E L F M A G N E T I C M O D E L
of M A T T E R & M I N D;
the O R I G I N O F L I F E; &
the A R T of H E A L I N G.

* * * * * * * * * * *

Theory, Experiments and Proofs

by

Andrija Puharich, M.D., LLD.

Director of Research

ESSENTIA RESEARCH ASSOCIATES
and
ELF COCOON CORPORATION

Route 1, Box 545, Dobson, N.C. 27017-9998

COPYRIGHT
February 1987

life originated on primitive earth from four atoms, C , O, H, and N which produced four molecules, CH_4 methane, NH_3 ammonia, H_2O water, and H_2 hydrogen. These molecules are known to exist in interstellar space (17, 105). These four molecules have also been formed into amino acids under laboratory conditions. (50, 21, 6). Twenty amino acids are the molecular foundation of all proteins. The unique feature of amino acids produced in living things is that they are all levo-rotary, i.e., they will rotate plane polarized light waves to the left (57) (14). In trying to understand this asymmetrical feature of life energies, I observed that all of the antagonistic physiological pairs of atomic elements are polarized magnetically. Table 1 shows this relationship ranked by proton number.

Table 2 shows these physiological pairs ranked by nuclear magnetic increments of 0.4 Bohr magnetons, μ . All the values for μ are ground state values. (13). From the data in these two tables we can make some deductions. First, we observe that the four atomic letters of life show a set of unique magnetic moment polarizations:

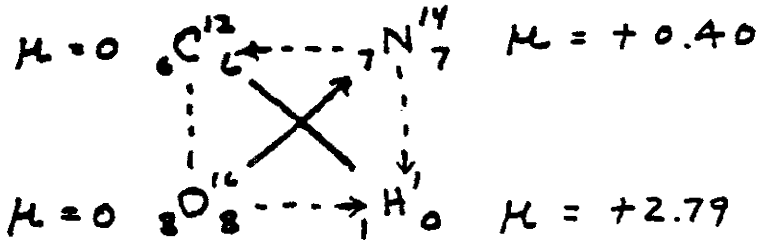

We shall refer to this asymetrical magnetic polarized group as the COHN set. The COHN set magnetic moment asymmetry

within amino acids may account for the l-amino acids of life. We can briefly characterize this asymmetry with the example of glycine, one of the simplest of amino acids and the one produced in the greatest abundance in the laboratory re-creation of life origins. The chemical formula below is from Pauling (60).

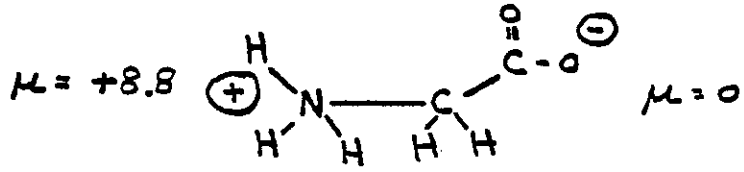

The base NH_3^+ group has a positive electric charge. The acidic COO^- group has a negative electric charge. But note that the molecule is also polarized magnetically with the NH_3^+ group carrying +8.8 μ while the COO^- group has zero magnetic moment. In this molecule the positive electric pole, and the positive magnetic moment are on the same end of the molecule, and rotation of this group may account for the optical rotation of amino acids.

I believe that this "life" asymmetry reflects the weak violation of parity that exists in the cosmos. I further believe that this violation is related to the preponderance of hydrogen atoms in the cosmos (90% by count) (17) and preponderance of hydrogen atoms in the human body (63% by count) (3). This possibility focussed my attention on the role of the proton in life processes.

PART 1 CONTENTS

Introduction	1
1) Problem of Life Origins.	1
Molecular Asymmetry and Proton Magnetic Basis	
2) Replication and Control in Life Processes	4
Proton Super-Conduction	
3) Normal Sensory Perception	10
Proton Precession Frequencies	
4) Artificial Sense Perception	16
C=O:H:N Semiconductor Ferroelectrics	
5) Memory in Brain	19
Modulation of Proton Spin	
6) Direct Brain Perception	25
Proton-Proton Spin Coupling. Water & Glia	
7) Direct Brain Action	28
Proton Synchrony with Gravity Waves.	
8) Memory in Nature	30
Cosmic Proton Matrix. Magnetic Matter	
9) Precognition	35
Mushrooming Proton Fields	
Concluding Remarks	38
Tables and Figures	41
References	46

PART 2 CONTENTS

1. Introduction to how the author got into cancer research. 1

2. Electrostimulation of humans with deafness 3
   This technology (the transdermal system, or T.D.) found to prevent blood clotting in animals.
   The TD system was found to efficiently split water by alternating current electrolysis.

3. Development of an energy cell to split water into H_2 and O_2. 4

4. The energy cell developed into a crucible for the biochemical origin of life. The chemistry of the origin of life. 5

5. The role of O_2 and O_3 (ozone) in the origin of life. 12
   O_3 found to be an effective and cheap treatment for cancer in mice. Discovery of quantasomes in cancer cells by Dr. Arnan. Development. Use of the TD system to treat cancer.

6. The rate of ELF magnetic fields in causing cancer. 17

7. Tables, and Figures. 24-73

8. Appendix A. Reprint from SCIENCE 74-77

9. Appendix B. NUCLEAR MAGNETISM. 78-82
   References. 83-94

PART 3 CONTENTS

1. U.S. PATENT. 4,394,230 PUHARICH 1
   Method and Apparatus for splitting water molecules.

2. Method of splitting the water molecule according to 21
   the theory of ELF PHONONS-HYDROAMPLIFICATION OF
   STIMULATED EMISSION RADIATION, i.e. the PHASER.
   Analysis of the Phonon generated in water by the
   TD signal generator.

3. Stationary harmonic waves generated in the skin 33
   by SKIN-STROKING due to a fundamental frequency
   of 8.00 Hz. Phonons.

4. Review of experiments in biochemical origin of life. 68
   Showed that 8.00 Hz ELF magnetic field is the guiding
   information necessary to create life. The development
   of living forms can be described by the mathematics
   of the Mandelbrot Fractal Geometry.

5. References. 79

PART 4 CONTENTS

A. Brief synopsis of the Nature of the Universe. 1

B. The Nature of Man. 3
Artificial Stimulation of hearing in the deaf. Researches with healers. Researches in psychometry. Researches of ESP in Faraday Cages. Precognition of Cosmic Ray Pulses coming to earth.

C. The quantum nature of ultimate physical particles - preons, and their guage fields. Clairvoyant vision of quarks and preons in 1895 by Besant & Leadbeater. This work anticipates quarks and preons. Super-string theory. 16

D. What can the theory predict? 27
It predicts the nature and solution of 22 problems of science. It predicts that a device can be built that will duplicate the normalizing effects of healers in disease.

E. A device is built that duplicates some of the healing effects of healers. It is called the TESLAR , and is packaged as a wrist watch. 35

SUMMARY 45

APPENDIX A 48

PAPER No.1

PROTOCOMMUNICATION

by

ANDRIJA PUHARICH

Presented at the

TWENTIETH INTERNATIONAL CONFERENCE
OF THE PARAPSYCHOLOGY FOUNDATION
Le Piol, St. Paul de Vence, France
August 27, 1971

July 7, 1971, New York, New York, U.S.A.
(Revised January 1987)

CONTENTS

Introduction	1
1) Problem of Life Origins.	1
Molecular Asymmetry and Proton Magnetic Basis	
2) Replication and Control in Life Processes	4
Proton Super-Conduction	
3) Normal Sensory Perception	10
Proton Precession Frequencies	
4) Artificial Sense Perception	16
C=O:H:N Semiconductor Ferroelectrics	
5) Memory in Brain	19
Modulation of Proton Spin	
6) Direct Brain Perception	25
Proton-Proton Spin Coupling. Water & Glia	
7) Direct Brain Action	28
Proton Synchrony with Gravity Waves.	
8) Memory in Nature	30
Cosmic Proton Matrix. Magnetic Matter	
9) Precognition	35
Mushrooming Proton Fields	
Concluding Remarks	38
Tables and Figures	41
References	46

INTRODUCTION

Progress in parapsychology and the advancement of the epistemological problem, it seems to me, are dependent on solving the modus operandi of certain phenomena:

1) The Origin of Life

2) Replication in the Life process

3) Sensory Perception

4) Memory in Brain

5) Artificial Perception and Intelligence

6) Direct Brain Perception

7) Direct Brain Action

8) Memory in Nature

9) Precognition

I feel that these phenomena have a common thread the pursuit of which has been my life's work. I shall describe what I have done and what others have done to untangle this thread from nature's fabric. Although this exploration is fragmentary and presented with utmost reserve, I believe that it may serve a useful function in stimulating discussion and experimentation.

1. PROBLEM OF THE ORIGIN OF LIFE

The consensus of scientific opinion (6, 50, 21) is that

The result is that the neutron's magnetic spin tends to cancel the magnetic spin of the proton. It is my considered opinion that this spin "shielding" effect is large enough to cancel the protonic "GO" command to divide. What we do not know is the locus and origin of the "GO" command - except that it is probably protonic.* But we shall pursue this question later. What is of interest is the role of water in the GO, NO-GO control mechanism.

Let us look at a situation where there is potentiation of the "GO" command in cell division and the growth and repair process. Grad (90) of McGill University has clearly shown that if a healer "treats" distilled water in glass bottles, and such treated water is used on plants, there is a significant potentiation of the growth process. Sister Justa Smith (88, 89, 90) has shown that distilled water treated by a healer's hands will significantly increase the hydrolytic action of the enzyme trypsin. The healer's "treatment" is exerted solely on the water, and the effect is most likely to be on the proton moments of the resonant hydrogen bonds of the water molecules. Further research should be directed to looking for nuclear magnetic resonant shifts either in magnetic field, ELF, or radio frequency. We shall return to the role of water in bio-control systems later. There remains the mystery of the "GO" command in egg division which I do not believe

* (1987) THIS HAS NOW BEEN IDENTIFIED AS THE MAGNETIC FIELDS EMANATING FROM THE MAGNETIC MONOPOLES RESIDING IN QUARKS WITHIN THE PROTON - AS OMEGONS (OR ALSO called PREONS).

modulation before he can hear sounds. (70) (44) (45). One of the first measurable effects of such AMAC electronic conditioning is that a barrier potential of about 0.6 volts develops across the energized tissues. This is due to dielectric polarization of the cell membranes of all cells in the signal path. (71) Once a barrier potential is present across tissue, one can evoke the following effect: One of the AMAC energized electrodes, when it is lightly stroked over the skin, produces the sensation of hearing both in the deaf and in normals. (32). During the hearing attendant upon skin-stroking one will observe on the oscilloscope that the sine wave carrier signal injected into the head becomes half-wave rectified with the positive half-wave being clipped. What tissue mechanism detects AMAC signals? (See figure 3).

Detection occurs when the keratin of the skin is stretched by the stroking action (24), which releases elf fields from the protons. The coils of the alpha helix configuration of the keratin are held together by hydrogen bonds in the form shown in figure 2 (72).

Under the combined effect of the barrier potential forming a DC bias across the carbonyl-H-imide bond, and the stretching of the distance across the H bond, the C=O:H:N system becomes a semiconductor which rectifies the sine wave carrier (71).

Chemical Content of Solution:

A. BEFORE ELECTROLYSIS

$NaCl$, HOH

Air Contaminants

N_2, O_2, Ar

pH 4.27

CO_2 - not detectable

B. AFTER SEVERAL HOURS VACUUM @ 60 μ

$NaCl$, HOH

N_2, O_2, Ar, CO_2 - not detectable

After 3 minutes of AC ELECTROLYSIS the solution contained the following elements:

$^{23}_{11}Na$ $^{35}_{17}Cl$ $^{2}_{1}H$ $^{16}_{8}O$

$^{63}_{29}Cu$ (from the centre electrode)

$^{56}_{26}Fe$ (from the annular electrode)

FIG 8

ELECTROLYSIS START @ 09:00 PM

Sample Identity:	#1-10:12 AM	#2-10:34	#3-11:01	#4-11:35	#5-12:00	#6-12:34 PM	#7-1:10
Constituents	Concentration, % by Volume						
Nitrogen	59+	37.6	18.2	11.0	11.5	9.6	5.0
Oxygen	18.7	9.6	0.98	0.88	0.86	0.87	0.44
Argon	0.87	0.77	0.40	0.37	0.50	0.30	0.174
Carbon Dioxide	ND	0.056	0.060	0.054	0.096	0.0137	0.0127
Hydrogen	21.0	51+	80+	87+	87+	89+	94+
Hydrogen, cc	3.6	NA	NA	NA	2.6	NA	NA
Oxygen, cc	3.2	NA	NA	NA	0.022	NA	NA
Amount of Gas Sampled, cc	0.12	0.44	0.44	0.50	0.46	0.35	0.49

Definitive Test

Sample Identity:	2:15P.M. 0 min	2:30 P.M. 15 min	2:45 P.M. 30 min	4:00 P.M. 0 min	4:30 P.M. 30 min
Constituents	Concentration, % by Volume				
Nitrogen	6.6	5.3	8.7	7.9	12.1
Oxygen	0.86	0.53	1.53	1.36	2.8
Argon	0.161	0.138	0.199	0.21	0.23
Carbon Dioxide	ND	0.0154	0.062	0.0058	0.082
Hydrogen	92+	94+	89+	90+	84+
Total Amount of Gas, cc	0.20	0.29	0.18	1.9	2.1
Hydrogen, cc	0.184	0.27	0.16	1.72	1.78
Oxygen, cc	0.0017	0.0015	0.00275	0.026	0.059

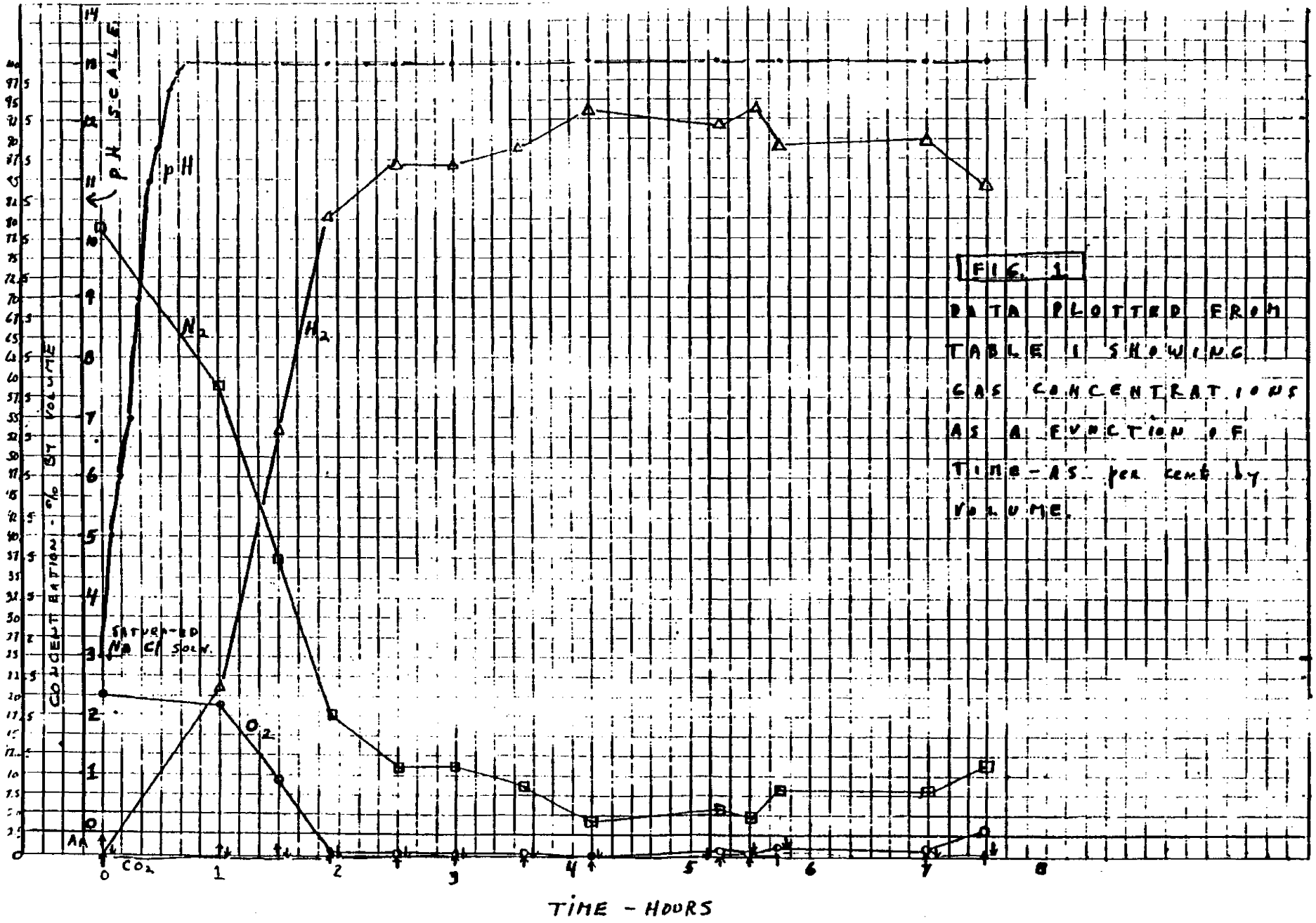

FIG. 1

DATA PLOTTED FROM TABLE I SHOWING GAS CONCENTRATIONS AS A FUNCTION OF TIME - As per cent by VOLUME.

WATER ELECTROLYSIS REACTIONS

I. $2NaCl + 4HOH \longrightarrow 2NaOH + 2H_2(g) + Cl_2$

$Fe + Cl_2 \longrightarrow FeCl_2$

II. $3FeCl_2 + 4HOH \xrightarrow[\text{CATALYST}]{Cu} FeO \cdot Fe_2O_3 + 6HCl + H_2(g)$

III. $Fe_3O_4 + 8HCl \longrightarrow 3FeCl_2 + 4HOH + Cl_2$

IV. $2Cl_2 + 2HOH \rightarrow 4HCl + O_2(g)$

FIG. II.

Glycine (Gly)

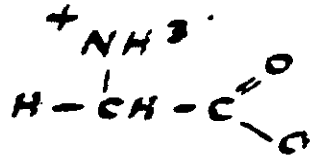

Alanine (Ala)



Valine (Val)

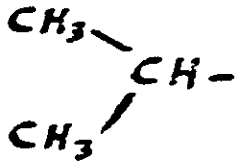

Leucine (Leu)

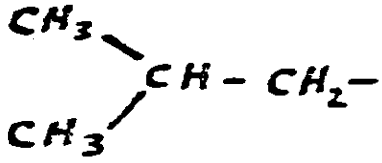

Isoleucine (Ileu)

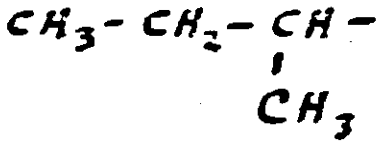

Serine (Ser)



Threonine (Thr)

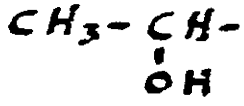

Phenylalanine (Phe)

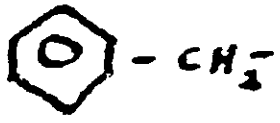

Tyrosine (Tyr)



Tryptophan (Trp)

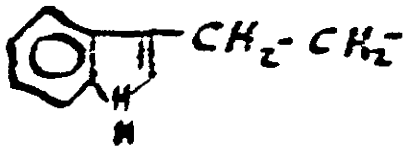

Histidine (His)



Proline (Pro)

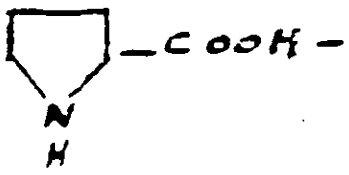

ORGANIC ACIDS IN SOLUTION

Formic	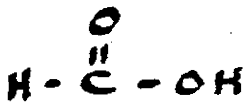
Acetic	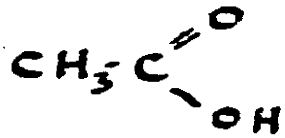
Proprionic	CH_3CH_2COOH
Oxalic	$HOOC-COOH$
Succinic	$HOOC(CH_2)_2COOH$
Benzoic	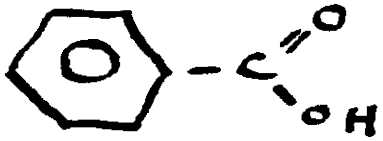

PYRROLES

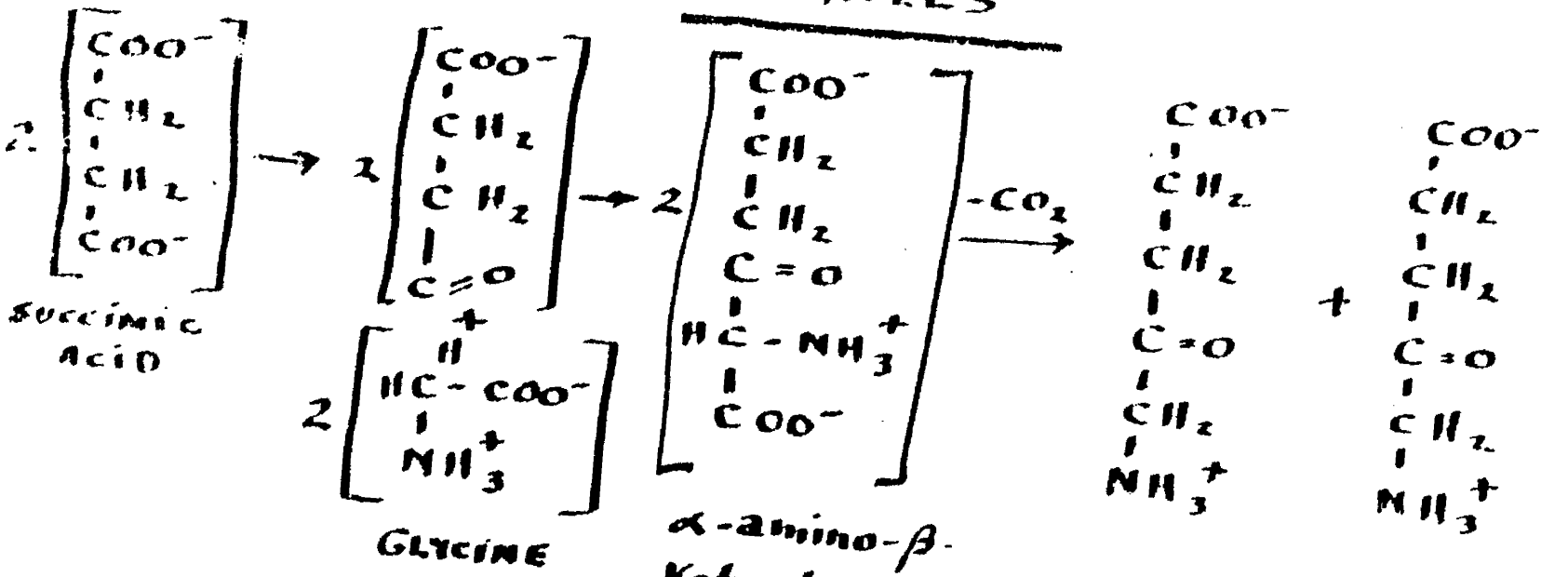
Succinic Acid
Glycine
α-amino-β-Keto adiptic Acid
-CO2
2 δ-amino levulinic Acid
-2H2O
Four Pyrrole Rings Join To Form Porphyrin
Many steps to Protoporphyrin IX + Fe

HEME

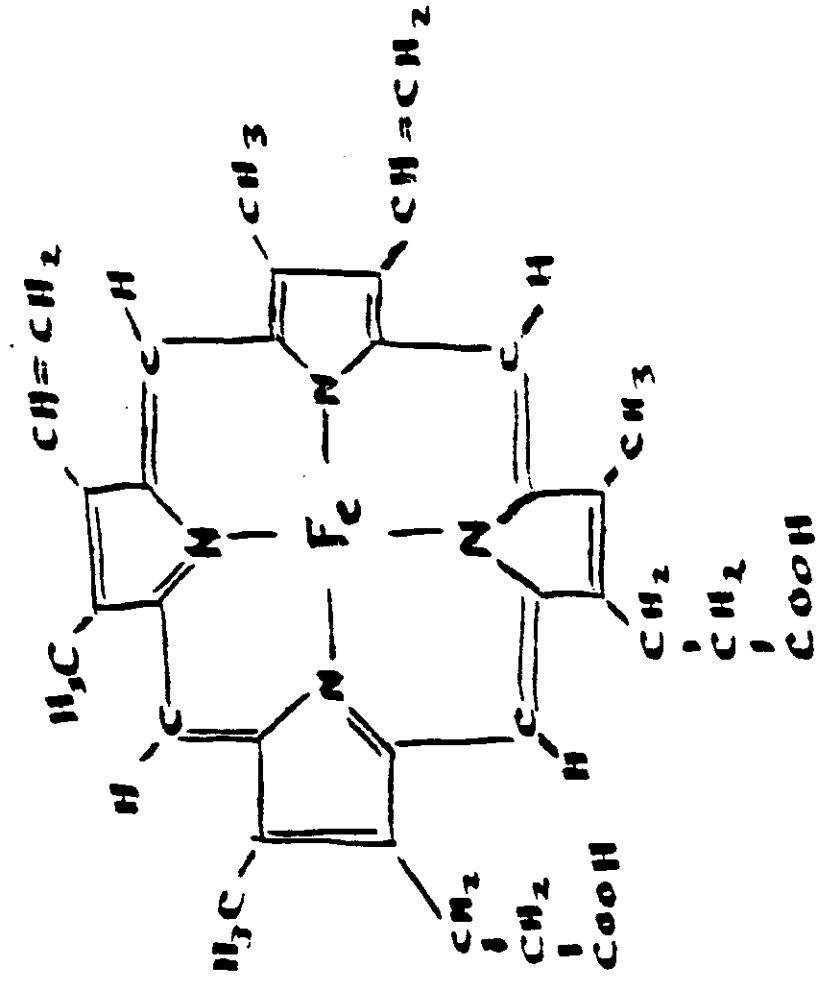

KERVRAN REACTION

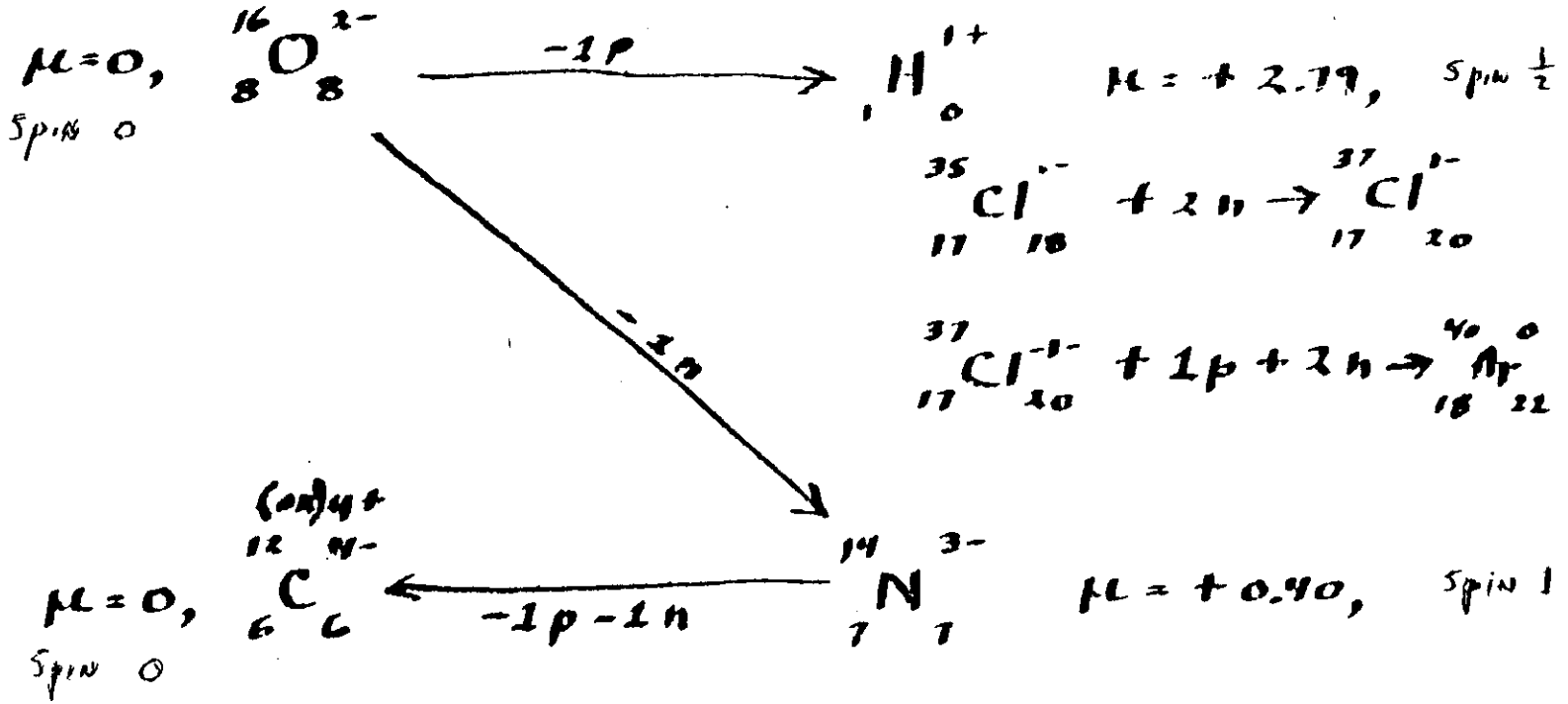

Feed stock for amino acid synthesis:

O → H, N, C

FIG 14

Commoner has shown that stretching of such proteins in a nerve fiber also produces an electron spin resonance signal during neural conduction (12).

The production of speech hearing capability in a deaf person by means of direct brain electro-stimulation has revealed some significant data about information processing. Empirically we found that the deaf hear words optimally at a carrier frequency of 20 KHz with amplitude modulation of audio signals (double side band) where the half-power band pass is about 3 KHz (67). This passes about 1.5×10^7 bits per second of information to the brain. This compares favorably to normal hearing where some 3×10^7 auditory nerve fibers with an average time constant of 5×10^{-3} sec. yields 6×10^7 bits of information per second.

Secondly, the power spectrum of the AMAC signal shows that the power pulse height of the side band curve is inversely proportional to frequency, and this accords well with the classic Fletcher-Munson curve for threshold of hearing. Thirdly, all evidence pointed to current pulses as being the signal mechanism of electrostimulation of hearing (67).

Fourthly, actual hearing of tones in the deaf is due to a beat frequency detection effect. For example, if a 100 Hz tone is the stimulus signal, it is impressed on a 20 KHz carrier

TABLE 2.2B The periodic table

IA	IIA	IIIB	IVB	VB	VIB	VIIB	VIII	VIII	VIII	IB	IIB	IIIA	IVA	VA	VIA	VIIA	O
1 H 1.00797																	2 He 4.0028
3 Li 6.939	4 Be 9.0122											5 B 10.811	6 C 12.01115	7 N 14.0067	8 O 15.9994	9 F 18.9984	10 Ne 20.183
11 Na 22.9898	12 Mg 24.312											13 Al 26.9815	14 Si 28.086	15 P 30.9738	16 S 32.064	17 Cl 35.453	18 Ar 39.948
19 K 39.102	20 Ca 40.08	21 Sc 44.956	22 Ti 47.90	23 V 50.942	24 Cr 51.996	25 Mn 54.9380	26 Fe 55.847	27 Co 58.9332	28 Ni 58.71	29 Cu 63.54	30 Zn 65.37	31 Ga 69.72	32 Ge 72.59	33 As 74.9216	34 Se 78.96	35 Br 79.909	36 Kr 83.80
37 Rb 85.47	38 Sr 87.62	39 Y 88.905	40 Zr 91.22	41 Nb 92.906	42 Mo 95.94	43 Tc (99)	44 Ru 101.07	45 Rh 102.905	46 Pd 106.4	47 Ag 107.870	48 Cd 112.40	49 In 114.82	50 Sn 118.69	51 Sb 121.75	52 Te 127.60	53 I 126.9044	54 Xe 131.30
55 Cs 132.905	56 Ba 137.34	57 *La 138.91	72 Hf 178.49	73 Ta 180.948	74 W 183.85	75 Re 186.2	76 Os 190.2	77 Ir 192.2	78 Pt 195.09	79 Au 196.967	80 Hg 200.59	81 Tl 204.37	82 Pb 207.19	83 Bi 208.980	84 Po (210)	85 At (210)	86 Rn (222)
87 Fr (223)	88 Ra (226)	89 †Ac (227)	104 Rf (257)	105 Ha (260)													

* Lanthanum Series

58 Ce 140.12	59 Pr 140.907	60 Nd 144.24	61 Pm (147)	62 Sm 150.35	63 Eu 151.96	64 Gd 157.25	65 Tb 158.924	66 Dy 162.50	67 Ho 164.930	68 Er 167.26	69 Tm 168.934	70 Yb 173.04	71 Lu 174.97

† Actinium Series

90 Th 232.038	91 Pa (231)	92 U 238.03	93 Np (237)	94 Pu (242)	95 Am (243)	96 Cm (247)	97 Bk (247)	98 Cf (249)	99 Es (254)	100 Fm (253)	101 Md (256)	102 No (253)	103 Lw (257)

Atomic Weights are based on C^{12}—12.0000

Figure 19-16
Simplified representation of the chemiosmotic-coupling hypothesis.

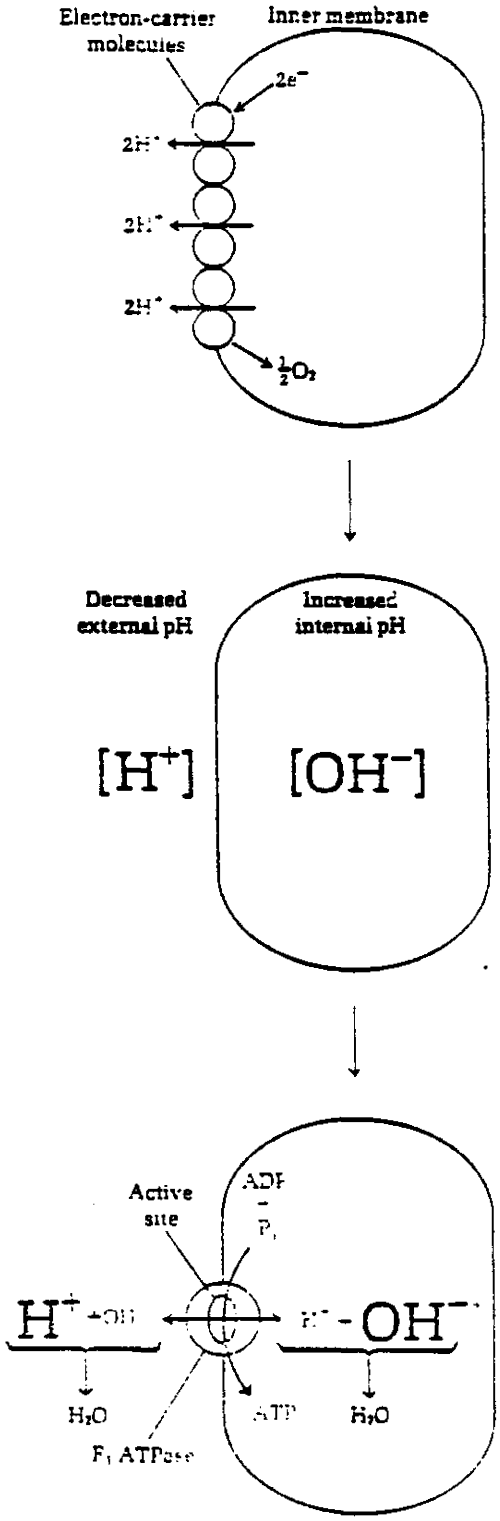

Electron transport causes H^+ ions to be pumped outward, across the inner membrane of the mitochondrion, to yield a gradient of H^+. This phase is shown in more detail in Figure 19-17.

The H^+ gradient is the energy-rich state into which electron-transport energy is transformed. The inner compartment becomes alkaline, the outer compartment more acid.

The H^+ gradient is the immediate driving force for the phosphorylation of ADP, which proceeds with the removal of HOH. The relatively high internal OH^- concentration pulls H^+ (color) from the active site of the F_1 ATPase and the relatively high external H^+ concentration pulls OH^- in the outward direction. Since the ion product of water ($K_w = [H^+][OH^-]$) is very low (10^{-14}), the sinks of OH^- and H^+ generated by electron transport are very effective traps for H^+ and OH^-, respectively. ATP formation is shown in more detail in Figure 19-18.

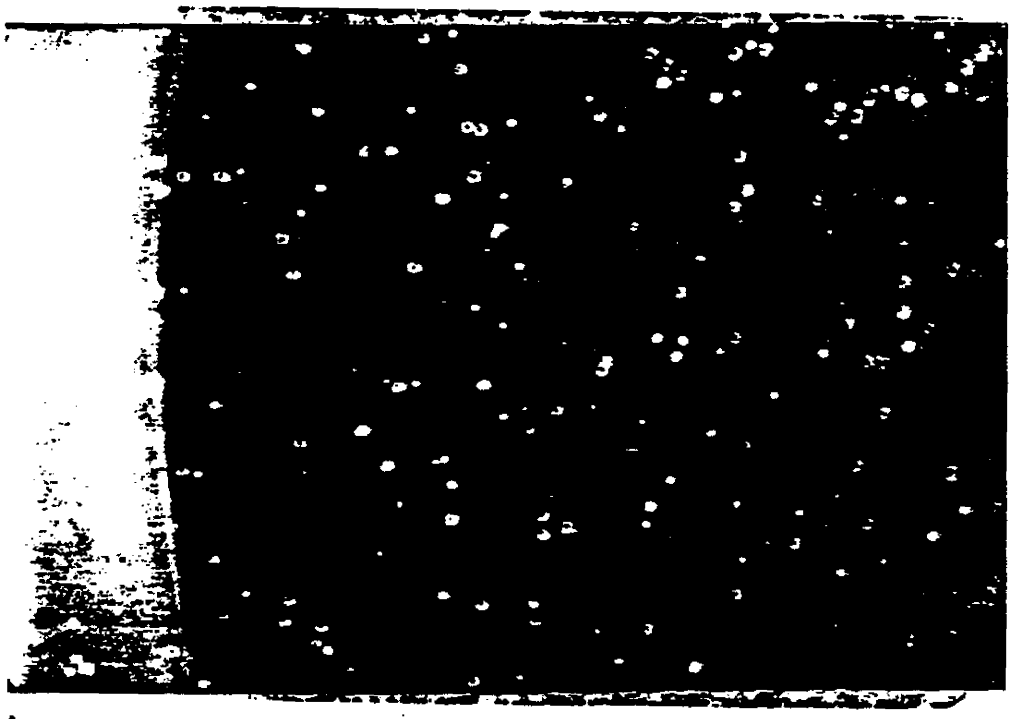

A.



B.

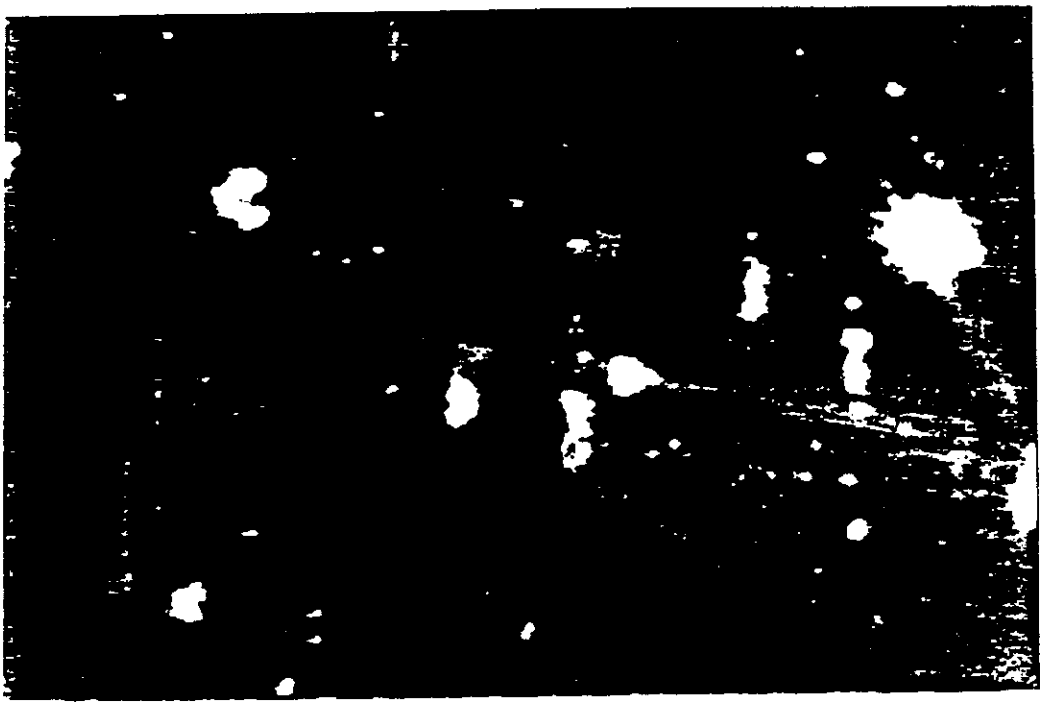

C.

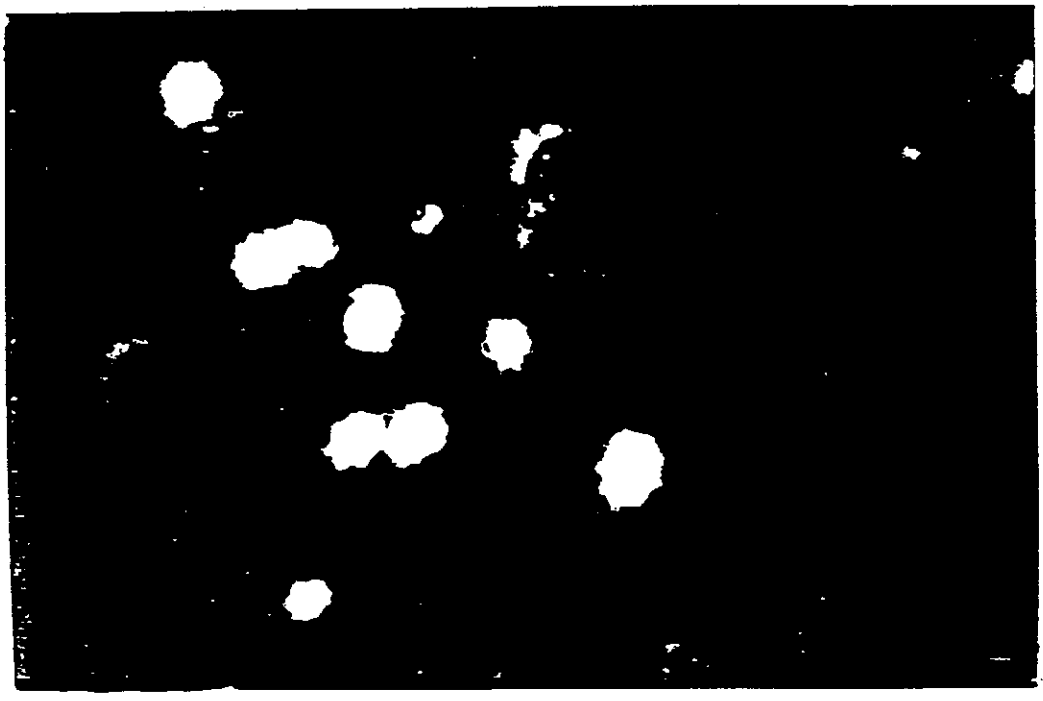

D.

ROTON AND CARBON-13 NMR SPECTROSCOPY

AN INTEGRATED APPROACH

R. J. Abraham
University of Liverpool

and

P. Loftus
Merchant Taylors' School, Crosby

HEYDEN
London · Philadelphia · Rheine

Table 3.1

Characteristic Proton–Proton Coupling Constants (Hz)

System	Coupling range	System	Coupling range
OPEN CHAIN			
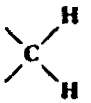	−10 to −18	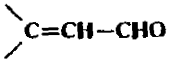	7 to 9
		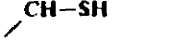	6 to 8
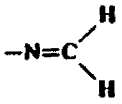	8 to 16	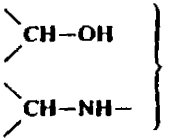	4 to 8
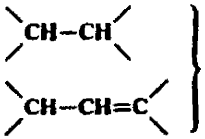	5 to 10	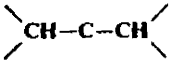	0 to 1
$CH_3.CH_2-$	7 to 8	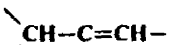	0 to −2
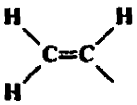	J_{gem} −3 to +7 J_{cis} 3 to 18 J_{trans} 12 to 24	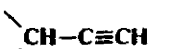	−2 to −3
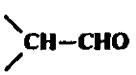	1 to 3		0 to 2
		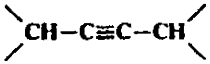	2 to 3

CYCLIC

Aromatic and olefinic	*ortho*	*meta*	*para*
Benzene derivatives	5–9	2–3	0–1

	J_{23}	J_{34}	J_{24}	J_{25}
Furan	1.8	3.5	0.8	1.6
Pyrrole	2.6	3.4	1.4	2.1
Thiophene	5.2	3.6	1.3	2.7
Cyclopentadiene	5.1	1.9	1.1	1.9

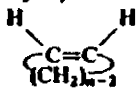

n =	3	4	5	6	7	8	9
	ca. 1	2.7	5.1	8.8	10.8	10.3	10.7

Saturated	J_{gem}	J_{cis}	J_{trans}
Cyclopropane	−4.5	9.2	5.4
Ethylene oxide	+5.5	4.5	3.2
Ethylene imine	+2.0	6.3	3.8
Ethylene sulphide	*ca.* 0	7.1	5.6
Cyclobutane derivatives	−11 to −15	6 to 11	3 to 9
Cyclopentane derivatives	−11 to −17	7 to 11	2 to 8
Cyclohexane derivatives	−12 to −15	J_{ax} 2 to 5	J_{aa} 8 to 13 J_{ee} 1 to 4

CARCINOGEN

-55-

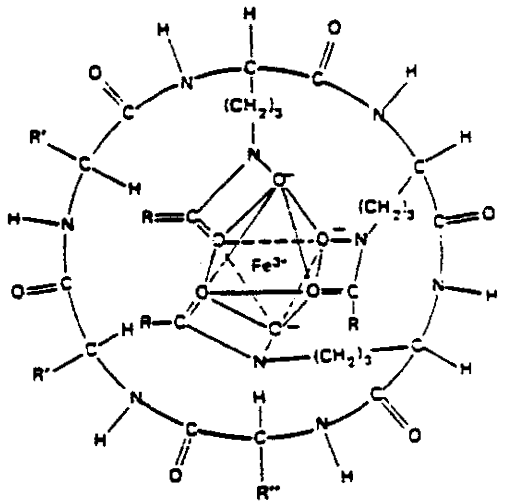

(a)

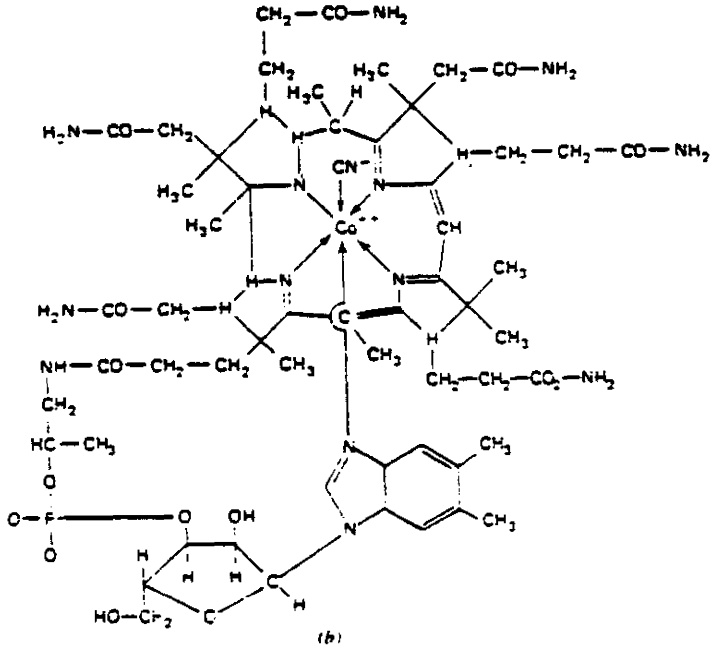

(b)

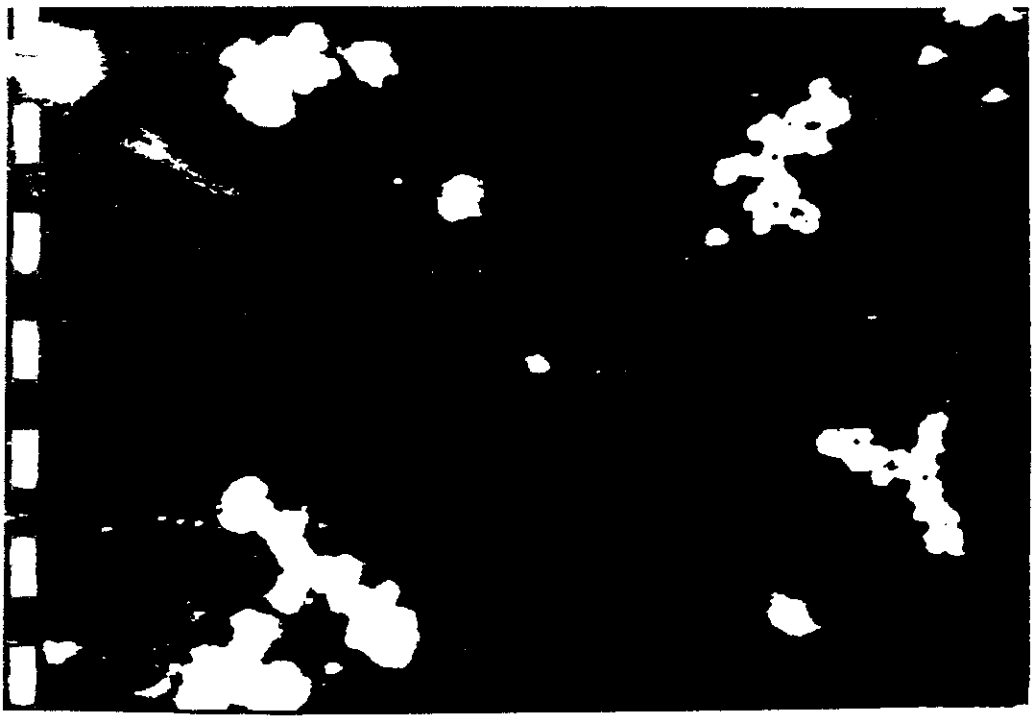

E.

Scanning electron micrograph of intact liver mitochondria in isolated state.

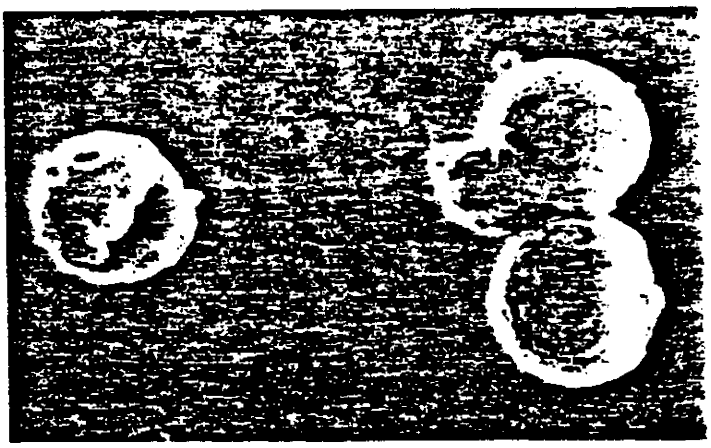

1.0 μm

E. H. Newcomer

Electron micrograph of a thin section of a mitochondrion in a bat pancreas cell.

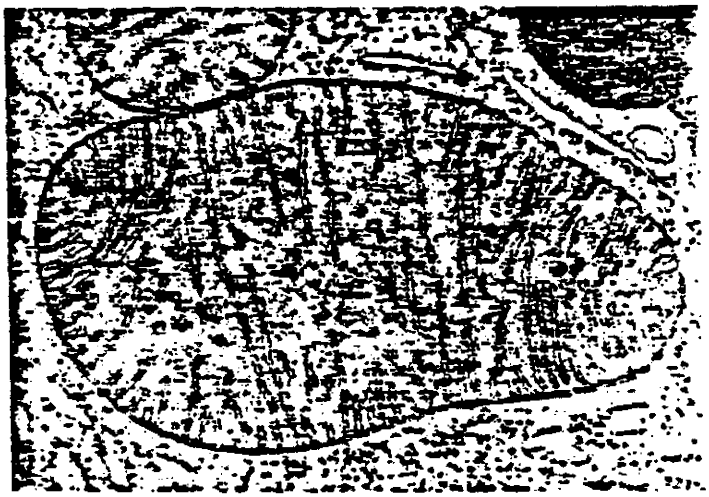

0.5 μm

K. R. Porter

Drawing of heart mitochondrion showing three-dimensional arrangement of membranes. (From Peter Raven and Helena Curtis. Biology of Plants. Worth Publishers, Inc., New York, 1970.)

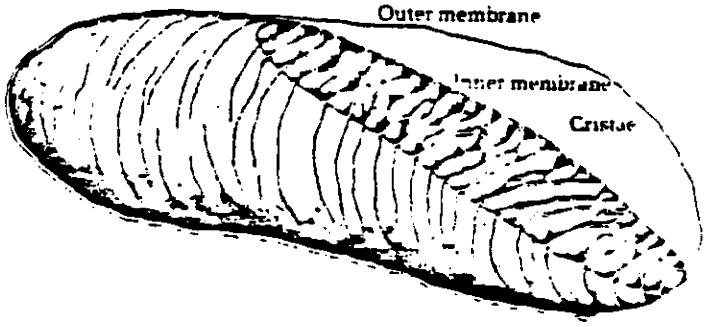



Rat liver (platelike)



Rat brown fat (septate)



Paramecium (tubular)

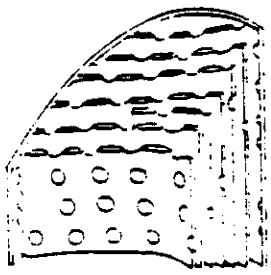

Blowfly flight muscle (perforated leaflets)

Figure 19-10
Electron micrographs showing the ultrastructural changes in mouse-liver mitochondria during the transition from resting (state 4) to active (state 3) respiration. This striking change in the structure and volume of the inner-membrane-matrix compartment appears to be caused by the binding of ADP to the ADP-ATP translocase molecules in the inner mitochondrial membrane.

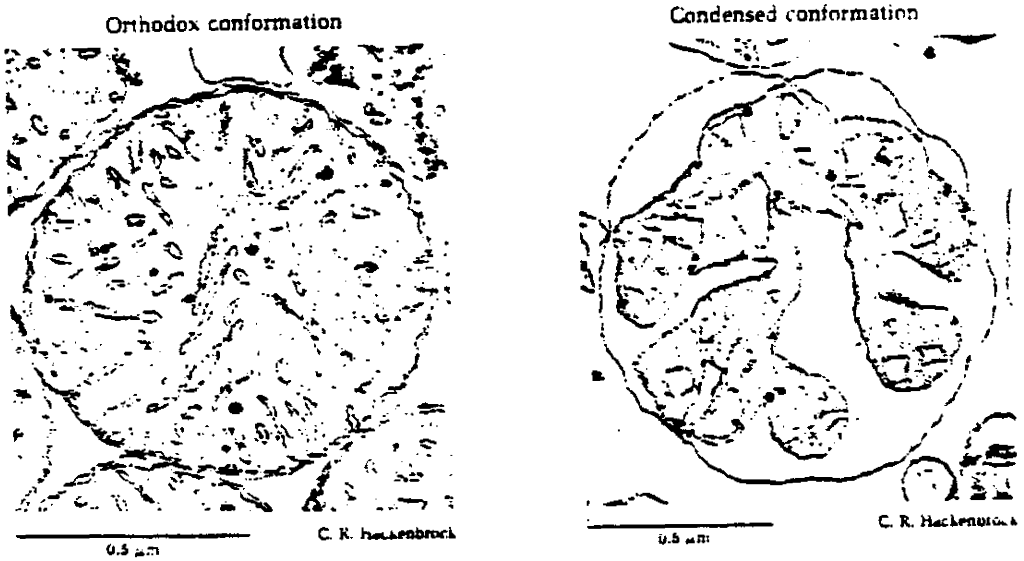

This analysis begins with the pair oxygen and hydrogen and their combination in water; and the pair carbon and nitrogen and their combination in amino acids and in nucleic acids. We shall develop the role of OH as the electron fuel cell of the organism (110), and HOH as the proton matrix end product of fuel cell hydrosynthesis and what this means for the storage of memories originating from life experience. We shall develop the role of CN groups as building blocks of proteins and nucleotides which become the memory bank for phylogenetic and ontogenetic experience..

2. REPLICATION AND CONTROL IN LIFE PROCESSES.

Cell division has two important goals, one is to perpetuate the species, and the other is to carry on orderly growth and repair in an organism. This process is under the control of the DNA system which is made up of four nucleic acid sentences whose active components are the 2 purine bases, adenine and guanine, and the 2 pyrimidine bases cytosine and thymine (16). It is of interest that these bases are made up of molecular building blocks that exist in interstellar space, NH_3, OH, and HCN (105). In fact, these molecules were used by Wöhler in 1828 to synthesise the first "organic" molecule, urea:

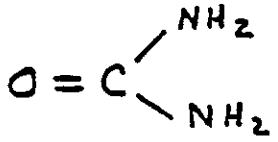

which is a building block of all the purines (55). The DNA

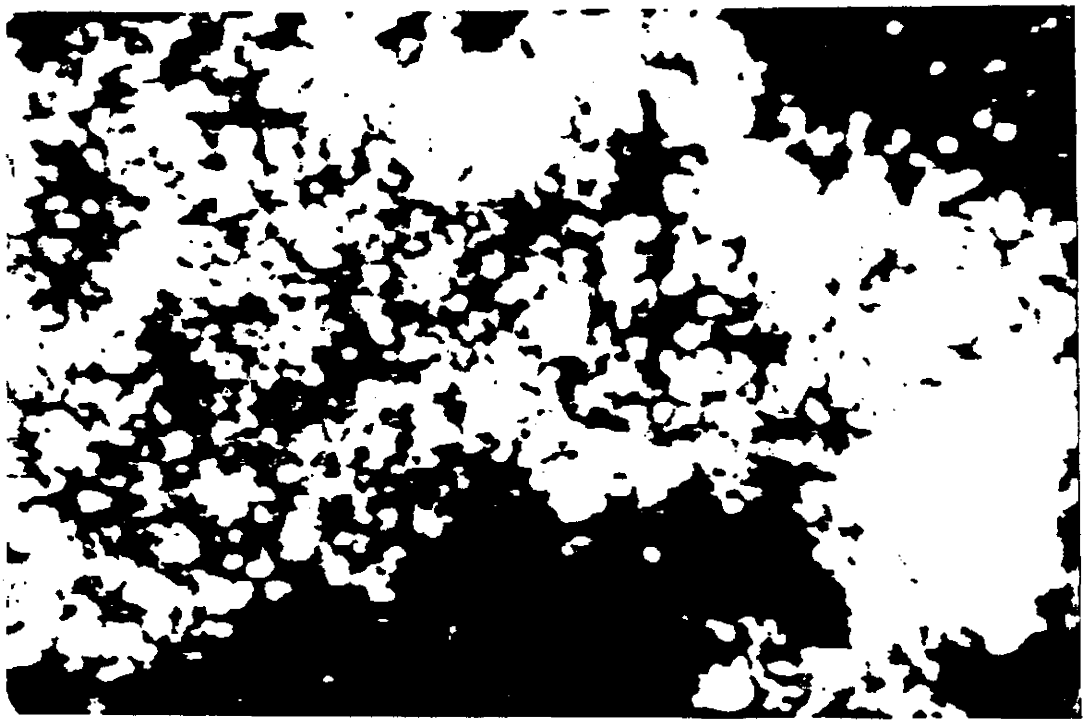

F.

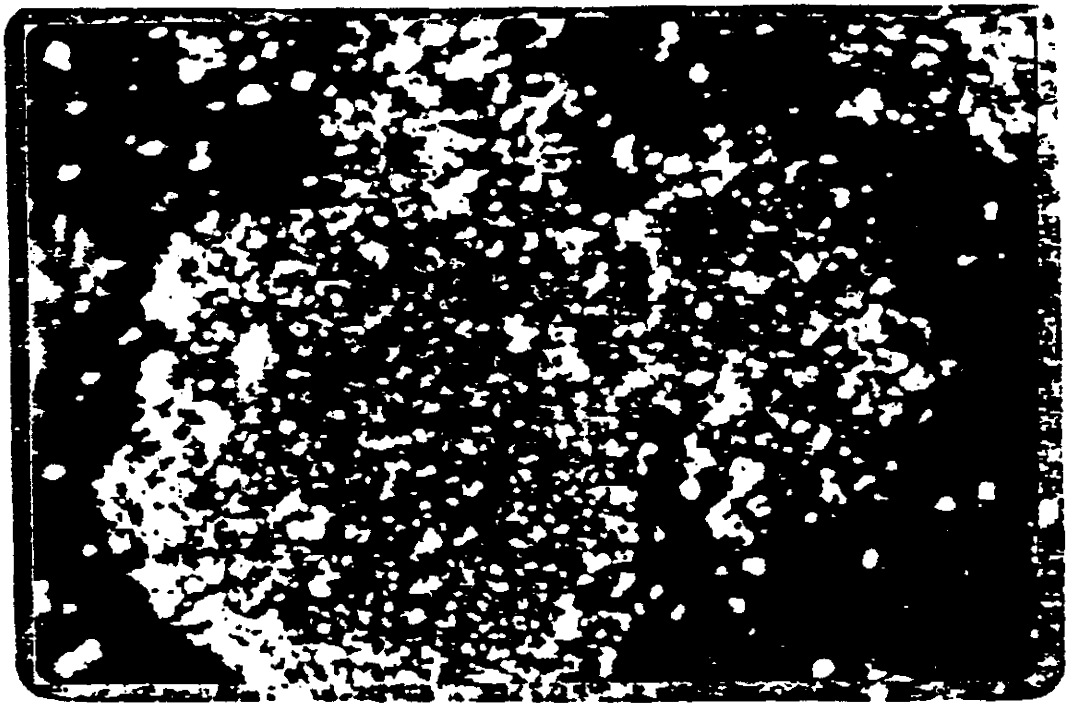

G.

Table 18-1 Standard oxidation-reduction potentials of some conjugate redox pairs expressed on the basis of two-electron transfers at pH near 7.0 and temperature 25 to 30 C

The standard potentials of the cytochromes and of ubiquinone vary somewhat with their state, i.e., whether isolated or present in the mitochondrial membrane; values given are for the latter case

Electrode equation	$E_{0'}$, V
Acetate + $2H^+ + 2e^-$ ⟹ acetaldehyde	−0.58
$2H^+ + 2e^-$ ⟹ H_2	−0.421
α-Ketoglutarate + $CO_2 + 2H^+ + 2e$ ⟹ isocitrate	−0.38
Acetoacetate + $2H^+ + 2e$ ⟹ β-hydroxybutyrate	−0.346
$NAD^+ + 2H^+ + 2e^-$ ⟹ NADH + H^+	−0.320
$NADP^+ + 2H^+ + 2e^-$ ⟹ NADPH + H^+	−0.324
Acetaldehyde + $2H^+ + 2e^-$ ⟹ ethanol	−0.197
Pyruvate + $2H^+ + 2e^-$ ⟹ lactate	−0.185
Oxaloacetate + $2H^+ + 2e$ ⟹ malate	−0.166
Fumarate + $2H^+ + 2e^-$ ⟹ succinate	−0.031
Ubiquinone + $2H^+ + 2e$ ⟹ ubiquinol	+0.10
2 cytochrome $b_{(Fe^{3+})}$ + $2e^-$ ⟹ 2 cytochrome $b_{(Fe^{2+})}$	+0.030
2 cytochrome $c_{(Fe^{3+})}$ + $2e^-$ ⟹ 2 cytochrome $c_{(Fe^{2+})}$	+0.254
2 cytochrome $a_{(Fe^{3+})}$ + $2e^-$ ⟹ 2 cytochrome $a_{(Fe^{2+})}$	+0.385
$\frac{1}{2}O_2 + 2H^+ + 2e^-$ ⟹ H_2O	+0.816

flow of electrons : RESPIRATION

PHOTOSYNTHESIS electron flow

OZONOSAN® PM 60

Deutsche und ausländische Schutzrechte

Bedienungsanweisung

Therapievorschläge

von Dr. med. H. Wolff

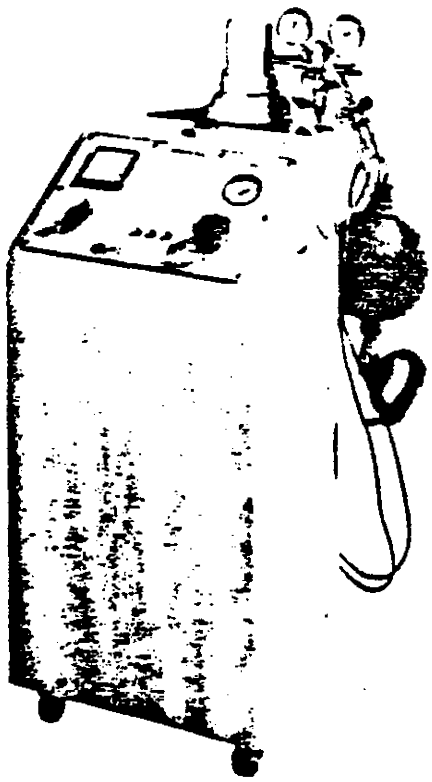

Konstante regelbare Ozonkonzentrationen
von 2 γ / ccm bis 100 γ / ccm

Keine Geruchsbelästigung
durch Destruktor und Spezialentnahmedüse

Dr. J. Hänsler KG · Medizintechnik

D - 7551 IFFEZHEIM, ROSENSTRASSE 3, TELEFON (0 72 29) 23 55

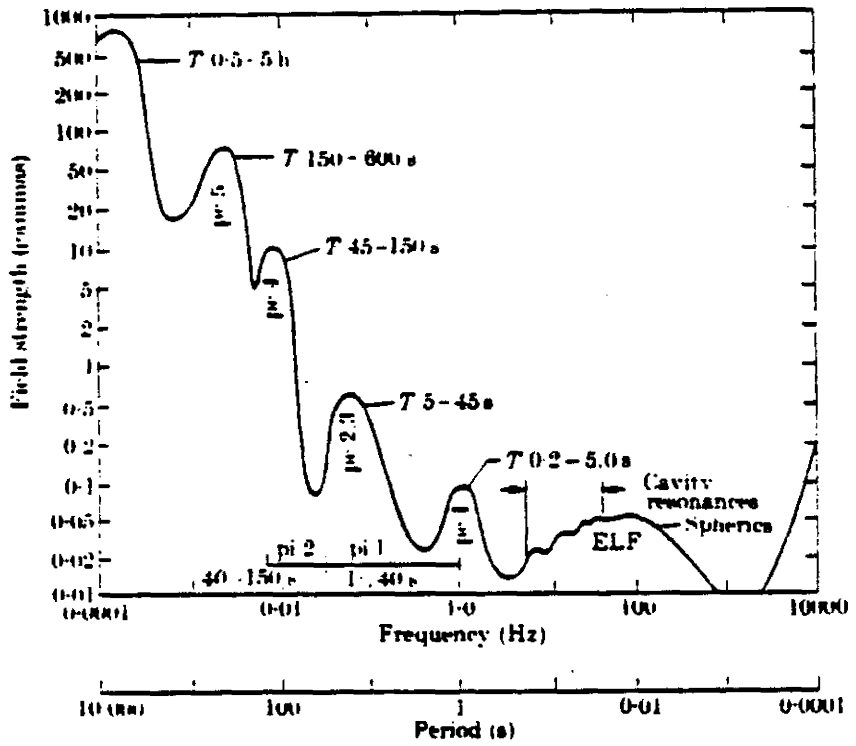

FIG. 6.44. The magnitude of geomagnetic micropulsations of different frequencies (or periods). After Campbell (1967).

The wave that travels with speed $V_A(1-\omega/\omega_i)^{\frac{1}{2}}$ is the pure Alfvén wave or the slow mode; the one that has the speed $V_A(1+\omega/\omega_i)^{\frac{1}{2}}$ is the modified Alfvén wave or the fast mode.

Obayashi (1965) computed the double-hop transit time τ of hydromagnetic waves along a geomagnetic field line; it is defined by

$$\tau = \int ds\, v_g^{-1},$$

where v_g denotes the group velocity, given by

$$v_g = V_A(1 \mp \omega/\omega_i)^{\frac{1}{2}}(1 \mp \omega/2\omega_i)^{-1}.$$

Assuming that the plasma density distribution is given by

$$n = n_0(a/r)^3,$$

we have

$$\tau = \frac{4aL^{\frac{1}{2}}}{B_0\sqrt{(4\pi n_0 m)}} \times$$

$$\times \int_0^{\lambda_m} \cos^4\lambda \left[\left\{1 \pm \frac{\omega}{2\omega_c}\frac{\cos^6\lambda}{\sqrt{(1+3\sin^2\lambda)}}\right\} \Big/ \left\{1 \pm \frac{\omega}{\omega_c}\frac{\cos^6\lambda}{\sqrt{(1+3\sin^2\lambda)}}\right\}^{\frac{1}{2}}\right] d\lambda.$$

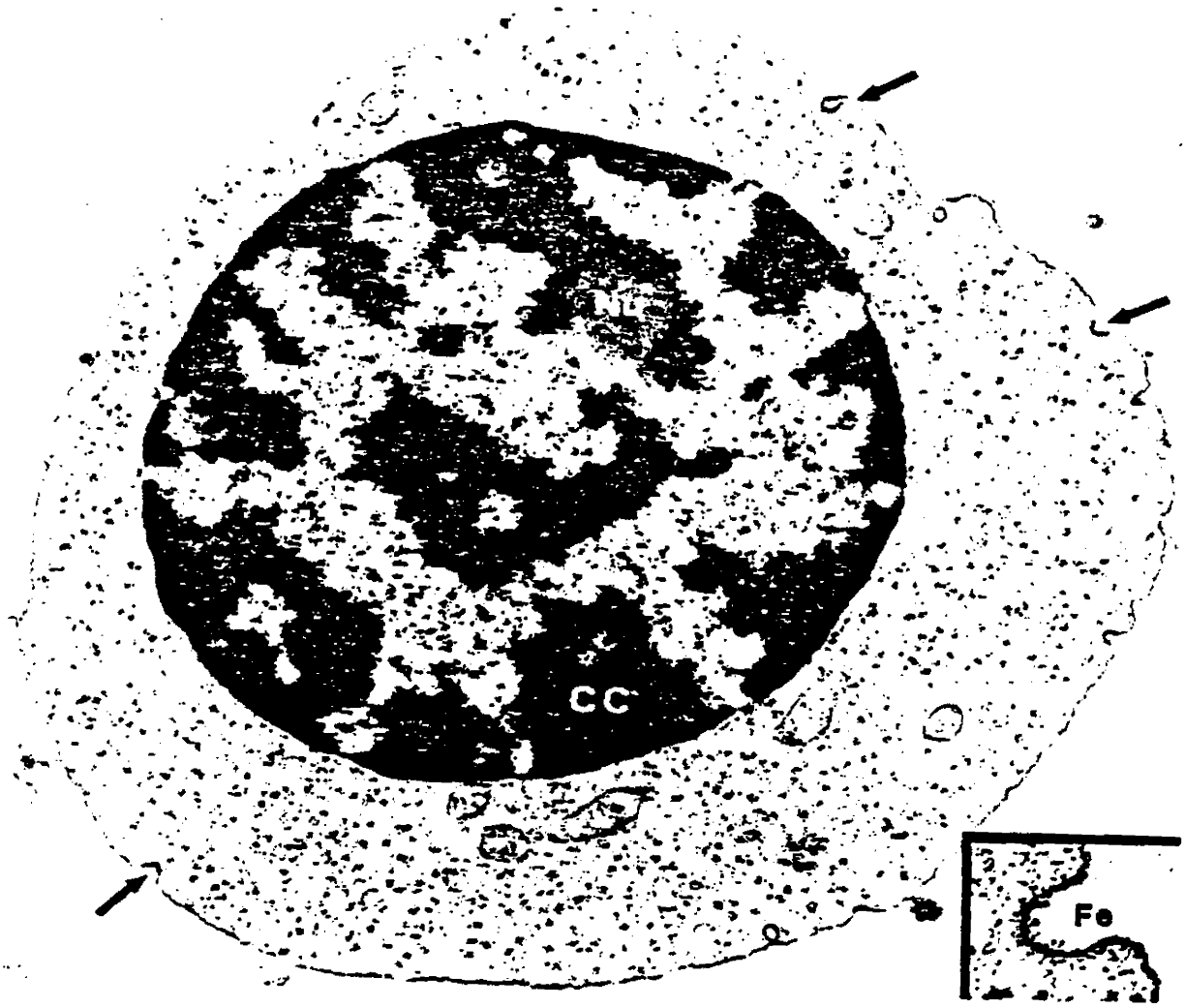

c

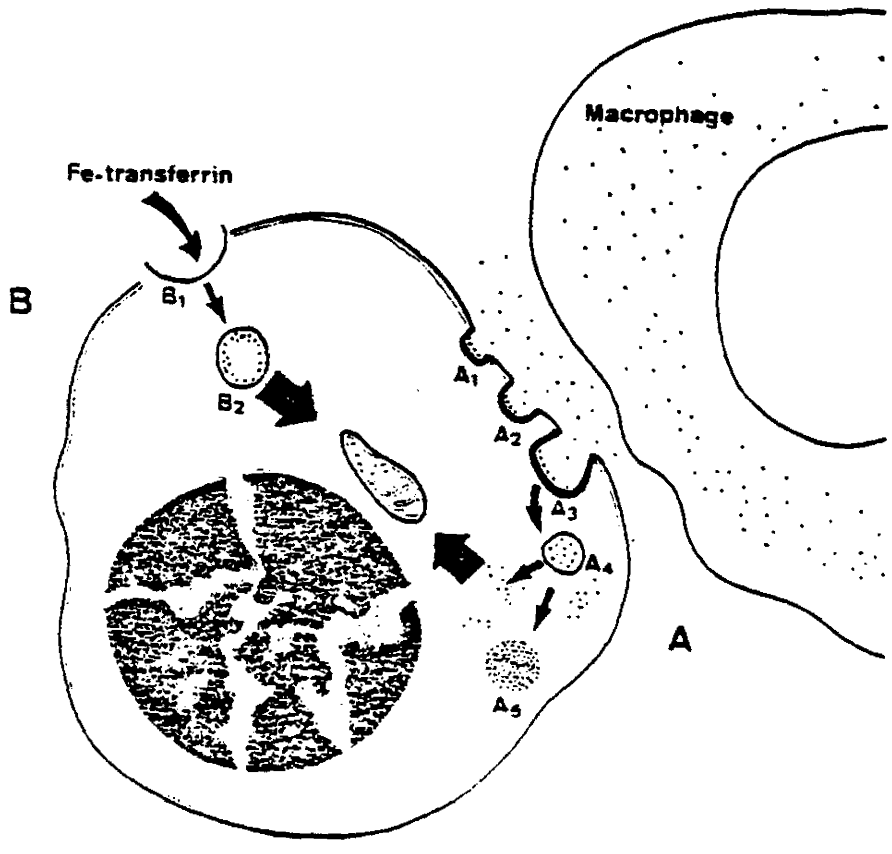

d



Fig. 7 **c)** *Basophilic erythroblast with clumps of condensed chromatin* (**CC**) *and only a vestigial nucleolus* (**Nu**). *Although the cytoplasm is still replete with polyribosomes which would account for the degree of basophilia on light microscopy, the grey background indicates the presence of hemoglobin. Several pinocytotic vesicles are detectable at the level of the cytoplasmic membrane, mainly related to absorption of iron in the form of ferritin molecules ("rhopheocytosis")* (× *18.000; Inset:* × *40.000).* **Fe.** *iron.*
Courtesy of Dr. D. Zucker-Franklin, Department of Medicine, New York University.

d) *Iron absorption in developing normoblasts. The mechanisms by which iron is delivered to the mitochondria of the developing normoblasts for the incorporation into heme, are still controversial. Two principal patterns are illustrated in this schematic drawing, where the stipples represent ferritin. According to pattern* **A**, *iron is transferred as preformed ferritin from a histiocyte (the "nursing" cell) to the adjacent normoblast. Bessis et al. have illustrated all the stages of this process which correspond to an invagination of the cell membrane progressively enclosing ferritin molecules* ($A_1 \longrightarrow A_5$) *[51, 52]. According to pattern* **B** *iron is selectively taken up by absorption to the erythroid cell surface of transferrin molecules, probably via specific receptors [53, 54]. Endocytosis of iron laden transferrin molecules or of transferrin-receptor complexes* ($B_1 \longrightarrow B_2$) *leads to the internalization of iron for heme synthesis. Ferritin accumulates in the cytoplasm in the form of dispersed molecules or aggregates which may be either free or contained in membrane-bound vacuoles (see* **e**). *Ferritin aggregates constitute a yellow-brown pigment known as* hemosiderin *and are responsible for positive staining of the erythroblasts with the Prussian blue reaction (Perls' reaction) [55] (see* **f**).

e) *Detail of an erythroblast from a patient with anemia of chronic disease associated with "ineffective" erythropoiesis. Note the large membrane-bound inclusions containing ferritin* (**arrows**). **G.** *Golgi apparatus;* **N.** *Nucleus (*× *63.000).*
Courtesy of Dr. D. Zucker-Franklin, Department of Medicine, New York University.

f) *Erythroblasts containing iron granules stained with Prussian blue dye (sideroblasts). Granules stain deep blue and show different size. Usually no more that three or four granules are recognizable by light microscopy under normal conditions.*

Figure 5. In lower right hand corner is the honey comb structured quantasome. 32,000 X

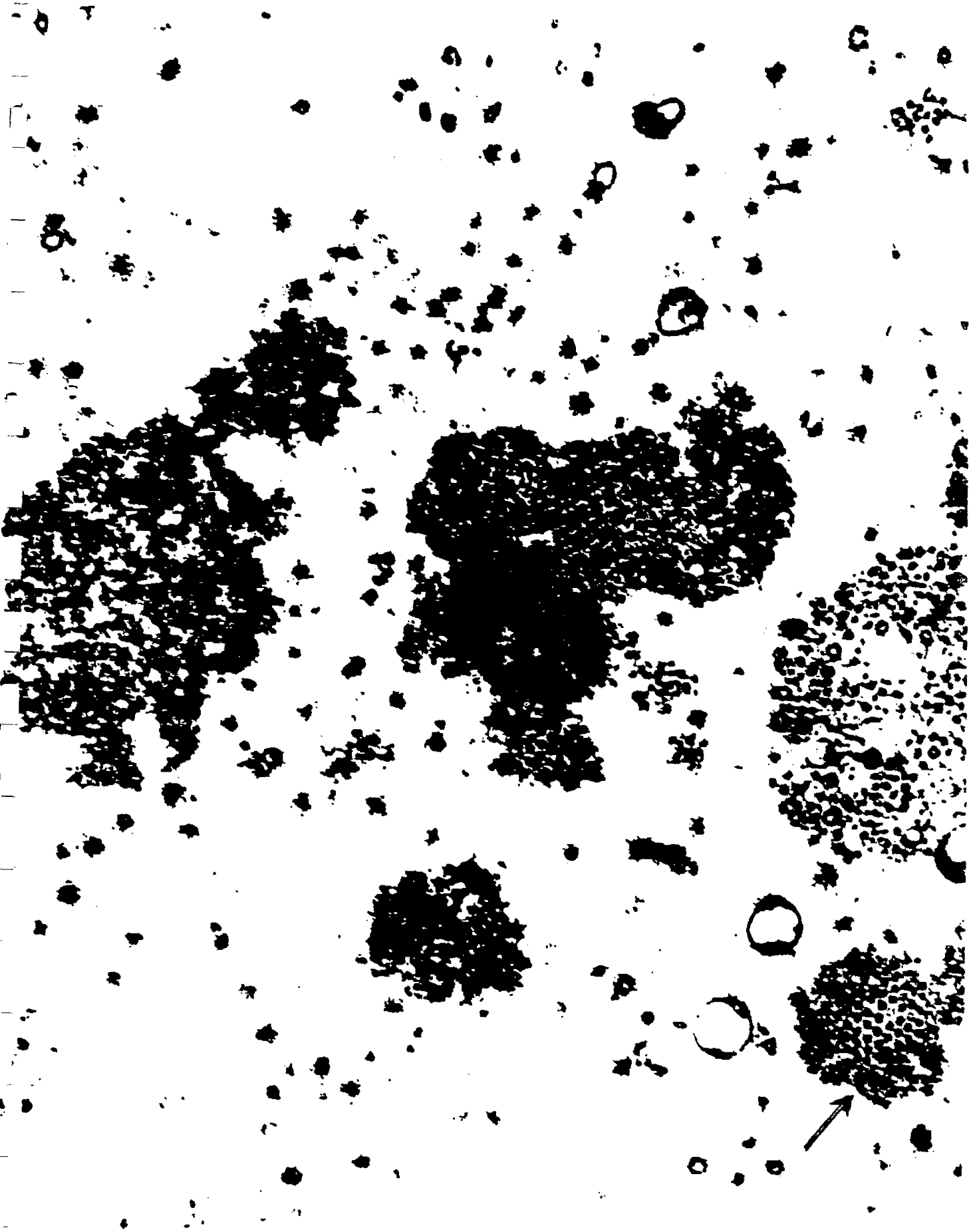

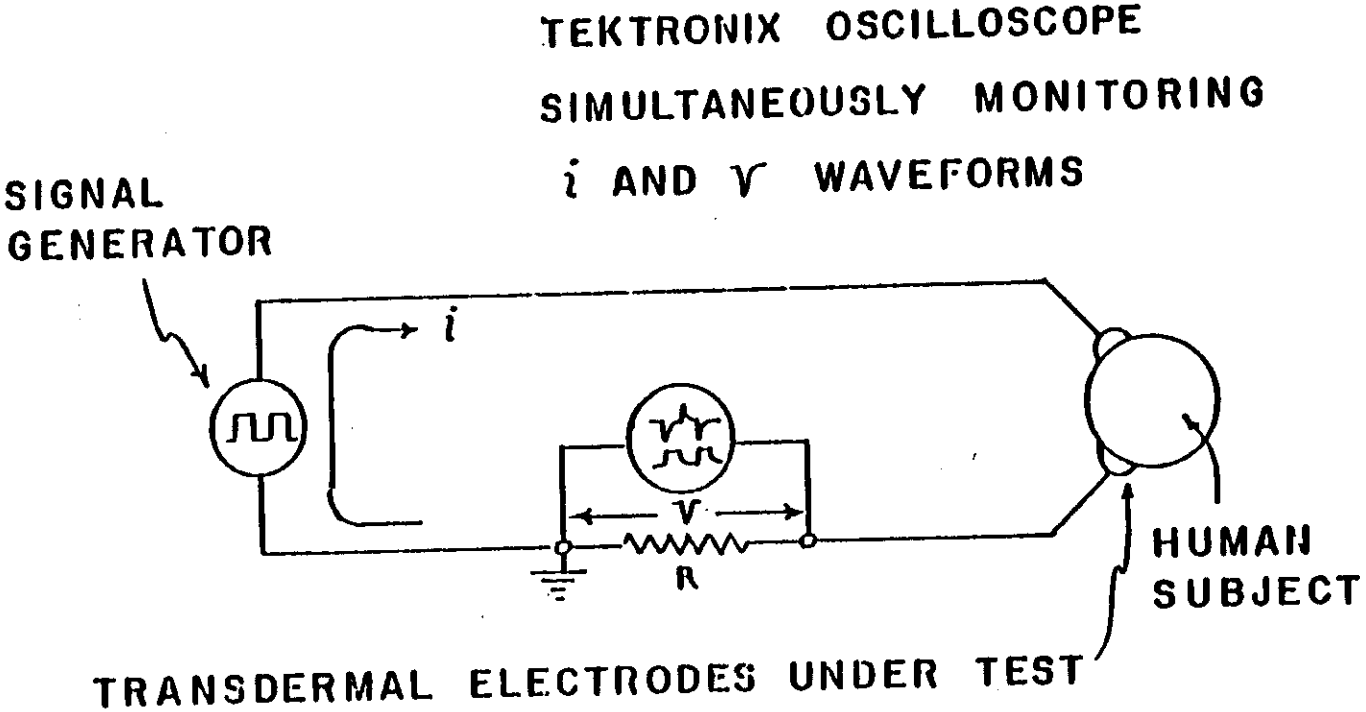

FIG. 28. TEST CIRCUIT TO MEASURE CURRENT AND VOLTAGE DECAY CURVES IN SQUARE WAVE SPECTROSCOPY OF ELECTRODE - HEAD CONFIGURATION.

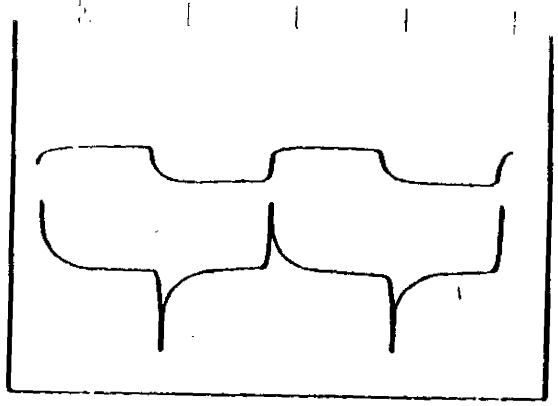

.30A. CASE IA ELECTRODES ACROSS HEAD.
15 OHM SERIES RESISTANCE. SEE FIG.28.
20 μsec PULSE WIDTH
UPPER TRACE: VOLTAGE DECAY CURVE
LOWER TRACE: CURRENT DECAY CURVE

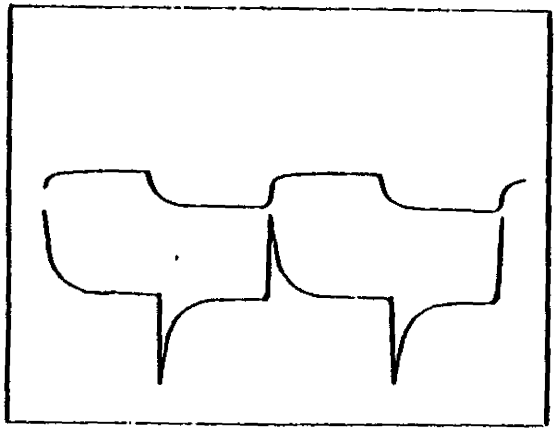

FIG.30B. CIRCUIT SYNTHESIZED (SEE FIG.31 CASE IA)
EQUIVALENT CIRCUIT OF HEAD.
UPPER TRACE: VOLTAGE DECAY CURVE
LOWER TRACE: CURRENT DECAY CURVE

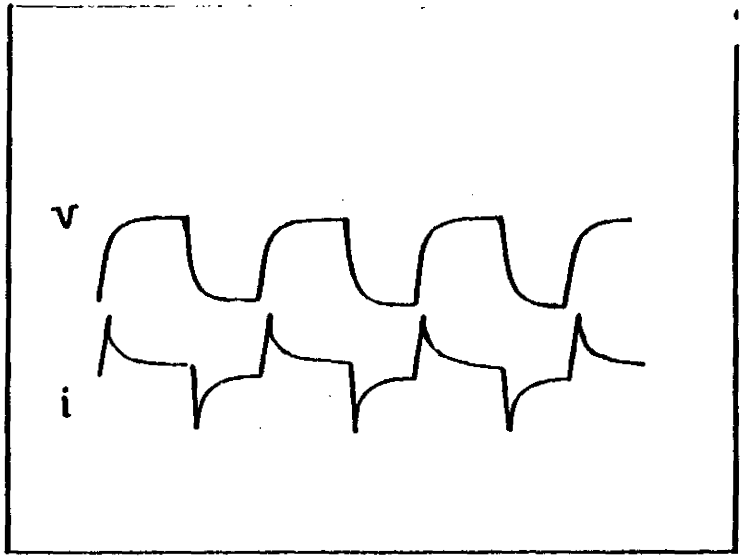

FIG. 29. CASE 1A ELECTRODES. 10 OHM SERIES RESISTANCE.
SEE FIG. 20.
SQUARE WAVE PULSE INPUT ACROSS CHEEK TISSUES.
20 μscc/cm TIME BASE
UPPER TRACE: VOLTAGE DECAY CURVE
LOWER TRACE. CURRENT DECAY CURVE

molecule is a double helix in which the two nucleotide strands are held together by hydrogen bonds. The hydrogen bonds hold together the base pairs guanine:cytosine (GC); and adenine:thymine (AT). What is of interest is that this simple four letter code GC and AT, replicated in unit aggregates of molecular weight of the order of 100,000,000, and contains complete instructions and operational control necessary to build a human body. Not only does this system contain an awesome stable memory capacity, and accuracy in carrying out instructions, but it must also be responsive to very small signals that tell it "GO" and "NO-GO" for growth and repair. (36,000,000,000 genom

In normal cell division the combination of the sperm and ovum trigger cell division. The start of DNA division is heralded by the appearance of a centrosome body. This latter body splits in two and the chromosomes containing DNA line up transverse to the lines connecting the two centrosomes. A classic spindle formation of microtubules occurs which is clearly visible under a microscope. At this point the hydrogen bonds holding the two strands of the DNA double helix cleave and the cell divides with a full complement of chromosomes going to each new cell.

Now we do not know what tells the DNA hydrogen bonds to divide, because the same effect can be artificially induced with D.C. electric pulses of the order of 30-40 volts (94).* The hydrogen bonds are of interest in that one of them is composed of the

* WE NOW KNOW (1987) THAT ELF FIELDS OF PRECISE FREQUENCIES TRIGGER H_2 DIVISION.

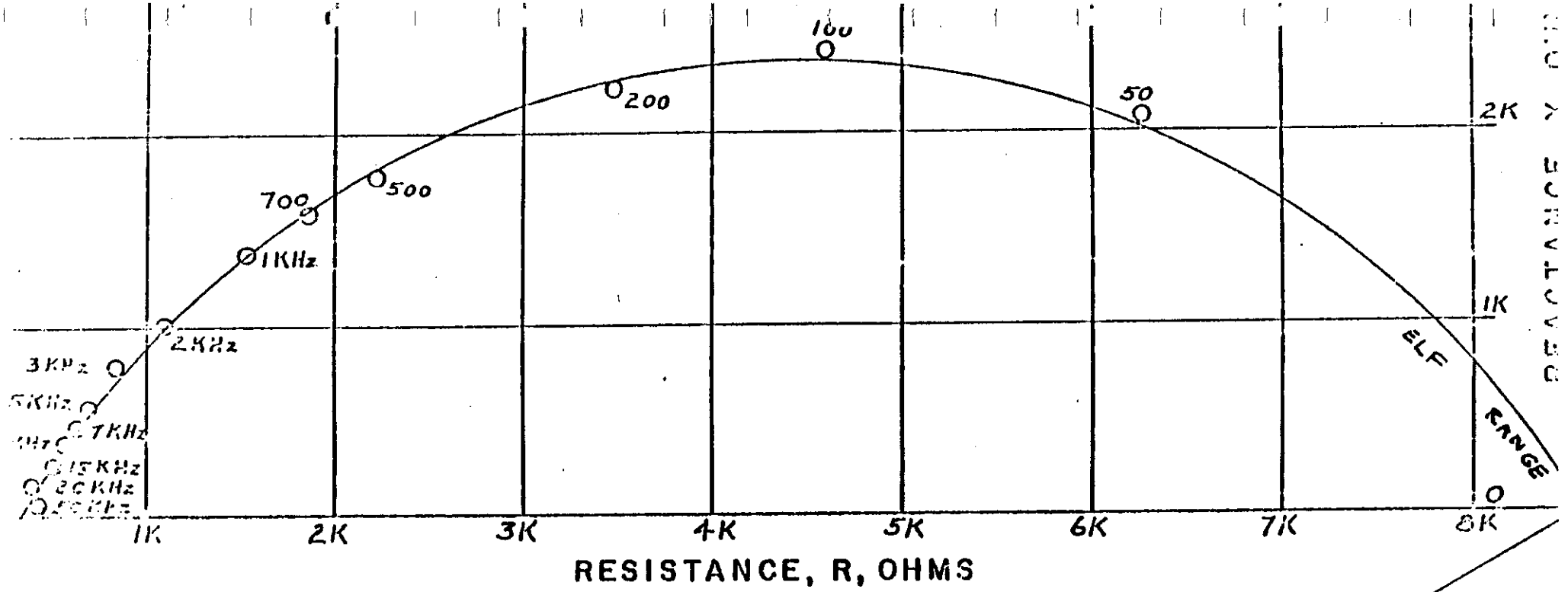

FIG. 35. COLE-COLE DIAGRAM OF IMPEDANCE LOCUS FOR CASE IA ELECTRODES ACROSS HUMAN HEAD. DRY ELECTRODES ON TRAGAL SKIN AT CONSTANT PRESSURE.

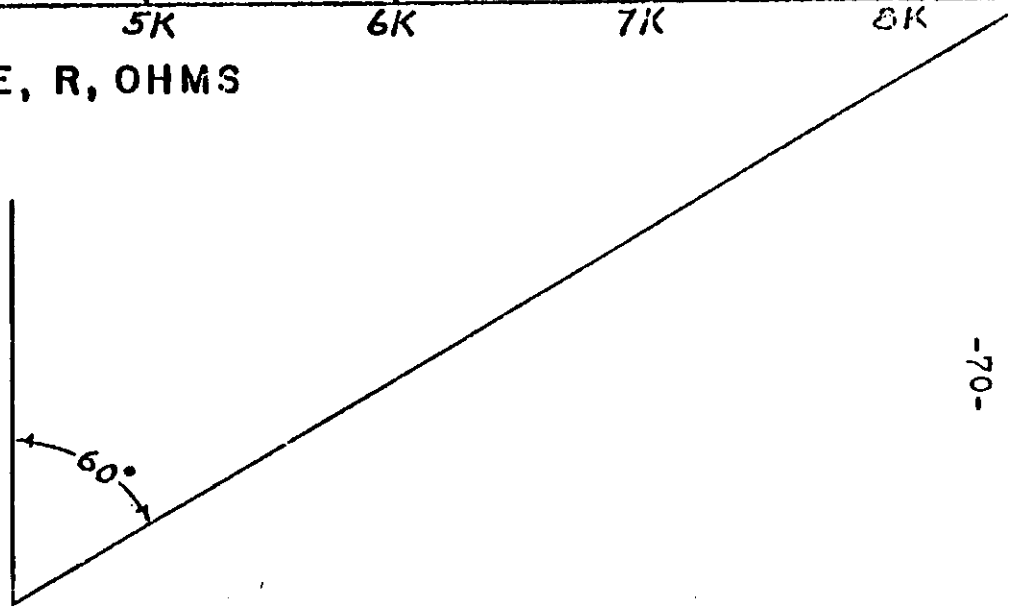

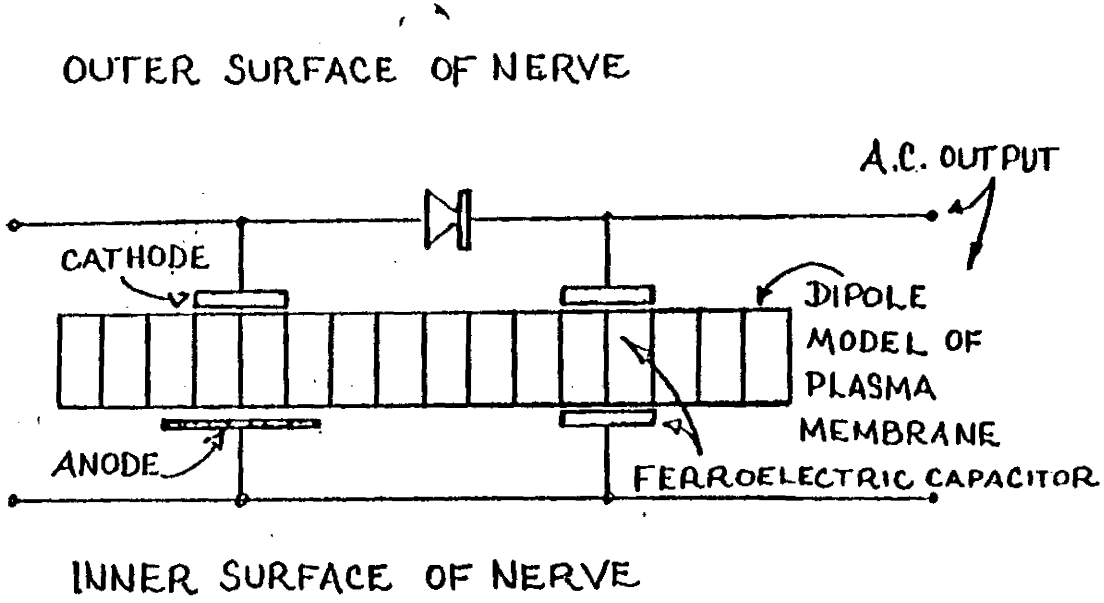

Figure 1. Ferroelectric Model Circuit Of One Domain Of The Nerve Plasma Membrane. The Load Is To The Right, The Input To The Left

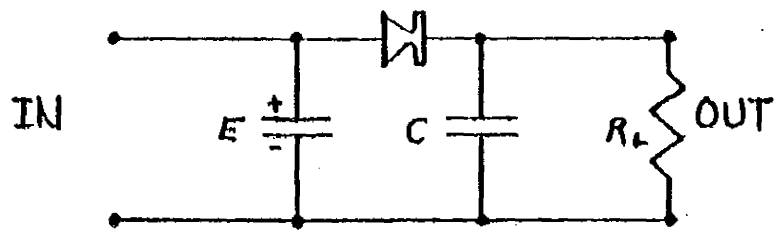

Figure 1A. Equivalent Circuit Of One Domain Of The Ferroelectric Model Plasma Membrane

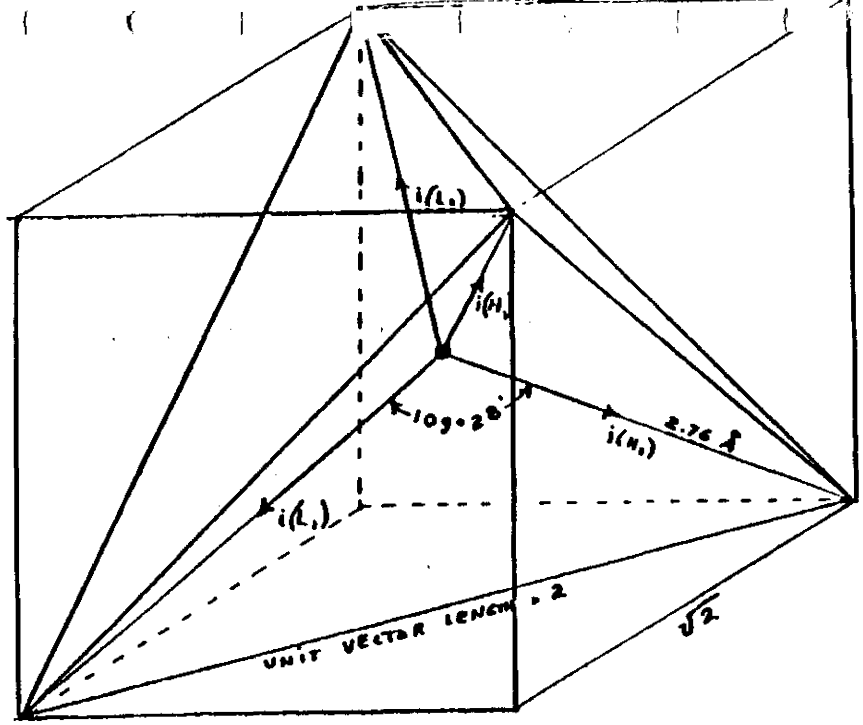

THE WATER MOLECULE IN TETRAHEDRAL FORM.

Hydrogen bonding occurs only along the four vectors pointing to the four vertices of a regular tetrahedron, and in the above drawing we show the four unit vectors along these directions originating from the oxygen atom at the center. $i(H_1)$ and $i(H_2)$ are the vectors of the hydrogen bonds formed by the molecule i as a donor molecule. $i(L_1)$ and $i(L_2)$ denote the unit vectors along the direction of the bonds formed by molecule i, as an acceptor molecule. These are assigned to the lone pair electrons. Molecules i are the neighboring oxygen atoms at each vertex of the tetrahedron.

FIG. 15

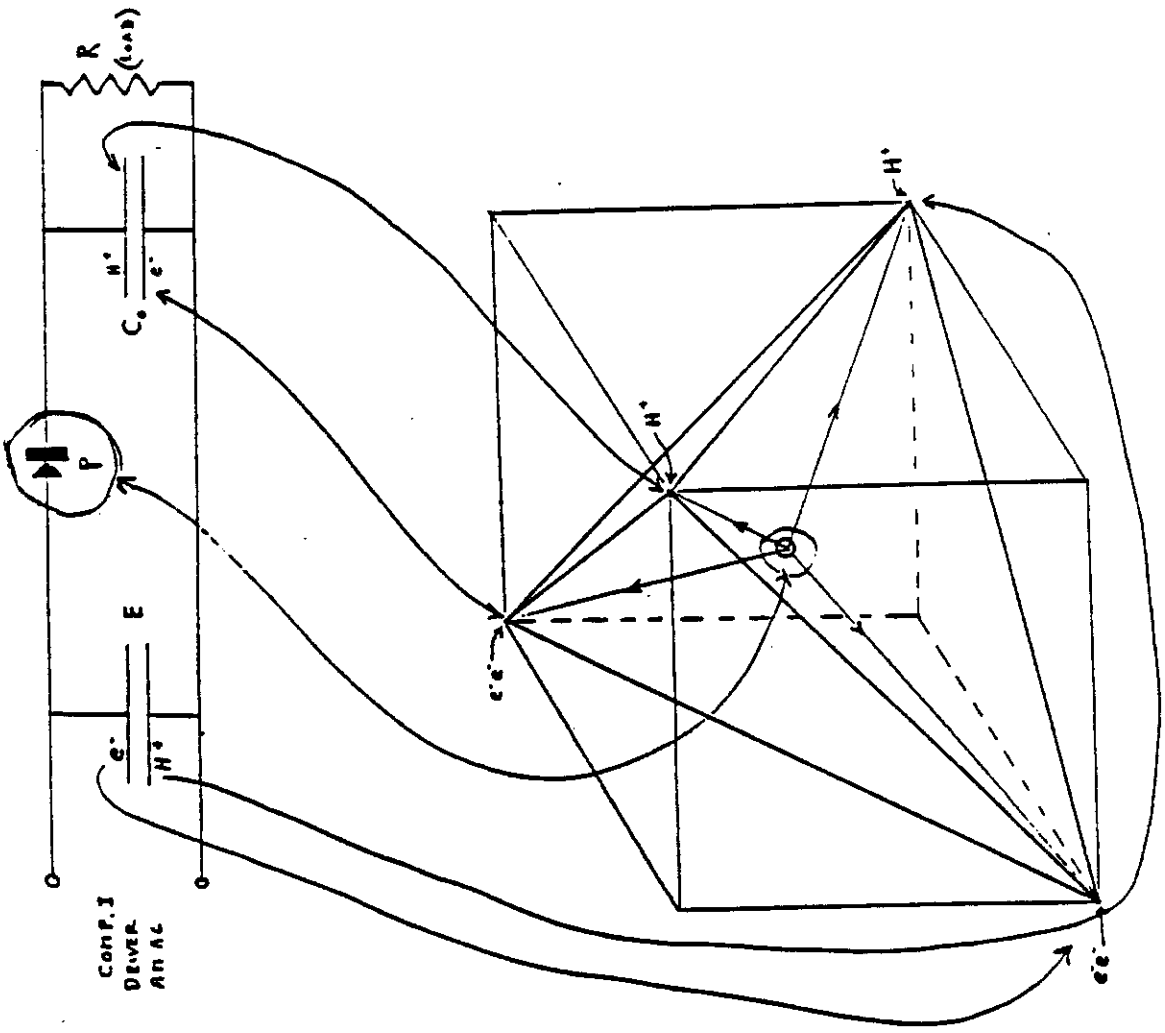

FIG. 22

REFERENCES

REFERENCES

1. Puharich and Lawrence
   (a) Hearing Aid. Great Britain Patent No. 982,934. September 21, 1959
   (b) Procede et Moyen Pour Amplifier ou Pour Retablir L'ouie. Republique Francaise No. 1.236.782. September 24, 1959. Brevet d'invention.
   (c) Schwerhorigengerat. Bundesrepublik Deutschland Patentamt 1120505. September 26, 1959
   (d) Procede et Moyen Pour Amplifier ou Pour Retablir L'ouie. Royaume de Belgique, Brevet d'invention No. 583.034 October 15, 1959
2. Puharich, H.K.
   Electrical Field Effects on Humans. Guest Speaker Annual Meeting of Institute of Radio Engineers, San Francisco Section, Berkeley, California. June 14, 1960
3. Puharich and Lawrence
   Procedimento ed Apparecchio per migliorare o ristabilire il senso dell'udito. Italy, Brevetto per invenzione industriale No. 615935, January 24, 1961.
4. Puharich, H.K.
   Experiments with Faraday Cage Apparatus. Darshan (India) Vol. 1, pp. 30-42, April, 1961.
5. Puharich and Lawrence
   Means for Aiding Hearing. U.S. Patent No. 2.995,633. August 8, 1961
6. Puharich, H.K.
   Computers, Chance, and Cholinergia (with Jeffery Smith and A. Kitselman). Darshana (India) Vol. 1, pp. 41-43, August, 1961.
7. Puharich and Lawrence
   (a) Dispositivo para la Transmision de Senales Auditivas a los Centros de Aduicion del Cerebro Humano. Republica Argentina, Patente de Invencion No. 127626, October 10, 1961.

(b) Method and Means for Aiding or Restoring Hearing. Canada Patent No. 634542. January 16, 1962.
(c) Method and Means for Aiding or Restoring Hearing. Japanese Letters Patent No. 307,053. August 27, 1962.
(d) Dispositifs d'aide a l'organe de l'ouie par stimulation electrique du systeme nerveux facial. Republique Francaise, Brevet d'invention No. 1.349.503, January 3, 1963.
(e) Schwerhorigengerat. Bundesrepublik Deutschland Patentamt No. 1,219,988. January 6, 1963.
(f) Dispositifs d'aide a l'organe de l'ouie par stimulation electrique du systeme nerveux facial. Royaume de Belgique, Brevet d'invention No. 626.742. January 15, 1963.
(g) Means for Aiding or Restoring Hearing. Commonwealth of Australia, Letters Patent No. 240,204. February 18, 1963.
(h) Dispositif d'audition a l'etat solide. Republique Francaise, Brevet d'invention No. 1.375.458. November 22, 1963.
(i) Ctofono o simile Apparecchio Elettronico a stato solido con Trasmissione Attraverso Nervi Facciali. November 23, 1963.
(j) Hearing Aid. Great Britain Patent No. 1,067,748. November 25, 1963.
(k) Solid State Hearing System. Commonwealth of Australia Letters Patent No. 281,219. November 26, 1963.
(l) Horgerat. Bundesrepublik Deutschland Patentamt 1202834. December 13, 1963.
(m) Hearing Aid. Great Britain Patent No. 1,075,430. December 30, 1963.
(n) Systeme d'ecoute a stimulation electrique avec signal de reaction. Royaume de Belgique, Brevet d'invention No. 642.183. January 7, 1964.

8. Puharich and Lawrence
Modulated Alternating Current Energy Used to Stimulate Audition in Totally Deaf Humans. Paper presented at the Annual Meeting of the Aerospace Medical Association Bal Harbour, Florida, May 13, 1964. Published as an abstract in: Journal of Aerospace Medicine, 35: May, 1964.

9. Puharich and Lawrence
(a) Dispositif d'audition a l'etat solide. Royaume de Belgique, Brevet d'invention No. 640.030. May 19, 1964.
(b) Systeme d'ecoute a stimulation electrique avec signal de reaction. Republique Francaise, Brevet d'invention No. 1.380.044. October 19, 1964.

10. Puharich, H.K.
How Many Channels Have Been Allocated to the Brain? Luncheon Address to the National Electronics Conference. Chicago, Illinois, October 20, 1964. Published in: Missiles and Rockets, October 26, 1964.

11. Puharich and Lawrence
Solid State Hearing System. U.S. Patent No. 3,156,787. November 10, 1964.

12. Puharich and Lawrence
Electrostimulation Techniques of Hearing Technical Documentary Report, No. RADC-TRD-64-18, December, 1964; Project No. 5534, Task No. 553401. Prepared under contract No. AF30 (602) - 3051, Intelectron Corporation, 432 West 45th Street, New York, New York, 10036. Published by: Defense Documentation Center, Alexandria, Virginia.

13. Puharich and Lawrence
(a) Dispositif pour assurer l'audition avec ou sans intervention de l'oreille. Confederation Suisse, Expose d'invention No. 384,041. January 29, 1965.

(b) Un dispositivo para impartir senales electricas moduladas a nervios viales del Sistema Facial de un sujeto. Republica Argentina. Patente de invencion No. 142889. February 9, 1965.

(c) Means for Aiding Hearing by Electrical Stimulation of the Facial Nerve System. U.S. Patent No. 3,170,993. February 23, 1965.

(d) Horeanordning. Norsk Patent Nr. 105 760. March 8, 1965.

(e) Solid State Hearing System: Canada Patent No. 708246. April 20, 1965.

(f) Werkwijze voor het hoorbaar maken van audiofrequente signalen bij doven. Octrooiraad Nederland, Octrooi Nr. 111 843. September 17, 1965.

(g) Electrically Stimulated Hearing with Signal Feedback. India. Patent No. 92045. April 16, 1966.

(h) Mejoras en Dispositivos Electronicos de Audicion. Republica Argentina, Patente de invencion No. 148047. May 10, 1966.

(i) Electrically Stimulated Hearing with Signal Feedback. U.S. Patent No. 3,267,931. August 23, 1966.

(j) Electrically Stimulated Hearing with Signal Feedback. Pakistan, Patent No. 115218. August 30, 1966.

(k) Means for Aiding Hearing by Electrical Stimulation of the Facial Nerve System. Commonwealth of Australia Letters Patent No. 269,970. September 13, 1966.

(l) Otofona del tipo a Stimolazione Elettrica del Sistema Nervoso Facciale con Circuito di Reazione. Italy, Brevetto per Invenzione Industriale No. 713017. September 20, 1966.

(m) Apparecchio per Aiutare L'udito mediante Stimolazion Electtrica del Sistema Nervoso Facciale. Italy, Brevetto per Invenzione Industriale No. 715786. October 1, 1966.

(n) Means for Aiding Hearing by Electrical Stimulation of the Facial Nerve System. Canada Patent No. 750503. January 10, 1967.

(o) Electrically Stimulated Hearing with Signal Feedback. Canada Patent No. 751001. January 17, 1967.

(p) Un aparato para estimular Electricamente el Sentido de Audicion de un Ser Humano con realimentacion de Senales a traves del Sistema Nervioso Facial. Republica Argentina, Patente de Invencion No. 153148. February 21, 1967.

(q) Processo e dispositivo para auxiliar ou restaurar a Audicao. Brasil, Patente de invencao No. 77775: February 28, 1967.

(r) Anordning for overforing av akustika signaler till manniskohnjarnans horselcentra. Sverige Patent Nr. 217 530. December 12, 1967.

(s) Electrically Stimulated Hearing with Signal Feedback. Commonwealth of Australia Letters Patent No. 282,485. April 22, 1968.

(t) Electroniskt Horsystem. Sverige Patent Nr. 301 337 September 12, 1968.

(u) Horapparat. Sverige Patent Nr. 305 669. February 13, 1969.

(v) Procedimento Ed Apparechio Per La Stimolazione, Elettroacustica de Sistema Auditivo, Brevetto per Invenzione Industriale, Italy, No. 854214, February 3, 1969.

(w) Transdermal Electrostimulation of Facial Nerve System with R-F Energy. U.S. Patent No. 3,497,637. February 24, 1970.

COHN set in the form,

$$C = O:H:N$$

(The dots (:H:) represent electron lone pairs)

and the other is composed of the NHN set in the form

$$N:H:N$$

In both bond sets the proton of the hydrogen atom is in a resonant state with the electron "lone pairs" on each side of it which gives the bond great stability. What kind of command is given which breaks this proton resonance stability in such an orderly way? The centrosome bodies behave like repulsive magnetic poles and the protons of the hydrogen bond system tend to line up in the inter-face repulsion region of low energy. The protons of the double helix ladder are paired in such a way that their center of momentum falls on the low energy inter-face where repulsive (magnetic) forces meet. This sets up a possible ELF mechanism for super-conductivity at body temperature (42) and protons can shift like a zipper opening up the ladder of H bonds.

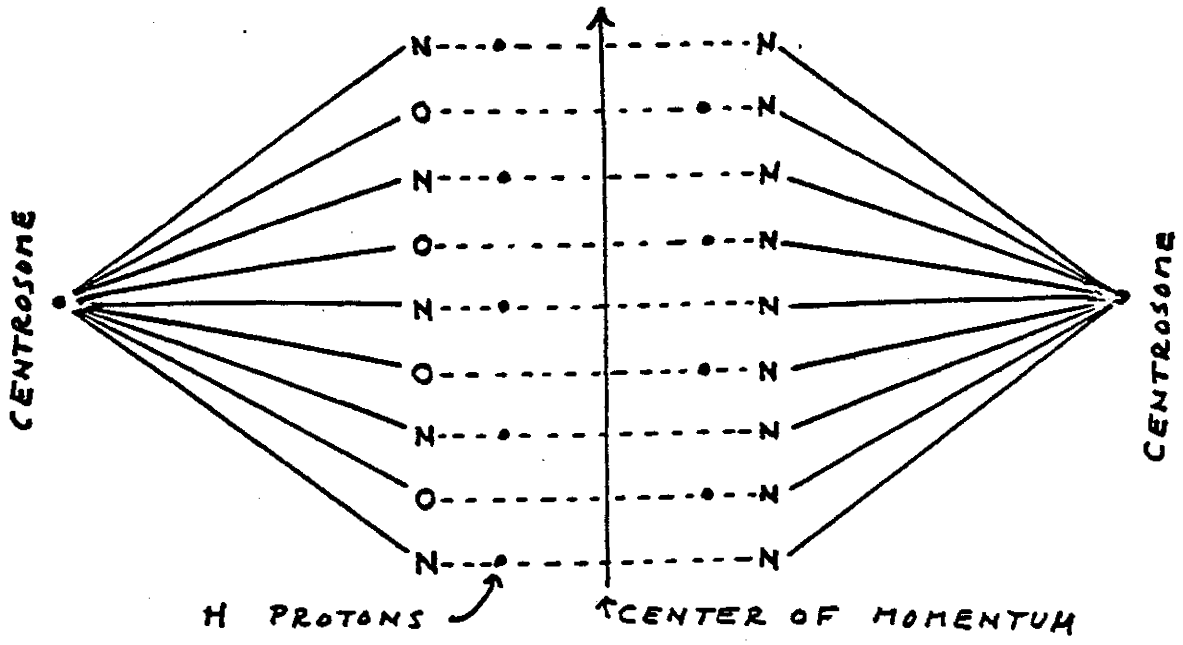

(x) Transducer for Stimulation of Facial Nerve System with R-F Energy. U.S. Patent No. 3,497,637. February 24, 1970.

(y) Method and Apparatus for Improving Neural Performance in Human Subjects by Electrotherapy. U.S. Patent No. 3,563,246. February 16, 1971.

14. Puharich and Lawrence
Hearing Rehabilitation by Means of Transdermal Electrotherapy in Human Hearing Loss of Sensorineural Origin. Acta Oto-Laryngologica, Vol. 67, Fasc. 1, pp. 69 - 83. January, 1969.

15. Puharich and Lawrence
Hearing Rehabilitation by Means of Transdermal Electrotherapy in Human Hearing Loss of Sensorineural Origin (II). Excerpta Medica International Congress Series No. 189. Ninth International Congress of Oto-Rino-Laryngology, Mexico, D.F., August 10-14, 1969.

16. Puharich, H.K.
Transdermal Electrostimulation of Hearing. (with J.L. Lawrence and R.S. Dugot). Presented at Thirteenth Annual Scientific Meeting, October 11, 1969, Committee for Research in Otolaryngology, Thorne Hall, Northwestern University School of Medicine, Chicago, Illinois. American Academy of Otolaryngology.

17. Puharich, H.K.
Electrodynamic Approach to Thrombus Prevention in a Ventricular Assist Device. (With George E. Reed, Luis E. Cortes, William R. Brewster and Joseph L. Lawrence). Paper presented at the 41st Annual Scientific Sessions of the American Heart Association, November 23, 1968, Miami Beach, Florida. Abstract published in Circulation, Vol. XXXVIII, No. 4, Supplement No. VI, page 162.

18. Puharich, H.K.
ELECTOACOUSTIC DECOMPOSITION OF WATER BY THE PHONON EFFECT. TOWARDS A VIABLE CLEAN FUEL SYSTEM. PACE Newsletter, Vol. 3, Nos. 2,3, December, 1981, p. 6. 100 Bronson Street, Ottawa, Ontario, Canada.

19. Puharich, H.K.
Methodology for the Evaluation of the Efficiency of Water Decomposition by Means of Alternating Current Electrolysis. Proceedings of the 1st International Conference on Non-Conventional Energy. Ed, Professor George Hathway, University of Toronto, Department of Physics, Toronto, Ontario, 1982.

20. Puharich, H.K.
Contibution to Molecular Evolution Studies and Relation to the Cause of Cancer. U.S. Psychotronic Association Annual Meeting, July 22-25, 1982, Colorado School of Mines - in press.

21. The FeO - Fe_2O_3 (Magnetite) Protoporphyrin Complex in Human Blood as a Possible ELF-EM Receptor-Detector in vitro and in vivo studies. A preliminary report. Proceedings of the June 1982 Conference of the Learned Societies of Canada - in press. Puharich.

22. Kervran, C. Louis
Transmutations Biologique et Physique Moderne. Maloine S.A., Editeur, 27, vue de l'Ecole de Medecine, 75006, Paris, 1982.

23. THE ICELAND PAPERS. Select papers on experimental and theoretical research on The Physics of Consciousness. Edited by Andrija Puharich M.D., LLD. with Foreward by Brian D. Josephson, Nobel Laureate, Physics. Published by Essentia Research Associates, 350 E. 52nd. Street, New York, N.Y. 10022. See Chap. V, p. 161 ff.; The expanding paradigm of the Einstein Theory of Olivier Costa de Beauregard.

24. C. Maxwell Cade, and Coxhead, N.
The Awakened Mind, Delta Books, Del Publishing Co., New York, N.Y., 1979.

25. Kamiya, Joe
Conscious Control of Brain Waves
Psychology Today, I:57, April, 1968.

26. The Imminence of ELF Magnetic Global Warfare.
Confidential. Report by H. Puharich, submitted March 13, 1977 to:
Hon. Pierre Elliot Trudeau, Prime Minister, Canada
Hon. James Carter, President, U.S.A.
Hon. Margaret Thatcher, Leader of the Opposition, Great Britain
(CLASSIFIED)
Report warns that the Soviet ELF signals broadcast since July 4, 1976 are psychoactive (in a predatory sense) and can lead to other biological effects.

27. NOTE: 1982, U.S. Navy confirms that Soviet ELF signals are indeed psychoactive and can cause mental depression at 6.66 Hz, and at 11 Hz can lead to manic and riotous behavior in humans.
(CLASSIFIED)

28. Abraham, R.J. and Loftus, P.
Proton and Carbon - 13 NMR Spectroscopy
Table 3.1, p. 41; Table 3.5, p. 46.
Heyden & Son, Ltd., London, 1981.

29. Parrish, Rob G., Kurland, R.J., and Janese, W.W. and Bakay, L.
Proton Relaxation Rates of Water in Brain and Brain Tumors. Science, Vol. 183, February 1, 1974.

30. Stumm, Werner and Morgan, JJ.
Aquatic chemistry second edition. Ferrichromes p. 378 - 382. John Wiley & Sons, New York, 1981

31. Domingue, Gerald J.
Cell Wall-Deficient Bacteria
Addison-Wesley Publishing Co.
Reading, Massachusetts, 1982

32. Lehninger, Albert L.
Principles of Biochemistry, p. 519
Worth Publishers, Inc., New York, N.Y. 10016, 1976

33. Ibid., p. 479

34. Akasofu, Syun-ichi, and Chapman, Sydney
Solar Terrestrial Physics, p. 439
Oxford, Clarendon Press, 1972

35. Becker, Robert O., Editor
Mechanisms of Growth Control
Charles C. Thomas, Publisher
Springfield, Illinois, 1981

36. Zucker-Franklin, D., et al
Atlas of Blood Cells, Function and Pathology
E.E. Edi. Ermes, Milano, Italy
Lea & Febiger, Philadelphia, 1981

37. Dominque, Gerald J. Op. Cit. (31)

38. Goubin, Gerald; Goldman, Debra S.; Luce, Judith; Neiman, Paul E.; and Cooper, Geoffrey M.
Molecular cloning and nucleotide sequence of a transforming gene detected by transfection of chicken B-cell lymphoma DNA
Nature, Vol. 302, 10 March 1938, pp. 114 and ff.

39. Franks, Felix, Editor
Water, a comprehensive trestise, six volumes.
Vol. 1, p. 139, Chapter 4. Properties of Ice
Plenum Press, New York, 1972

40. (a) Whalley, W.B.
Radio Frequency Eradication of Tumours
Electronics and Power, May 1977

(b) Le Veen, H.H., Wapnick S., Piccone, V., Falk, G. and Ahmed, N.
Tumour Eradication by Radio Frequency Therapy
J. Am. Med. Assoc., V. 235, 2198-2200, 1976.

41. Winfree, Arthur T.
Sudden Cardiac Death: A problem in Topology.
Scientific American, Vol. 248, No. 5, May, 1983

42. Abragam, A, and Goldman, M.
Nuclear Magnetism: Order and Disorder
Oxford, Clarendon Press, 1982
See Appendix 1.

43. Op. Cit (23) See pp. 161 ff for time reversal theory.

44. Gross, Paul R., and Spindel, W.
Heavy water inhibition of cell division. An approach to mechanism.
Annals of the New York Academy of Sciences, Vol. 90, Art. 2, pp. 345-613
Second Conference on the mechanisms of cell divison
Editor, Franklin N. Furness, October 7, 1960

45. Winter, R.
Cancer-causing Agents
Crown Publishers, Inc., New York, 1979

APPENDIX

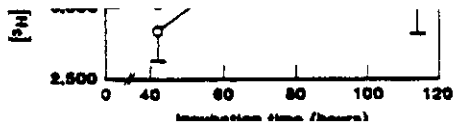

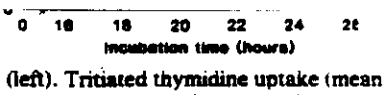

Fig. 1 (left). Tritiated thymidine uptake (mean counts per minute ± standard error) in human

APPENDIX

After the protons shift up the ladder one step and the magnetic repulsive force separates the two strands of the double helix the mechanism for ELF super-conductivity collapses. Now in order to understand this phenomen ON of cell division more fully let us consider what happens when we block cell division.

This can be reversibly accomplished in any system of dividing eggs by replacing about 20% to 30% of the water of the medium with deuterium oxide, D_2O (26). While cell division is arrested as though a motion picture of the process had stopped it, the metabolic activities of the cell go on. If the D_2O is removed from the medium, cell division will resume normally. This is a phenomena of great interest because the D_2O has counter-manded the "GO" command to divide with a reversible "NO-GO" command. Where does it act? Normal H_2O and D_2O differ only in that the hydrogen atom contains a neutron in addition to the proton. Thus the mass of the hydrogen atom is doubled hence the term "heavy water". The essential difference between H_2O and D_2O is not chemical, but nuclear. It turns out that the neutron (n) has a spin opposite to that of the proton (p) where (13)

$$n = -1.91\ \mu$$
$$p = +2.79\ \mu$$
$$\text{and, } {}_1H^2 = +0.85\ \mu$$

signal. Thus the head neurons see the following signal:
20 KHz + 100 Hz = 20, 100 Hz: 20 KHz - 100 Hz = 19,900 Hz.
The 20,100 Hz and the 19,900 Hz beat against the center frequency of 20,000 Hz and the result is that the deaf person "hears" 100 Hz. Certain proton nuclear magnetic resonant (NMR) signals in the nerve system may be of this nature where the actual perceived signal may be a side-band signal. For example, Nelson has shown that the HCH group of ethyl alchhol has a NMR at 200 MHz, but that each proton has a separate side band line 7 Hz above and below the center frequency. These side bands are due to proton-proton spin couplings (53). Such proton-proton spin couplings may have great importance in memory induction.

5. MEMORY IN BRAIN

We have shown in the skin-stroking effect that both the carrier potential across the C=O:H:N set, and stretching the H bond length produces semiconduction, and also gates AMAC signals. Let us examine this phenomenon as it applies to awareness, anesthesia, and memory.

Becker (7) has clearly shown the relationship of body surface barrier potentials to alertness and anesthesia. During alert states there is a barrier potential (30 mV) between the neuraxis and the skin periphery, the neuraxis being positive in sign, and the skin being negative in sign. Anesthetic

agents in the first stage of anesthesia lower this potential to zero and may even cause a reversal in sign. Hypnosis (if effective for surgery, as an example) shows the same pattern of lowering of barrier potential, as shown for chemical anesthesia.

Randt and Mazzia (74) have shown that the earliest sign of stage 1 anesthesia (Plane 1) is characterized by a spontaneous dissociation of eye ball movements, so-called ocular divergence. In this condition humans can perform simple calculations, respond to questions and other stimuli, but do not retain any memory of such mental performance. Yet, at the same time it is possible to perform major surgery during this state. Apparently, ocular divergence is a precision measure of the titer of anesthetic molecules required to uncouple perceptive-motor acts from memory imprinting. Let us analyse this important effect.

According to Pauling's(58) theory of Anesthesia, anesthetic chemical agents act by forming clathrate hydrates. For example, in the case of the inert anesthetic gas xenon, the hydrate which forms around the xenon atom has been shown to be a dodecahedron of HOH molecules. Pauling states that such "water cages" produce anesthesia by a kind of plasma membrane water control rod function which damps the electrical oscillation of the neurons. All tests of this theory since Pauling first

announced it in 1961 tend to confirm his concept of perineural water cage formation in anesthesia.

In addition to the Pauling concept of perineural water cages, I wish to bring up Hydén's concept (31) of the perineural role of glia in the memory process:

"In an acute learning situation, the modulated frequencies (time patterns) set up by the neuron are also transferred to the glia. The glia are characterized by potentials of a 500 to 1000 fold longer duration than those recorded from nerve cells. When the neural frequency is changed a lock-in effect brings the slow frequency of the glia in synchrony (with nerve pulse frequency). The difference being a multiple. This coupling of the frequencies of the neuron and the glia forms an information system. The glial ionic equilibrium is disturbed and substrates in the form of nucleotides are transferred from the glia to the neuron to release the repressed chromosome (DNA) region, and induce the necessary enzyme synthesis for the RNA production.

" This lock-in mechanism would, therefore, constitute the information system whereby the specific RNA was synthesized, triggered, or mediated by the glia as a regulator. As was stressed in the discussion earlier, the glia have many features of a feedback system.

"The glia are composed of multiple, thin membranes. Such a composition is well suited for rapid processes, for example proton transfer."

"Both the glia and the neuron constitute a unit. As I see it, that is the functional unit of the nervous system."

"Modulated frequencies set up in neurons of specific areas would specify RNA and proteins. These alterations would be stable for the best part of an individuals life time. After the first chemical specification, the proteins response on the same electrical pattern that once specified the RNA would be to dissociate rapidly. A molecular fragment would be provided which will react in an activation of the transmitter substance. In view of the fast reaction, the modulated frequency could affect fluctuating charges existing between basic groups of the protein and their attached protons." (31)

Basic to our theory of memory in a brain is that the permanent spin of the proton is considered to be the seat of information. Inputs or outputs from this seat of information occur by modulating the precession frequency (75). The macroscopic structure of the memory system is believed to be ferroelectric, as described. Ferroelectric properties have been found in RNA by Stanford and Lorey (93). We propose the

is a simple question of sperm and ovum meeting nor of electro-shock stimulation of an ovum (94). The life pattern of the Pacific Salmon illustrates the larger framework of the problem.

The Salmon hatches in an inland fresh water lake or pond in the spring of the year. It finds its way to the open sea by the autumn, and then moves as far as 4000 miles in the open sea from its place of birth. Five years later it begins the return voyage to its place of birth and arrives in time for optimal conditions for egg hatching. It finds a mate en route, and the two salmon ritually lay the eggs and fertilize them and then die within 4 to 7 days. This annual event which has gone on since time immemorial has these problems for us:

What is the nature of the imprinting on the egg (at time of fertilization?) that brings the Salmon back to this spot five years later? This imprinting requires a precise fix on a point on an earth that is spinning in orbital motion. The instructions require a timer for maturation, mating, and return in the right timing for optimum weather for egg hatching. The instructions require a command to go to the sea, navigate out and return in synchrony with physiological changes required for fresh to salt water adaptation. The final timing is of course the prescribed death following egg production and fertilization.

following scheme for the memory function in the central nervous system.

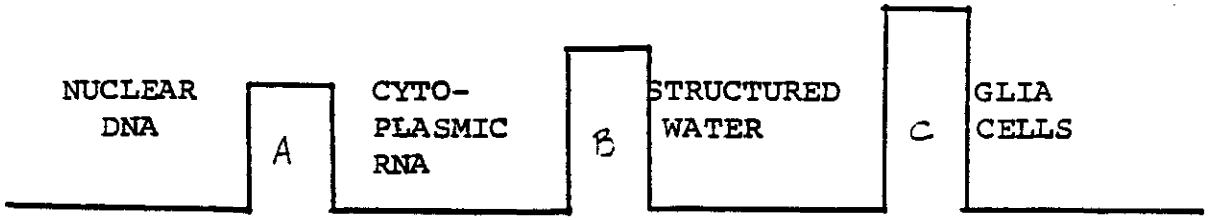

A) is the cell nucleus membrane barrier and is a conduction band semiconductor.

B) is the cytoplasmic plasma membrane barrier and is a tunnelling semiconductor.

C) is the structured water-glia interface in the peri-neural region - with proton ELF semiconduction (87).

When the nerve impulse fires across B, the sodium ion goes in to the cell, and the magnesium ion is activated to damp the action of the sodium. The Mg^{++} and the electronic pulse tells the nuclear DNA proton to produce RNA (77). As the electric pulse first started, the K^{+} ion went out of the cell across B, and perturbed the water (82) proton lattice so that a proton ELF FIELD hops into the glia to activate RNA. The DNA proton and the glia RNA proton, if activated by the same energy in coincidence, come into proton-proton spin coupling at a definite precession frequency controlled by the quantum rules of current density:

magnetic field described earlier. This spin coupling is transmitted through the water structure in the peri-neural area where a third proton freed by the hydrosynthesis process is also imprinted with the precession frequency of the other two protons. By this scheme the brain becomes an enormous set of interference patterns of magnetic waves generated by the ELF proton precession frequencies. (37) It is these interference patterns which I believe humans subjectively experience as imagings, memories, and all the other mind dynamics. The requirement of the brain for oxygen and glucose for maintenance of both consciousness, memory and structure will now be considered.

Let us quickly place this question in perspective. In the biological world mammals are not capable of cracking water, i.e. hydrolysis, to obtain free oxygen and hydrogen. Only algae, bacteria and plants are capable of hydrolysis - furnishing man with oxygen, the flame of his consciousness, and with hydrogen (in glucose) as the fuel of that flame. In all of man's metabolic processes the end result is the combination of 4 H with 2 O to form 2HOH and of course CO_2 (99). Thus every metabolic act of the brain, every nerve cell electrical impulse is accompanied by the formation of water, hydrosynthesis (81). The forms that such water take in the nerve cell, and around

each nerve cell, etc. is a matter of vigorous research today (73). The announcement of polywater by Deryagin has stirred this research to the highest level in history (22). What is emerging is a concept first formulated by McCulloch (49) which states that mind processes are mediated by crystalline water structures, and that the nerve cell is a supporting skeletal structure for such water forms (96).

Since consciousness is maintained only by a continuous supply of oxygen, and the integrity of brain structure (largely as water crystals) is also dependent on a continuous supply of oxygen we must consider continuous hydrosynthesis as a fundamental aspect of consciousness and mind operations. The modulation of mental states by anesthetic agents, hallucinogenic drugs, trance, hypnosis, etc, in order to influence Direct Brain Action (DBA)and DBP performance can best be understood in terms of crystalline water states in the brain.

6. DIRECT BRAIN PERCEPTION

By direct brain perception, DBP, I mean the process of obtaining new information by a person without using the channels of sense, the memory bank or deductive logic. The perception originates from a person at a distance (telepathy), or is a vision of a scene beyond the range of sight (clairvoyance), or is the audition of a voice beyond the reach of the ears (clairaudience

There are empirical psychological states, used over the centuries, to set the stage for the experience of DBP, Amongst these are self-induced trance - a dissociative state; release of cortical inhibitory states by the use of small amounts of alcohol, or other drugs; a state between waking consciousness and Stage 1, Plane 2 anesthesia; the REM state of sleep; cholinergia induced by drugs of the muscarinic group, e.g., AMANITA MUSCARIA. (64) What is it that these various states and techniques have in common?

One of the keys as to how this process works can be illustrated with telepathy experiments where high scoring is controlled with negative ion inhalation, and low scoring is controlled with positive ion inhalation (63). This effect can be rationalized by the principle of electronegativity which states that atoms have varying degress of power to attract and hold electrons. If we saturate the respiratory air with negative ions (O_2^- and free electrons) certain atoms in the CNS*will become saturated with the maximum number of electrons they can hold. For example, the muco-polysaccharide coatings of cells will carry a high negative surface charge (41). This will obviously create a large barrier potential. In

* CNS= Central Nervous System

general, we can predict that each atom will have maximum quantum orbital stability when its power of electonegativity is saturated, and this is the ground state of that atom. On a large scale this will create a condition wherein the core of each cell will be positively charged, and the cell periphery will be negatively charged.

If we induce such a state in a human subject by means of negative ion inhalation we can further stabilize these ground quantum energy level states by shielding the person from photonic and electronic perturbations within a Faraday Cage (64). Under these conditions, namely,

a) Self-induced Trance on the part of a clairvoyant,

b) Negative ion inhalation,

c) Faraday Cage shielding,

I have been able to show consistent, repeatable, statistically significant scoring in DBP tests designed as telepathy tests (68).

It is my opinion that the quantum orbital electron stability so induced further acts by building and maintaining the proper types of water protonic structures favorable to DBP.

The techniques cited thus far all act to quench the electronic noise of the neuronal system. The self-imposed dissociative techniques act to shift attention to the para neural information system - peri neural water: glia cell system.

When the slow oscillations of this system dominate the electrical activity of the brain, the so-called alpha waves, in the frequency range from 8 to 14 Hz, the protons of the water structure are receptive to similar signals (specifically 8.00 Hz) at a distance. (69) The best example of this phenomenon is the synchrony of alpha waves in identical twins by Direct Brain Action and Direct Brain Perception - or more scientifically proton ELF resonance at-a-distance between two brains. The unique feature here is that protons are not to be thought of as points of energy in space, but rather as energy systems whose ELF magnetic waves mushroom out over regions of space. We shall take up this concept in a later section.

7. DIRECT BRAIN ACTION

By Direct Brain Action, DBA, I mean the power of a person to induce a physical action-at-a-distance without the use of any known transducers, such as the muscular system. DBA is also known as psychokinesis in connection with dice tests, levitation in connection with lifting objects, poltergeists in connection with erratic movement of objects, table rapping, and metal-bending.

One of the common manifestations of DBA is in the phenomena of healing. I have already mentioned Grad's work on the induction of healing in animals, and growth induction in plants;

and the transfer of healing energy from a person to water which potentiates enzyme activity. I have had occasion to study healing for a number of years in Arigó, the recently deceased Brazilian healer who did major surgery without anesthetics and without pain or shock. But the most interesting healing action I have studied was in the case of a healer, Mrs. H., who uses non-contact hand passes over a patient. This healer had previously cured a patient of a ventricular arrhythmia. The healer, Mrs. H., passed her hands over the spine of this patient, who with eyes closed, was in a prone position, covered with a white sheet. When the healer's hands passed (in the air) over the TIO to C1 vertebrae of the patient the normal asynchronous EEG waves showed an immediate high amplitude alpha wave synchrony of 8Hz. This was readily repeatable. I conclude that non-contact healer's manual passes over a patient induce a short range (78) magnetic transmission to the hydrogen bond water protons of the brain causing them to precess in the frequency range from 7 to 14 Hz. This interpretation is compatible with the nuclear magnetic resonance frequency predicted by the Larmor equation for the parameters involved (Body magnetic field of 10^{-6} Gauss) (78, 100, 107). If the proton is in fact the universal carrier of information, per se, it would not only encode this information in quantum magnetic moments,

precession frequencies, and quantum electro-dynamic resonances, but must logically do work at a distance.

Recent evidence suggests that gravity waves exist (101) with a frequency in the audio range, and detection has repeatedly occurred at 1660 Hz.(109). We have considered proton-proton spin coupling between brains at the so-called alpha frequencies. It will be recalled that protons have a not-insignificant mass. We raise the very real question as to the possibility of the weak interaction between proton spin couplings, proton magnetic moment couplings and gravity waves showing in-phase locking at frequencies that are in the physiological range, i,e. from .2Hz to 30KHz, accounting for direct brain action? (109). In my experience (64) all the DBA phenomena I have observed are very short range - a few meters at most. Such short range action is compatible with the suggestion I have made.

8. MEMORY IN NATURE

If protons in a biological matrix are the carrier of information, per se, then protons in the cosmos as a whole would also be vehicles of proto-communication.

Hannes Alfvén has sharply reminded us that until the advent of recent space probes in peri-planetary and solar space, scientists were under the impression that deep space was a

pure vacuum (1). This impression is wrong. We now know that deep space is alive with plasmas, ELF magnetic fields, electrostatic double layers, and currents.(2). It is estimated that about 90% of the atoms of the cosmos are made up of hydrogen atoms, and that there is on the average about one H atom per cubic cm. of space.(1). This cosmic distribution of H atoms existing as a proton matrix can be treated as a universal framework for protocommunication. Since about 63% of the human body also consists of hydrogen atoms we can look for a resonance between its protonic magnetic spin and precession systems and the protonic ELF matrix of the cosmos as a whole. This effect would be most prominent in the perisolar region which we now know is alive with energetic protons streaming out from the sun (54). The magneto-sheath of the earth is now also known to form a gigantic shock wave against this protonic flux from the sun. The entire picture is that of a mushroom cap facing the sun with the earth at the point of attachment of the stem to the cap and the stem reaching out as a tube far into space. In short all space is alive with protons so that any communication from proton to proton can occur through a chain-like coupling. These protons exist in an enormous energy range from highly energetic relativistic protons to hydrogen-bond resonant quasi-static protons.

One of the curious reasons that protons in the cosmic matrix, nd protons in the bio-matrix can resonate is that they can n fact, under certain conditions exist at the same thermal nergy level (62). It is a fact that at temperatures of 00°K, and in the cold of deep space, proton nuclear spin systems re like dilute ideal gases in the simplicity and universality f their thermodynamics (75).

If one applies a static magnetic field, and an RF field o a nuclear spin system at room or body temperatures one can roduce within the nuclear spin system temperatures of 1°K. his is due to 3 properties of such a system (75):

1) In a magnetic field all the protons will precess at the same frequency.
2) Because the spin moments are all polarized opposite to the magnetic field, the energy of the system has a distinct upper and lower boundary.
3) The system is subjected to a monochrome RF frequency.

We have seen that an effect similar to 1). 2). and 3) occurs in manual alpha wave induction: DBA and DBP induction of alpha waves between twins, and in transfer of a healer's power to water hydrogen bond systems. Since these effects are due to protons in elements common to planet earth, C,O,H,N, and found in interstellar space we expect to find the same information carried throughout all nature. In fact, the phenomenon

I believe that a solution of these problems should be a top priority for SCIENCE because it comes close to the heart of the mystery behind the general phenomenon. I believe that the postulate of proton super-conductivity OF ELF FIELDS is a necessary condition for such rapid and complex imprinting of the fertilized egg. The super-conductivity hypothesis is supportable for protons based on the theory of nuclear spin thermodynamics in the rotating frame (75). This theory describes the mechanism whereby proton spin systems attain spin temperatures in the region of $1^{\circ}K$, while the solid they are in, is at room temperature ($300^{\circ}K$).

3. NORMAL SENSORY PERCEPTION - AUDITION

Within biological systems one of the more highly developed environmental information transfer systems is the neural network. I shall use the acoustic neural system as a model for these systems. Let us consider the perception of a 1 KHz sine wave air conducted tone by a human at the threshold level of sensation. The interface between the bio-system and the air is the ear drum which transmits the analog wave into the system with a displacement of 10^{-8} cm= 1Å (0.3Å = Radius of a hydrogen atom). The 1 KHz wave is then transmitted by ossicular coupling to a fluid medium - the cochlear perilymph which transfers the wave or energy to the Basilar Membrane (B.M.). At the threshold of hearing the 1 KHz sine wave displaces the B.M. about 10^{-11} cm. (20).

of object-reading by DBP (psychometry) is one where the object carries information which may be detected by touching and by skin-stroking. I have treated this subject extensively under the title "Memory capacity of Objects" (64). What concerns us here is the question of the basic nature of information, per se, in nature. I have treated this question in this paper, and indicated that life begins with a proton magnetic bias in nature which produces biassed levorotatory molecules. I have tried to show that proton ELF magnetic spin properties are ubiquitous in the human sensory, and memory systems, and that these extend into so-called "inanimate" nature. Julian Schwinger (83) (84) has recently proposed a new theory called "A Magnetic Model of Matter." While this theory is unproven, it addresses itself directly to the questions I have raised. Schwinger points out that even though the Maxwell equations call for a symmetry between electric charge and magnetic charge, the cold fact is that no magnetic counterpart to electric charge is known. Yet the unit of electric charge is unvarying in its universality. Why? He further notes that common to all nuclear particles is isotopic spin and hypercharge which has no explanation. In addition he wonders why there exists in the universe a weak violation of charge-parity (CP) symmetry. He proposes an answer to these

our disturbing questions - which are too complex to go into ere. Nevertheless, he does deduce a unit of basic magnetic harge: He shows that electric charge is given by

$$e^2/\hbar c \approx 1/137$$

nd the magnetic charge becomes for ground states,

$$g_o^2/\hbar c \approx 4(137)$$

His new charge unit which he calls the DYON is a fractional nit compared to the universal unit of electric charge now nown, where

$$\text{DYON} = e_o = 1/3\ e$$

The same type of fractional charge has been proposed for he proton and the neutron, called quarks, or partons (39).

If these theories of fractional charge, consisting of electric charge and magnetic charge are proven, we shall have a truly scientific basis for the theory of protocommunication proposed herein.

We speculate that on a cosmic scale protons are imbedded in a magnetic field matrix which gives them spatial orientation. The cosmic gravitational field determines the lattice spacing of such protons. These two fields determine the gestalt of the proton lattice, and input and output of "information" is mediated by quantum boson, pion, electronic, and photonic

pulses. This concept of a brain applies equally to the bio-domain, or the cosmic domain.

It now remains to illustrate features of protocommunication and the nature of protons which can only come from observations of precognition.

9) PRECOGNITION

Nineteen years ago (August 1952) this month I conducted an experiment with Eileen Garrett (68). The target she was seeking clairvoyantly was created by big cosmic ray pulses incident upon a coincidence counter housed 0.3 miles away from her. This target source gave a purely random distribution of events. Her direct hits in calling the time of arrival of the cosmic rays were at a P level of 10^{-6} (68). This gave me confidence that the experimental design and procedure were valid.

One of the striking findings of this study was the precognition hits made by Mrs. Garrett, not only for their statistical significance ($P = 10^{-3}$), but for the verbal description of the "coming" event. I must state that the counter was so set that only the big cosmic (C.R.) ray events triggered the detectors. In this way during the course of the experiment the average C.R. pulse interval was about 6 minutes with a range of 1 to 30 minutes. By clairvoyant knowledge alone, Mrs Garrett was able to see and describe the components

and function of the C.R. detector. In this way we knew unambiguously when she "saw" the pen recording device, the amplifier circuits, the coincidence counter tube, the Faraday Cage in which this apparatus was housed, or the arrival of the cosmic ray showers. She was able to sense and describe the coming of a cosmic ray as long as 116 seconds before it hit the detector circuit, and then to call, within a second or two, the final movement of the pen that recorded the C.R. event. Here is a description by Mrs. Garrett of one such event starting 33 seconds before the pen recorded the event:

" I see little particles coming down. A formation of particles. The particles look like mercurial globules assembling. They have a fluid, magnetic quality. The particles gather together, they pile up in the tube (Note by author: The coincidence counter tube). The particles strike and make a sound as they hit -it has a shrill quality. The sound is transmitted into a light. NOW! The pen moves!" The Target Pen recorded the cosmic ray event at 23'05" of the experiment. Mrs. Garrett said "NOW" at 23'06" of the experiment. This is clearly both a brilliant precognition hit, and a hit synchronous in time.

I, and all my colleagues (seven of them) present at the experiments were impressed with this power of description of an event 3×10^{10} meters out in space, or about half the

diameter of the sun. I personally am convinced that her mind locked onto those protons in space which were headed on a collision course for a point on a rotating planet. If all this be true how do we account for it? Let us examine some of the facts.

Interstellar space is filled with a plasma made up of magnetic fields of the order of 10^{-6} gauss, and atoms and ions such as protons making what Hannes Alfvén (1,2) has called a viscous medium. Protons moving at relativistic velocities are profoundly influenced by the magnetic field while their rest mass is not significantly altered, their total energy, particularly the magnetic component, is increased. It is my opinion that the quantum concept of a point proton is not valid under these conditions. Rather we should think of a spread out, an ELF-field, mushroom-shaped proton, if you will. If we accept this point of view the proton now has a frame of reference which (depending on its energy) may have a wave length which is equal to the radius of the solar system. Thus we do not have to be concerned with Einstein's limiting velocity of light, c, nor with Feinberg's velocities that exceed c. We need only be concerned with spin temperatures and plasma temperatures which determines resonant conditions between protons in the clairvoyant's

brain, and those in space. Protons in interstellar space can have temperatures ranging from 1°K to 10,000°K. It would seem that the two protons in question must be at the lower end of this scale in order to be at thermal equilibrium. If this condition can be met and it is within the physiological range, I see no diffuculty in bringing the bioproton and the cosmoproton sets into resonance (75,15,34,35,62,76,79). It requires an extraordinary quality of perception on the part of a clairvoyant to come into resonance with such an elusive target (97, 98,102,109,106). Now what can we say about more long range precognition? Does the proton plasma in which all planets and life are immersed act as a giant brain?

CONCLUDING REMARKS

Let me briefly review the essential points that I want to make as a concluding statement.

In order to find some place in the greater order of nature for our personal experience of the brain as mind-qualities, I have been led by my biophysical and parapsychological researches to examine the most common unit in the universe - the proton.

I find that a magnetic basis for matter, as proposed by Schwinger, is required in order to explain l-amino acid molecular asymmetry of life processes operating through proton magnetic asymmetry.

I find that the DNA hydrogen bond system is a suitable matrix for proton ELF superconductivity which may account for basic bio-control mechanisms that must operate in cell division, cell growth and repair, and abnormalities such as cancer.

I find that the C=O:H:N set is a good molecular basis for semiconduction, ferroelectricity, and proton precession effects with which to build a sensory apparatus.

Biological memory finds a rational basis in the simple concept of modulated proton ELF spin states. The same concept applied to a paraneural domain of water-glia is a possible basis for direct brain perception (DBP). However, this latter mechanism is intimately linked to the concept of a cosmic protonic plasma brain built into all of nature, connected thru ELF fields.

I feel that no man should put forth a serious theory without suggesting experiments that will test its validity. I want to propose, very briefly, a number of such experiments.

I believe that if the proton-proton spin coupling exists in DBP it should be possible to shield a sender from a receiver in a telepathy experiment. This may be done by placing one of the participants in an enclosure of D_2O. I predict this will stop, or attenuate DBP. A control for this experiment would place the subject in a charged Faraday Cage Enclosure whose walls could be emptied, or filled of D_2O without perturbing the subject.

Long range precognition and detection of protons, as was described for Mrs. Garrett, can best be done by astronauts in a satellite in space. On earth we would have a clairvoyant. In space, an astronaut with a helmet that would detect when an energetic proton went through his brain. The clairvoyant would try to guess when the astronaut's brain is activated by a proton. The experiment could be reversed with the astronaut trying to guess when a person on earth had a cosmic ray event pass through his brain. This experiment would be highly important in determining proton energy levels, spin temperatures, and the role of the earth's magneto-sheath in direct brain perception.

Another experiment would involve driving two brains in synchrony using the techniques of nuclear ELF magnetic resonance. It would be desirable to have the two brains at matching thermal equilibria, and at driving frequencies such as the 8 Hz. alpha frequency. We would look for either increased, or decreased DBP transmission between the two subjects.

The most important study would be a long term study of the life cycle of the salmon. I believe that this study could yield more basic information about geo-cosmic information imprinting than any other study of which I can conceive. The most important phase for study would be the ritual egg laying and egg fertilization.

P	At.	N	μ	μ	P	At.	N
1	H	0	2.79	-1.91	0	n	1
1	H	1	0.85	0	2	He	2
3	Li	3	0.82	-1.17	4	Be	5
5	B	5	1.80	0	6	C	6
7	N	7	0.40	0	8	O	8
9	F	10	2.62	0	10	Ne	10
11	Na	12	2.21	0	12	Mg	12
13	Al	14	3.64	0	14	Si	14
15	P	16	1.13	0	16	S	16
17	Cl	18	0.82	0	18	Ar	22
19	K	20	0.39	0	20	Ca	20
21	Sc	22	4.52	0	22	Ti	26
23	V	28	5.14	0	24	Cr	28
25	Mn	30	3.46	0	26	Fe	30
27	Co	32	4.65	0	28	Ni	32
29	Cu	34	2.22	0	30	Zn	34
53	I	74	2.80	0	54	Xe	78
83	Bi	126	4.08	0	84	Po	126

TABLE 1. COMPLEMENTARY PHYSIOLOGICAL PAIRS OF ELEMENTS RANKED BY PROTON NUMBERS.

(SOURCE OF DATA, REF. 11)

P= PROTON NUMBER

At=SYMBOL OF ELEMENT

N= NEUTRON NUMBER

μ = BOHR NUCLEAR MAGNETON NUMBER

MULTIPLE OF 0.4 UNIT	P	At	N	μ	μ	P	At	N
FUNCTION								
I. NEURON POTENTIAL	19	K	20	0.39	0	20	Ca	20
OXIDATION	7	N	7	0.40	0	8	O	8
II. ELECTROLYTE, CLATH RATE	17	Cl	18	0.82	0	18	Ar	22
NEGATIVE-LIFE	1	H	1	0.85	0	2	He	2
III. ENERGY SOURCE	15	P	16	0.13	0	16	S	16
IV. STRUCTURAL	5	B	5	0.80	0	6	C	6
V. NEURON POTENTIAL	11	Na	12	2.21	0	12	Mg	12
TRACE ELEMENTS	29	Cu	34	2.22	0	30	Zn	34
VI. BONE STRUCTURE	9	F	10	2.62	0	10	Ne	10
VII. REDUCTION	1	H	0	2.79				
METABOLIC HORMONE, I	53	I	74	2.80	0	54	Xe	78
CLATHRATE, Xe								
VIII. OXYGEN CARRIER, Fe	25	Mn	30	3.46	0	26	Fe	30
TRACE ELEMENT								
IX. TRACE ELEMENTS	13	Al	14	3.64	0	14	Si	14
X. TRACE ELEMENTS	83	Bi	126	4.08	0	84	Po	126
XI. TRACE ELEMENTS	27	Co	32	4.65	0	28	Ni	33
XII. TRACE ELEMENTS	23	V	28	5.14	0	24	CR	25

TABLE 2 COMPLEMENTARY PHYSIOLOGICAL PAIRS OF ELEMENTS RANKED BY MAGNETIC MOMENT UNITS (0.4μ).

(SYMBOLS AS IN TABLE 1. Ref. 11)

The radius of a nucleus - e.g., proton is 1.5×10^{-13} cm. (103).

Note: The distance from O to N in the COHN system ranges from 2.60 Å to 2.90Å.

AVERAGE = 2.72 Å in alpha helix (28)

This mechanical displacement of the B.M. is transferred to the auditory sensor - the hair cell wherein the 1 KHz sine wave undergoes transduction to produce an analog 1 KHz sine electrical signal - the cochlear microphonic signal (16). Up to this point the information transfer process is linear. But the hair cell is now excited to generate a chemical pulse which it discharges across the synapse (Deiter) at the first order auditory neuron (43, 36). Encoding occurs, and the information (1 KHz sine wave) is now transferred along the nerve as a series of time distributed digital pulses, the classical "action potential" electrical pulses.

The actual mechanism of auditory encoding at the Deiter's synapse is not known in spite of great efforts to solve it (43). What I present here is a highly speculative solution for which we can make certain assumptions. The first is that hair cells can resonate to one cycle per second intervals over the range of 16 Hz to 30 KHz (65,66). The second assumption is that the higher the audio frequency the greater will be the current density flow for the constant level voltage of each action potential pulse (70).

As the hair cells go into vibration in resonance with the

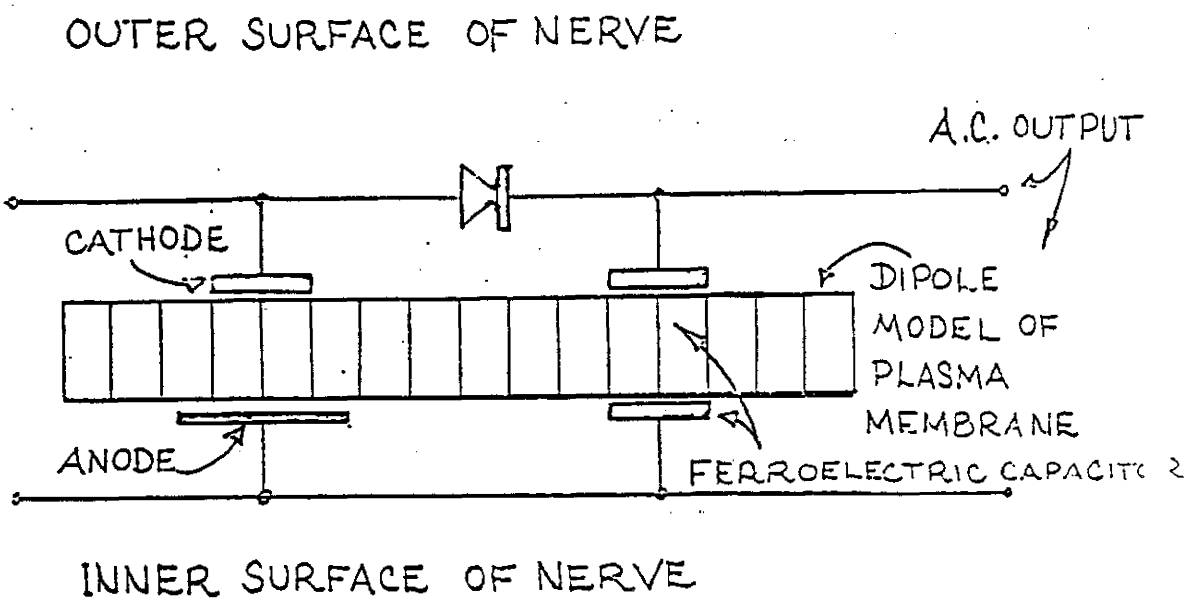

Figure 1. Ferroelectric Model Circuit Of One Domain Of The Nerve Plasma Membrane. The Load Is To The Right, The Input To The Left

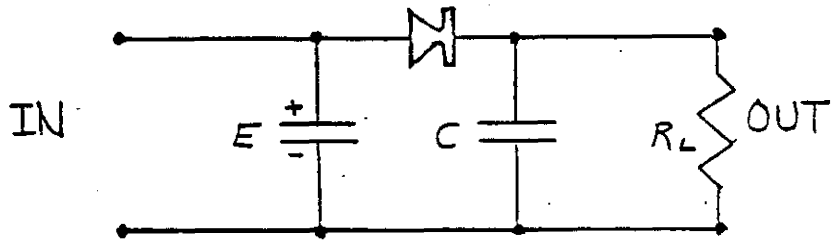

Figure 1A. Equivalent Circuit Of One Domain Of The Ferroelectric Model Plasma Membrane

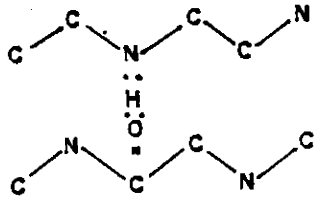

FIG. 25 A

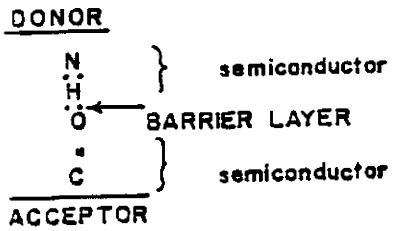

FIG. 25 B

PART 1

REFERENCES

REFERENCES

1. Alfvén, Hannes — Antimatter and Cosmology
   Scientific American — April 1967, pp. 106

2. Alfvén, Hannes; Elvius, Aina — Antimatter Quasi-stellar Objects, and the Evolution of Galaxies
   Science, vol. 164 — May 23, 1969, pp. 911-917

3. Andrews, Donald Hatch — The Symphony of Life
   Unity Books, Lee's Summit, MO., USA — 1966, p. 200

4. Baker, Peter F. — The Nerve Axon
   Scientific American — March 1966, pp. 74

5. Barclay, M.; Barclay, R. K.; Essner, E. S.; Skipski, V. P.; Terebus-Kekish O. — Plasma Membranes of Rat Liver: Isolation of Lipoprotein Macromolecules
   Science, vol. 156 — May 5, 1967, pp. 665-667

6. Bar-Nun, A.; Bar-Nun, N.; Bauer, S. H.; Sagan, Carl — Shock Synthesis of Amino Acids in Simulated Primitive Environments

7. Becker, Robert O., M.D. — Some Observations Indicating the Possibility of Longitudinal Charge Carrier Flow in the Peripheral Nerves
   Presented at the Second Annual Bionics Symposium, Ithaca, New York — 31 August 1961

8. Bobeck, Andrew H.
Scovil, H.E.D.
Magnetic Bubbles

Scientific American
June 1971, pp. 78 - 90

9. Bolef, D. I.
Acoustic Techniques in Magnetic Resonance

Science
May 4, 1962, vol. 136, pp. 359-369

10. Brandt, Werner
Channeling in Crystals

Scientific American
March, 1968, p. 91

11. Calvin, Melvin
Androes, G. M.
Primary Quantum Conversion in Photosynthesis

Science
November 23, 1962, vol. 138
pp. 867 - 873

12. Commoner, Barry
Woolum, John C.
Larsson, Ernst
Electron Spin Resonance Signals in Injured Nerve

Science
August 15, 1969, vol. 165
pp. 703 - 704

13. Condon, E. U., Ed.
Odishaw, Hugh
Handbook of Physics
Table 3.1 Nuclear Moment Values.
Section 9-93

McGraw-Hill Book Co.
2nd Ed. 1967 New York.

14. Corrigan, John J.
D-Amino Acids in Animals

Science, vol. 164
April 11, 1969, pp. 142 - 149

15. Crane, H. R.
The g Factor of the Electron

Scientific American
Jan., 1968, pp. 76-85

16. Crick, F. H. C. — On the Genetic Code
Science — February 8, 1963, vol. 139, no. 3554 pp. 461 - 464

17. Donn, Bertram — Interstellar Molecules and Chemistry
Science — Dec. 4, 1970, vol. 170, pp. 1116-1117

18. Eccles Sir John — The Synapse
Scientific American — January 1965, pp. 56+

19. Essman, Walter B. — Some Neurochemical correlates of altered memory consolidation
Trans. N.Y. Acad. Sciences — Dec. 1970, pp. 947-973

20. Flanagan, James — Computer Simulation of Basilar Membrane Motion and Electronic Artificial Larynx
1965 IEEE International Convention Record, Part 12 — p. 40

21. Fox, Sidney W — Synthesis of Amino Acids by the Heating of Formaldehyde and Ammonia
Science, — Nov. 27, 1970. vol. 170, pp. 984-986

22. Frank, Henry S — The Structure of Ordinary Water
Science — August 14, 1970. vol. 169, no. 3946, pp. 635-641

23. Gesteland. Robert — Biological Mechanisms for Monitoring Atmospheric Composition and Pollution in Closed Air Force Environments
Defense Documentation Center Report #T10996, July 16, 1970 — Primary Number Code 62202F 7233 05 006

31. Hydén, Holgar — Activation of Nuclear RNA of Neurons and GLIA in learning. (p. 178-239)

in: The Anatomy of Memory. Ed. Daniel P. Kimble Science and Behavior Books, Inc.. Palo Alto, Calif. — 1965. (Quote from p. 231)

2. Ingalls, Clyde E., E.E. — Sensation of Hearing in Electromagnetic Fields

New York State Journal of Medicine — Nov. 15, 1967, vol. 67. no. 22. pp. 2992 - 2997

33. Jardetzky, Oleg — Magnetic Resonance in Biological Systems

Science. — Oct. 23, 1964, vol. 146, pp. 552-553

34. Jensen, L. H. Sundaralingam, M. — Hydrogen Atom Thermal Parameters

Science — September 11, 1964 vol. 145. pp. 1185-1187

35. Johnson, Charles Y. Young, J. M. Holmes, J. C. — Magnetoglow: A New Geophysical Resource

Science — Jan. 29, 1971. vol. 171 pp. 379-381

36 Kaneko, Y. Daly, J. F. — Activity of Acetylcholinesterase on the Endolymphatic Surface of Outer Hair Cells

Acta Oto-Laryngologica, — June 1969, vol. 67, fasc. 6, pp. 602 - 610

37. Kastler, Alfred — Optical Methods for Studying Hertzian Resonances

Science — October 13. 1967, vol. 158 pp. 214-221

38.	Pipkin, Francis M	1966 Nobel Laureate in Physics: Alfred Kastler
	Science	November 11, 1966 vol. 154 pp. 747-749
39.	Kendall, Henry W Panofsky, Wolfgang. K. H.	The Structure of the Proton and the Neutron
	Scientific American	June 1971, pp. 61-77
40	Koshland, Jr., D. E.	Correlation of Structure and Function in Enzyme Action
	Science	Dec. 20 1963, vol. 142 no. 3599 pp. 1533-1541
41.	Lippman, Muriel. S.S.J.	A Proposed Role for Mucopolysaccharides in the Initiation and Control of Cell Division
	Transactions of the New York Academy of Sciences	Jan. 1965, Series II , vol. 27, pp. 342-360
42.	Little, W. A.	Superconductivity at Room Temperature
	Scientific American	February 1965, vol. 212, no. 2, pp. 21-27
43.	Lummis, R. C.	The Secret Code of Hearing
	Bell Laboratories Record	Sept. 1968, pp. 261-266
44.	Manfredi, A.. Bombelli, U.	Radioacoustic Treatment of Deafness (Originally published in Atti della Fondazione Giorgio Ronchi, nov-dec 1963, anno XVIII no. 6, pp. 603-616),
	Pubblicazioni dell'Istituto Nazionale di Ottica, Arcetri Firenze. Serie IV, no. 408	

45. Manfredi, A.
Bombelli, U.

Explanatory Notes on Radio-Acoustic Treatment of Deafness

Presented at the VII Congress of the International society of Audiology

August 24, 1964 Copenhagen

46. Marsh, James T.
Worden, Frederic G.
Smith, James C.

Auditory Frequency-Following Response: Neural or Artifact?

Science

vol. 169 Sept. 18, 1970, pp. 1222-1223

47 Mauro, Alexander

Space Charge Regions in Fixed Charge Membranes and the Associated Property of Capacitance

Biophysical Journal

1962, vol. 2, no. 2, Part 1, pp. 179-198

48. Mayer, Maria Goeppert

The Shell Model

Science

Sept. 4, 1964. vol. 145 pp. 999-1006

49. McCulloch, Warren S.

The Biological Sciences in the Great Ideas Today

Encyclopedia Britannica. Chicago

1966, pp. 288,334

50. Miller, S. L.

The Formation of Organic Compounds on the Primitive Earth

Ann. New York Acad. Sci.

1957, 69:260

51 Murray, Margaret R.
Benitez, Helen H

Deuterium oxide: Direct Action on Sympathetic Ganglia Isolated in culture

Science

vol. 155, Feb. 24 1967, pp. 1021-1024

52.	Myers, R. D. Veale, W. L.	Body Temperature: Possible Ionic Mechanism in the Hypothalamus Controlling the Set Point
	Science	Oct. 2, 1970, vol. 170 pp. 95-97
53.	Nelson, F. A. Weaver, H. E.	Nuclear Magnetic Resonance Spectroscopy in Superconducting Magnetic Fields
	Science	Oct. 9, 1964, vol. 146, pp. 223-232
54.	Ness, Norman F.	Earths Magnetic Field: A New Look
	Science	vol. 151, March 4,,1966, pp. 1041-1052
55.	Oró, J. Kimball, A. P.	Synthesis of Purines under possible primitive earth conditions. 1. Adenine from Hydrogen Cyanide
	Arch. Biochem. Biophys.	94:217-227, 1961
56.	Parisi, Mario Rivas, Emilio De Robertis, E.	Conductance Changes Produced by Acetylcholine in Lipidic Membranes Containing a Proteolipid from Electrophorus
	Science	vol. 172, April 2, 1971, p. 56-57
57.	Pauling. Linus	Nature of the Chemical Bond
	Cornell University Press	Ithaca, New York 1948, 450 pp.
58.	Pauling, Linus	A Molecular Theory of General Anesthesia
	Science	July 7, 1961, vol. 134, no. 3471 pp. 15 - 21

1 KHz signal, the acoustic phonon displacement of 10^{-11} cm is sufficient to strain the C=O:H:N set to open the membrane gate for the sodium pump. As the current flows (the higher the frequency, the higher the current density) it will set up a magnetic field. (75). The magnetic field will be picked up by the hydrogen proton of the C=O:H:N set and cause it to precess. The higher the magnetic field the higher the frequency of precession.

The magnitude of the current density across the membrane will determine the number of molecules of chemical transmitter such as acetylcholine that will be released at the pre-synaptic membrane (18). Thus we have two parallel related events:

1) Energy release (current density) linear to audio frequency which triggers chemical transmitter molecules.
2) Proton precession triggered by the magnetic field generated by current density - and such precession frequency is linear to audio input.

The acetylcholine activating the post-synaptic membrane transfers phonons of thermal energy to the axon whose energy is equivalent to the original acoustic phonon at the hair cell. This phonon repeats the events already described. It is to be noted that each C=O:H:N: set is activated serially thus

59.	Pauling, Linus	Orthomolecular Psychiatry
	Science	April 19, 1968, vol. 160 pp. 265-271
60.	Pauling, Linus Hayward Roger	The Architecture of Molecules
	WH Freeman & Co San Francisco	1964 Plate 45
61.	Pohl, Herbert A	Theoretical Aspects of Dielectrophoretic Deposition and Separation of Particles
	Journal of the Electrochemical Society,	June 1968, vol. 115 no. 6 pp. 155c-161c
62.	Porter, William S.	Hydrogen Energy Levels: Perturbation Caused by Proton Structure
	Science	March 20, 1964, vol. 143 pp. 1324-1325
63.	Puharich, (Andrija) H.K.	Sacred Mushroom
	Doubleday & Co. Inc.	New York, 1959 262 pp.
64.	Puharich, (Andrija) H.K.	Beyond Telepathy
	Doubleday & Co. Inc,	New York 1962, 312 pp.
65.	Puharich, H.K. Lawrence, J.L.	Means for Aiding Hearing
	US Patent No. 2,995,633	August, 1961
66.	Puharich, H.K. Lawrence, J.L.	Alternating Current Energy Used to Simulate Audition in Deaf Humans
	Paper presented at 35th Annual Convention Aerospace medical assoc. Miami, Florida	May 13, 1964

67. Puharich, H. K.
Lawrence, J.L.

Electrostimulation Techniques of Hearing

Technical Documentary Report December, 1964
Defense Documentation
Center, Virginia

68. Puharich, H.K.

Electric Field Reinforcement of ESP

International Journal of Neuropsychiatry

vol. 2 No. 5. pp. 474-486 1966

69. Puharich, H. K.
Smith, J.
Kitselman, A

Computers, Chance & Cholinergia

Darshana (India)

1: 41-43 August 1961

70. Puharich, H.K.
Lawrence, J.L.

Hearing Rehabilitation by Means of Transdermal Electrotherapy in Human Loss of Sensorineural Origin (I)

Acta OtoLaryngologica, 1969

vol. 67, Fasc. 1 pp. 69-83

71. Puharich, H.K.
Lawrence, J.L.

Hearing Rehabilitation by Means of Transdermal Electrotherapy in Human Hearing Loss of Sensorineural Origin (I

Excerpta Medica International Congress Series no. 189 containing abstracts of papers read at the Ninth International Congress of Oto-Rhino-Laryngology

Mexico. D.F. August 10-14, 1969

72. Puharich. H.K.
Lawrence. J.L.
Dugot, R.S.

Transdermal Electrostimulation of Hearing

Presented at 13th Annual Scientific Meeting Committee for Research in Otolaryngology, American Academy of Opthalmology and Otolaryngology, Chicago, Illinois, October 11 1969.

3. Rabideau, S.W.
Florin, A.E.

Anomalous Water: Characterization by Physical Methods

Science

July 3, 1970 vol. 169, pp. 48-52

4. Randt, Clark T.
Mazzia, Valentino D. B.

Recent Memory Fixation in Man

Reprint from Transactions of the American Neurological Association,

1965. pp. 141-144

5. Redfield, Alfred G.

Nuclear Spin Thermodynamics in the Rotating Frame

Science

May 30, 1969, vol. 164 no. 3883 pp. 1015-1023

6. Reines, Frederick
Sellschop, J.P.F.

Neutrinos from the Atmosphere and Beyond

Scientific American

February 1966, pp. 40

7. De Robertis, Eduardo

Molecular Biology of Synaptic Receptors

Science

Vol..171, March 12. 1971 pp. 963-971

8. Rocard, Y.

Actions of a Very Weak Magnetic Gradient: The Reflex of the Dowser

La Nature, No. 3343

pp. 468-472 Nov. 1963

9. Romig, Mary F.
Lamor, Donald L.

Anomalous Sounds and Electromagnetic Effects Associated with Fireball Entry

The Rand Corporation. Santa Monica, Calif.

July 1963, Memorandum RM-3724-ARPA

80. Rose, Birgit — Junctional Membrane Permeability: Restoration by Repolarizing Current
Science — August 7, 1970 vol. 169 pp. 607-609

81. Rosenberg, Barnett; Postow, Elliot — Semi Conduction in Proteins and Lipids - Its Possible Biologic Import pp. 161-190
Ann. of the NY Acad. Sci. vol. 158 art. 1 pp. 1-438 — Editor Philip Reigelson, May 16, 1969

82. Runnels, L.K. — Ice
Scientific American — Dec, 1966, pp. 118-126

83. Schwinger, Julian — Relativistic Quantum Field Theory
Science — vol. 153 no. 3739 Aug. 26, 1966 pp. 949-953

84. Schwinger, Julian — A Magnetic Model Of matter
Science — August 22, 1969 vol. 165, no. 3895 pp. 757-761

85. Segrè, Emilio — Physics in the Last Twenty Years
Science — March 4, 1966 vol. 151 pp. 1052-1055

86. Seipel, J.; Morrow, R. — The Magnetic Field Accompanying Neuronal Activity
Journal of the Washington Academy of Sciences — p. 1, 1960 (No vol. no. on reprint)

87. Shah, Dinesh O.; Hamlin, Jr., Roy M. — Structure of Water in Microemulsions: Electrical, Birefringence, and Nuclear Magnetic Resonance Studies
Science — February 5, 1971 vol. 171 pp. 483-485

88. Smith, Sister M. Justa — Effect of a Homogeneous Magnetic Field on Enzymes

Third International Biomagnetic Symposium, University of Illinois. Chicago. Illinois 1967, pp. 22-25

89. Smith, Sister M. Justa — Considerations Regarding the Mechanism of the Action of Magnetic Fields on Enzymes

Third International Biomagnetic Symposium. University of Illinois, Chicago, Illinois 1967, pp. 26-27

90. Smith, Justa — Are These Healing Hands?

Response, vol. 11 no. 2 Publication of Rosary Hill College, Buffalo, NY — p. 18 Spring 1968

91. Solomon, Arthur K. — Pores in the Cell Membrane

Scientific American — December 1960 pp. 146+

92. Sproull, Robert L — The Conduction of Heat in Solids

Scientific American — December 1962, pp. 92-104

93. Stanford, A.L.Jr. Lorey, R. A. — RNA's Function in Memory: Lingering Polar Alignment?

Dateline in Science — October 18, 1968, vol. 3 No. 20 p. 1

94. Tarkowski, A. K. — Spermless Egg-Activation is Achieved in the Mouse

Dateline in Science — May 15, 1970 vol. 5 no. 10 p. 1

95. Taylor, Barry N. Langenberg, Donald N. Parker, William H. — The Fundamental Physical Constants

Scientific American — October 1970 p. 62

96. Teorell, Torsten — Electrokinetic Considerations of Mechanoelectrical Transduction

Annals of the New York Academy of Sciences — pp. 950-966 vol. 137 Art. 2 pages 403-1048, July 14 1966

97. Valentinuzzi, Maximo — Theory of Magnetophosphenes

The American Journal of Medical Electronics — April-June 1962. PP. 112-121

98. Volkers, W.. — Detection and Analysis of High Frequency Signals From Muscular Tissues with Ultra-Low Noise Amplifiers, Technical Report No. TR 76

Millival Division of COHU Electronics, Inc — Schenectady, New York

99. Walker, Jr., J .L. — Unified Account of the Variable Effects of Carbon Dioxide on Nerve Cells

Science — March 13, 1970 vol. 167, pp. 1502-1504

100. Walsh, Jr. W. M. — Magnetic Resonances and Waves in Simple Metals

Science, January 8, 1971 — vol. 171, pp. 36-42

101. Weber, Joseph — Evidence of Gravity Waves Reported

The New York Times — June 15, 1961 p. 1

102. Wei, Ling Y. — Role of Surface Dipoles on Axon Membrane

Science — January 17, 1969. vol 163. pp. 280-282

103.	Weisskopf, Victor F.	The Three Spectroscopies
	Scientific American	May 1968 vol. 218, no. 5 pp. 15-29
104.	Weissler, Alfred Pecht, Israel Anbar, Michael	Ultrasound Chemical Effects on Pure Organic Liquids
	Science	vol, 150 Dec, 3 1965, pp. 1288-1289
105.	Wick, Gerald L.	Interstellar Molecules: Chemicals in the Sky
	Science	October 9. 1970 vol, 170 pp. 149-150
106.	Wiener, N.	CYBERNETICS
	John Wiley & Sons Inc. New York	1948 p. 166
107.	Wigner, Eugene P.	Events. Laws of Nature and Invariance Principles
	Science	September 4. 1964, vol. 145. pp. 995-1006
108.	Wilkins. MHF	Molecular Configuaration of Nucleic Acids
	Science	May 31. 1963 vol. 140 no. 3570 pp. 941-950
109.	Witteborn, Fred C.	Data Confirm Faint Gravity Pulls Free Electrons in Magnetic Field
	Dateline in Science	January 20, 1967 p. 1
110.	Yeager, Ernest	Fuel Cells
	Science	October 20, 1961 vol. 134 pp.1178-1186

PAPER No.2

SUCCESSFUL TREATMENT OF NEOPLASMS IN MICE WITH GASEOUS SUPEROXIDE ANION (O_2^-) AND OZONE (O_3): WITH A RATIONALE FOR THE EFFECT.

by

H. Andrija Puharich, M.D., LLD.
Director of Research

ESSENTIA RESEARCH ASSOCIATES
350 East 52nd Street
New York, N.Y. 10022

and

ESSENTIA RESEARCH LABORATORY
Route 1, Box 545
Dobson, N.C. 27017
U.S.A.

SIXTH OZONE WORLD CONGRESS, OF THE
INTERNATIONAL OZONE ASSOCIATION 1983
May 22 - 26, 1983
Washington, D.C. U.S.A.

PAPER 2. CONTENTS

1. Introduction to, how the author got into cancer research. 1

2. Electrostimulation of humans with deafness 3
   This technology (the transdermal system, or T.D.) found to prevent blood clotting in animals.
   The TD system was found to efficiently split water by alternating current electrolysis.

3. Development of an energy cell to split water into H_2 and O_2 . 4

4. The energy cell developed into a crucible for the biochemical origin of life. The chemistry of the origin of life. 5

5. The role of O_2 and O_3 (ozone) in the origin of life. 12
   O_3 found to be an effective and cheap treatment for cancer in mice. Discovery of quantasomes in cancer cells by Dr. Arnan. Development. Use of the TD system to treat cancer.

6. The rate of ELF magnetic fields in causing cancer. 17

7. Tables, and Figures. 24-73

8. Appendix A. Reprint from SCIENCE 74-77

9. Appendix B. NUCLEAR MAGNETISM. 78-82
   References. 83-94

setting up the mechanism for a delay line which accounts for the slow conduction of the nerve impulse. The current density pulse besides metering out "quanta" of chemical transmitter material has another function which is to act on perineural water shells with a hydrolysis-like action. This effect on water protons becomes, in my theory, the basis for memory. This topic will be discussed later as a brain effect when we consider more fully the subject of brain memory.

Within this model is the well-known sodium pump mechanism which maintains a DC barrier potential across the cell membrane (4) With nerve excitation K^+ goes out of the cell, and Na^+ goes into the cell. Each of these ions has an opposing ion which acts to damp its action; K^+ is damped by Ca^{++}, and Na^+ is damped by Mg^{++}. What is not gemerally recognized is that K^+ has a positive (0.4) magnetic moment, and Ca^{++} has a zero moment; Na^+ has a positive (2.2) magnetic moment, and Mg^{++} has a zero magnetic moment, Table 2. We would expect a short range transfer of ELF magnetic information from the precessed proton to Na^+ and K^+ via the acetylcholine molecule (47). This would tell the post-synaptic membrane whether it is to be excited, a process which opens the membrane to sodium ions, or to be inhibited, a process which closes the membrane to sodium ions (18, 57). This information would

I want to make it clear at the outset that I had no intention of doing cancer research when I started my career. Furthermore, I do not claim to be an expert in cancer research. In working toward my Ph.D. in Physiology under A.C. Ivy at Northwestern University Medical School, I did research on methods of electroanesthesia in animals. When I got my M.D. degree, I became an internist. In 1948 I became Dr. Sam Rosen's surgical assistant on his invention of the Stapes Mobilization operation for conductive deafness. From him I learned about hearing problems, and got interested in alleviating the problem of sensorineural hard-of-hearing, and deafness.

In conjunction with Warren S. McCulloch, one of the founders of Cybernetics, we found a patient at Bellevue Hospital in New York City, who had been committed for "hearing voices". We determined that, outside of hearing voices, his psychiatric profile was normal. We found out that his job was the key to the diagnosis. He ground metal castings against carborundum wheels. Dental examination showed that his metal fillings were coated with carborundum dust. We placed him in a Faraday Cage, which eliminates all common electrical and radio signals, and found that his voices ceased. We found that he was precisely tuned to radio station WOR in New York City. His teeth were cleaned, and he was cured of the "psychiatric" problem. I set out to find the scientific basis for this phenomenon of "hearing radio waves".

It was obvious that the carborundum behaved like the "crystal" rectifier in the old crystal radio sets of the 1920's. Joe Lawrence, a dentist, joined me in this research in the early 1950's, when we were stationed at the Army Chemical Center, Edgewood, Maryland. We began to do research on the phenomenon of hearing radio waves. [1,2] Referring to (p.23) Fig. 46 we found that when a person, standing in the near

field of a low power radio transmitter, stroked a wire resting on his cheek, he could hear a voice signal, and increase the RF (radio frequency) field on his skin from +200 mv to +250 mv. When the wire was clamped between the teeth and stroked there was a 10 db gain in hearing. Fig. 44. When a plastic box was cemented around the wire, it was found that (p.24) sound was being generated in the wire - an electroacoustic effect. [3,4] It is to be noted that hearing sensation occurred only when the wire was stroked by the skin. The (p.25) mystery of skin-stroking a wire in the presence of amplitude modulated RF was solved (Fig. 47) when it was found that an ordinary diode held in the teeth without stroking, gave the sensation of hearing. A model of this (p.26) effect is shown in Fig. 45. The actual wave-shaping by the non-linear element, i.e., either skin stroking, or the use of a rectifier element such as a crystal, or a diode, (p.27) is shown in Fig. 3. In 1A we see a normal amplitude modulated radio wave. In 1B we see that stroking will clip the positive half of the wave form, and allow the negative pulses to pass across the tissues giving perfect hearing sensation to both normal, and sensorineural impaired humans. Fig. 42 showes the power spectrum, and the side bands. [5,6,7] (p.28).

From this basic finding, Lawrence and I, and our engineering staff, developed the manually controlled laboratory instrument shown in Fig. 4., with which we learned (p.29) how to get deaf subjects to hear words and speech. [8] We found that before a deaf person could hear, he had to undergo a one to two month course of transdermal (TD) electrotherapy daily. This consisted of repetitively sweeping the head, via electrodes, with pure tones over the frequency range from 20 Hz to 10,000 Hz modulating a 30 to 50 KHz carrier wave for one hour each day. This clinical work resulted in (p.30) the development of a completely automatic treatment program in the instrument shown in Fig. 7. Lest we forget, we did solve the technology of hearing radio waves through the teeth, as shown in some of the patents issued, Figs. 8, 9, and 10. [9,10,11,12,13] (p. 31, 32, 33.

In carrying out large scale Transdermal Electrotherapy in cooperation with several medical schools on patients with sensorineural hearing loss, other beneficial effects were uncovered.[14] It was found that Meniere's disease could be cured in two weeks of treatment.[15] In elderly senile patients there was a restoration of short term memory. There was an acceleration of bone healing in refactory fractures. Significant improvement was found in cases of impaired vascular circulation.[16] In the course of safety and hazard studies on animals, it was found that blood coagulation was significantly delayed, in vitro and in vivo. A joint research program was carried with New York University Medical Center, Cardiovascular Research Laboratory. The team was made up of Dr. George Reed, Dr. William Brewster, Dr. Luis Cortes, and myself. Our goal was to prevent blood coagulation in an articial heart device by using the TD electrotherapy signal on the blood. We were successful.[17] In Fig. 3 we see a dilute suspension of red blood cells (p. 34) (p. 35) under a microscope without the TD signal energization. The cells clump and settle out in about four minutes. In Fig. 5 we see the TD energized red blood cells in the same cell as Fig. 3, but now they are energized by the TD signal; they develop a negative charge, and repel each other so that they do not clump, do not settle down, and in vivo do not coagulate in an artificial heart pump in animals. Fig. shows the method of doubling the shelf life of stored whole blood by means of continuous TD signal charging, and Fig. shows the method applied to a human.

One day, while I was studying the effects of the TD electrical fields on the dynamics of a dilute suspension in Ringers solution of red blood cells under a microscope, I observed bubbles coming from both of the electrodes. I ran a gas analysis on the Ringers solution, and found that

I had been observing the splitting of water molecules by electrolysis at incredibly low power levels, i.e., 0.16mw. It was this single observation that turned me in the direction of studying cancer. I shall now describe how this came about.

I had been heavily influenced by Dr. Warren S. McCulloch to believe that water structure was the basis of life structure and organization. So I began an intense study of water structure and the electrolysis of water by means of the TD signal generator.

The block diagram of the water electrolysis equipment (p.37) is shown in Fig. 1. Component I is the same TD signal generator as was used in the hearing experiments. Component I is coupled to Component II (shown in top view as a coaxial electrode arrangement) by a series inductive-capacitance circuit. Fig. 2 is a side view of Component (p. 38) II, and the space between the copper center electrode and the concentric iron electrode is filled with a 0.9% saline solution termed Component III. The center copper electrode is surrounded by a high temperature-fired ceramic jacket which is porous to water molecules. Fig. 3 shows more (p.39) clearly, the geometry of Component III. My initial goal was to measure the efficiency of this system for the production of hydrogen and oxygen as a fuel.[18] Fig. 14 (p.40) shows in a simplified way the thermodynamics of water decomposition in (b), and the exergonic reaction when hydrogen and oxygen gases are brought together and burned to release energy. I measured all of the gas production by the Mass Spectrometer, and measured the electrical power consumed in the endergonic reaction with precision calibrated instrumentation, and with this data calculated the efficiency of the system.[19] I was able to attain a 90% efficiency in the first half-hour of electrolysis, and thereafter it steadily declined to about 11%. The mass spectrometer revealed that the oxygen was being consumed in some unknown chemical reaction.

All conditions of the experiment were sterile, run under a high vacuum, and contamination, or loss, from an outside source was impossible. Yet at the end of each experiment when the apparatus was taken apart it was found that Component III was filled with a flocculent albuminoid material which had a fish-like odor.

I shall very briefly review the course of chemical (p. 41) events. The first slide shows the chemical content of the solution before electrolytic action started. The second (p. 42) slide shows the chemical content of the solution after three minutes of electrolysis. The main addition is copper and iron electrolytically removed from the electrodes. The (p 43) next slide shows a computer print-out of the mass spectrometer analysis of the products of electrolysis, and the next (p. 44) graph plots the significant data. The pH rises in the first 30 minutes of electrolysis from 4.27 to pH 13.0. This is due to the production of hydroxyl ions. The oxygen drops from 21% to a fraction of 1% in two hours. The hydrogen rises from zero to about 90% by volume in several hours. The nitrogen drops from 78% to about 5% in four hours. The CO_2 starts at a non-detectable level, and slowly rises to about the 2% level in seven and a half hours. And the Argon does not disappear with vacuum pumping, but tends to increase as a function of time. The next few slides (p 45, 46, 47, 48, 49) show the chemicals that were synthesized in the electrically pulsed Component III solution.[19] What is very wrong with this experiment is that when all the nitrogen was removed and replaced with helium, there was carbon in the solution, and there was nitrogen in the solution. Now where did the nitrogen and the carbon come from? In order to test a hypothesis the Component III solution was changed from a sodium chloride solution, to a sodium hydroxide solution.

When this was done, no organic compounds were formed, as had been the case with the sodium chloride solution, and no carbon or nitrogen was formed in the solution. [21] This finding forced me to reluctantly accept the possibility that we were looking at the Kervran reaction in vitro. [22] The next slide shows the Kervran reaction. (p.50).

The Kervran reaction has been studied in vivo for many years, and confirmed by many workers. As far as I know, this is the first time that it has been observed in vitro. The nuclear control systems of these biochemical reactions are of the type developed by the theoretical physicist, Olivier Costa de Beauregard, Director of the Institute Henri Poincare in Paris. [23]

$$n \rightarrow p + e^- + \bar{\nu} \qquad (1)$$

$$p + \nu \rightleftharpoons p' + \nu' \qquad (2)$$

$$p \rightleftharpoons p' + \bar{\nu} + \nu' \qquad (3)$$

The equations imply the conversion of a neutron (n) to a proton (p) by virtual exchange processes, the neutral currents of Weinberg. These processes produce protons (p and p') of different energy levels; and two neutrinos (ν and ν') of different energy levels. ($\bar{\nu}$) represents the antineutrino, and (e-) the electron. In one state the proton will be bound to an atomic nucleus, and in the other state it will be relatively free in a chemical binding. Kervran reactions, or as they are sometimes called, biological weak transmutations, have been observed for the elements marked with an arrow in the Table of Elements. For example, the oxygen atom can (p. 51) enter into a virtual nuclear reaction with p or n to yield, ^{14}N, or ^{19}F. The normal flow of electrons in the terminal respiratory chain in the mitochondria will yield $2H + \frac{1}{2}O_2 \rightarrow H_2O$, an exergonic yield of energy. However, if this normal reaction is blocked by the chemical reaction, $^{1}_{1}H^{+}_{0} + {}^{16}_{8}O_8 \rightarrow OH^-$, there will be an increase of pH inside the mitochondrial as shown (p in the diagram. Such an increase in the pH inside the mitochondrial membrane can have profound effects on the electron flow and energy yield. We will take this topic up later.

We now describe our light microscopy studies of the organic matter that appeared in the sodium chloride solution energized by amplitude modulated carrier signals. As usual the solution and apparatus were sterilized, and vacuum pumped to remove the contaminating gases, nitrogen, carbon dioxide, and argon before the TD electrical field was applied. The microscope was a Wild research microscope with 100X planapochromat objective, and 32X bifocal eyepieces to give a maximum gain of 3200X at high resolution. I used the dark field method of illumination. Here is a (p 53 A) microphotograph of what a sterile solution of 0.9% sodium chloride looks like before it is electrolysed with the TD signal. It is surprising that the individual crystals of sodium chloride can be located as tiny doughnuts, or toroids, against the dark field.

Now here is what the sodium chloride solution looks like after three minutes of electrical energization at 50 mw. (p 53 B) This frame is a one second exposure. When one observes this scene with the eyeball one notes that the particles are flickering and oscillating. A critic would say that these eight-pointed light patterns are merely lense artefacts. When one uses a strobe light to stop the action it measures an oscillation of eight flashes per second. This effect occurs only in the early stages of electrolysis, and is not found later.

Eventually, I identified the molecule that was oscillating, but more of that later. In 1960 I was in Mexico with my friend Aldous Huxley and his wife Laura. In the course of a long discussion, I found that Laura practiced "laying on of hands" therapy. We arranged for a test of this alleged ability in Los Angeles, California on August 15, 1960 at the Sepulveda Veterans Hospital. Dr. Barbara Brown ran the electroencephalograph equipment. The design of the experiment was to see if Laura could exert any effect on a

patient with ventricular extra-systoles, and occasional mild cardiac fibrillation. The subject and the operator were both connected to the EEG machine with additional readouts for respiration, EKG, and skin resistance. Laura was not allowed to touch the patient, but merely bring her hands within a few inches of the patient. The main finding was that when Laura brought her hands within four inches of the patient's thoracic spine - Laura's EEG suddenly showed high amplitude 8 Hz waves, and at the same time the patient's brain waves were entrained at 8 Hz with phase locking. I might add that a five year follow-up showed that the patient had been cured of her cardiac problem. This experiment has since been repeated by many workers. [24] Thereafter, Joe Kamiya developed a teaching method so that people could train themselves to autogenically evoke (8 Hz) Alpha waves. [25] When the Soviets went on the air in July 4, 1976 with their 100 megawatt transmissions of extremely low frequency waves (ELF) the intelligence community of the U.S. was caught, unaware, of this new technology. The Soviet ELF pulses covered the frequency range of the human brain. No one knew what the purpose of this new technology was. I had a hypothesis that this was a new mind control weapon that could entrain a human being's EEG. Bob Beck and I designed an experiment that conclusively proved that the Soviet transmissions could indeed entrain the human brain, and thereby induce behavioural modification. I reported this finding to the intelligence community in the U.S., and my paper was promptly classified. [26] A CIA commission of inquiry reported to President Carter that there was no substance to our findings. Today, five years later, all of our findings have been confirmed by various agencies of the U.S. Government. However, they went one step beyond

our findings, and proved that a certain ELF frequency (3.21 Hz) will cause cancer.[27*] I have repeated these experiments, and found this to be true. The mechanism of this effect is that the ELF frequency modifies the function of DNA and of the RNA transferases so that amino acid sequences are scrambled and produce unnatural proteins. The ELF exerts its' effect on the atomic nuclear level, more specifically, the nuclear magnetic resonant property of the nucleus. The (p. 55) table shows the spin-spin coupling constants of various common chemical chains. Note the common chemical groupings with coupling constants around 8 Hz.[28] Note that a powerful carcinogen, ethylene dioxide, has coupling constants around 3 to 5 Hz. Note that another powerful carcinogen, formaldehyde, has a coupling constant around 41 Hz. Parrish, et al,[29] have found that the spin-spin coupling constants for water in malignant brain tumors (in humans and dogs) range from 4.8 to 13.4 Hz., whereas normal brain gray matter ranges from 8.6 Hz to 11.3 Hz. Thus malignancy shows a spread of frequencies from low to high ELF range i.e. with respect to normal brain EEG's, and carcinogens have a wide spread from 3 Hz to about 41 Hz around the center frequency for normalcy of 8 Hz. However, a single ELF frequency can produce cancer.

However, let us return to an examination of what we found in the electrically energized sodium chloride solution. (p. 53 (2)) Here again is the control - normal saline solution before electrical energization. Now the oscillating particles were entrained by the earth's natural oscillating magnetic field at 7.83 Hz (rounded off to 8 Hz). We determined eventually that the particle responsible for the oscillation was Ferrichrome, one of the strongest complex formers known for Fe (III).[30] The iron binding center is an octahedral arrangement of six oxygen donor atoms of trihydroxamate. (p. 56)

27*. SEE APPENDIX A for FEB. 24, 1984. Release of This information by the U.S. NAVY IN SCIENCE VOL. 223, p. 818-820. 24 Feb. 1984

Ferrichromes are most important in the biosynthetic pathways of very complex compounds of iron, and Vitamin B12 (cyanocobalamin) is shown in the lower part of the figure. The next slide shows material that is an aggregate of several cocci-like masses of a bluish-green hue. This picture was taken at the 18th minute of electrical energization. The next slide shows forms that have a high mobility looking very much like bacteria. The next slide shows the form that evolved after one hour of electrolysis. There was no further evolution of "cell" form after this form had been reached. At this point in my research, I remembered that highly active mitochondria take a form very much as shown in the last slide. Here, in this slide we have pictures of what mitochondria look under different conditions. [31] In the next slide we see that mitochondria can take an arboreal form when they go from the resting state to the active state. [32] I then remembered from my medical school days, when we studied the blood of syphilitic patients under the dark field microscope, that we occasionally saw pleiomorphic bacteria. When I asked my instructor what these were, I was told that they were just debris, and to forget it. So I now went back to the microscope, and began to study these pleiomorphic bacteria afresh. In the forty years since medical school days a whole literature had been built up around these lowly bodies. [31] I became convinced that what I now saw in the blood of patients, particularly those with cancer, was very similar to what I was seeing in my <u>in vitro</u> preparations.

My next step was to take these arboreal forms out of the TD cell, and place them on a microscope stage heated to 37° C. and nurture them with D-glucose 6-phosphate in 5% solution. In a matter of minutes, the branch-like forms were covered with little beads of yellow, orange, green and blue

have to be delivered to the proton of the COHN system which acts as a gating switch on the post-synaptic membrane.

The information to be transmitted, a 1 KHz sine wave, must reach the temporal lobe cortex without distortion, and be stored in such a way that a person can vocally mimic this sound at some later time. Such storage may occur in a single nerve cell's membrane surrounding glial cells and water shells (31). This would require domain formation (ferroelectric type) in which the proton magnetic moment poles are arranged in north pole and south pole regions (29). Access to this memory bank requires that the action potential pulse and the proton magnetic dipole interact to perform ELF FIELD functions of write-in; read-out; numerical functions; store; hold; search; erase; etc (8). The basic scheme of nature has the fixed hydrogen bond proton matrix scanned by travelling waves of electric AND ELF MAGNETIC pulses. The distinctive aspect of this scheme is that the protons form the storage, and hence the gestalt of the system; while input and output access is mediated by quantum electronic and photonic pulses.

We propose an extremely simple model and equivalent circuit of an unit element of the plasma membrane. This is shown in Figure 1. The EMF source is shown at the left and can represent any stimulus; the potential (DC) shown across the cathode-anode

(p.60 F.)

material.*_n The next slide shows the branched material (p.60 G.) beginning to clump and organize. At this point the morphology of the arboreal forms, and the metabolic events just cited, led me to entertain the hypothesis that I was dealing with a very primitive metabolic chemistry in which iron compounds like ferritin, ferrodoxin, and transferrins were serving as electron acceptors for electrons (H) arising from water. When I stopped the electrolysis of the saline solution, I found that the general reaction,

$$H_2O + A \xrightarrow[\text{energy}]{\text{electr.}} A\,H_2 + \tfrac{1}{2}O_2$$ ceased.

A represents the electron acceptor, and in this case is an iron compound, of the type just cited. An important feature of this Hill reaction is that electrons are induced to flow away from water molecules to acceptor A, thus yielding molecular oxygen from the water. In order to appreciate the meaning of this electrochemistry we see in the Table (p.61.) that in animal metabolism in the terminal respiratory chain electrons flow from the negative sign to the positive sign to produce water. [33] In the plant the electron flow is reversed and goes from the positive sign to the negative sign, a sort of uphill flow, electronically speaking. It occurred to me at this time that nature might have worked out a system to account for spontaneous cancer cures by reversing the flow of electrons in the mitochondrial terminal respiratory chain, and thereby producing more molecular oxygen to combat the cancer process. It also occurred to me that increased oxygen would tend to pull the proton/proton spin-spin coupling closer to the 8 Hz normative center frequency of biological systems. But I had no proof for these speculations. I did have some experience however

* These forms did not replicate after prolonged culture in various media. The reason is that I withheld sulfur from the solution in all my experiments.

in the clinical area from 1975 and on when I bought an (p. 62) ozone producing machine, the OZONOSAN PM 60, and did research on decubitus ulcers with Dr. Harry Beckman at the Veterans Hospital in Montrose, N.Y. We found that hyperoxygenation and ozone gas treatment cleared up chronic decubitis ulcers in a matter of weeks. In a sense, this experience with ozone prepared me for the next step, which was a meeting with Migdalia Arnan, M.D., a Board Certified Pathologist, and her colleagues.

I will briefly summarize her main findings, because her paper will follow mine. Dr. Arnan found that a normal human cell, when immersed in formaldehyde gas, converts to a cancer cell in a few minutes. She then found that a human cancer cell if irradiated with intense white light under a microscope would undergo a (thermal) death in twelve minutes. She then discovered, under bright light microscope illumination, that unstained human cancer cells, (p. 66) as seen in the next slide, had pale green bodies in the cytoplasm about the size of mitochondria. It was at this point that we both gave a "Eureka" yell, and realized that her clinical discoveries, and my electrical and chemical investigations clarified each other. Furthermore, she and her colleagues had proven that if ozone gas is administered directly into a malignant tumor in mice, the tumor would dissolve in a matter of seconds to minutes and leave the normal surrounding tissue unaffected.

It is not yet generally recognized in the biological sciences that all life is immersed in an oscillating magnetic field that originates from protons in the sun. The slide (p. 63) shows the magnetic oscillations from the sun.[34] These ELF waves have a sharp resonance on earth due to cavity resonances, peaking at 7.81 to 7.83 Hz. This is the center frequency of the electromagnetic power spectrum of the human brain, the so-called Alpha frequency, of 8 Hz. We have already indicated that a "healthy" ELF center frequency exists for proton-proton spin-spin coupling in the chemistry of the body,

particularily in such control functions as genes and enyzymes for DNA and RNA. We have indicated that certain ELF frequencies at extremely low power, can induce cancer. I might add that the amount of power required to induce cancer at the correct ELF stimulus is measured in the range of microwatts. In short, ELF frequencies at **super** low power levels can control the well-being of organisms.

Now what happens when an organism is deeply insulted by chemicals, injury, or amputation? Let us take the most extreme case, i.e., amputation of a limb in a salamander. Robert Becker, M.D. has shown that the salamander limb can be regenerated if certain procedures are followed. [35] First, a skin flap of epidermis only (no dermal tissue allowed) is placed over the stump. Under this epidermal flap it has been found that regeneration occurs when red blood cells in the wound site undergo de-differentiation, i.e. revert to very primitive cells, the blastema. The figure shows red (p.64,65) blood cells in their earliest stage when they still have a nucleus. [36] Such an early RBC form is what a de-differentiated cell looks like. Note the way in which such a cell takes up Iron transferrin and feeds it to the mitochondria.

My evidence indicates that the pleiomorphs found in the blood in association with cancer, as first reported by J.F. Glover, M.D. in Canada in 1923, [37] and verified by many workers subsequently, are in fact mitochondrial fragments from de-differentiated red blood cells that are released in response to the insult of cancer. These pleiomorphs carry a type of transferrin (not yet identified) that serve two functions. The first, as recently reported, by Goubin, et al, [38] in Nature, vol. 302, 10 March 1983, shows that the nucleotide sequence of a cloned transforming gene, that induces cancer in chickens, suggests that it encodes a

protein that is partially homologous to the amino acid terminus of transferrin and related proteins, although it is only about one-tenth the size of transferrin. The second function of this type of transferrin, I believe, is to reverse the electron flow in the mitochondria by changing one of the heme molecules into a chlorophyll type of molecule. The purpose of nature in this electron flow reversal is to electrolyze water in order to produce more oxygen to swing to local ELF frequency toward 8 Hz using both the Kervran nuclear transmutation mechanism, and the known effect of oxygen to lower the NMR spin-spin coupling of a solution.

The findings of Dr. Arnan also show that the mitochondrium is not only transformed in the reversal of electron flow, but actually produces Quantasomes, the chlorophyll bearing bodies of plants, as shown in one of her electron micrographs. (p.66) This is a Quantasome found in a human cancer cell and accounts for the pale green bodies easily found in human cancer cells, if one just looks, and is not color blind. Now how does this theoretical mechanism account for the efficacy of ozone in the treatment of cancer tumors?

The analysis begins with an understanding of skin and membrane properties. One begins with square wave electrical spectroscopy according to the method shown in the slide. (p.67) This yields various decay curves for voltage and current as shown in the next two figures. One also plots the impedance (p.70) locus of the skin which shows loci for ELF, and for kilohertz frequencies. From this data one develops equivalent circuits for the various configurations of signal used on the skin, membranes, and water. A typical equivalent circuit for nerve is shown in Fig. 1A which also holds for the skin in (p.25) the ELF range. Our studies, as well as that of others shows

that the water molecule has the tetrahedral form as shown. (p.72.) The equivalent circuit for the water molecule is shown (p.73) in Fig. 22. Von Hippel and others have established that the water molecule has a dielectric resonance in the 8 Hz range.[39] The importance of water in biological structure and function is well known. Suppose that one were to substitute a molecule that mimicked the water molecule, for the true water molecule? We don't really know what would happen because there is nothing known quite like a water molecule. But I have a proposal to make. If one looks at the last figure, and conceives that ozone could actually have a tetrahedral form (and no one knows its true form) what would it behave like? The only change required is to substitute the Hydrogen atoms with O^+ atoms. The net effect of this ozone geometry would be to reverse the polarity of the EMF source at the left, and the polarity of the ferroelectric capacitor on the right, and reverse the diode so that the P semiconductor would face the capacitor. The circuit would now reverse the electron flow. In addition the ozone tetrahedron would have far more oxidizing power than water. Thus ozone would behave in the following manner as a therapeutic agent:

1) It would easily substitute for water in terms of geometrical fit into any biological structure. Wherever water would fit, ozone would fit.
2) Ozone would seek out the H_2 molecule by the following reaction: $H_2 + O_3 \longrightarrow H_2O + O_2^-$

This is a powerful exergonic reaction which would not only be a bond breaker, but release enough heat at the molecular level to melt the altered conformational states of proteins, oncogenes and various go/no go genetic switches.

I have tested this possibility, in the late sixties, while doing safety and hazard studies of the TD system on dogs. I used old and sick dogs in some of my studies, and some of them had surface malignant tumors. The procedure was as follows: In running high voltage hazard studies on animals I observed in a very dark room (a Faraday Cage) that a bluish plasma glowed between the electrode face and the skin. I could also smell ozone in the air. This effect occurred at 1100 volts (p-p) and 11 mA (rms) current. I found that I could tolerate this level of signal on myself without any discomfort, and the dogs could tolerate this signal after some training. I treated three dogs that had malignant tumors under the skin one hour a day for three weeks with this high voltage ozone-generating signal. There was no damage to the skin of the dog, and the tumors melted away under the skin during the three weeks. Others have repeated this type of radio frequency treatment of malignant tumors, subsequently.[40]

SUMMARY

We have presented a theory of a probable cause of cancer supported by some fragmentary experimental evidence. There are many further tests that can be made of the theory. I must emphasize that this is only a preliminary formulation. The theory, both empirically and experimentally led from separate sources to a rational therapy for malignant neoplasms in animals. The essence of the theory is that nuclear spin properties form an integrating topology for the development of chemical evolution centered on proton-proton spin-spin coupling in water. It is well to recall

here that the human body is made up of some two thirds, by mass, of water. It is also well to recall that the human body is made up, by count, 92%,of hydrogen atoms. The dynamics of hydrogen and oxygen are of great importance in the structure and function of the human body. For example, if the brain is deprived of oxygen for several minutes, the person will not only become unconscious, but permanent damage may result in the organization of the brain at a molecular level. There is another disintegrative pathology called "cardiac fibrillation" wherein the individual myocardial fibrils suddenly cease to beat in synchrony, and death can result within five minutes, if the condition is not normalized. A topological theory has been advanced by Winfree which shows that tiny electrical pulses intercalated at a precise phase angle in the normal heart natural period, called a topological singularity, or a "black hole", is sufficient to initiate fibrillation of the heart. [41] In NMR there is a spin echo technique called the "magic sandwich" in which certain magnetic and radio frequency phase cancellation operations are carried out in an orthonormal sequence, and a phase coherence in the spin system that appears to be lost, is restored. [42] This experiment, carried out with Calcium Fluoride (with the ^{19}F isotope) has the uncanny property of reversing the Hamiltonian in the equations, which is equivalent to making the time flow backwards at half the normal speed. See Appendix B. This is a situation where the Kervran transmutation from $^{16}_{8}O_{8}$ to $^{19}_{9}F_{10}$ can place this form of fluorine at a critical point in the mitochondrial apparatus and cause time to flow backwards: or in other words, reverse the flow of electrons in time, as positrons. [43] These are some of the possibilities of the theory. We can now summarize the main points by reference to the graphic display.

An electrical signal generator was developed which proved to have rehabilitative effects on humans. The same signal pattern proved to be efficient in the electrolysis of sodium chloride solutions. A by-product of such electrolysis was a new insight into the dynamics of chemical evolution leading to organism. These insights were applied to the problems of cancer cause and control. These insights were sharpened by the experimental work of Dr. Arnan and her colleagues, in controlling and dissolving mammary neoplasms in female mice by injecting O_2^- and O_3 gas into the tumors. This theoretical and experimental work pointed to the disruption of ELF NMR proton spin-spin coupling mechanisms as a probable cause of some types of cancer. This probable mechanism is summarized in the flow chart, and the top line shows the ELF range of such coupling constants. Many considerations indicate that 8 Hz is <u>the</u> center frequency that "pulls" all other frequencies toward it, to maintain biological organizational integrity. Such biological integrity can be quantized by reference to an arbitrary rate of cell division scale, pointing from left to right on line two. On the left is shown the well-known fact that deuterated water, 27% concentration, or higher, will stop all cell division in many species.[44] When the deuterated water is removed from the cell suspension - the cells resume normal cell division. This type of control is exerted, in general, by elements as shown, with spin 1, and a positive magnetic moment.

(p.20) Fig.

In the center column we list those stabilizing elements with Spin ½, and magnetic moment, μ, having a positive multiple of 0.4 Bohr magnetons, and these are elements with odd number mass; or of even number mass, Spin 0, and $\mu = 0$. We have indicated that DNA and RNA transferases can be disorganized by microwatt levels of magnetic ELF radiation. It is theorized that such ELF waves affect the DNA and RNA transferases at a precise phase angle that triggers a topological singularity.

The column above this line shows some of the many possible pre-conditions which essentially disperse the gaussian distribution around the power spectrum center frequency of 8 Hz., and this effect in turn, stimulates the rate of cell division locally, and may then later manifest as cancer. The dispersive mechanism originally acts to trigger the release of iron compounds from the red blood cell membrane due to altered amino acid sequences in both the cell wall, and the iron compounds. This in turn triggers red blood cell de-differentiation (backward in time) to a primitive stage of evolution. In this primitive stage, which we associate with the mitochondrial fragment "pleiomorphs" found in the blood of some cancer patients, the normal mammalian electron flow in the mitochondrial terminal respiratory chain is reversed, so that it flows in the direction found in plant cells. This effect is triggered and fed by a Hill reaction in which the electron acceptor molecules are iron compounds. Chlorophyll and quantasomes then appear in the cytoplasm of cancer cells. The correct dose of ozone gas easily substitutes for water molecules in the "plant-like" terminal respiratory chain, and releases both oxidative the thermal effects which dissolve the neoplastic-forming molecules, and restores the normal respiratory electon flow in the normal tissue surrounding the neoplasms. This process re-integrates the atoms and molecules around the 8 Hz center frequency ELF NMR.
In its essence this is a theory of nuclear control of cell division processes operating through spin properties, and nuclear magnetic resonant fields in the extremely low frequency range.

Figure 1

ELF NMR Spin-Spin COUPLING FREQUENCY SCALE

-64 Hz	-32 Hz	-16 Hz	0 Hz	8.00 Hz	16 Hz	32 Hz	64 Hz

Direction of increasing rate of Cell Division ⟶

Factors that Decrease Cell Div.

When cells are placed in H_2O suspensions that contain 27% $^2_1H_1$ or more, of deuterated water, cell division stops, reversibly.

$^2_1H_1$ = Spin I = 1, μ = 0.85

$^{14}_7N_7$ = Spin I = 1, μ = 0.40

$^6_3Li_3$ = Spin I = 1, μ = 0.82

Nitrogen acts as an anesthetic, and Lithium is a cell depressant.

normal

STABILIZING ELEMENTS

$^1_1H_0$ = I = ½, μ = 2.79, and all elements with spin ½, or integral ½ spins with odd number mass and μ = 0; or with spin 0 and even number mass.

All proton-proton, spin-spin coupling energies pull toward 8 Hz.

RNA transferases

Tetrahedral forms of H_2O

OZONE TREATMENT: ⟶

Normal Terminal Respiratory Chain electron flow restored, as well as normal rate of cell division.

Factors that increase Cell Div. and may lead to cancer.

Genetic susceptibly
Chemical Pollution
- Industrial
- Automobile emissions
- Cigarette smoking
- Food Additives
- Water pollution

Ionizing radiation
ELF radiation
Geographic soil factors
Nutrition
Trace elements deficiency
Viruses
Cosmic ray flux
Neutrino flux
Telluric ELF
Weak transmutations

ABNORMAL: All proton-proton spin-spin couplings pull away from 8 Hz + or -

⟶ Topological Singularity initiating local desynchronization.

ABNORMAL

Polypeptide and protein transcription errors leading to - RBC de-differentiation, and increasing Iron losses of:
- Ferritin
- Ferredoxin
- Transferrins

Changing electron flow (reversal), and producing:
- Chlorophyll
- Quantasomes

Initiating photosynthesis by the Hill reaction,

$H_2O \longrightarrow H_2 + \frac{1}{2}O_2$

$CO_2 + 2H_2 \longrightarrow H_2CO + \frac{1}{2}O_2$

$(H_2CO)_n \longrightarrow$ Hexoses

FLOW CHART RELATING NUCLEAR SPIN PROPERTIES, MAGNETIC MOMENT PROPERTIES TO THE RATE OF CELL DIVISION, AND TO ELF NMR COUPLING ENERGIES

plates is determined by the polarized state of the dipoles; and its current flow by the depolarization release of potassium and sodium ions from the lattice structure of the plasma membrane. In the resting state of the nerve, the ferroelectric capacitor, C_o is charged to a constant voltage, V, and the charge ,Q, on the capacitor $=C_oV$. All linear current flow in the system is through the conducting fluids on both sides of the plasma membrane. However, the plasma membrane, on its outer surface, is covered by a coating made up of lipoid-protein layers. Conduction through this protein material is non-linear, and is represented by the C=O :H:N element shown as a semiconductor in Figure 2.

It is postulated that nerve stimulation , or depolarization will only occur by a decrease in the capacitance of the ferroelectric capacitor, and this is fundamentally dependent on the dielectric polarizibility, ϵ_α of the plasma membrane. ϵ_α, is dependent on the electronegativity of the neutral bound atoms of the plasma membrane, and can be lowered by DC biassing, by the choice of AC frequency, by pressure (strain) effects, by change in chemical composition, hydration, hydrolysis, thermal variations, etc. We will illustrate this triggering condition with the not-so-obvious case of thermal fluctuation stimulation. We assume that there is a Curie temperature, T_c, transition point, at 38°C.

P	Atom	N	I	μ	μ	P	Atom	N	I
1	* H	0	½	2.79	* -1.91	0	n	1	½
1	H	1	1	0.85	0	2	He	2	0
3	* Li	3	1	0.82	-1.17	4	Be	5	3/2
5	* B	5	3	1.80	0	6	*C	6	0
7	* N	7	1	0.40	0	8	*O	8	0
9	* F	10	½	2.628	0	10	Ne	10	0
11	* Na	12	3/2	2.21	0	12	*Mg	12	0
13	* Al	14	5/2	3.64	0	14	*Si	14	0
15	* P	16	½	1.13	0	16	*S	16	0
17	* Cl	18	3/2	0.82	0	18	Ar	22	0
19	* K	20	3/2	0.39	0	20	*Ca	20	0
21	Sc	22	7/2	4.52	-0.788	22	Ti	25	5/2
23	* V	28	7/2	5.14	-0.474	24	*Cr	28	3/2
25	* Mn	30	5/2	3.46	+0.090	26	*Fe	31	½
27	* Co	32	7/2	4.65	±0.75	28	*Ni	33	3/2
29	* Cu	34	3/2	2.22	+0.875	30	*Zn	37	5/2
53	* I	74	5/2	2.80	-0.776	54	Xe	75	½
83	Bi	126	9/2	4.08	0	84	Po	125	½

TABLE 1. COMPLEMENTARY PHYSIOLOGICAL PAIRS OF ELEMENTS RANKED BY PROTON NUMBERS.
(SOURCE OF DATA, REF. 11) Handbook of Physics, Condon.

P = PROTON NUMBER

ATOM = SYMBOL OF ELEMENT

N = NEUTRON NUMBER

μ = BOHR NUCLEAR MAGNETON NUMBER , I = SPIN

I = SPIN , $h/2\pi$

* = ESSENTIAL TO LIFE

The Respiratory chain of mitochondria in which the electron flow proceeds in the direction of NADH to oxygen. See below.

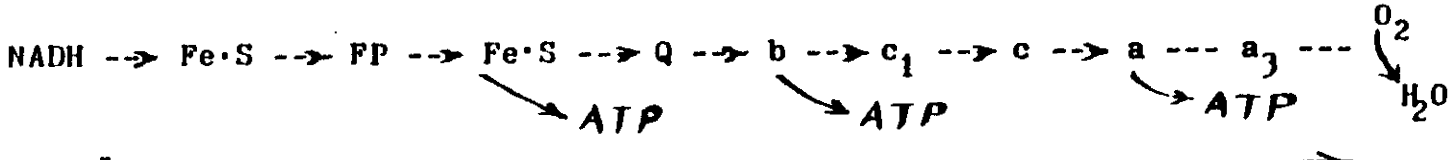

The photosynthetic electron transport chain, showing the flow of electrons from H_2O to $NADP^+$ via a sequence of electron carriers. See Key. See below.

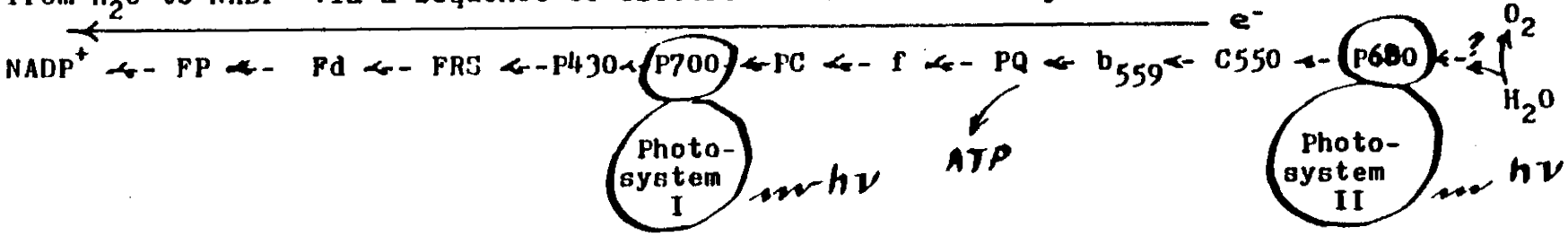

Key:

c_{550} = cytochrome c_{550}

b_{559} = cytochrome b_{559}

PQ = plastoquinone

f = cytochrome f

PC = plastocyanin

P430 = Pigment 430

FRS = Ferredoxin-reducing substance

NADH = nicotinamide adenine dinucleotide, reduced form.

Fd = ferredoxin

FP = Ferredoxin-$NADP^+$

F·S = Ferrosulfate

Q = Quinone

c_x = cytochromes

ATP = Adenosine Tri-Phosphate

$NADP^+$ = nicotinamide adenine dinucleotide phosphate, oxidized form

$h\nu$ = photon

Figure 4.

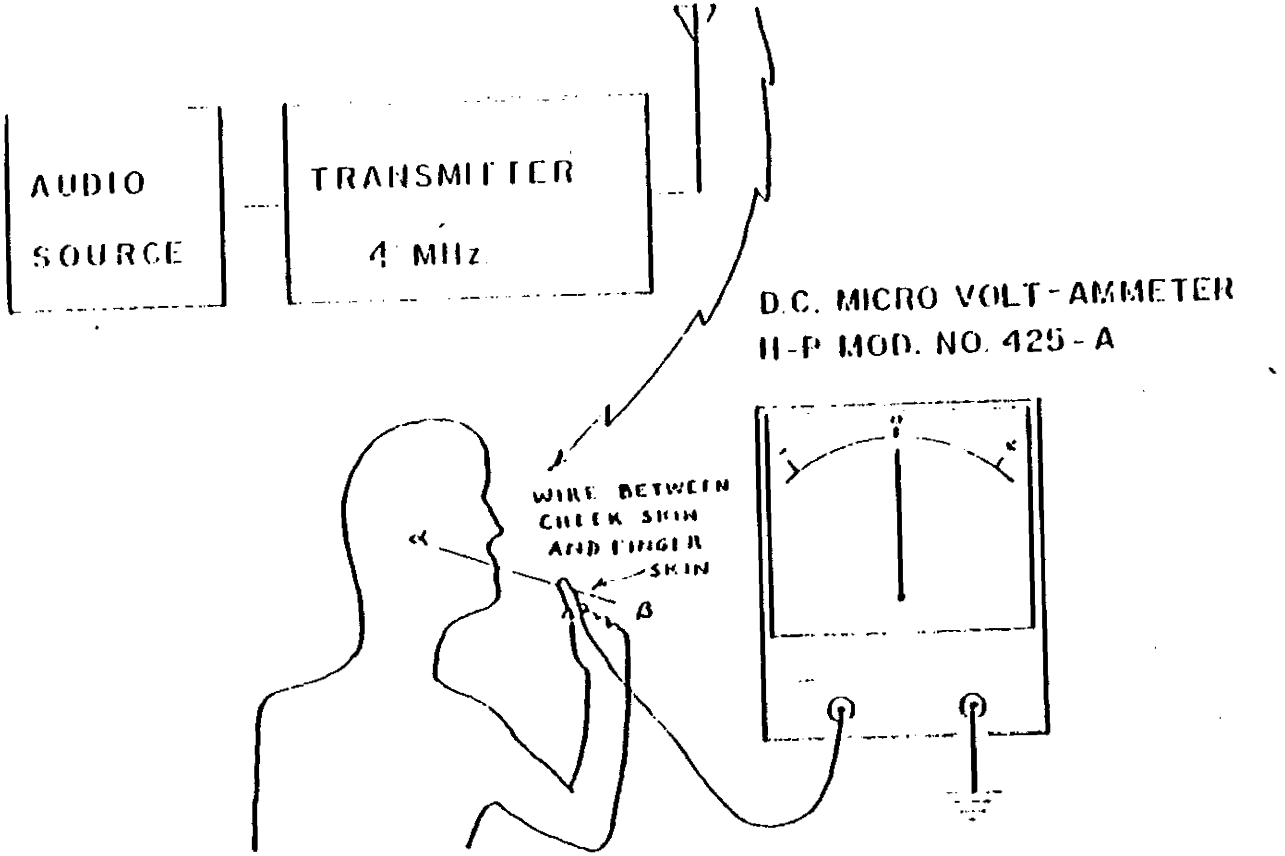

FIG. 46. MEASUREMENT OF DC SKIN POTENTIAL IN SHIELDED ROOM. RANGE OF DC OBSERVED IN 25 SUBJECTS.

1. WITHOUT RF FIELD: -60.5 mv TO +59.5 mv. (STATIONARY FINGER)
2. WITH RF FIELD: +200mv FOR ALL SUBJECTS (STATIONARY FINGER)
3. WITH RF FIELD: +200 → +250 mv WITH EACH STROKE OF FINGER ON WIRE WHEN HEARING OCCURS WITH EACH STROKE OF FINGER ON WIRE.

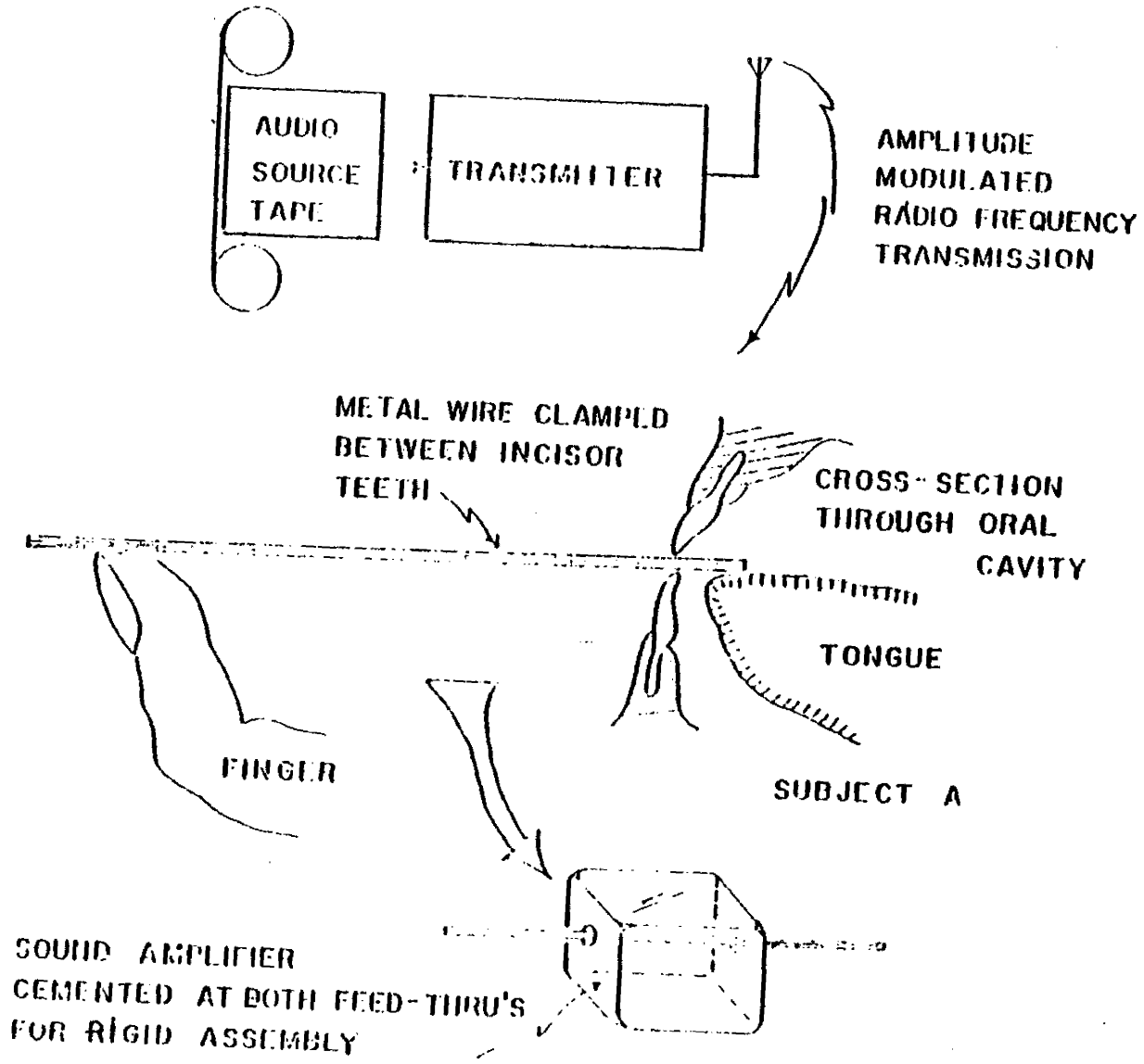

FIG. 44. RADIO FREQUENCY STIMULATION OF HEARING WITH WIRE MODEL.

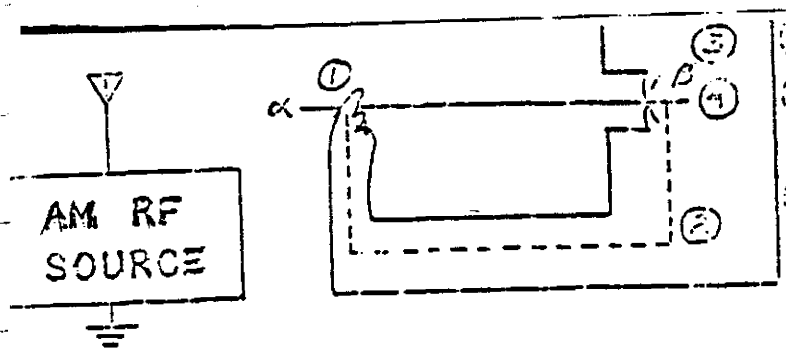

(1) FINGER-STROKING AT α
(2) POSITIVE FEEDBACK THROUGH BODY.
(3) TRANSDUCTION AT β
(4) TISSUE AT β END.

A. PHYSICAL RELATIONSHIPS IN SKIN-STROKING OF WIRE

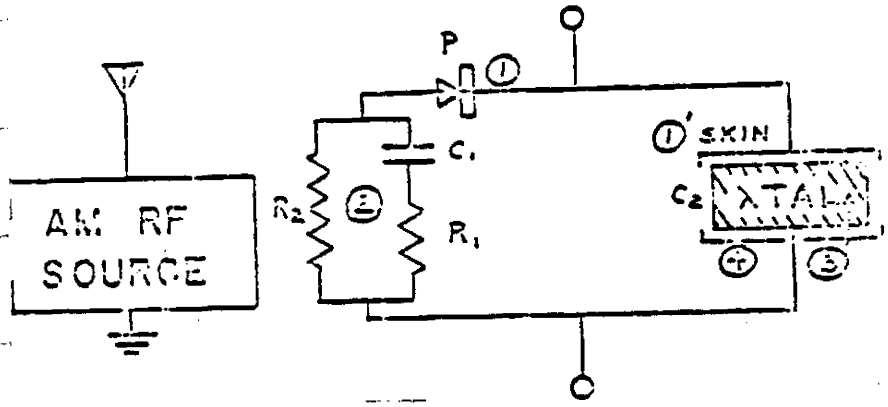

(1) DETECTOR: DIODE.
(1') P DONOR
(2) RC TISSUE NETWORK.
(3) PULSE GENERATOR: PZT
C_2 SPACE CHARGE REGION.
(4) P ACCEPTOR

B. MODEL OF SKIN-STROKING

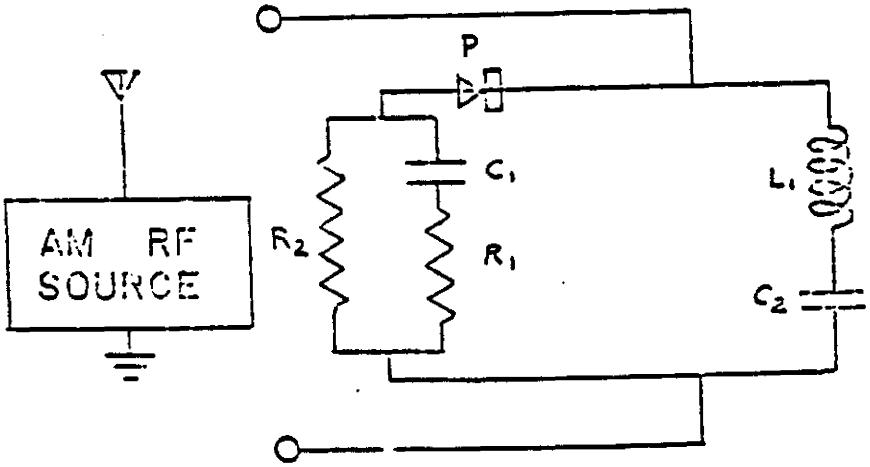

P = NON-LINEAR ELEMENT
R_1, C_1 = RELAXATION OSCILLATOR
L_1, C_2 = PULSE GENERATOR (EQUIVALENT CIRCUIT)

C. EQUIVALENT CIRCUIT OF SKIN-STROKING MODEL.

FIG. 47. MODEL FOR HEARING RADIO WAVES BY SKIN-STROKING, AND

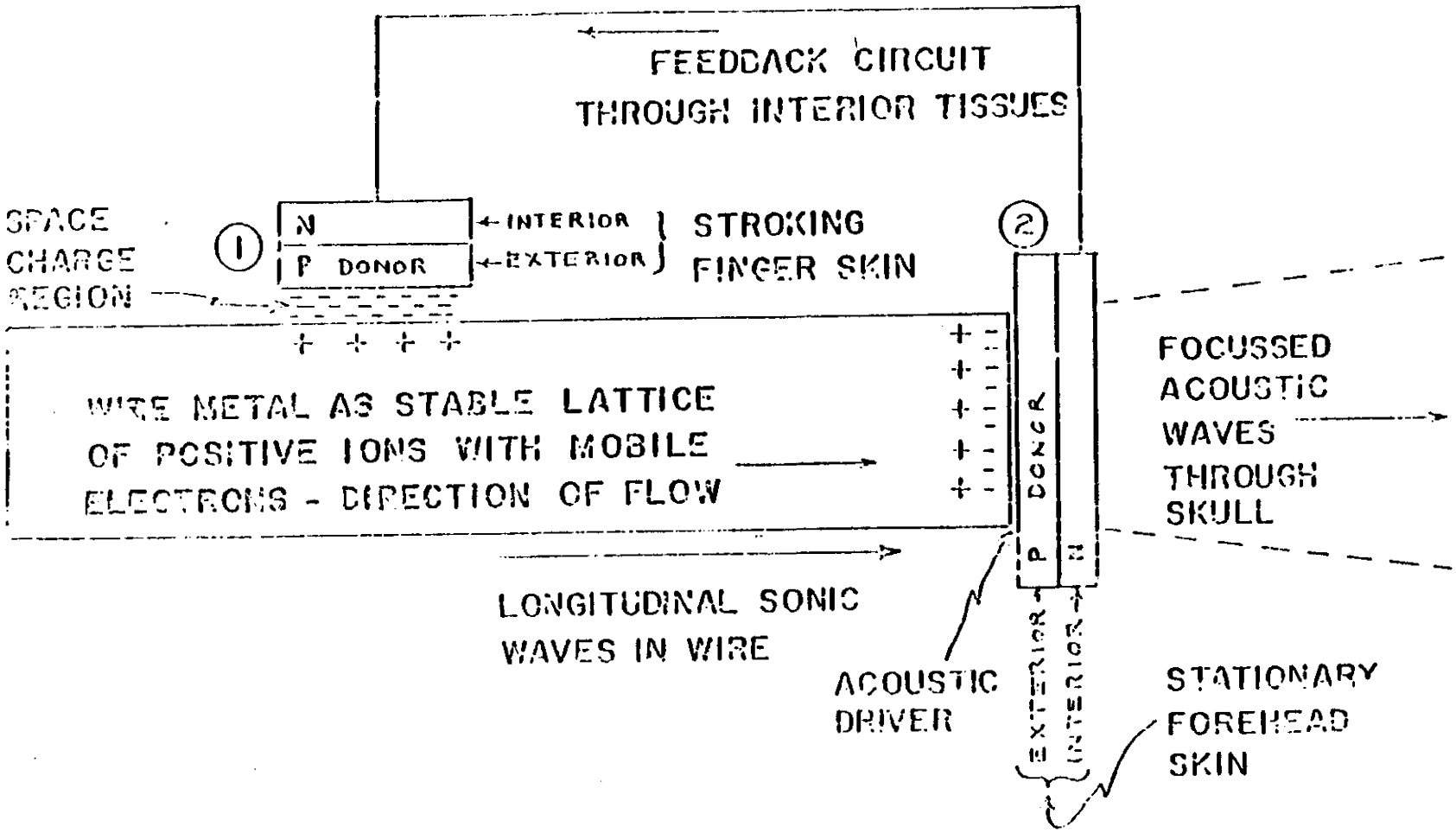

FIG. 45. WORKING HYPOTHESIS TO EXPLAIN HEARING BY "FINGER STROKING OF A WIRE" PRODUCING A FOCUSSED NARROW ACOUSTIC BEAM.

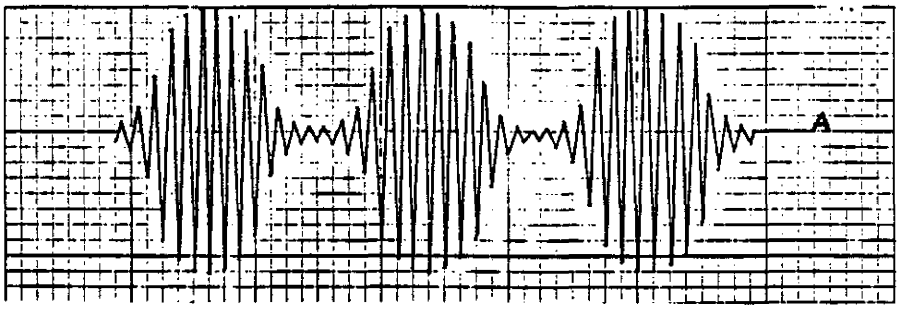

Figure 1A - Case IA.

One KHz AM carrier signal input across head. Bare metal electrodes stationary on skin. The same input and output signal is observed for Case II.

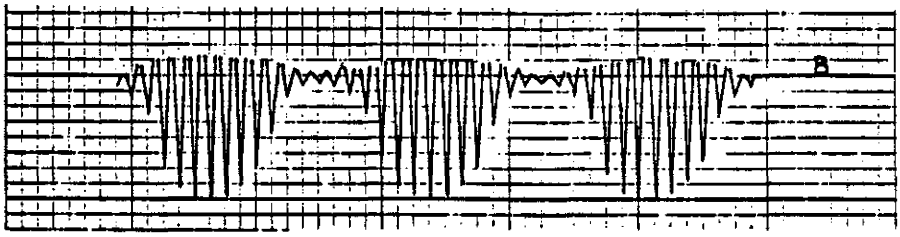

Figure 1B - Case IB.

TD input signal as shown in Figure 1A. Bare metal electrodes stroked on skin across head. Output is full half-wave rectification of 1 KHz AM carrier signal.

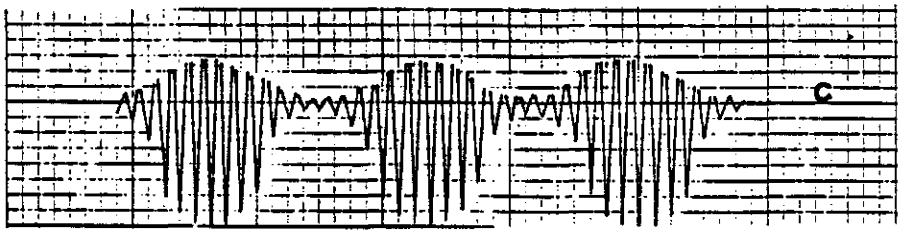

TD input signal as shown in Figure 1A. One bare metal electrode and one mylar covered electrode stationary on skin across head. Output is partial half-wave rectification of 1 KHz AM carrier signal.

FIG 3. EFFECTS OF HEAD TISSUES ON TD SIGNAL WAVE FORMS WITH VARIOUS ELECTRODE CONFIGURATIONS

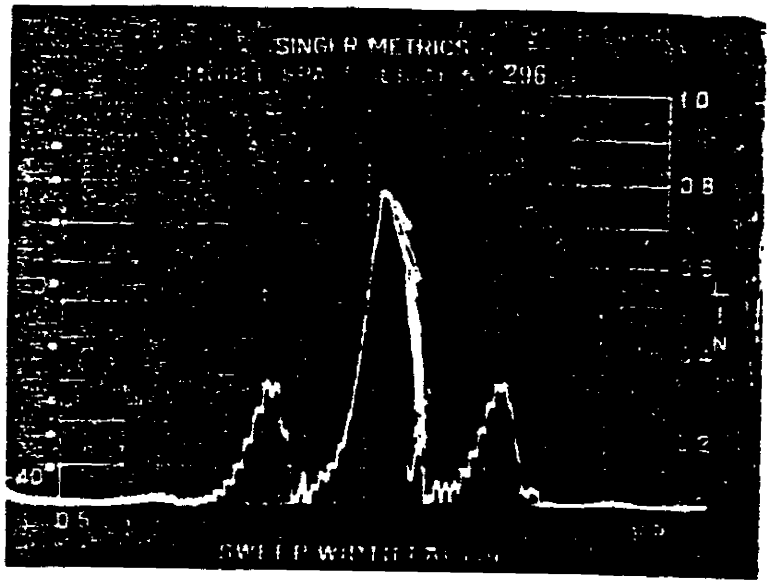

A. FIGURE SHOWING SINGLE SWEEP.

TRANSDERMAL HEARING SYSTEM
AMPLITUDE MODULATION, CASE II.
50 KHz CARRIER - 150 V (p-p) 10 m A.
1 KHz SINE MODULATION

SPECTRUM ANALYSER
50 KHz CENTER FREQUENCY
5 KHz BANDWIDTH SWEEP
100 DB ATTENUATION

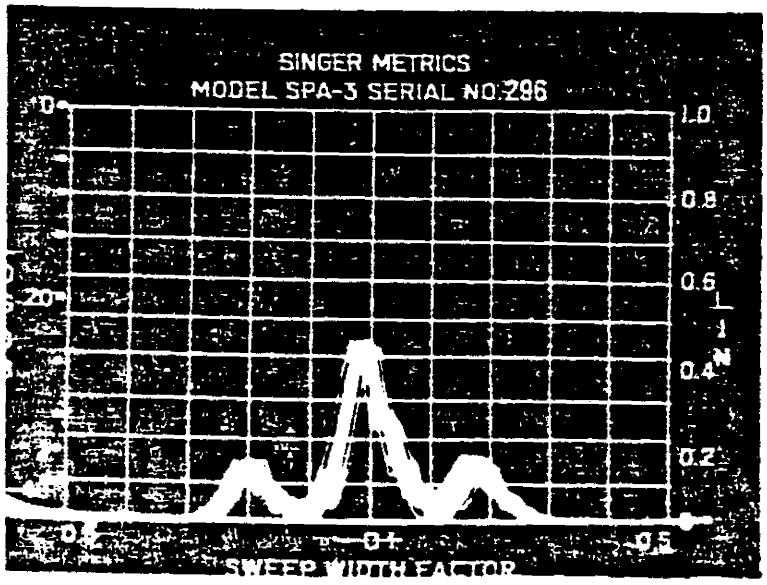

B. FIGURE SHOWING REPETITIVE SWEEPS.

FIG. 42. POWER SPECTRUM OF TD SYSTEM OUTPUT

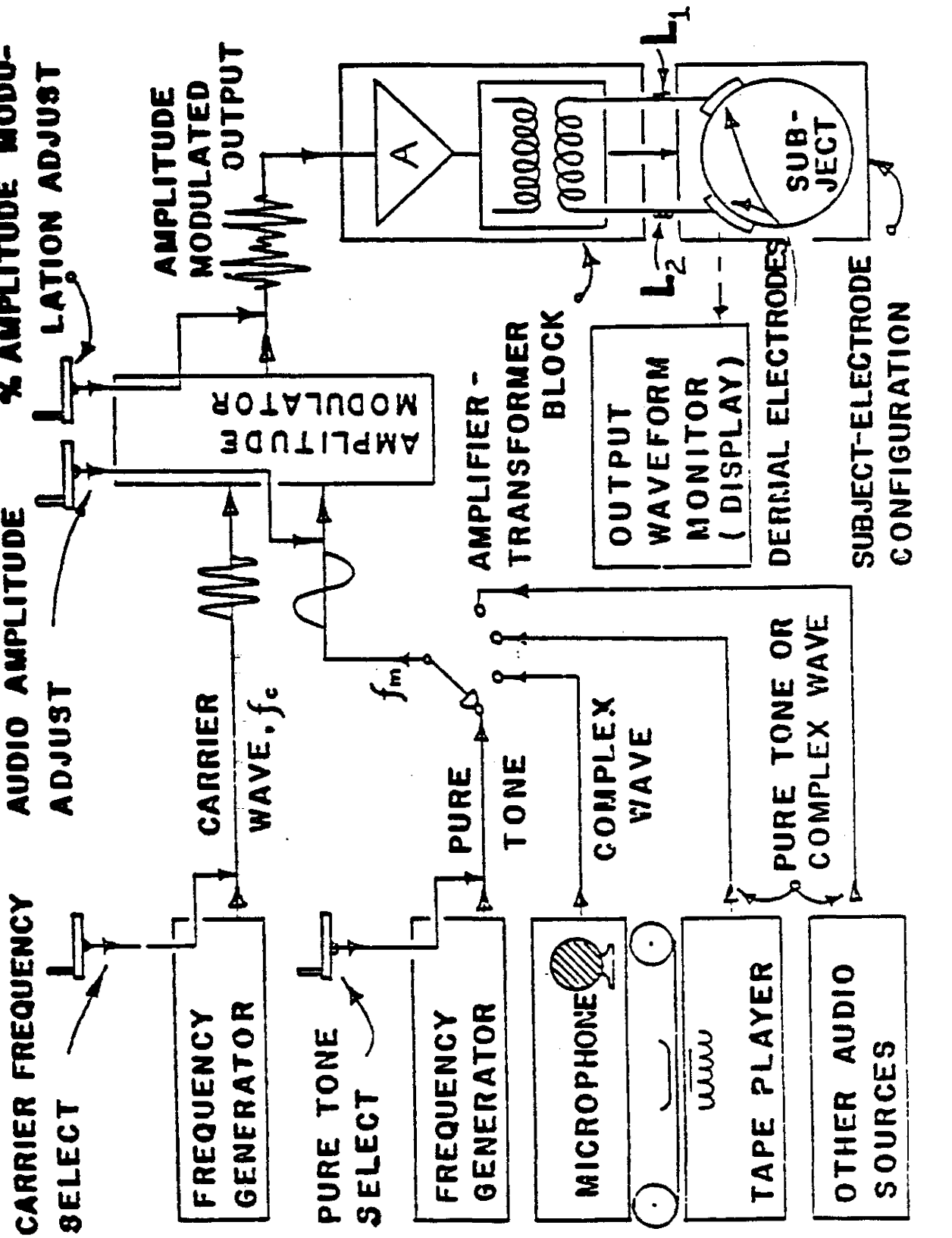

FIG. 4. MANUAL TRANSDERMAL AMRF SYSTEM BLOCK DIAGRAM

THE INTELECTRON MODEL TD-100
PROFESSIONAL TRANSDERMAL THERAPY INSTRUMENT

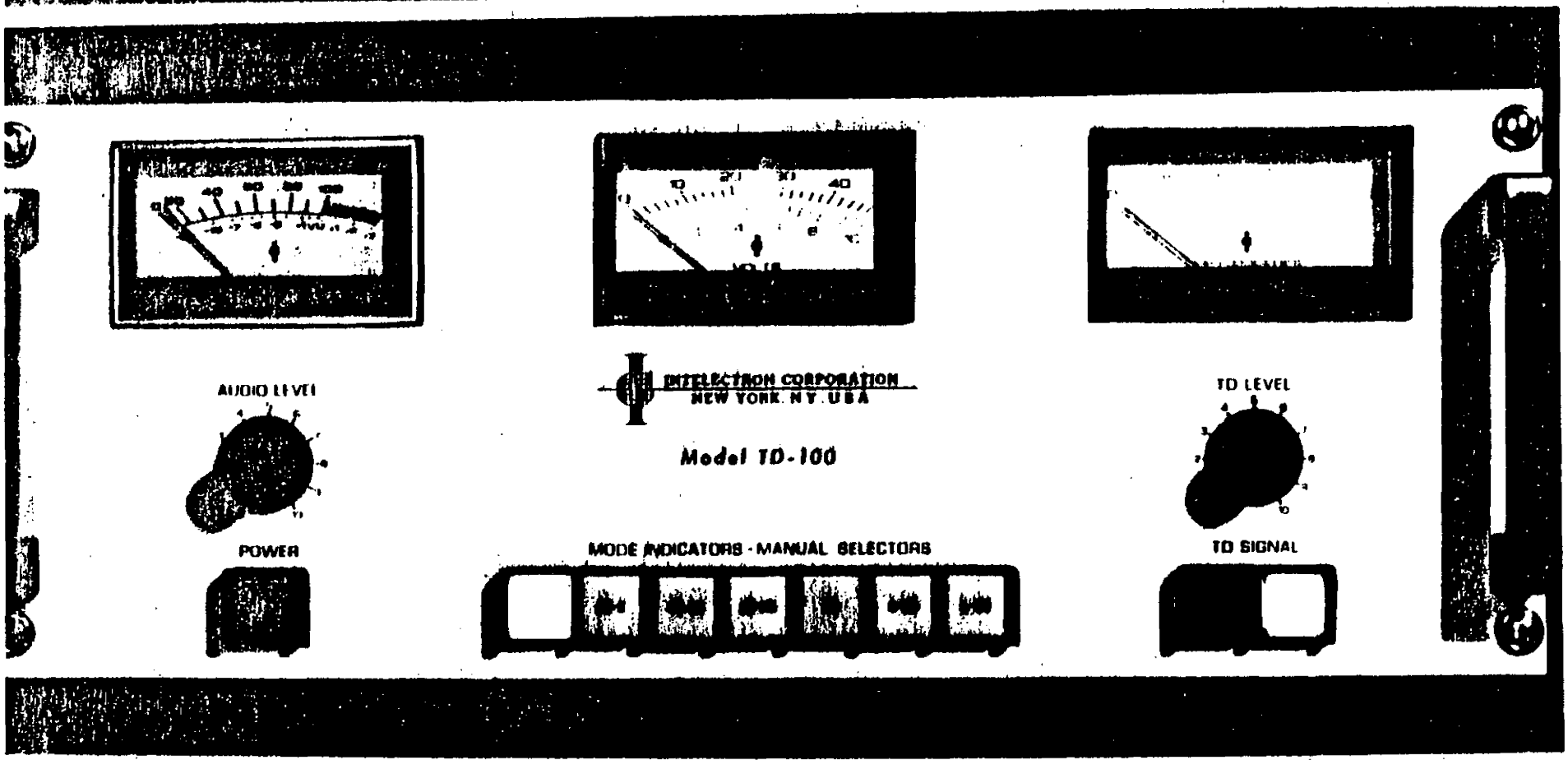

A temperature change above or below T_c, will decrease the capacitance and this will cause a current to flow to the load, since current flow through the EMF source is blocked by the non-linear semiconductor element. The capacitive discharge will in itself generate additional heat, and this represents part of the positive heat observed during the action potential phase of nerve firing. It has been observed in nerve firing that the positive heat phase is followed at times by negative heat, or absorption cooling effects. Thus the thermal cycle is completed by an increase in capacitance, causing a reverse flow of current through the load from the EMF source establishing the original charge on the capacitor. The net result is an AC output.

4. ARTIFICIAL SENSE PERCEPTION

My colleague, J.L. Lawrence, and I invented and developed an electronic system which makes it possible for a totally deaf person to hear speech sounds by Direct Brain Perception (DBP) using as stimulus to the brain an amplitude modulated alternating current carrier signal (AMAC) (65).

The AMAC signal is applied to the dry neck skin below the mastoid areas bilaterally via gold plated circular electrodes. This placement directs the AMAC signal to the brain stem region (56). The deaf patient requires several weeks of electronic signal conditioning of such tissues with audio frequency band pure tone

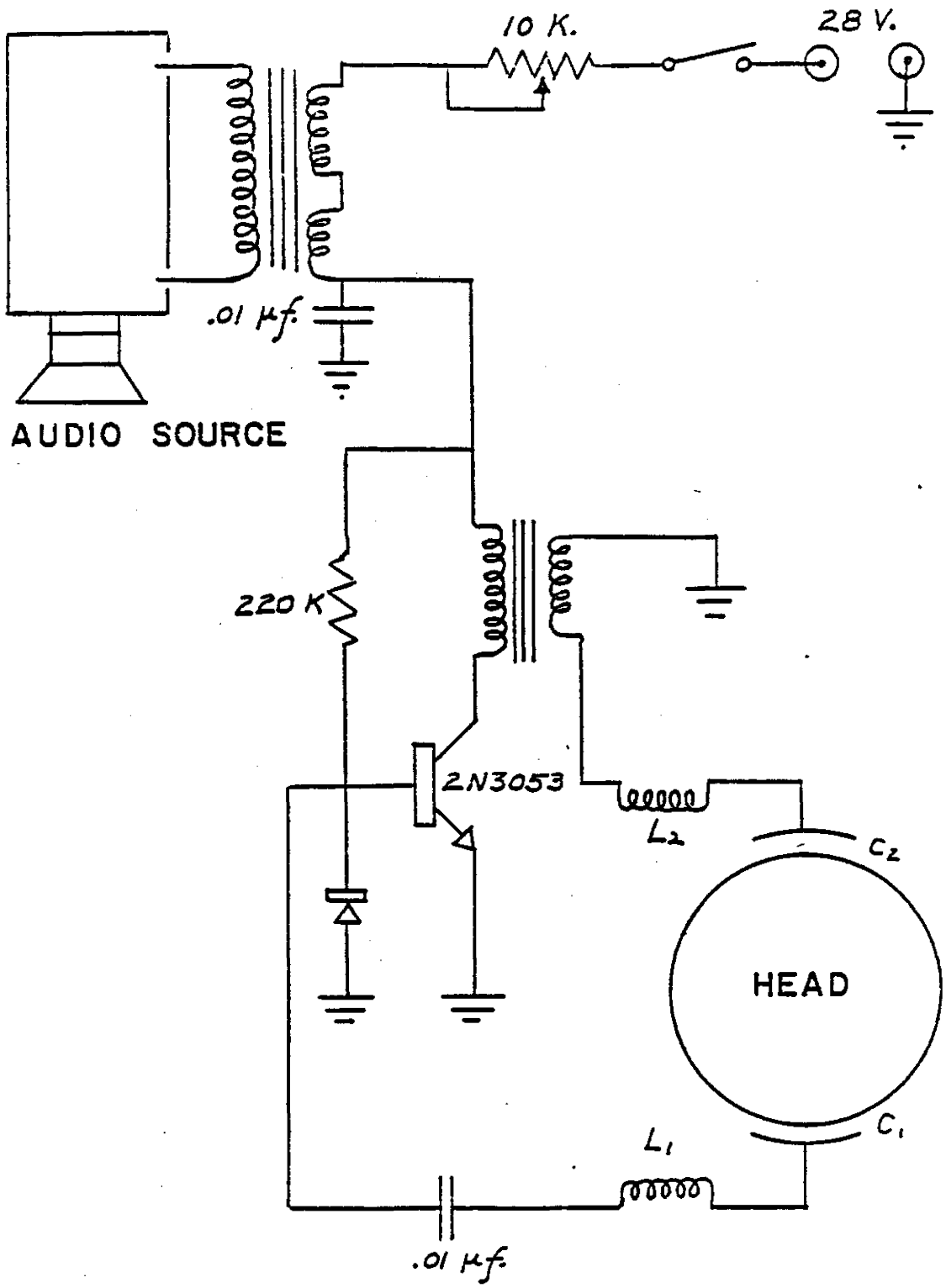

FIG. 5. TRANSDERMAL SYSTEM SIGNAL GENERATOR WITH AUTOMATIC RESONANT CARRIER FREQUENCY CONTROL

FIG. 3

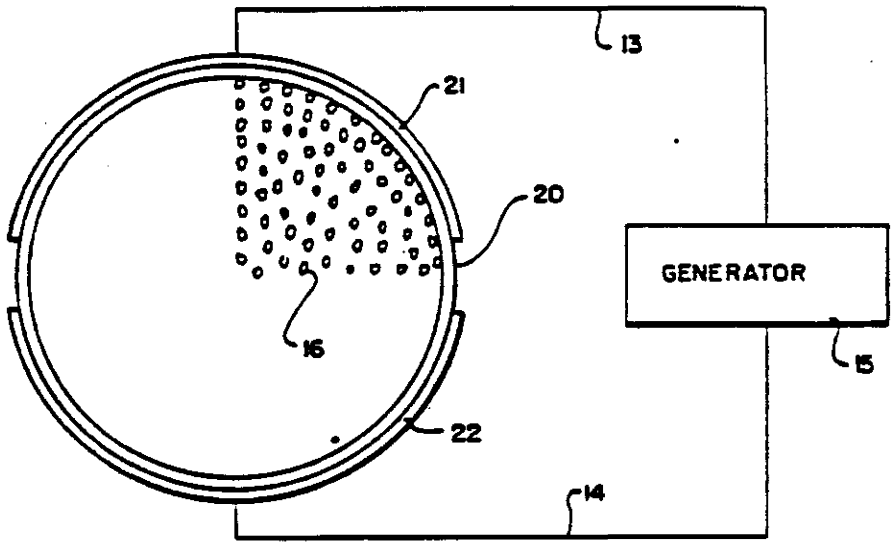

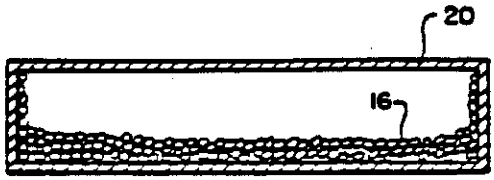

FIG. 4

INVENTOR
HENRY K. PUHARICH

BY Mandeville & Schweitzer
ATTORNEYS

Aug. 8, 1961 H. K. PUHARICH ET AL 2,995,633
MEANS FOR AIDING HEARING
Filed Sept. 25, 1958 2 Sheets-Sheet 2

FIG. 2

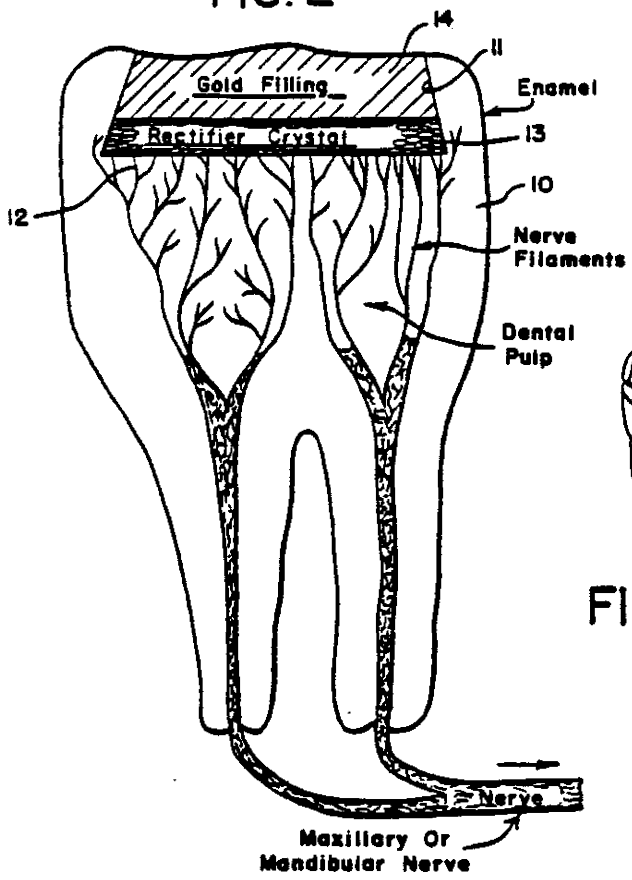

FIG. 4

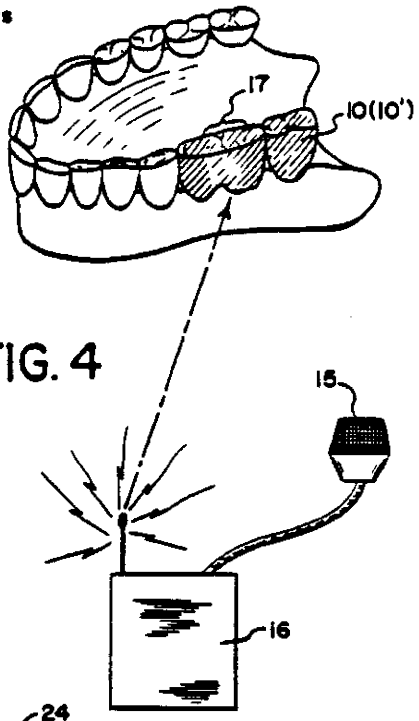

FIG. 3

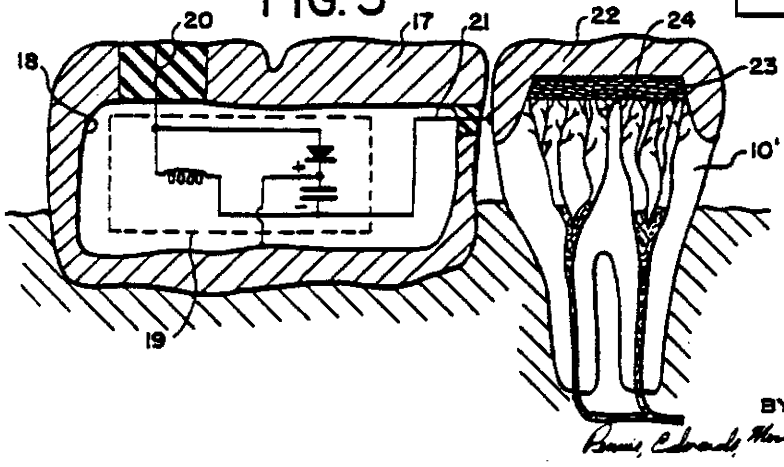

INVENTORS
HENRY K. PUHARICH
BY JOSEPH L. LAWRENCE
Pennie, Edmonds, Morton, Barrows & Taylor
ATTORNEYS

April 10, 1973 H. K. PUHARICH 3,726,762

BLOOD STORAGE METHOD

Original Filed Dec. 26, 1967 4 Sheets-Sheet 3

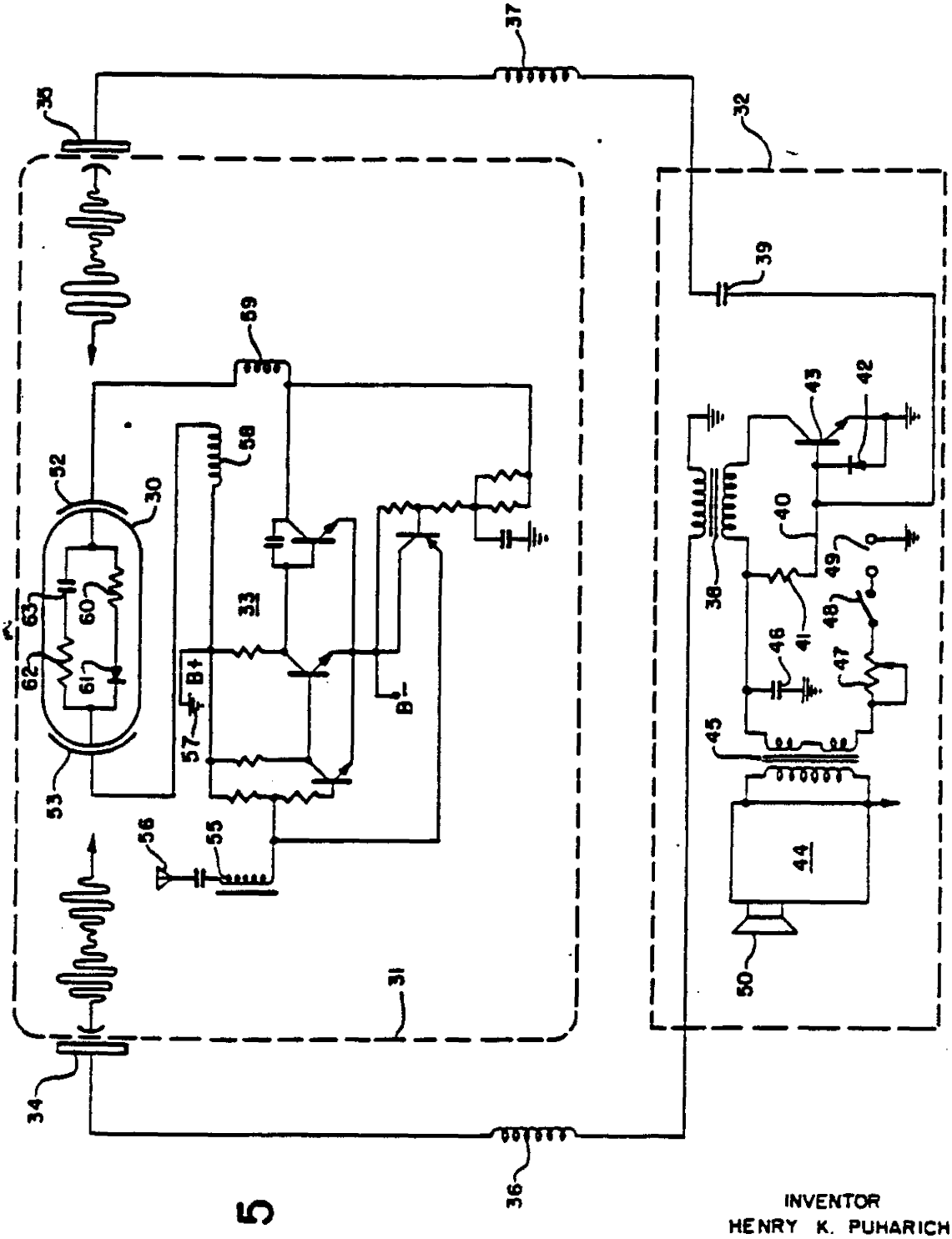

FIG. 5

INVENTOR
HENRY K. PUHARICH

BY
Mandeville & Schweitzer
ATTORNEYS

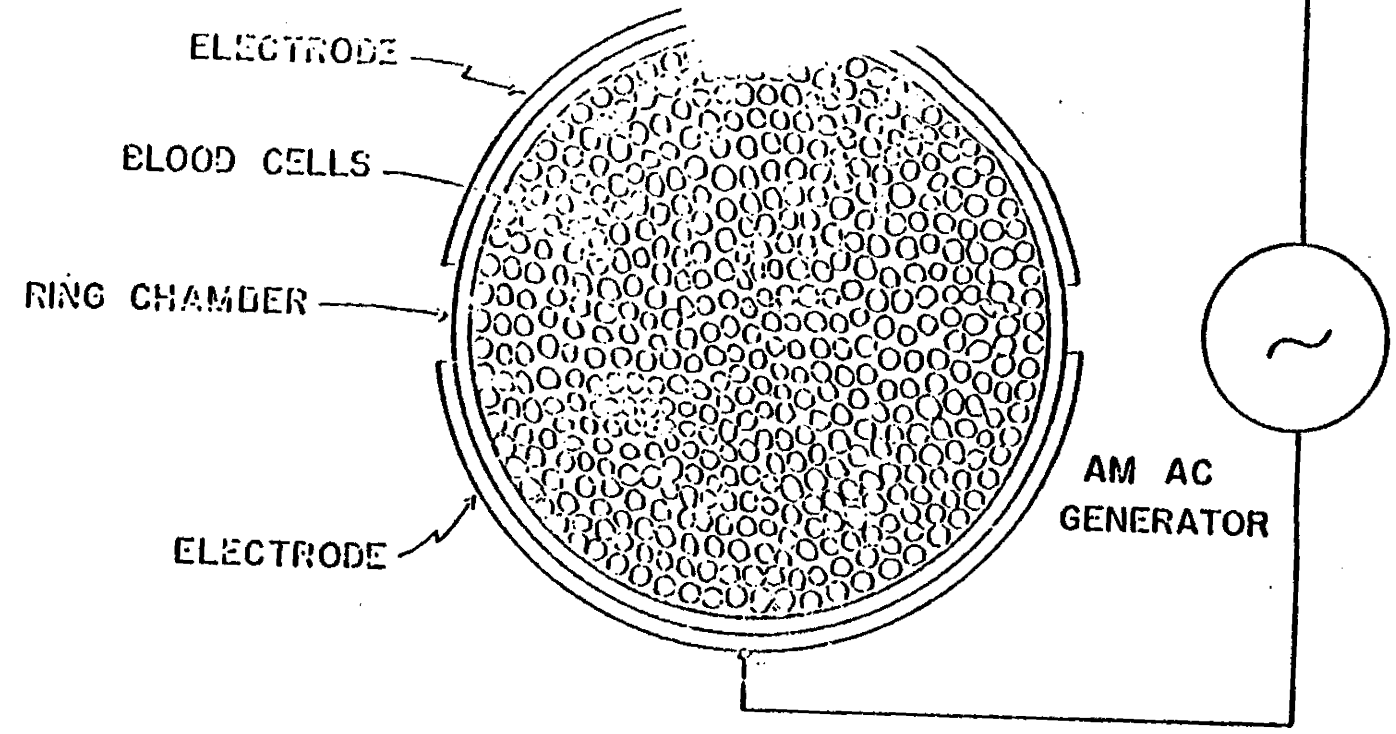

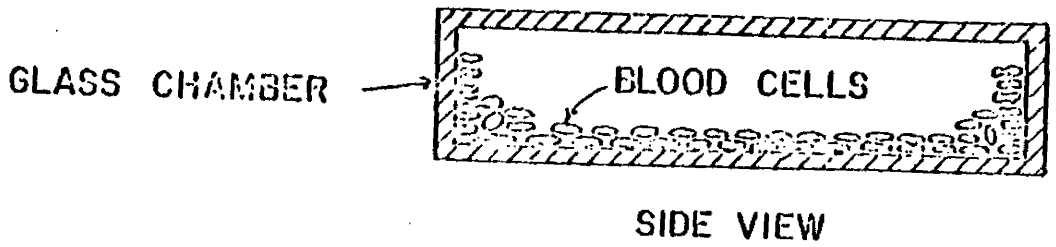

FIG. 52 GLASS MICROCHAMBER

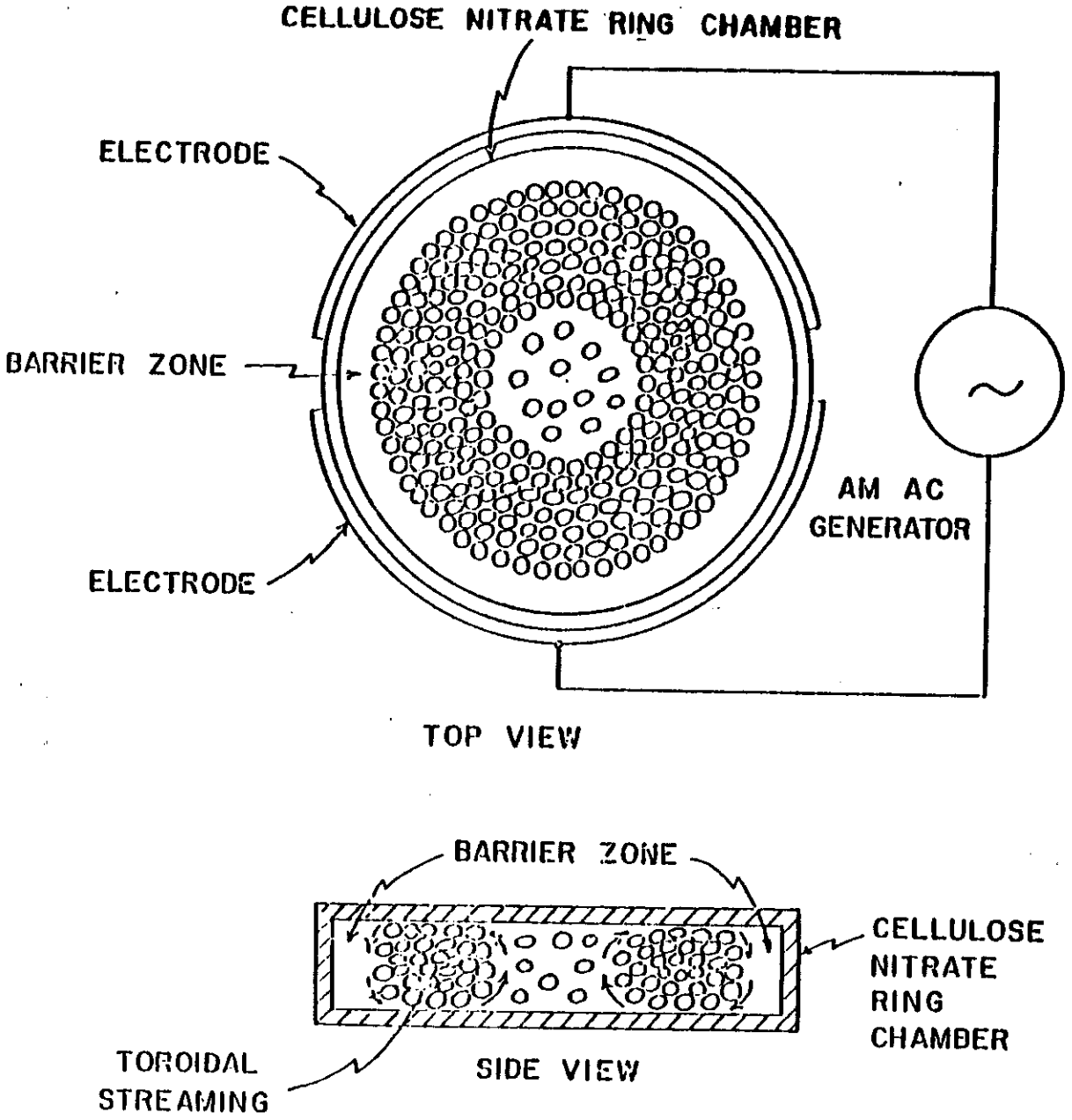

FIG. 5 CELLULOSE NITRATE RING CHAMBER

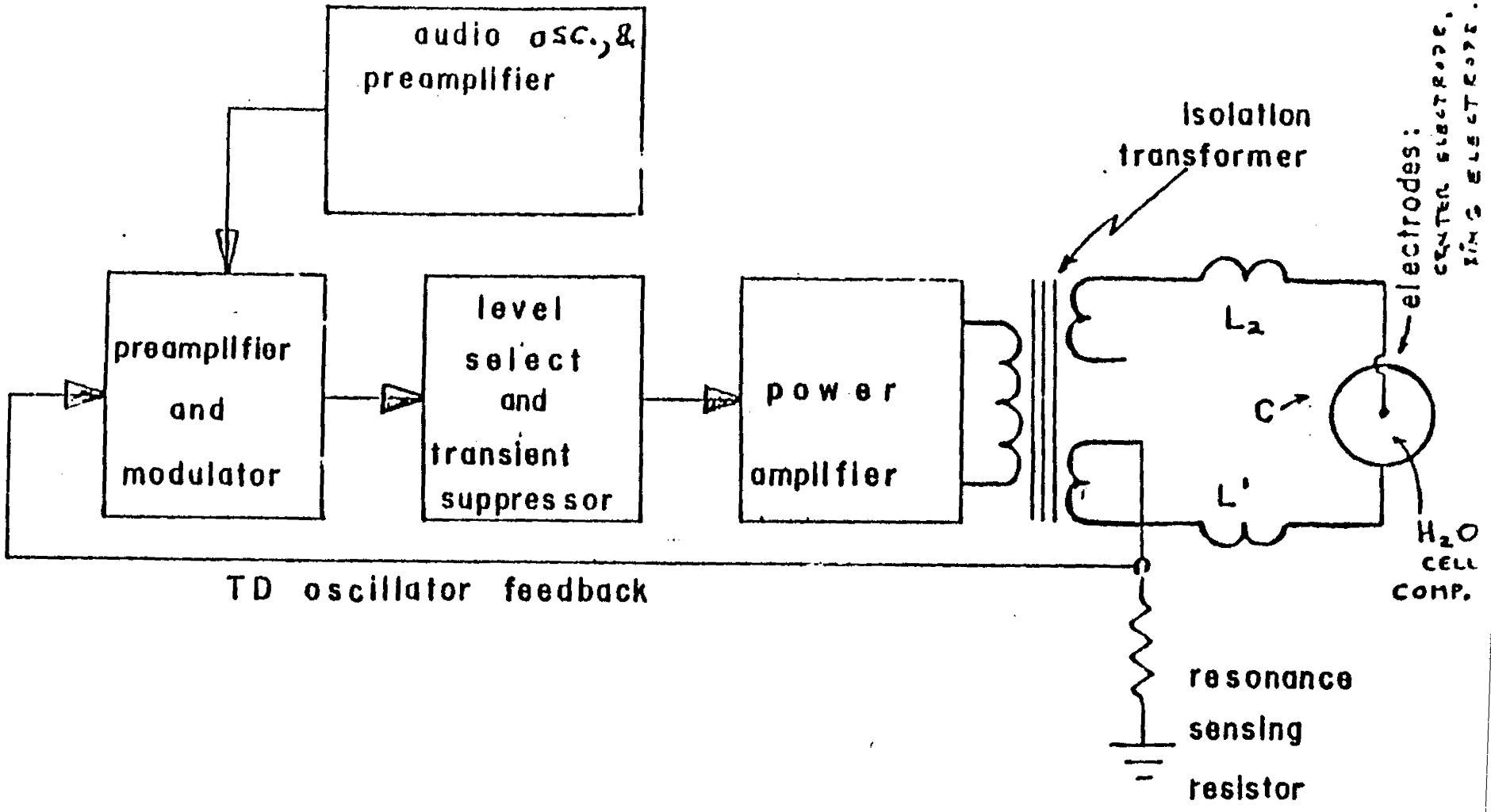

Fig. 1. COMPONENT I. SIGNAL GENERATOR BLOCK DIAGRAM.

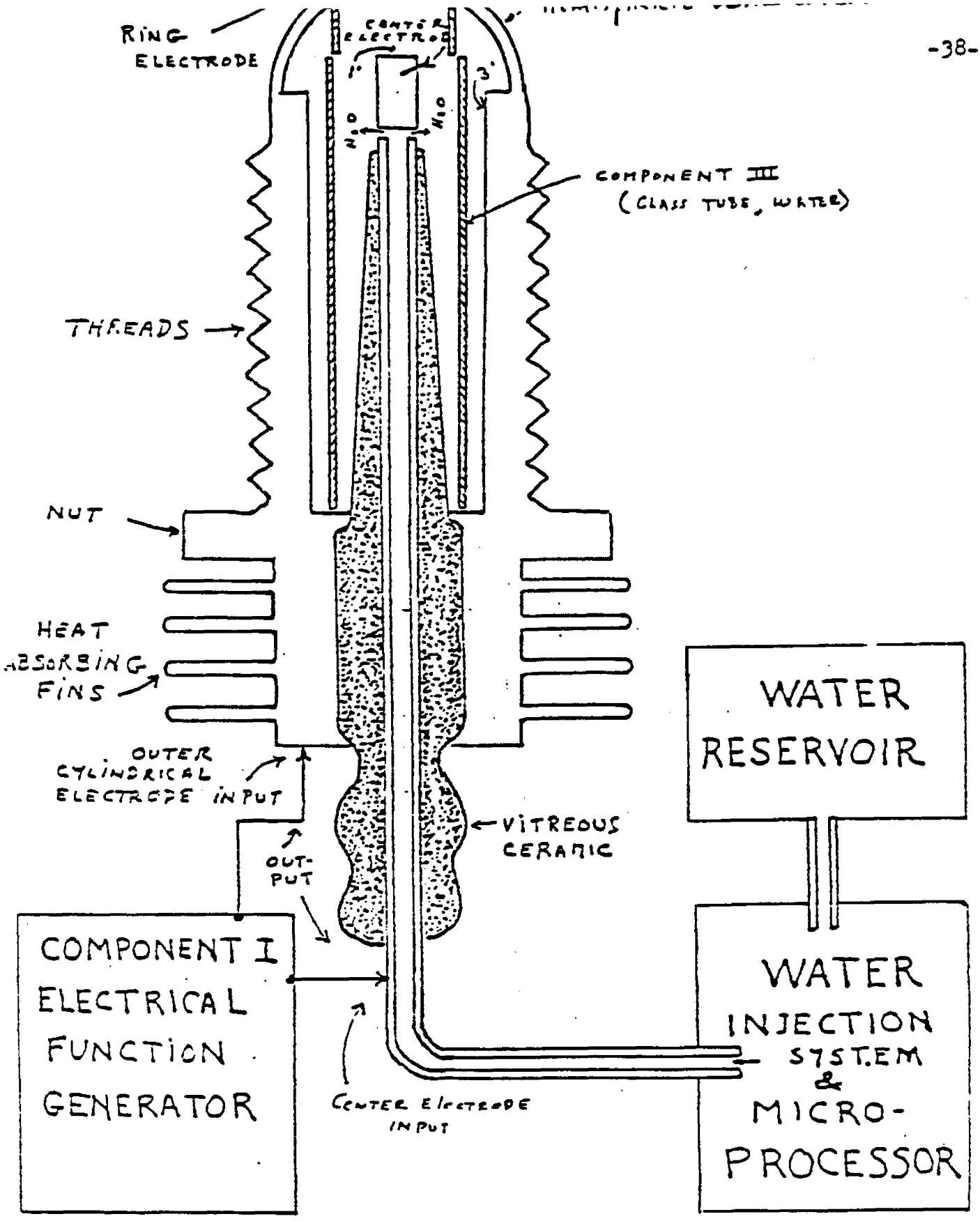

FIGURE 2.
COMPONENT II. THERMODYNAMIC DEVICE (TD).
(Side view - cross section)

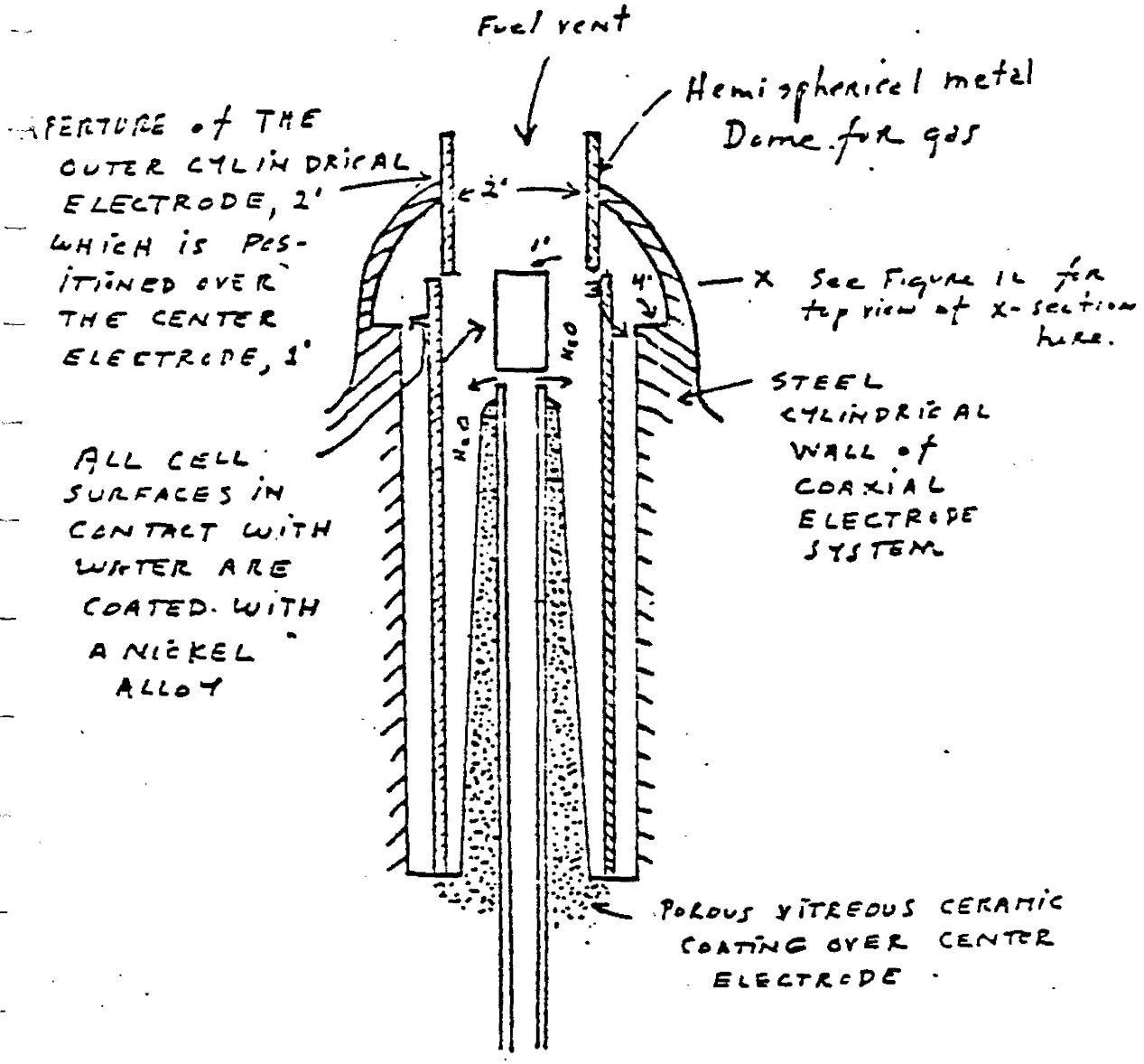

Fig. 3. COMPONENT III. The water cell Section of Component II.

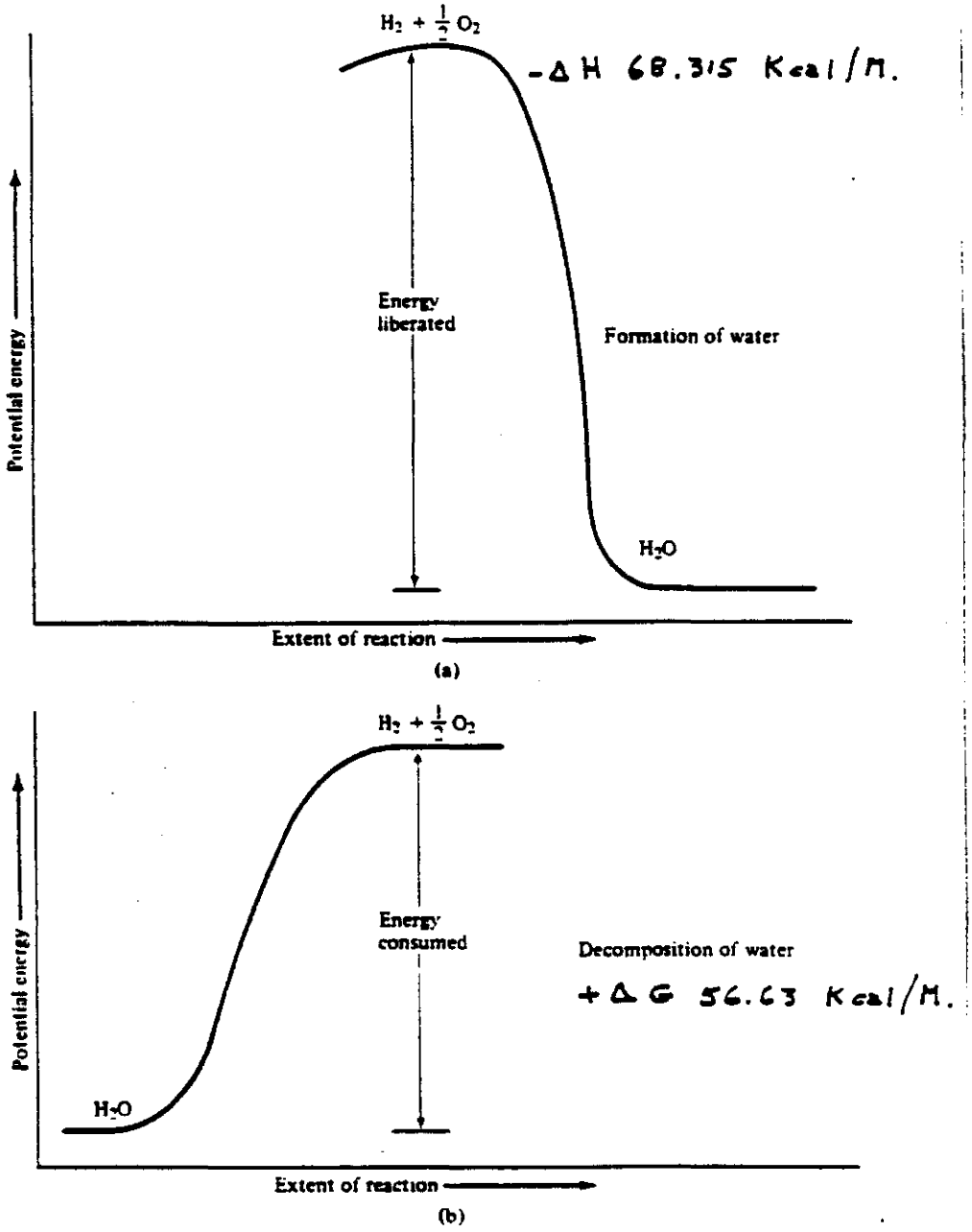

FIGURE 4.1. (a) An exorgonic reaction. Products have a lower potential energy than reactants, therefore, energy is released. (b) An endergonic reaction. Products have a higher potential energy than reactants, causing energy to be consumed.

APPENDIX A

Time-Varying Magnetic Fields: Effect on DNA Synthesis

Abstract. *Human fibroblasts have exhibited enhanced DNA synthesis when exposed to sinusoidally varying magnetic fields for a wide range of frequencies (1.5 hertz to 4 kilohertz) and amplitudes (2.3×10^{-6} to 5.6×10^{-4} tesla). This effect, which is at maximum during the middle of the S phase of the cell cycle, appears to be independent of the time derivative of the magnetic field, suggesting an underlying mechanism other than Faraday's law. The threshold is estimated to be between 0.5×10^{-5} and 2.5×10^{-5} tesla per second. These results bring into question the allegedly specific magnetic wave shapes now used in therapeutic devices for bone nonunion. The range of magnetic field amplitudes tested encompass the geomagnetic field, suggesting the possibility of mutagenic interactions directly arising from short-term changes in the earth's field.*

Most studies of the effect of static magnetic fields on living systems have yielded negative or inconsistent results (*1*); the exception is studies of species that incorporate ferromagnetic materials as geomagnetic sensory elements (*2*). Experiments on time-varying magnetic fields have been fewer and more difficult to interpret (*3*). A therapeutic technique for accelerating repair in bone nonunions that subjects the site to a time-varying magnetic field (*4*) has achieved a measure of acceptance in the clinical community (*5*). However, the mechanism underlying this procudure is still largely unexplained, in part because the narrow and repetitive pulse shape of the wave form, allegedly specific to the therapy, makes it difficult to perform and interpret in vitro cellular experiments (*6*).

We sought to determine the effect of sinusoidally varying magnetic fields on DNA synthesis in cell culture, particularly the frequency and intensity response, if any. A pair of matched incubators were fitted with modified Helmholtz coils (0.5 m, inside diameter; 0.25 m long), providing a horizontal magnetic field with an active field uniformity of less than 3 parts out of 17. Either could be an experimental or control (no field) unit. Periodically the roles were switched and, at other times, both were used simultaneously as controls. An a

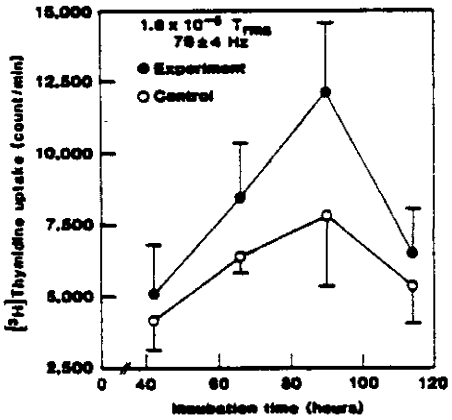

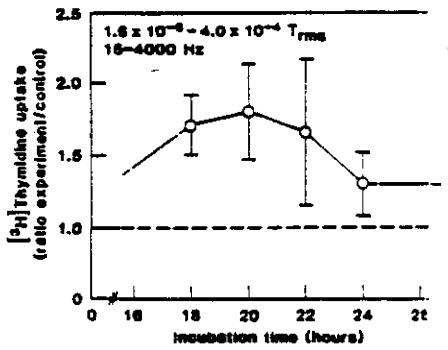

Fig. 1 (left). Tritiated thymidine uptake (mean counts per minute ± standard error) in human foreskin fibroblastic cells exposed to a magnetic field of amplitude 2.3×10^{-5} T oscillating at 76 ± 4 Hz in the horizontal plane (experiment) and uptake in unexposed cells (control). Mean levels differ at $P = 0.0001$, as determined from the pooled variances. The ambient 60-Hz magnetic field in the area of the incubators was $\leq 1 \times 10^{-7}$ T_{rms}. Note that the approximate intensity of the geomagnetic field is 5×10^{-5} T. Fig. 2 (right). Mean ratios and standard errors of [^{3}H]thymidine uptake exposed cells to that in control cells for ten different combinations of frequencies and fields. The dotted line indicates the expected response if there is no effect due to a magnetic field. The peak at 20 hours corresponds to the middle of the S phase of the cell cycle. The dashed lines below 18 and above 24 hours represent the expected, but inexact trends, in these data.

5. C. A. L. Bassett, S. N. Mitchell, S. R. Gaston, *J. Am. Med. Assoc.* **247**, 623 (1982); editorial comment in *ibid.*, p. 669; J. S. Kort, *et al.*, *Clin. Orthop. Relat. Res.* **165**, 124 (1982); M. L. Sutcliffe and A. A. J. Goldberg, *ibid.* **166**, 45 (1982).
6. G. A. Rodan, L. A. Bourret, L. A. Norton, *Science* **199**, 690 (1978); L. A. Norton, *Clin. Orthop. Relat. Res.* **167**, 280 (1982); R. A. Luben, C. D. Cain, M. C. Chen, D. M. Rosen, W. R. Adey, *Proc. Natl. Acad. Sci. U.S.A.* **79**, 4180 (1982); R. Goodman, C. A. L. Bassett, A. S. Hendersen, *Science* **220**, 1283 (1983).
7. Cell line HFS-15, HEM Research, Inc., Rockville, Md. (catalog number 4-404).
8. Costar, Cambridge, Mass.; seeding in 0.02 ml of Delbecco's minimum essential medium (DMEM) plus 10 percent fetal calf serum (FCS) (Gibco, Grand Island, N.Y.) per well; incubation at 36.5° ± 0.4°C, 5.0 ± 0.1 percent CO_2, and 95 percent air.
9. New England Nuclear, Boston, Mass. (1 μCi per well).
10. R. J. Hartzman, M. L. Bach, F. H. Bach, G. B. Thurman, K. W. Sell, *Cell. Immunol.* **4**, 182 (1972).
11. Costar, Cambridge, Mass. Seeding in 1.0 ml DMEM plus 10 percent FCS per well; incubation at 36.5° ± 0.4°C, 5.0 ± 0.1 percent CO_2, 95 percent air.
12. These measurements were made by J. Gauger (personal communication).
13. J. M. R. Delgado, J. Leal, J. L. Monteagudo, M. G. Gracia, *J. Anat.* **134**, 533 (1982).
14. J. D. Hays, *Geol. Soc. Am. Bull.* **82**, 2433 (1971).
15. We acknowledge the technical assistance of C. Winiling and A. Alicea, as well as advice from L. Homer. This research was supported by the Naval Medical Research and Development Command Research Work Unit 3M161102BS10.BA.436 and MR04101O0-5.0004.
• Present address: Department of Physics, Oakland University, Rochester, Minn.

4 May 1983; accepted 14 December 1983

APPENDIX B

NUCLEAR MAGNETISM:
Order and Disorder

A. ABRAGAM
AND
M. GOLDMAN
Collège de France and Centre d'Etudes Nucléaires de Saclay

CLARENDON PRESS · OXFORD
1982

86

PREFACE

TWENTY years ago one of the authors wrote a comprehensive book on *The principles of nuclear magnetism* ('*The Principles*' for brevity). Ten years later the other author wrote a more specialized monograph on *Spin temperature and nuclear magnetic resonance in solids* ('*Spin Temperature*' for brevity).

Although the present book does deal with the principles of nuclear magnetism and although spin temperature is one of its key concepts, it should be made emphatically clear at the outset that this is not a new edition of either one of the earlier books.

The motivations for preparing a new edition of a book are manifold but can be summed up as a wish to add and a wish to suppress: to add, because in a field which remains alive, new directions of research, new theories, new experimental results keep cropping up and want coverage; to suppress, because these new experiments and theories make some of the former descriptions and explanations incomplete or even incorrect, and rob some others of much of their interest.

Through care, foresight, caution and sheer luck, it has turned out that there is very little to suppress in our former books, or so we think. On the other hand at least for the more comprehensive of the two, *The Principles*, there is far too much to add. It is our considered opinion that today no single author (nor even a couple of authors) could cover in a single volume (or even in a couple of volumes) the whole field of nuclear magnetism. This is why in spite of its size this new book covers only a limited part of the field, which does not overlap with either *The Principles* or *Spin Temperature*.

Nuclear magnetism is both a tool and a field that is an object of study for its own sake. With respect to its first aspect, to quote from the preface to *The Principles*: 'it has become a major tool in the study of the finer properties of matter in bulk. Structure of molecules, reaction rates and chemical equilibria, chemical bonding, crystal structures, internal motions in solids and liquids, electronic densities in metals, alloys, and semiconductors, internal fields in ferromagnetic and antiferromagnetic substances, density of states in superconductors, properties of quantum liquids, are some of the topics where nuclear magnetism has so far provided specific and detailed information.' Twenty years later, with biologists and biochemists taking now the lion's part among the users, the role of nuclear magnetism as a scientific tool is greater than ever. The amount of factual information gathered is staggering. The techniques and instrumentation of nuclear magnetic resonance (NMR) and above all of high resolution in liquids have reached new heights of sophistication and efficiency, thanks in particular to the tremendous progress in the art of computers.

nuclear magnetic behaviour which has no counterpart anywhere else in nuclear magnetism. In trying to understand the theoretical explanations of this behaviour we realized how ill-prepared for this task, through their background, were most students of nuclear magnetism, including ourselves. This chapter is an earnest attempt to spare the reader some of the difficulties that the authors experienced in going through the original papers and the review articles. It is a painstaking, somewhat pedestrian account of the magnetic properties of superfluid ^{3}He, which does not assume any previous knowledge of the theory of Fermi liquids let alone that of the BCS theory of superconductivity.

With this chapter ends what may be considered as the first part of the book, although it is not so formalized in the table of contents. It differs from the second part, formed by the last four chapters, at two levels.

The spin temperatures encountered in the first part are high: whenever Boltzmann statistics applies to the spins, the first order expansion of the Boltzmann exponentials is an adequate approximation. This is not so in the second part and in particular in the chapter on the long range ordering where all expansions in powers of the inverse temperature break down.

The second distinction between the two parts is of a personal nature. In contrast with the first, the second part covers subjects on which the authors have worked actively for a long time. To use an image that we applied earlier to nuclear spins: spectators in the first part, actors in the second.

CHAPTER 5. *Spin systems at low temperatures* plays for part II the role that chapter 1 played for part I. The theoretical methods necessary for dealing with spin systems at very low temperatures are developed. The expansion of expectation values of various physical observables in powers of inverse temperature, valid in the paramagnetic range is performed by the diagrammatic method, with what the *cognoscenti* may deem excessive detail but others may find useful. General relations, valid also in the ordered states, are established and experimental illustrations are given.

CHAPTER 6. *Thermal contact between nuclear spins and paramagnetic impurities: nuclear relaxation and dynamic polarization.* These studies are not new since they are already dealt with in both *The Principles* and *Spin Temperature*. However the advances in this field, resulting both in a better understanding of the various processes involved and in a large harvest of new and spectacular results, warrant a new chapter in a new book. Indeed this is one of the very few topics where *The Principles*, and even the more recent *Spin Temperature*, could do with some little suppressions. The duality field-tool appears again. Dynamic nuclear polarization, a field of study in its own right is a tool for building polarized targets for nuclear, neutron, and elementary particle physics. It is also a tool for another field of nuclear magnetism, namely dipolar magnetic ordering.

CHAPTER 7. *Nuclear magnetism and neutrons: nuclear pseudomagnetism.* The nuclear forces between slow neutrons and nuclei have a spin-dependent part which can be conveniently described by assigning to each nuclear species a fictitious pseudomagnetic moment. The various aspects of the interaction of the neutron spin with a system of nuclear spins are likewise referred to as nuclear pseudomagnetism. Nuclear pseudomagnetism exhibits some very interesting features of its own such as pseudomagnetic resonance and pseudomagnetic precession. It is however chiefly a tool for the study of long range nuclear magnetic ordering, its structures, and its imperfections.

CHAPTER 8. *Nuclear dipolar magnetic ordering.* This is the key chapter of the second part of this book. All the methods and results described in the three previous chapters converge towards the realization of a goal pursued over the years namely the prediction, production, observation, and study by various techniques, of magnetically ordered structures of nuclear spins produced by their dipolar magnetic interactions.

The ordering of nuclear spins of ^{3}He is described in far less detail in view of the preliminary character of the experiments and of the tentative character of the theory. The so-called enhanced nuclear magnetism with its potentialities for ordering nuclear spins is not considered at all. It is felt that because of its strong dependence on the magnetism of the electronic clouds surrounding the nuclei, which give rise to it, its description belongs in a book on electron magnetism.

A few more topics such as the nuclear magnetism of solid hydrogen and solid methane could arguably have been included in this book. Among other arguments against their inclusion, such as the few uncertainties still present in the experimental results and in their interpretation, was the wish to complete in a finite time a book of finite size.

Like its predecessors (*The Principles* 1961, *Spin Temperature* 1970) this book reflects the spirit of our laboratory, dedicated for more than twenty-five years now to the study and progress of nuclear magnetism. To all our coworkers past and present, too numerous to be cited here but not too many to be all very present in our mind, our heartfelt thanks.

We are grateful to Professor Bleaney for suggesting the title of this book which is a concise and accurate statement of its contents.

This manuscript could never have been prepared in the allotted time without the kind and competent assistance of Madame Porneuf and her staff. Special thanks are due to Madame Neveux who typed most of the preliminary draft and to Madame Parent who produced the final typescript.

We thank the authors and the publishers of the scientific journals who kindly gave us permission to reproduce the figures.

Orme des Merisiers A.A.
August 1981 M.G.

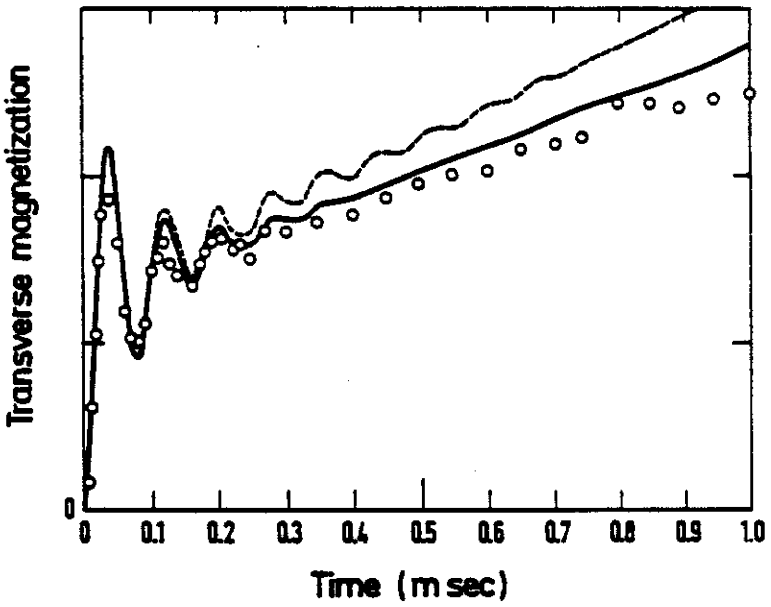

FIG. 1.5. Short-term transient variation of ^{43}Ca transverse magnetization during thermal coupling between ^{43}Ca effective Zeeman reservoir and dipole–dipole reservoir in CaF_2 with $H_0 \| [111]$. Dashed curve: exponential approximation. Solid curve: Gaussian memory function approximation. (After Demco *et al.*, 1975.)

However striking the present success of the Gaussian approximation for the memory function of $G(t)$, one should remember that this approximation does not arise from any real theory. There is no fundamental argument as to why this memory function should be Gaussian, and no way to tell how good this approximation would be in another case.

In nuclear magnetism where as a rule correlation functions have rather complicated shapes, it is a noticeable fact that in the present problem such simple mathematical functions as the Lorentzian and the Gaussian fit so well, respectively the shape of $G(t)$ and that of its memory function.

C. On the validity of the concept of spin temperature

(*a*) *The random phase assumption*

The concept of spin temperature has over the years proved extremely beneficial to the development of nuclear magnetism in solids. The validity of the underlying assumptions has been verified in many instances not only in the domain of high temperature considered so far, but also at very low spin temperatures as will appear in chapters 5 and 8.

However, ingenious and elaborate experiments have been performed in more recent years, whose results seem to contradict the usual assumptions of spin temperature or at any rate to set limits to its validity, narrower than had been thought previously. The discussion of these limits is the theme of this section.

It will appear that such limitations are in fact intrinsically associated with the concept of temperature in general and exist even for the more usual thermodynamic systems. If they emerge more conspicuously in the field of nuclear magnetism it is because interacting nuclear spins can be manipulated more subtly and observed more sharply than most thermodynamic systems.

We begin by recalling briefly some of the steps which lead to the concept of temperature in statistical mechanics.

(i) The density matrix of a macroscopic system evolves according to the equation:

$$\sigma(t) = \exp(-i\mathcal{H}t)\sigma(0)\exp(i\mathcal{H}t). \tag{1.172}$$

Its matrix elements in a basis where the Hamiltonian $\mathcal{H}$ is diagonal, have the following well-known behaviour:

the diagonal elements are time independent,

$$\langle i|\sigma(t)|i\rangle = \langle i|\sigma(0)|i\rangle; \tag{1.173}$$

the off-diagonal elements oscillate without damping,

$$\langle i|\sigma(t)|j\rangle = \langle i|\sigma(0)|j\rangle \exp\{-i(\mathcal{H}_i - \mathcal{H}_j)t\}. \tag{1.174}$$

(ii) The expectation value of an operator Q with *no* diagonal matrix elements is a sum of oscillating terms:

$$\langle Q\rangle = \sum \langle i|\sigma(0)|j\rangle\langle j|Q|i\rangle \exp\{-i(\mathcal{H}_i - \mathcal{H}_j)t\}. \tag{1.175}$$

When the frequencies $\mathcal{H}_i - \mathcal{H}_j$ form a quasi-continuous spectrum the destructive interference of the various terms leads to a decay of $\langle Q\rangle$ towards zero in a time T_2 of the order of the inverse width of the frequency spectrum.

Thus, if at time $t = 0$ the system was prepared in a state where the expectation values $\langle Q\rangle$ of off-diagonal operators Q are different from zero, the *assumption* is made that after a time of the order of several times T_2 it is permissible to 'forget' the off-diagonal part of the density matrix $\sigma(t)$ and to replace it by a 'truncated' density matrix σ_d reduced to the diagonal (and time-independent part) of $\sigma(t)$.

(iii) For macroscopic operators with diagonal matrix elements only, it is then assumed that the truncated matrix σ_d can be represented with good accuracy, (the better the larger the number of degrees of freedom of the system), by the canonical density matrix,

$$\sigma(\beta) = \exp(-\beta\mathcal{H})/\mathrm{Tr}\{\exp(-\beta\mathcal{H})\}, \tag{1.176}$$

where β is chosen to give the same value for the total energy E of the system as the original density matrix σ_d (or $\sigma(0)$, or $\sigma(t)$ which all give the same result).

$$\mathrm{Tr}\{\mathcal{H}\sigma(t)\} = \mathrm{Tr}\{\mathcal{H}\sigma_d\} = \mathrm{Tr}\{\mathcal{H}\sigma(0)\} = E. \tag{1.177}$$

We shall not examine here the validity of the replacement of $\sigma(t)$ by σ_d. This problem, well known in statistical mechanics has been discussed in the literature at great length and over many years and there is nothing in the nature of interacting spin systems to warrant a more specialized discussion.

On the other hand the random phase approximation where the off-diagonal part of the density matrix is 'forgotten' has special aspects for spin systems and deserves more careful consideration.

A first point is that in the usual thermodynamic systems the time required to perform a measurement is in general far longer than the time constant T_2 for the randomization of the phases. Thus for every physical quantity one usually measures a time-average to which the oscillating off-diagonal matrix elements of $\sigma(t)$ bring a negligible contribution.

The originality of the nuclear spin systems resides in part in the fact that the measurements can be performed on a time scale far shorter than T_2: oscillatory behaviour of longitudinal or precessing magnetization and of other quantities such as dipolar energy can be observed *without* the time averaging which in most thermodynamical systems wipes out the oscillations. This puts more stringent conditions on the validity of the random phase approximation for nuclear spin systems than for conventional systems.

We have already discussed in detail in section **B**(e) an experiment which illustrates the decay of the oscillations in the trend toward an equilibrium or quasi-equilibrium regime described by a spin temperature (or temperatures).

A second example, of a somewhat different nature, which demonstrates that the establishment of a spin temperature is not instantaneous is given below. We then describe a very remarkable experiment which shows how the effects of the off-diagonal matrix elements of $\sigma(t)$, apparently buried in the graveyard of spin temperature can be brought to life again.

(*b*) *The trend toward spin temperature: production and observation of dipolar order in high field: An example*

We had stated in section **A**(c)1 that in high field whatever the initial conditions a quasi-equilibrium state of the spin system was expected to occur after a time interval of the order of a few times T_2, described by the density matrix (1.29):

$$\sigma = 1 - \beta_Z \omega_0 I_z - \beta \mathcal{H}'_D. \tag{1.178}$$

In such a state the expectation values $\langle Z\rangle = \langle \omega_0 I_z\rangle$ and $\langle \mathscr{H}'_D\rangle$ are given respectively by:

$$\langle Z\rangle = -\beta_Z \omega_0^2 \operatorname{Tr}\{I_z^2\} \qquad \langle \mathscr{H}'_D\rangle = -\beta \operatorname{Tr}\{\mathscr{H}'^2_D\}. \tag{1.179}$$

β_Z and β can be measured from the signals $\langle I_x(t)\rangle$ and $\langle I_y(t)\rangle$, following a pulse of angle θ around $0x$ (in the rotating frame) given by (1.43) and (1.44). The ratio of these signals is:

$$\frac{\langle I_x(t)\rangle}{\langle I_y(t)\rangle} = \frac{\beta}{\beta_Z}\cos\theta \frac{1}{\omega_0}\frac{1}{G}\frac{dG}{dt} = \frac{1}{\omega_0 T_2}\frac{\beta}{\beta_Z}. \tag{1.180}$$

Since $\omega_0 T_2 \gg 1$ in high field, a dipolar order can only be observed through $\langle I_x(t)\rangle$ if $|\beta/\beta_Z| \gg 1$, that is if the dipolar energy is much colder than the Zeeman energy, hardly a surprising result, since $\mathscr{H}'_D \ll Z$. One of the methods for achieving the dipolar cooling is the ADRF described in A(*b*)3. We recall here another method due to Jeener and Broekaert (1967), (and described in Goldman, 1970), because it serves as an illustration of the trend of the system to the quasi-equilibrium state (1.29). The procedure is the following.

Starting from $\sigma_0 = 1 - \beta_Z^0(\omega_0 I_z + \mathscr{H}'_D) \simeq 1 - \beta_Z^0 \omega_0 I_z$, a $(\pi/2)$ pulse around $0y$ is applied, followed τ seconds later by a $(\pi/4)$ pulse around $0x$. t seconds after the second pulse the density matrix is:

$$\sigma(\tau, t) = 1 - \beta_Z^0 \omega_0 \exp(-i\mathscr{H}'_D t)\exp(-i(\pi/4)I_x)\exp(-i\mathscr{H}'_D\tau)I_x$$
$$\times \exp(i\mathscr{H}'_D\tau)\exp(i(\pi/4)I_x)\exp(i\mathscr{H}'_D t). \tag{1.181}$$

The expectation values of Z and $\mathscr{H}'_D$ at time $(t+\tau)$,

$$Z(\tau, t) = \omega_0 \operatorname{Tr}\{I_z \sigma(\tau, t)\}, \qquad \langle \mathscr{H}'_D(\tau, t)\rangle = \operatorname{Tr}\{\mathscr{H}'_D \sigma(\tau, t)\}, \tag{1.182}$$

are easily calculated using the transformation properties of $\mathscr{H}'_D$ following from (1.11*a*) and (1.9*b*). They are:

$$\langle Z(\tau, t)\rangle = 0; \tag{1.183a}$$

$$\langle \mathscr{H}'_D(\tau, t)\rangle = \beta_Z^0 \frac{\omega_0}{2} \operatorname{Tr}\{I_z^2\}\left(\frac{dG}{dt}\right)_{t=\tau}. \tag{1.183b}$$

We see that at *any time* after the second pulse these expectation values, independent of t, are according to (1.179) and (1.183) rigorously the same as if the density matrix at that time were the spin temperature matrix (1.178) with:

$$\beta_Z = 0; \qquad \beta = -\beta_Z^0 \frac{\omega_0}{2D^2}\left(\frac{dG}{dt}\right)_{t=\tau}. \tag{1.184}$$

Can we conclude that at a time t after the second pulse we can replace the *real* density matrix (1.181) by the spin temperature matrix (1.178), with

$\beta_Z = 0$, which gives for *any* t the same expectation values of Z and $\mathcal{H}'_D$? The answer is yes if the time t is long compared to T_2, no if t is much shorter than T_2.

The first answer is based solely on experiment. After *preparing* the spin system by a pulse $(\pi/2, 0y)$ and a pulse $(\pi/4, 0x)$ separated by a time τ it is possible to *look* at it by a pulse $(\theta, 0x)$ t seconds later. When $t \gg T_2$ it has indeed been found experimentally (Jeener and Broekaert, 1967) that $\langle I_y \rangle = 0$ and that the time-dependence of $\langle I_x(t) \rangle$ is given by (1.44) where β has the value given by (1.184):

$$\langle I_x(t') \rangle = -\beta_Z^0 \frac{\omega_0}{2D^2} \sin\theta \cos\theta \, \mathrm{Tr}\{I_x^2\} \left(\frac{dG}{dt}\right)_{t=\tau} \left(\frac{dG}{dt}\right)_{t=t'}. \quad (1.185)$$

Its dependence on τ and t' is $(dG/d\tau)(dG/dt')$.

The second answer is a straightforward consequence of quantum mechanics. If the observation pulse $(\theta, 0x)$ occurs shortly after the pulse $(\pi/4, 0x)$, then $\sigma(\tau, t)$ does *not* behave at all as a spin temperature matrix. As an example assume that the observation pulse $(\theta, 0x)$ occurs immediately after the pulse $(\pi/4, 0x)$ and that θ is given the value $-\pi/4$. The two pulses cancel each other and t' seconds later:

$$\begin{aligned} \langle I_x(t') \rangle &= -\beta_Z^0 \omega_0 \, \mathrm{Tr}\{I_x \exp(-i\mathcal{H}'_D t') \exp(-i\mathcal{H}'_D \tau) I_x \exp(i\mathcal{H}'_D \tau) \exp(i\mathcal{H}'_D t')\} \\ &= -\beta_Z^0 \omega_0 \, \mathrm{Tr}\{I_x^2\} G(\tau + t'), \end{aligned} \quad (1.186)$$

a dependence on τ and t' quite different from (1.185). This discrepancy is due to the fact that while $\langle Z \rangle$ and $\langle \mathcal{H}'_D \rangle$ are unaffected by the off-diagonal matrix elements of $\sigma(\tau, t)$ in (1.181), the transverse component $\langle I_x \rangle$ is, and one must therefore wait for the randomization of the phases before attempting a measurement of β_Z and β.

(c) *Phase refocussing: the magic sandwich*

1. *The argument for irreversibility*

In the early years of magnetic resonance Erwin Hahn had performed an experiment, the spin echo, which to the uninitiated, had appeared little short of miraculous. The transverse nuclear magnetization of a liquid sample, precessing in an inhomogeneous magnetic field, once it had decayed to zero, could be restored to its full, or almost full value, by an appropriate r.f. pulse, and this after a time far longer than the decay time.

The principle of Hahn's spin echo is too well known to be discussed here in any detail. The gist of it is that the Larmor precession frequencies of the different parts of the sample, although spread over an interval $\Delta\omega$, whence their destructive interference and the magnetization decay in a time of the order of $(\Delta\omega)^{-1}$, are constant in *time*. A π pulse, by reversing at a time

$\tau' \gg (\Delta\omega)^{-1}$ after the beginning of the precession all the phase angles accumulated by the various spins, brings them automatically into phase again at time 2τ, if the precession velocities have remained constant; whence comes the 'resurrection' of the magnetization.

On the contrary, in a solid where the decay of the nuclear magnetization is due to the dipolar interaction $\mathcal{H}'_D$, this decay has been for a long time considered as completely irreversible.

The case for this irreversibility has rested on various arguments, some more convincing than others.

(i) It has been argued that in the solid each spin precesses in the local field of its neighbours. Because of flip-flops between the spins this field is not constant in time but fluctuates in a random and hence, irreversible manner: the accumulated phase lags or advances cannot be retrieved. One must beware of arguments of that type. It was a similar argument which, before the historical spin temperature experiment of Pound, had led to the belief that the loss of magnetization after a demagnetization into zero field was always irreversible: it was argued that in zero field fast random reversals of one spin, or of two spins in the same direction, (processes forbidden by energy conservation in high field but allowed in zero field), would destroy for ever the magnetization in a time T_2, a conclusion that contradicts both the experiment and the spin temperature theory.

(ii) A second argument is to state that because of the bilinear nature of the dipolar Hamiltonian $\mathcal{H}'_D$ the refocussing effect of a pulse *à la* Hahn would be nil. This is quite true but only shows that the decayed precessing magnetization cannot be retrieved by *that* particular method.

(iii) By far the most cogent argument for irreversibility was the spin temperature assumption.

Immediately after a $\pi/2$ pulse around 0x the density matrix of the spin system is, in the rotating frame: $\sigma(0) = 1 - \alpha\omega_0 I_y$ and the transverse magnetization:

$$\langle I_y \rangle_0 = \mathrm{Tr}\{I_y \sigma(0)\} = -\alpha\omega_0 \,\mathrm{Tr}\{I_y^2\}. \tag{1.187}$$

After a time $t \gg T_2$ the transverse magnetization has completely disappeared and according to the spin temperature assumption and to all the experimental evidence backing this assumption we expect $\sigma(t)$ to be represented with good accuracy by the expression: $\sigma = 1 - \beta_Z \omega_0 I_z - \beta \mathcal{H}'_D$ where the quasi-invariants $\mathcal{H}'_D$ and $Z = \omega_0 I_z$ have the same expectation values:

$$\langle Z \rangle = -\beta_Z \omega_0^2 \,\mathrm{Tr}\{I_z^2\}, \qquad \langle \mathcal{H}'_D \rangle = -\beta \,\mathrm{Tr}\{\mathcal{H}'^2_D\} \tag{1.188}$$

as at the time $t = 0$:

$$\langle Z \rangle_0 = \omega_0 \,\mathrm{Tr}\{I_z \sigma(0)\} \qquad \langle \mathcal{H}'_D \rangle = \mathrm{Tr}\{\mathcal{H}'_D \sigma(0)\}. \tag{1.189}$$

The latter however are clearly zero and so therefore are β_Z and β. The spin temperature density matrix should thus be the unit matrix and no magnetic signal could seemingly be extracted from it.

'Nothing will come out of nothing.' And yet $\cdots$.

2. *The magic sandwich*

After a pulse $(\pi/2, 0x)$ at time $t = 0$ and once the precessing magnetization has disappeared presumably for ever, the following sequence of pulses called 'magic sandwich' is applied (Rhim *et al.* 1971).

(i) At time $T_A \gg T_2$ a pulse $(\pi/2, 0y)$ followed by the sudden application for a duration $T_B \gg T_2$ of a strong r.f. field $H_1 = -\omega_1/\gamma$ along 0x.

(ii) At time $(T_A + T_B)$ the field H_1 is cut off and a pulse $(-\pi/2, 0y)$ applied.

After the magic sandwich sequence one looks for the appearance of a signal. Indeed if $T_B \gg T_2$, has been chosen greater than $2T_A$ a signal shaped like an echo of the initial decay, does appear at a time $T_C = \frac{1}{2}T_B - T_A$ after the magic sandwich!

The theory of this echo is actually quite straightforward. The unit operator $U_M(T_B)$ which corresponds to the magic sandwich is:

$$\begin{aligned} U_M(T_B) &= R_y^{-1}\left(\frac{\pi}{2}\right) \exp\{-iT_B(\omega_1 I_x + \mathcal{H}'_D)\} R_y\left(\frac{\pi}{2}\right) \\ &= \exp\left\{-iT_B R_y^{-1}\left(\frac{\pi}{2}\right)[\omega_1 I_x + \mathcal{H}'_D] R_y\left(\frac{\pi}{2}\right)\right\} \\ &= \exp\left\{-iT_B\left[\omega_1 I_x + R_y^{-1}\left(\frac{\pi}{2}\right)\mathcal{H}'_D R_y\left(\frac{\pi}{2}\right)\right]\right\}. \end{aligned} \tag{1.190}$$

According to (1.10*a*),

$$R_y^{-1}\left(\frac{\pi}{2}\right)\mathcal{H}'_D R_y\left(\frac{\pi}{2}\right) = -\tfrac{1}{2}\mathcal{H}'_D + G_2 + G_{-2}, \tag{1.191}$$

where G_2 and G_{-2} transform under rotation like the tensor operators T_2 and T_{-2}. If $\omega_1 I_x \gg G_2$, G_{-2}, $\mathcal{H}'_D$, that is if $H_1 \gg H'_L$ we can within first order perturbation theory disregard the effects of the off-diagonal terms $G_2 + G_{-2}$ whence:

$$U_M(T_B) \simeq \exp\{-i(-\tfrac{1}{2}\mathcal{H}'_D + \omega_1 I_x)T_B\}. \tag{1.192}$$

If furthermore we choose T_B such that $\omega_1 T_B = 2n\pi$ (which, as a more elaborate discussion shows, is not really necessary) $U_M(T_B)$ becomes:

$$U_M(T_B) \simeq \exp\{-i[-\tfrac{1}{2}\mathcal{H}'_D T_B]\}. \tag{1.193}$$

The magic sandwich has the uncanny property of reversing the effective sign of $\mathcal{H}'_D$, which is equivalent to making the time flow backwards (at half

the normal speed). The evolution operator of the system at time $T_A + T_B + T_C$ becomes:

$$U(T_A + T_B + T_C) = \exp(-i\mathcal{H}'_D T_C) U_M(T_B) \exp(-i\mathcal{H}'_D T_A)$$
$$= \exp(-i\mathcal{H}'_D (T_C - \tfrac{1}{2}T_B + T_A)). \quad (1.194)$$

The magic sandwich is thus capable of cancelling the sum of the phase $-i\mathcal{H}'_D T_A$ accumulated before it and of the phase $-i\mathcal{H}'_D T_C$ accumulated after it if:

$$T_A + T_C = T_B/2. \quad (1.195)$$

It thus restores the initial density matrix $\sigma(0)$ and the initial signal $\langle I_y(0)\rangle$ (Fig. 1.6).

It would thus appear that a decayed precessing magnetization can always be retrieved whatever the time elapsed after its decay (within the limitations caused by spin-lattice relaxation). There are actually other limitations. The formula (1.192) for the effect of the magic sandwich is only approximate. The effective Hamiltonian for U_M is:

$$\mathcal{H}_{eff} = \omega_1 I_z - \tfrac{1}{2}\mathcal{H}'_D + G_2 + G_{-2}. \quad (1.196)$$

The off-diagonal term $G_2 + G_{-2}$ does induce a departure of $U_M(T_B)$ from the approximate expression (1.192).

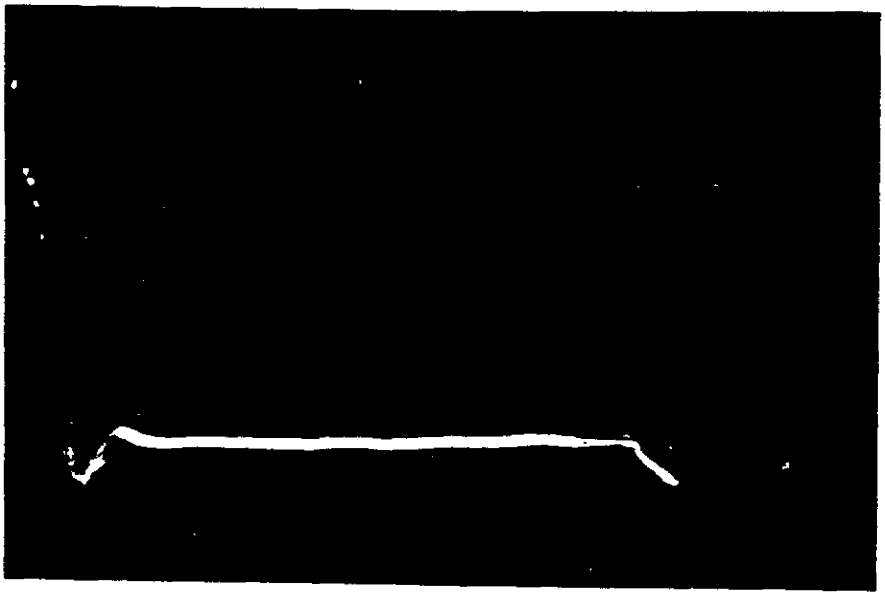

FIG. 1.6. 'Magic sandwich' experiment in CaF_2 with $H_0 \| [111]$. Free induction decay and 'magic' echo of ^{19}F spins. (After Rhim *et al.*, 1971.)

ɔnger the time T_B during which it acts, the larger the departure of from (1.192) and either, the poorer the phase cancellation by the andwich, or conversely the larger the value required for ω_1 to ı this cancellation.

ıually, the magnetization would be lost because its retrieval would impossibly high values of the r.f. field H_1 and irreversibility wins. his experiment shows that phase coherence in the spin system may or times much longer than was thought previously.

it mean that one should give up the concept of spin temperature, it has been used successfully in innumerable experiments? The n the opinion of the authors is no. The point is not whether after a he order of a few T_2 the off-diagonal matrix elements of the density have 'disappeared', a philosophical question, but whether their e can have observable consequences in a given experimental situa- turns out that unless an elaborate experiment, like the magic h, has been designed with the express purpose of tracking down -diagonal matrix elements, the usual criterions for the validity of the ıperature assumption keep their usefulness.

ew contribution of the magic sandwich experiment is to deepen our nding of the meaning of the spin temperature assumption and to careful assessment of the experimental conditions lest an accidental ing of the phases occurs.

-lattice relaxation

ıus places in the foregoing, eqn (1.25), eqn (1.38) we have introduced omenological parameters spin-lattice relaxation times for various ırators, such as T_{1z} and T_{1D} for the Zeeman and dipolar energies and the relaxation of the transverse magnetization. A detailed micro- heory of spin-lattice relaxation can be found in Abragam (1961), ; VIII and IX and, with special reference to spin temperature, in ın (1970), chapter 3.

s section we shall show how the formalism of spin-lattice relaxation derived as a consequence of the generalized Provotorov equations

rinciple is very simple. In order to study the spin-lattice relaxation of ator Q of the spin system such as, say, I_z or I_x (in the rotating frame) ve choose this operator as an 'operator of interest' in the sense of the $\mathbf{B}(b)$ and $\mathbf{B}(c)$. As a second 'operator of interest' we choose the ɔnian $\mathcal{H}$ of the 'lattice' which is a physical system whose variables te with those of the nuclear spin system.

attice is assumed to be at all times in internal thermal equilibrium inverse 'lattice' temperature β_L. In the course of the coupling

PAPER No. 3

A NEW CONTROL AND INFORMATION SYSTEM DISCOVERED IN BIOLOGY AND MEDICINE: Extremely Low Frequency Magnetic Fields (ELF)

by

Andrija Puharich, M.D., LLD
Essentia Research Associates
Devotion, North Carolina, 27017, USA

February 1987

PART 3 CONTENTS

1. U.S. PATENT. 4,394,230 PUHARICH 1
   Method and Apparatus for splitting water molecules.

2. Method of splitting the water molecule according to the theory of ELF PHONONS-HYDROAMPLIFICATION OF STIMULATED EMISSION RADIATION, i.e. the PHASER. Analysis of the Phonon generated in water by the TD signal generator. 21

3. Stationary harmonic waves generated in the skin by SKIN-STROKING due to a fundamental frequency of 8.00 Hz. Phonons. 33

4. Review of experiments in biochemical origin of life. Showed that 8.00 Hz ELF magnetic field is the guiding information necessary to create life. The development of living forms can be described by the mathematics of the Mandelbrot Fractal Geometry. 68

5. References. 79

United States Patent [19]

Puharich

[11] **4,394,230**

[45] **Jul. 19, 1983**

[54] **METHOD AND APPARATUS FOR SPLITTING WATER MOLECULES**

[76] Inventor: **Henry K. Puharich**, Rte. 1, Box 97, Delaplane, Va. 22025

[21] Appl. No.: 272,277

[22] Filed: **Jun. 10, 1981**

[51] **Int. Cl.**[3] **C25B 1/04**; C25B 1/10; C25B 9/04

[52] **U.S. Cl.** **204/129**; 204/228; 204/260; 204/263; 204/266

[58] **Field of Search** 204/129, 228, 260, 263, 204/266

[56] **References Cited**

U.S. PATENT DOCUMENTS

3,563,246	2/1971	Puharich	331/47
3,726,762	4/1973	Puharich	128/422
4,107,008	8/1978	Horvath	204/129

Primary Examiner—R. L. Andrews

Attorney, Agent, or Firm—Mandeville and Schweitzer

[57] **ABSTRACT**

Disclosed herein is a new and improved thermodynamic device to produce hydrogen gas and oxygen gas from ordinary water molecules or from seawater at normal temperatures and pressure. Also disclosed is a new and improved method for electrically treating water molecules to decompose them into hydrogen gas and oxygen gas at efficiency levels ranging between approximately 80–100%. The evolved hydrogen gas may be used as a fuel; and the evolved oxygen gas may be used as an oxidant.

9 Claims, 20 Drawing Figures

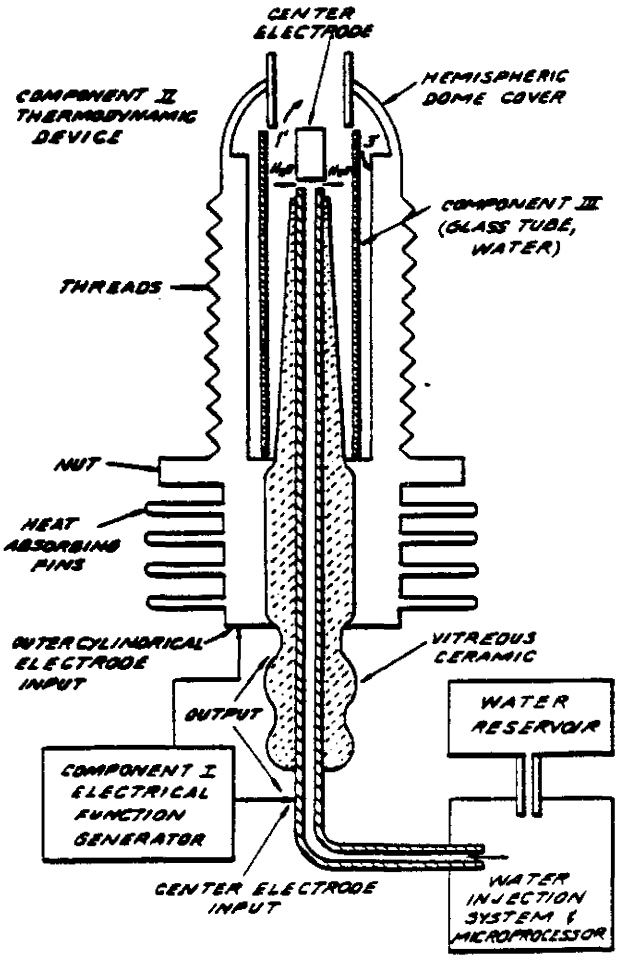

FIG. 1

COMPONENT I
SIGNAL GENERATOR
BLOCK DIAGRAM

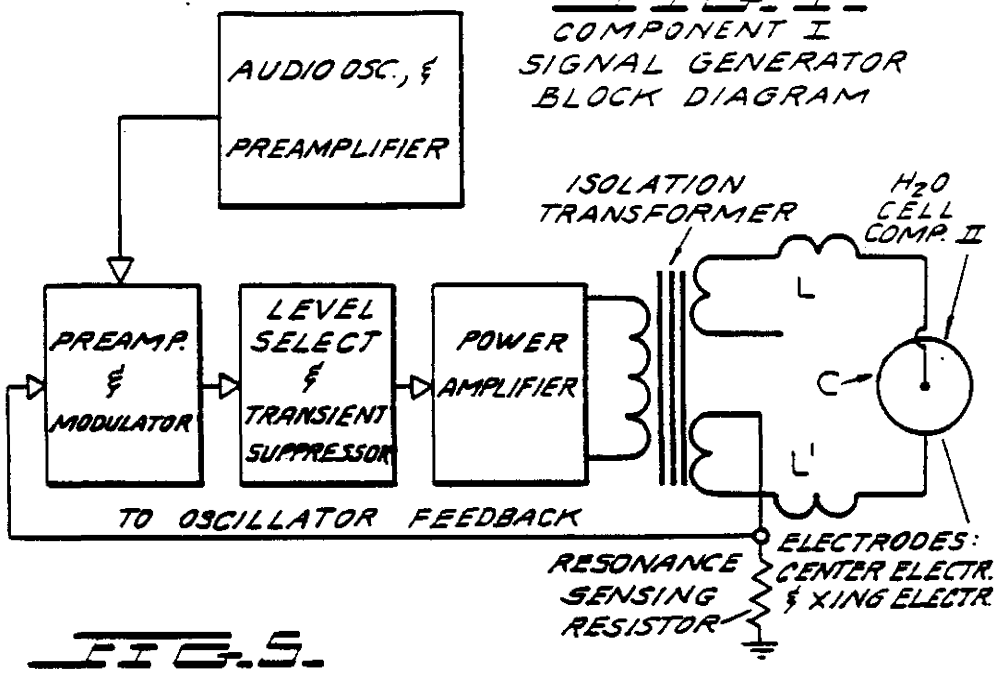

FIG. 5

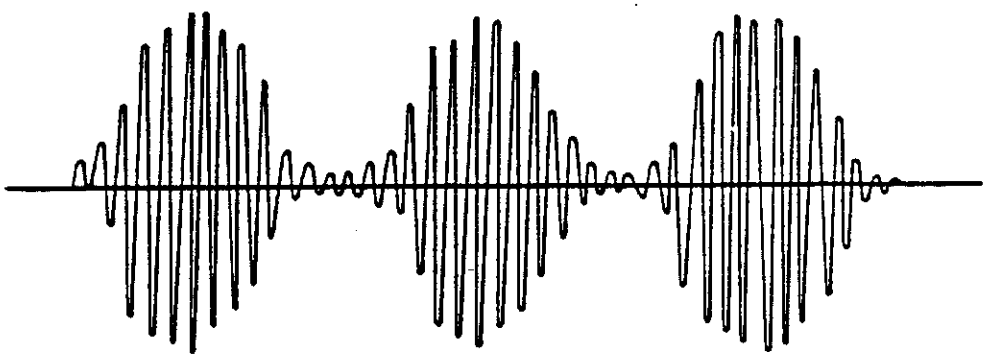

AMPLITUDE MODULATED 90° CARRIER SINE WAVE

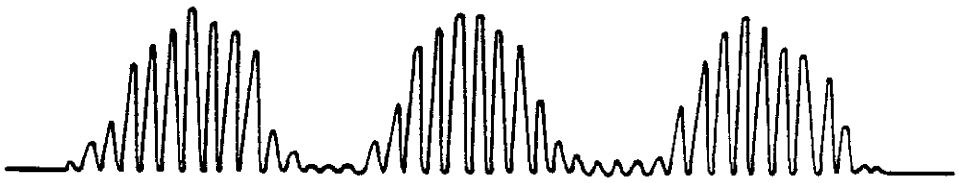

HALF-WAVE VECTIFICATION OF ABOVE SIGNAL

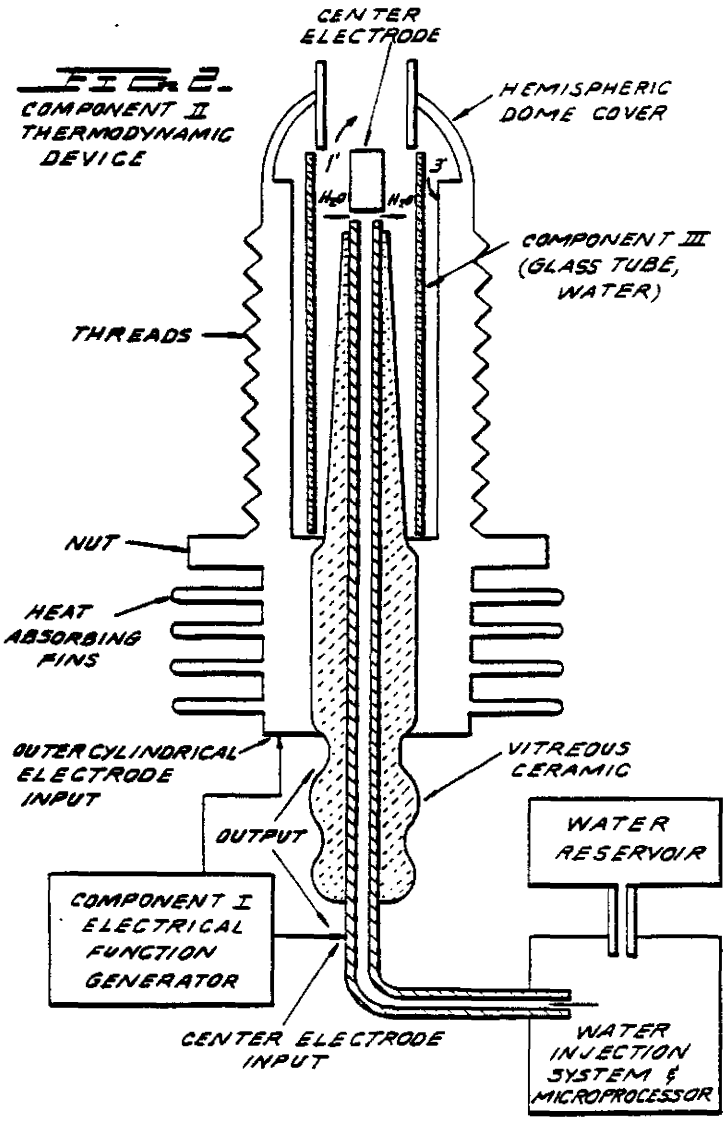
FIG 2-
COMPONENT II
THERMODYNAMIC
DEVICE
CENTER
ELECTRODE
HEMISPHERIC
DOME COVER
1'
3'
COMPONENT III
(GLASS TUBE,
WATER)
THREADS
NUT
HEAT
ABSORBING
FINS
OUTER CYLINDRICAL
ELECTRODE
INPUT
VITREOUS
CERAMIC
OUTPUT
WATER
RESERVOIR
COMPONENT I
ELECTRICAL
FUNCTION
GENERATOR
CENTER ELECTRODE
INPUT
WATER
INJECTION
SYSTEM &
MICROPROCESSOR

FIG. 3.

COMPONENT III.
THE WATER CELL SECTION
OF COMPONENT II

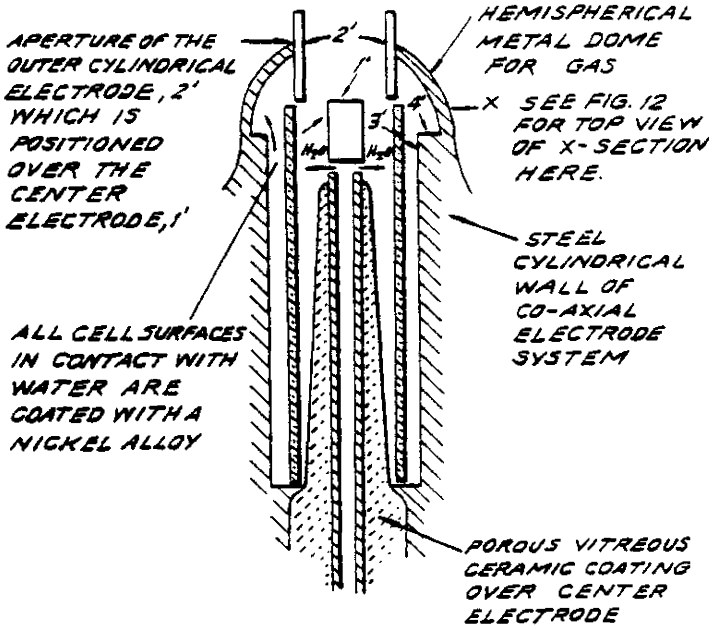

FIG. 4.

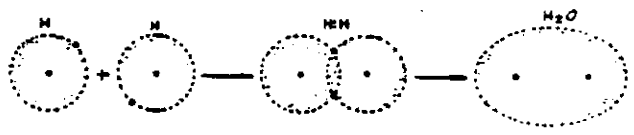

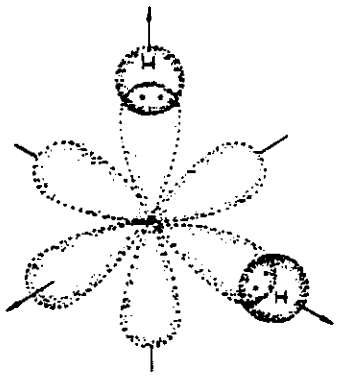

FIG. 4A.
UNHYBRIDIZED ORBITAL INTERACTION IN WATER BOND ANGLE IS 104° RATHER THAN 90° AS PREDICTED

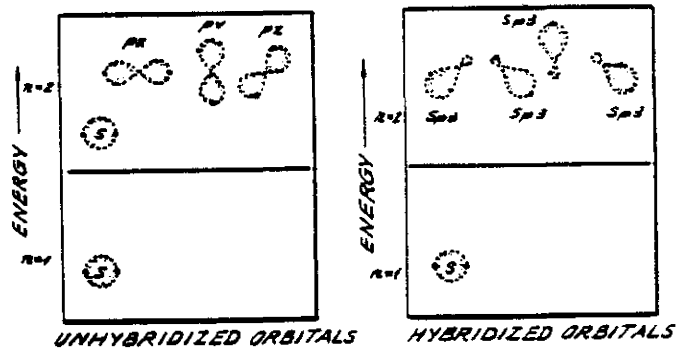

FIG. 4B.
FORMATION OF sp^3 HYBRID ORBITALS

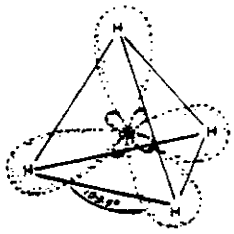

HYBRIDIZED METHANE MOLECULE CH_4

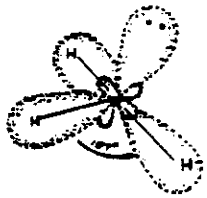

HYBRIDIZED AMMONIA MOLECULE NH_3

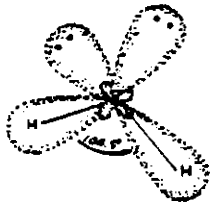

HYBRIDIZED WATER MOLECULE H_2O

FIG. 4C.
GEOMETRY OF METHANE, AMMONIA, AND WATER MOLECULES

FIG. 6.

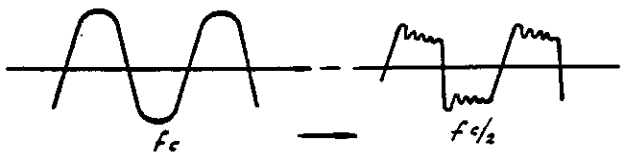



FIG. 6A.

FIG. 11.

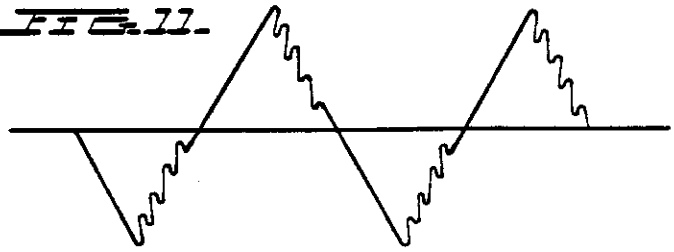

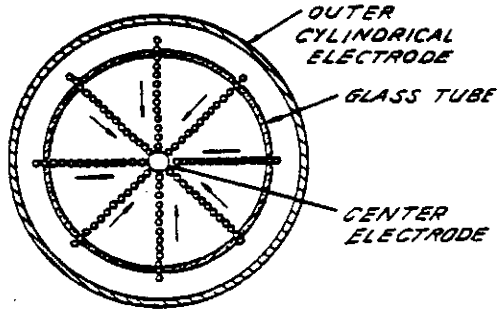

FIG. 12.
PEARL CHAIN FORMATION OF HYDROGEN GAS BUBBLES IN COMPONENT III AS SEEN FROM ABOVE

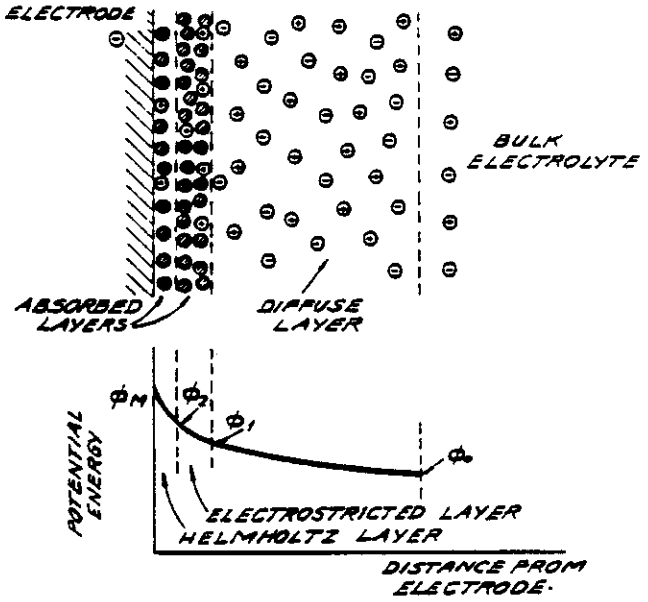

FIG. 7.

DIAGRAM OF THE DOUBLE LAYER CLOSE TO A NEGATIVE ELECTRODE. THE POTENTIAL ENERGY OF POSITIVE IONS IN THIS REGION WHEN NO CURRENT IS FLOWING IS SHOWN IN THE LOWER DIAGRAM. $\phi_M - \phi_2$ IS THE ELECTRON TRANSFER POTENTIAL: $\phi_2 - \phi_1$ IS RELATED TO THE ACTIVATION OVERPOTENTIAL: AND $\phi_1 - \phi_o$ IS RELATED TO THE DIFFUSION OVERPOTENTIAL

KEY
- ● SOLVENT MOLECULE = H_2O
- ⊕ POSITIVE ION = H^+
- ⊖ NEGATIVE ION = O^-

FIG. 8.

EQUIVALENT TETRAHEDRAL BONDING ORBITALS OF WATER

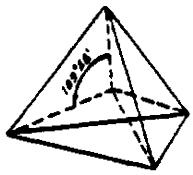

GEOMETRIC TETRAHEDRON

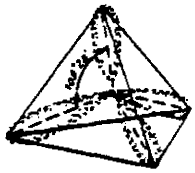

HYBRIDIZED BONDING ORBITALS OF WATER

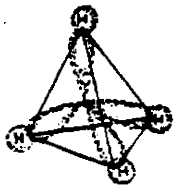

(a)

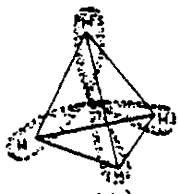

(b)

METHANE OVERLAP OF SPHERICAL 1s ORBITAL OF HYDROGEN WITH sp3 BONDING ORBITALS OF CARBON (a) RESULTS IN EQUIVALENT SIGMA BONDS, THE MOLECULAR ORBITALS OF (b).

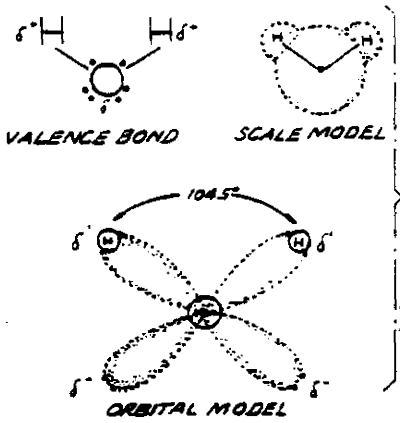

FIG. 9.
THE WATER MOLECULE. THE WATER DIPOLE RESULTS FROM UNEVEN CHARGE DISTRIBUTION.

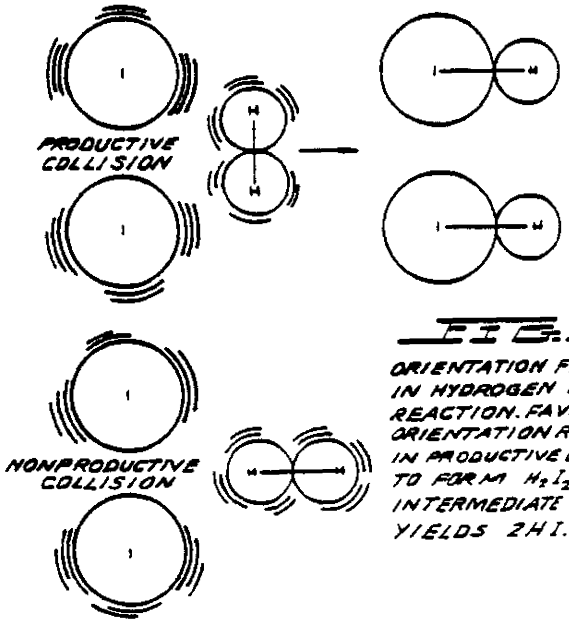

FIG. 10.
ORIENTATION FACTOR IN HYDROGEN IODIDE REACTION. FAVORABLE ORIENTATION RESULTS IN PRODUCTIVE COLLISION TO FORM H_2I_2 INTERMEDIATE WHICH YIELDS 2HI.

FIG. 13

A PLOT OF THE COURSE OF THE ONSET OF THE BARRIER EFFECT, AND UNBLOCKING IT WITH MECHANICAL TAPPING TO COMPONENTS II, III.

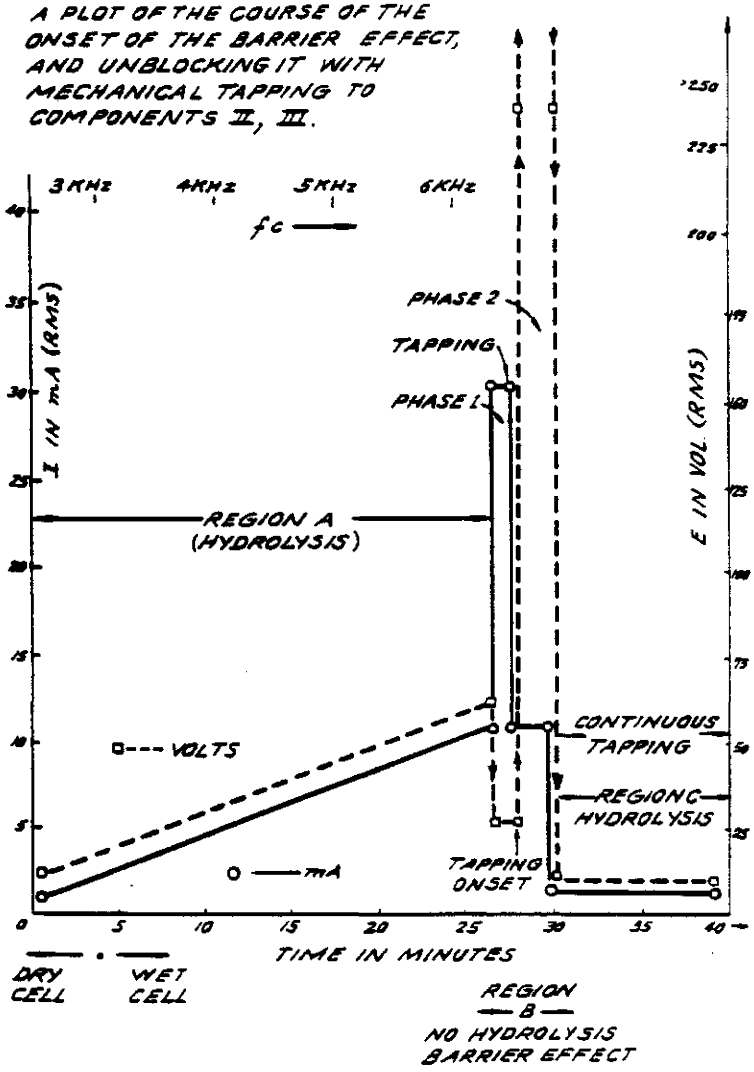

FIG. 14A.

(a) AN EXERGONIC REACTION. PRODUCTS HAVE A LOWER POTENTIAL ENERGY THAN REACTANTS, THEREFORE, ENERGY IS RELEASED.

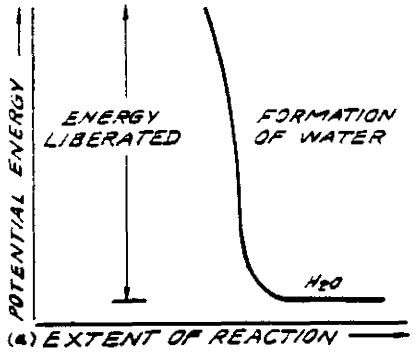

FIG. 14B.

(b) AN ENDERGONIC REACTION PRODUCTS HAVE A HIGHER POTENTIAL ENERGY THAN REACTANTS, CAUSING ENERGY TO BE CONSUMED.

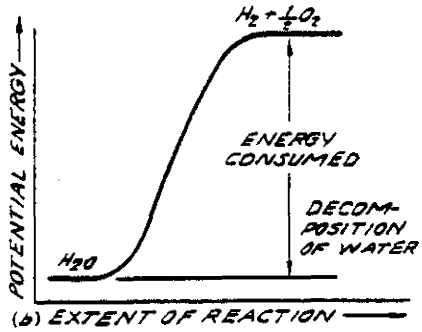

FIG. 14C.

ENERGY DIAGRAM FOR EXERGONIC REACTION. ACTIVATION ENERGY IS BARRIER TO BE OVERCOME FOR REACTION TO PROCEED, ⚡ IS SUPPLIED AS A "SPARK" TO THE GASES TO GET IGNITION.

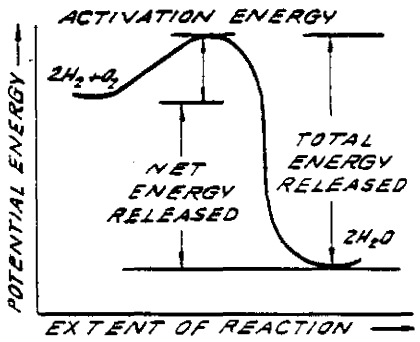

METHOD AND APPARATUS FOR SPLITTING WATER MOLECULES

BACKGROUND OF THE INVENTION

The scientific community has long realized that water is an enormous natural energy resource, indeed an inexhaustible source, since there are over 300 million cubic miles of water on the earth's surface, all of it a potential source of hydrogen for use as fuel. In fact, more than 100 years ago Jules Verne prophesied that water eventually would be employed as a fuel and that the hydrogen and oxygen which constitute it would furnish an inexhaustible source of heat and light.

Water has been split into its constituent elements of hydrogen and oxygen by electrolytic methods, which have been extremely inefficient, by thermochemical extraction processes called thermochemical water-splitting, which have likewise been inefficient and have also been inordinately expensive, and by other processes including some employing solar energy. In addition, artificial chloroplasts imitating the natural process of photosynthesis have been used to separate hydrogen from water utilizing complicated membranes and sophisticated artificial catalysts. However, these artificial chloroplasts have yet to produce hydrogen at an efficient and economical rate.

These and other proposed water splitting techniques are all part of a massive effort by the scientific community to find a plentiful, clean, and inexpensive source of fuel. While none of the methods have yet proved to be commercially feasible, they all share in common the known acceptability of hydrogen gas as a clean fuel, one that can be transmitted easily and economically over long distances and one which when burned forms water.

SUMMARY OF THE PRESENT INVENTION

In classical quantum physical chemistry, the water molecule has two basic bond angles, one angle being 104°, and the other angle being 109°28'.

The present invention involves a method by which a water molecule can be energized by electrical means so as to shift the bond angle from the 104° configuration to the 109°28' tetrahedral geometrical configuration.

An electrical function generator (Component I) is used to produce complex electrical wave form frequencies which are applied to, and match the complex resonant frequencies of the tetrahedral geometrical form of water.

It is this complex electrical wave form applied to water which is contained in a special thermodynamic device (Component II) which shatters the water molecule by resonance into its component molecules—hydrogen an oxygen.

The hydrogen, in gas form, may then be used as fuel; and oxygen, in gas form is used as oxidant. For example, the thermodynamic device of the present invention may be used as a hydrogen fuel source for any existing heat engine—such as, internal combustion engines of all types, turbines, fuel cell, space heaters, water heaters, heat exchange systems, and other such devices. It can also be used for the de-salinization of sea water, and other water purification purposes. It can also be applied to the development of new closed cycle heat engines where water goes in as fuel, and water comes out as a clean exhaust.

For a more complete understanding of the present invention and for a greater appreciation of its attendant advantages, reference should be made to the following detailed description taken in conjunction with the accompanying drawings.

DESCRIPTION OF THE DRAWINGS

FIG. 1 is a schematic block diagram illustrating the electrical function generator. Component I, employed in the practice of the present invention;

FIG. 2 is a schematic illustration of the apparatus of the present invention, including a cross sectional representation of the thermodynamic device. Component II;

FIG. 3 is a cross-sectional view of Component III of the present invention, the water cell section of Component II;

FIG. 4 is an illustration of the hydrogen covalent bond;

FIG. 4A is an illustration of the hydrogen bond angle;

FIG. 4B is an illustration of hybridized and un-hybridized orbitals;

FIG. 4C is an illustration of the geometry of methane ammonia and water molecules;

FIG. 5 is an illustration of an amplitude modulated carrier wave;

FIG. 6 is an illustration of a ripple square wave;

FIG. 6 A is an illustration of uni-polar pulses;

FIG. 7 is a diagram showing ion distribution at the negative electrode;

FIG. 8 is an illustration of tetrahedral bonding orbitals;

FIG. 9 is an illustration of water molecules;

FIG. 10 is an illustration of productive and non-productive collisions of hydrogen with iodine;

FIG. 11 is a wave form found to be the prime characteristic for optimum efficiency;

FIG. 12 is an illustration of pearl chain formation;

FIG. 13 is a plot of the course of the onset of the barrier effect and the unblocking of the barrier effect; and

FIGS. 14A, B, and C are energy diagrams for exergonic reactions.

DETAILED DESCRIPTION OF INVENTION

Section 1—Apparatus of Invention

The apparatus of the invention consists of three components, the electrical function generator, the thermodynamic device, and the water cell.

COMPONENT I. The Electrical Funtion Generator

This device has an output consisting of an audio frequency (range 20 to 200 Hz) amplitude modulation of a carrier wave (range 200 Hz to 100,000 Hz). The impedance of this output signal is continuously being matched to the load which is the second component, the thermodynamic device.

The electrical function generator represents a novel application of circuitry disclosed in my earlier U.S. Pat. Nos. 3,629,521; 3,563,246; and 3,726,762, which are incorporated by reference herein. See FIG. 1 for the block diagram of Component I.

COMPONENT II. The Thermodynamic Device

The thermodynamic device is fabricated of metals and ceramic in the geometric form of coaxial cylinder made up of a centered hollow tubular electrode which is surrounded by a larger tubular steel cylinder, said two

-13-

g. carrier wave form
h. RPM of an internal combustion engine (if used)
i. ignition control system
j. temperature of region to be heated;

(C) An electrical ignition system to ignite the evolved hydrogen gas fuel.

The important aspects of Component III are the tubu-

ammonia, NH_3 where there is only one lone pair, the repulsion is not so great and the bond angle is 107°. Carbon forms typical tetrahedral forms and components the simplest being the gas methane, CH_4. (See FIGS. 4C and 8). The repulsion of lone pair electrons affects charge distribution and contributes to the polar-

Section 2—Electrodynamics (Pure Water)

The electrodynamics of Components I, II, and III described individually and in interaction during the progress of purewater reaction rate in time. The reactions of saline water will be described in Section 3. It is to be noted that the output of Component I automatically follows the seven stages (hereinafter Stages A–F) of the reaction rate by varying its parameters of resonant carrier frequency, wave form, current voltage and impedance. All the seven states of the reaction herein described are not necessary for the practical operation of the system, but are included in order to explicate the dynamics and novel aspects of the invention. The seven stages are applicable only to the electrolysis of pure water.

STAGE A

Dry Charging of Component II by Component I

To make the new system operational, the Component I output electrodes are connected to component II, but no water is placed in the cell of Component III. When Component I output is across the load of Component II we observe the following electrical parameters are observed:

Range of current (I) output with (dry) load:
0 to 25 mA (milliamperes) rms.
Range of voltage (E) output with (dry) load:
0 to 250 Volts (AC) rms.

There is no distortion of the amplitude modulated (AM), or of the sine wave carrier whose center frequency, f_c

Ranges between 59,748 Hz to 66, 221 Hz
with f_c average=62, 985 Hz

The carrier frequency varies with the power output in that f_c goes down with an increase in amperes (current). The AM wave form is shown in FIG. 5. It is to be noted here that the electrical function generator, Component I, has an automatic amplitude modulation volume control which cycles the degree of AM from 0% to 100%, and then down from 100% to 0% at every 3.0 seconds. This cycle rate of 3.0 seconds corresponds to the nuclear spin relaxation time, τ/sec, of the water in Component III. The meaning of this effect will be discussed in greater detail in a later section.

In summary, the principal effects to be noted during Stage A -dry charging of Component II are as follows:

a. Tests the integrity of Component I circuitry.
b. Tests the integrity of the coaxial electrodes, and the vitreous ceramic materials of Component II and Component III.
c. Electrostatic cleaning of electrode and ceramic surfaces.

STAGE B

Initial operation of Component I, Component II, and with Component III containing pure water. There is no significant electrolysis of water during Stage B. However, in Stage B the sine wave output of Component I is shaped to a rippled square wave by the changing RC constant of the water as it is treated:

There is an 'Open Circuit' reversible threshold effect that occurs in Component III due to water polarization effects that lead to half wave rectification and the appearance of positive unipolar pulses; and

There are electrode polarization effects in Component II which are a prelude to true electrolysis of water as evidenced by oxygen and hydrogen gas bubble formation.

Appearance of Rippled Square Waves

Phase 1: At the end of the Stage A dry charging, the output of Component I is lowered to a typical value of:

$I = 1mA.$ $E = 24VAC$ f_c about 234 Hz.

Phase 2: Then water is added to the Component III water cell drop by drop until the top of the center electrode, 1', in FIG. 3 is covered, and when this water just makes contact with the inner surface of the top outer electrode at 2'. As this coupling of the two electrodes by water happens, the following series of events occur:

Phase 3: The f_c drops from 66,234 Hz. to a range from 1272 Hz to 1848 Hz. The current and voltage both drop, and begin to pulse in entrainment with the water nuclear spin relaxation constant, $\tau = 3.0$ sec. The presence of the nuclear spin relaxation oscillation is proven by a characteristic hysteresis loop on the X-Y axes of an oscilloscope.

$I = 0$ to 0.2mA surging at τ cycle

$E = 4.3$ to $4.8VAC$ surging at τ cycle

The sine wave carrier converts to a rippled square wave pulse which reflects the RC time constant of water, and it is observed that the square wave contains higher order harmonics. See FIG. 6:

With the appearance of the rippled square wave, the threshold of hydrolysis may be detected (just barely) as a vapor precipitation on a cover glass slip placed over the Component III cell and viewed under a low power microscope.

The 'Open Circuit' Reversible Threshold Effect

Phase 4: A secondary effect of the change in the RC constant of water on the wave form shows up as a full half wave rectification of the carrier wave indicating a high level of polarization of the water molecule in tetrahedral form at the outer electrode.

With the already noted appearance of the rippled square wave, and the signs of faint vapor precipitation which indicate the earliest stage of electrolysis, it is possible to test for the presence of a reversible hydrolysis threshold. This test is carried out by creating an open circuit between Components I and II, i.e., no current flows. This is done by lowering the water level between the two electrodes in the region—1' and 2' shown in FIG. 3; or by interrupting the circuit between Component I and II, while the Component I signal generator is on and oscillating.

Immediately, with the creation of an 'open circuit' condition, the following effects occur:

(a) The carrier frequency, f_c, shifts from Phase 4 valve 1272 Hz to 1848 Hz to 6128 Hz.

(b) The current and voltage drop to zero on the meters which record I and E, but the oscilloscope continues to show the presence of the peak-to-peak (p-p) voltage, and the waveform shows a remarkable effect. The rippled square wave has disappeared, and in its place there appear unipolar (positive) pulses as follows in FIG. 6A.

The unipolar pulse frequency stabilizes to ca. 5000 Hz. The unipolar pulses undergo a 0 to 1.3 volt pulsing amplitude modulation with τ at 3.0 seconds.

Thus, there exists a pure open circuit reversible threshold for water electrolysis in which the water molecules are capacitor charging and discharging at their characteristic low frequency RC time constant of 0.0002 seconds. It is to be noted that pure water has a very high dielectric constant which makes such an effect possible. The pulsing amplitude modulation of the voltage is determined by the Hydrogen Nuclear Spin Relaxation constant, where τ_H=3.0 seconds. It is to be noted that the positive pulse spikes are followed by a negative after-potential. These pulse wave forms are identical to the classic nerve action potential spikes found in the nervous system of all living species that have a nervous system. The fact that these unipolar pulses were observed arising in water under the conditions of reversible threshold hydrolysis has a profound significance. These findings illuminate and confirm the Warren McCulloch Theory of water "crystal" dynamics as being the foundation of neural dynamics; and the converse theory of Linus Pauling which holds that water clathrate formation is the mechanism of neural anesthesia.

Phase 5: The effects associated with reversible threshold electrolysis are noted only in pauses since they reflect events which are occurring on the electrode surfaces of Component II, the Thermodynamic Device.

A principal effect that occurs in Stage B, Phase 3, in Component II, the thermodynamic device, is that the two electrodes undergo stages of polarization. It has been observed in extensive experiments with different kinds of fluids in the cell of Component II i.e., distilled water, sea water, tap water, Ringers solution, dilute suspensions of animal and human blood cells, that the inner surface of the outer ring electrode at 3' in FIG. 3 (the electrode that is in contact with the fluid) becomes negatively charged. Referring to FIG. 7, this corresponds to the left hand colummar area marked, Electrode ⊖.

Electrode Polarization Effects at the Interface Between Components II and III

Concurrently with the driver pulsing of Component I at the τ constant cycle which leads to electrode polarization effects in Component II, there is an action on Component III which energizes and entrains the water molecule to a higher energy level which shifts the bond angle from 104° to the tetrahedral form with angle 109°28' as shown in FIGS. 8 and 15. This electronic pumping action is most important, and represents a significant part of the novel method of this invention for several reasons. First, the shift to the tetrahedral form of water increases the structural stability of the water molecule, thereby making it more susceptible to breakage at the correct resonant frequency, or frequencies. Second, increasing the polarization of the water molecule makes the lone pair electrons, S— connected with the oxygen molecule more electronegative; and the weakly positive hydrogen atoms, S+ more positive. See FIG. 9 and FIG. 22.

As the outer electrode becomes more electronegative, the center electrode concomitantly becomes more electropositive as will be shown. As the polarity of the water molecule tetrahedron increases, a repulsive force occurs between the two S+ apices of the water tetrahedron and the negatively charged electrode surface within the region of the Helmholtz layer, as shown in FIG. 7. This effect "orients" the water molecule in the field, and is the well-known "orientation factor" of electrochemistry which serves to catalyse the rate of oxygen dissociation from the water molecule, and thereby causes the reaction rate to proceed at the lowest energy levels. See FIG. 10 for an example of how the orientation factor works.

Near the end of Stage B, the conditions are established for the beginning of the next stage, the stage of high efficiency electrolysis of water.

STAGE C

Generation of the complex wave form frequencies from Component I to match the complex wave form resonant frequencies of the energized and highly polarized water molecule in tetrahedral form with angles, 109°28' are carried out in Stage C.

In the operation of the invention active bubble electrolysis of water is initiated following Stage B, phase 3 by setting (automatically) the output of Component I to:

I=1mA. E=12VAC—rms

causing the rippled square wave pulses to disappear with the appearance of a rippled sawtooth wave. The basic frequency of the carrier now becomes, f_c=3980 Hz.

The wave form now automatically shifts to a form found to be the prime characteristic necessary for optimum efficiency in the electrolysis of water and illustrated in FIG. 11. In the wave form of FIG. 11, the fundamental carrier frequency, f_c=3980 Hz., and a harmonic modulation of the carrier is as follows:

1st Order Harmonic Modulation (OHM)=7960 Hz.
2nd Order Harmonic Modulation (II OHM)=15,920 Hz.
3rd Order Harmonic Modulation (III OHM)=31,840 Hz.
4th Order Harmonic Modulation (IV OHM)=63,690 Hz.

What is believed to be happening in this IV OHM effect is that each of the four apices of the tetrahedron water molecule is resonant to one of the four harmonics observed. It is believed that the combination of negative repulsive forces at the outer electrode with the resonant frequencies just described work together to shatter the water molecule into its component hydrogen and oxygen atoms (as gases). This deduction is based on the following observations of the process through a low power microscope. The hydrogen bubbles were seen to originate at the electrode rim, 4', of FIG. 3. The bubbles then moved in a very orderly 'pearl chain' formation centripetally (like the spokes of a wheel) toward the center electrode, 1' of FIG. 3. FIG. 12 shows a top view of this effect.

Thereafter, upon lowering the output of Component I, the threshold for electrolysis of water as evidenced by vapor deposition of water droplets on a glass cover plate over the cell of Component III, is:

I = mA.
E = 10 volts
} = 10 rms

with all other conditions and waveforms as described under Stage C, supra. Occasionally, this threshold can be lowered to:

I = mA

-continued

E = 2.0 volts } = 2.0 min.

This Stage C vapor hydrolysis threshold effect cannot be directly observed as taking place in the fluid because no bubbles are formed—only invisible gas molecules which become visible when they strike a glass plate and combine into water molecules and form droplets which appear as vapor.

STAGE D

Production of hydrogen and oxygen gas at an efficient rate of water electrolysis is slowed in Stage D when a barrier potential is formed, which barrier blocks electrolysis, irrespective of the amount of power applied to Components II and III.

A typical experiment will illustrate the problems of barrier potential formation. Components I, II, and III are set to operate with the following parameters:

I = 1 mA. } = 11.2 min. (at the start)
E = 11.2 volts } (rising to 100 min.)

This input to Component III yields, by electrolysis of water, approximately 0.1 cm^3 of hydrogen gas per minute at one atmosphere and 289° K. It is observed that as a function of time the f_c crept up from 2978 Hz to 6474 Hz over 27 minutes. The current and the voltage also rose with time. At the 27th minute a barrier effect blocked the electrolysis of water, and one can best appreciate the cycle of events by reference to FIG. 13.

STAGE E

The Anatomy of the Barrier Effect

Region A: Shows active and efficient hydrolysis

Region B: The barrier region effect can be initiated with taps of the finger, or it can spontaneously occur as a function of time.

Phase a: The current rose from 1 mA to 30 mA. The voltage fell from 22 volts to 2.5 V.

Phase b: If component II is tapped mechanically during Phase a supra—it can be reversed as follows: The current dropped from 30 Ma to 10 Ma. The voltage shot up from 5 volts to over 250 volts (off scale).

Throughout Phase a and Phase b, all hydrolysis has ceased. It was observed under the microscope that the inner surface of the outer electrode was thickly covered with hydrogen gas bubbles. It was reasoned that the hydrogen gas bubbles had become trapped in the electrostricted layer, because the water molecule tetrahedrons had flipped so that the S+ hydrogen apices had entered the Helmholtz layer and were absorbed to the electronegative charge of the electrode. This left the S− lone pair apices facing the electrostricted layer. This process bound the newly forming H^+ ions which blocked the reaction

$$H^+ + H^+ + 2e \rightarrow H_2(gas)$$

STAGE F

Region C. It was found that the barrier effect could be unblocked by some relatively simple procedures:

(a) Reversing the output electrodes from Component I to Component II, and/or:

(b) Mechanically tapping the Component III cell at a frequency T/2 = 1.5 seconds per tap.

These effects are shown in FIG. 12 and induce the drop in barrier potential from:

E = 250 volts to 4 volts } = 4 min. (final state)
I = 10 mA to 1 mA

Upon unblocking of the barrier effect, electrolysis of water resumed with renewed bubble formation of hydrogen gas.

The barrier potential problem has been solved for practical application by lowering the high dielectric constant of pure water, by adding salts (NaCl, KOH, etc.) to the pure water thereby increasing its conductivity characteristics. For optimum efficiency the salt concentration need not exceed that of sea water (0.9% salinity) in Section 3, "Thermodynamics of the Invention", it is to be understood that all water solutions described are not "pure" water as in Section B, but refer only to *salinized* water.

Section 3—The Thermodynamics of the Invention (Saline Water)

Introduction (water, hereinafter refers to salinized water)

The thermodynamic considerations in the normal operations of Components I, II, and III in producing hydrogen as fuel, and oxygen as oxidant during the electrolysis of water, and the combustion of the hydrogen fuel to do work in various heat engines is discussed in this section.

In chemical reactions the participating atoms form new bonds resulting in compounds with different electronic configurations. Chemical reactions which release energy are said to be exergonic and result in products whose chemical bonds have a lower energy content than the reactants. The energy released most frequently appears as heat. Energy, like matter, can neither be created nor destroyed according to conservation law. The energy released in a chemical reaction plus the lower energy state of the products is equal to the original energy content of the reactants. The burning of hydrogen occurs rather violently to produce water as follows:

$$2H_2 + O_2 \rightarrow 2H_2O - \Delta H\ 68.315\ Kcal/mol$$ (this is the enthalpy, or heat of combustion at constant pressure)

(18 gms) = 1 mol)

The chemical bonds of the water molecules have a lower energy content than the hydrogen and oxygen gases which serve as the reactants. Low energy molecules are characterized by their ability. High energy molecules are inherently unstable. These relations are summarized in the two graphs of FIG. 14. It is to be noted that FIG. 14 (*b*) shows the endergonic reaction aspect of the invention when water is decomposed by electrolysis into hydrogen and oxygen. FIG. 14 (*a*) shows the reaction when the hydrogen and oxygen gases combine, liberate energy, and re-form into water. Note that there is a difference in the potential energy of the two reactions. FIG. 14 (*c*) shows that there are two components to this potential energy. The net energy released, or the energy that yields net work is labelled in the diagram as Net Energy released, and is more prop-

erly called the free energy change denoted by the Gibbs function, $-\Delta G$. The energy which must be supplied for a reaction to achieve (burning) spontaneity is called the activation energy. The sum of the two is the total energy released. A first thermodynamic subtlety of the thermodynamic device of the invention is noted in Angus McDougall's FUEL CELLS, Energy Alternative Series, The MacMillan Press Ltd., London, 1976. page 15 it is stated:

"The Gibbs function is defined in terms of the enthalpy H, and the entropy S of the system:

$G = H - TS$ (where T is the thermodynamic temperature)

A particularly important result is that for an electrochemical cell working reversibly at constant temperature and pressure, the *electrical* work done is the *net work* and hence,

$\Delta G = -w_e$

For this to be a reversible process, it is necessary for the cell to be on 'open circuit', that is, no current flows and the potential difference across the electrodes is the EMF, E. Thus,

$\Delta G = -zFE$

(where F is the Faraday constant—the product of the Avogadro Constant $\div N_A = 6.022045 \times 10^{23}$ mole^{-1}, and the charge on the electron, $e = 1.602189 \times 10^{-19}$ C—both in SI units and z is the number of electrons transported.) When the cell reaction proceeds from left to right."

It is to be noted that the activation energy is directly related to the controlling reaction rate process, and thus is related to the Gibbs free energy changes.

The other thermodynamic subtlety is described by S. S. Penner in his work:

Penner, S. S. and L. Icerman, ENERGY, Vol. II, Non-Nuclear Energy Technologies. Addison-Wesley Publishing Company, Inc. Revised Edition, 1977. Reading, Mass. Page 140 ff.

"It should be possible to improve the efficiency achieved in practical electrolysis to about 100% because, under optimal operating conditions, the theoretically-attainable energy conversion by electrolysis is about 120% of the electrical energy input. The physical basis for this last statement will now be considered.

"A useful definition for energy efficiency in electrolysis is the following: the energy efficiency is the ratio of the energy released from the electrolysis products formed (when they are subsequently used) to the energy required to effect electrolysis. The energy released by the process

H_2 (gas) + $(\frac{1}{2})O_2$ (gas) $\rightarrow H_2O$ (liquid)

under standard conditions (standard conditions in this example are: (1) atmospheric pressure = 760 mm Hg and (2) temperature = 298.16° K. = 25° C. = 77° F.) is 68.315 Kcal and is numerically equal to the enthalpy change (ΔH) for the indicated process. On the other hand, the *minimum* energy (or useful work input) required at constant temperature and pressure for electrolysis equals the Gibbs free energy change (ΔG). There is a basic relation derivable from the first and second laws of thermodynamics for isothermal changes, which shows that

$\Delta G = \Delta H - T\Delta S$

where ΔS represents the entropy change for the chemical reaction. The Gibbs free energy change (ΔG) is also related to the voltage (E) required to implement electrolysis by Faraday's equation, viz.

$E = (\Delta G/23.06n)$ volts

where ΔG is in Kcal/mol and n is the number of electrons (or equivalents) per mol of water electrolyzed and has the numerical value 2.

"At atmospheric pressure and 300° K., $\Delta H = 68.315$ Kcal/mol of H_2O (l) and $\Delta G = 56.62$ Kcal/mole of H_2O (l) for the electrolysis of liquid water. Hence, the energy efficiency of electrolysis at 300° K. is about 120%."

$\frac{\Delta H}{\Delta G} = 120\%$

"(When) H_2 (gas) and O_2 (gas) are generated by electrolysis, the electrolysis cell must absorb heat from the surroundings, in order to remain at constant temperature. It is this ability to produce gaseous electrolysis products with heat absorption from the surroundings that is ultimately responsible for energy-conversion efficiencies during electrolysis greater than unity."

Using the citations of these two authorities, it is possible to make a rough calculation of the efficiency of the present invention.

Section 4—Thermodynamic Efficiency of the Invention

Efficiency is deduced on the grounds of scientific accounting principles which are based on accurate measurements of total energy input to a system (debit), and accurate measurements of total energy (or work) obtained out of the system (credit). In principle, this is followed by drawing up a balance sheet of energy debits and credits, and expressing them as an efficiency ratio, η.

$$\eta = \frac{\text{Credit}}{\text{Debit}} = \frac{\text{Energy Out}}{\text{Energy In}} = < 1$$

The energy output of Component I is an alternating current looking into a highly non-linear load, i.e., the water solution. This alternating current generator (Component I) is so designed that at peak load it is in resonance (Components I, II, III), and the vector diagrams show that the capacitive reactance, and the inductive reactance are almost exactly 180° out of phase, so that the net power output is reactive, and the dissipative power is very small. This design insures minimum power losses across the entire output system. In the experiments which are now to be described the entire emphasis was placed on achieving the maximum gas yield (credit) in exchange for the minimum applied energy (debit).

The most precise way to measure the applied energy to Components II and III is to measure the Power, P, in Watts, W. This was done by precision measurements of

the volts across Component II as root mean square (rms) volts; and the current flowing in the system as rms amperes. Precisely calibrated instruments were used to take these two measurements. A typical set of experiments (using water in the form of 0.9% saline solution =0.1540 molar concentration) to obtain high efficiency hydrolysis gave the following results:

rms Current = I = 25 mA to 38 mA (0.025 A to 0.038 A)

rms Volts = E = 4 Volts to 2.6 Volts

The resultant ratio between current and voltage is dependent on many factors, such as the gap distance between the center and ring electrodes, dielectric properties of the water, conductivity properties of the water, equilibrium states, isothermal conditions, materials used, and even the presence of clathrates. The above current and voltage values reflect the net effect of various combinations of such parameters. The product of rms current, and rms volts is a measure of the power, P in watts:

$$P = I \times E = 25\ ma \times 4.0\ volts = 100\ mW\ (0.1\ W)$$

$$P = I \times E = 38\ ma \times 2.6\ volts = 98.8\ mW\ (0.0988\ W)$$

At these power levels (with load), the resonant frequency of the system is 600 Hz (±5 Hz) as measured on a precision frequency counter. The wave form was monitored for harmonic content on an oscilloscope, and the nuclear magnetic relaxation cycle was monitored on an X-Y plotting oscilloscope in order to maintain the proper hysteresis loop figure. All experiments were run so that the power in Watts, applied through Components I, II, and III ranged between 98.8 mW to 100 mW.

Since, by the International System of Units—1971 (SI), One-Watt-second (Ws) is exactly equal to One Joule (J), the measurements of efficiency used these two yardsticks (1 Ws = 1 J) for the debit side of the measurement.

The energy output of the system is, of course, the two gases, hydrogen (H_2) and oxygen ($\frac{1}{2}O_2$), and this credit side was measured in two laboratories, on two kinds of calibrated instruments, namely, a Gas Chromatography Machine, and, a Mass Spectrometer Machine.

The volume of gases, H_2 and $(\frac{1}{2})O_2$, was measured as produced under standard conditions of temperature and pressure in unit time, i.e., in cubic centimeters per minute (cc/min), as well as the possibly contaminating gases, such as air oxygen, nitrogen and argon; carbon monoxide, carbon dioxide, water vapor, etc.

The electrical, and gas, measurements were reduced to the common denominator of Joules of energy so that the efficiency accounting could all be handled in common units. The averaged results from many experiments follow. The Standard Error between different samples, machines, and locations is ±10%, and only the mean was used for all the following calculations.

Section 5—Endergonic Decomposition of Liquid Water

Thermodynamic efficiency for the endergonic decomposition of liquid water (salinized) to gases under standard atmosphere (754 to 750 m.m. Hg), and standard isothermal conditions @ 25° C. = 77° F. = 298.16° K., according to the following reaction:

$$H_2O(l) \rightarrow H_2(g) + (\tfrac{1}{2})O_2(g) - \Delta G 56.620\ KCal/mole$$

As already described, ΔG is the Gibbs function (FIG. 14*b*). A conversion of Kcal to the common units, Joules, by the formula, One Calorie = 4.1868 Joules was made.

$\Delta G = 56.620\ Kcal \times 4.1868\ J = 236.954\ J/mol$ of H_2O (1) where, 1 mole is 18 gms.

ΔG = the free energy required to yield an equivalent amount of energy from H_2O in the form of the gases, H_2 and $(\frac{1}{2})O_2$.

To simplify the calculations, the energy required to produce 1.0 c.c. of H_2O as the gases, H_2 and $(\frac{1}{2})O_2$ was determined. There are (under standard conditions) 22,400 c.c. = V, of gas in one mole of H_2O. Therefore,

$$\frac{\Delta G}{V} = \frac{236.954\ J}{22{,}400\ cc} = 10.5783\ J/cc$$

The electrical energy required to liberate 1.0 cc of the H_2O gases (where $H_2 = 0.666$ parts, and $(\frac{1}{2})O_2 = 0.333$ parts, by volume) from liquid water is then determined. Since P = 1 Ws = 1 Joule, and V = 1.0 cc of gas = 10.5783 Joules, then,

$$PV = 1\ J \times 10.5783\ J = 10.5783\ J = 10.5783\ Ws$$

Since the experiments were run at 100 mW (0.1 W) applied to the water sample in Component II, III, for 30 minutes, the ideal (100% efficient) gas production at this total applied power level was calculated.

$$0.1\ Ws \times 60\ sec \times 30\ min = 180.00\ Joules\ (for\ 30\ min)$$

The total gas production at Ideal 100% efficiency is,

$$180.00\ J / 10.5783\ J/cc = 17.01\ cc\ H_2O\ (g)$$

The amount of hydrogen present in the 17.01 cc H_2O (g) was then calculated.

$$17.01\ cc\ H_2O\ (gas) \times 0.666\ H_2\ (g) = 11.329\ cc\ H_2\ (g)$$

$$17.01\ cc\ H_2O\ (g) \times 0.333(\tfrac{1}{2})O_2\ (g) = 5.681\ cc\ (\tfrac{1}{2})O_2\ (g)$$

Against this ideal standard of efficiency of expected gas production, the actual amount of gas produced was measured under: (1) standard conditions as defined above (2) 0.1 Ws power applied over 30 minutes. In the experiments, the mean amount of H_2 and $(\frac{1}{2})O_2$ produced, as measured on precision calibrated GC, and MS machines in two different laboratories, where the S.E. is ±10%, was,

Measured Mean	=	10.80 cc H_2(g)
Measured Mean	=	5.40 cc $(\frac{1}{2})O_2$(g)
Total Mean	=	16.20 cc H_2O(g)

The ratio, η, between the ideal yield, and measured yield,

$$\eta = \frac{\text{Measured } H_2(g)}{\text{Ideal } H_2(g)} = \frac{10.80\ cc}{11.33\ cc} = 91.30\%$$

Section 6—Energy Release

The total energy release (as heat, or electricity) from an exergonic reaction of the gases, H_2 and O_2, is given by,

$H_2(g) + (\frac{1}{2})O_2(g) \longrightarrow H_2O(l) - \Delta H$ of 285 Kcal/mol =

$(-\Delta H$ 286,021 Joules)/mol

It is possible (Penner, Op. Cit., p. 128) to get a total heat release, or total conversion to electricity in a fuel cell, in the above reaction when the reactants are initially near room temperature (298.16° K.), and the reactant product (H_2O) is finally returned to room temperature. With this authoritative opinion in mind, it is desirable to determine the amount of energy released (ideal) from the exergonic experiment. The total energy of 1.0 cc of H_2O (l), as above is:

$$1.0 \text{ cc } \Delta H = \frac{286,021 \text{ J/mol}}{22,400 \text{ cc/mol}} = 12.7687 \text{ J/cc } H_2O \text{ (l)}$$

for $H_2 = 12.7687 \times 0.666 = 8.509$ J/0.66 cc H_2
for $O_2 = 12.7687 \times 0.333 = 4.259$ J/0.33 cc $(\frac{1}{2})O_2$

The energy produced from the gases produced in the experiments in an exergonic reaction was,

16.20 cc H_2O (g) $\times$ 12.7687 J/cc $H_2O = 206.8544$ J.

The overall energy transaction can be written as,

$$\frac{\text{EXERGONIC}}{\text{ENDERGONIC}} = \eta = \frac{-\Delta H}{+\Delta G} = \frac{206.8544 \text{ J}}{180.000 \text{ J}} =$$

1.14919 = 114.919%

In practical bookkeeping terms the balance of debits and credits, $n = (-\Delta H) - (+\Delta G)$, so, $n = 206.8544$ J $- 180.0 = +26.8544$ J (surplus)

Since, in the invention, the gas is produced where and when needed, there is no additional cost accounting for liquifaction, storage, or transportation of the hydrogen fuel, and the oxygen oxidant. Therefore, the practical efficiency, is

$$\eta_p = \frac{26.8544 \text{ J}}{180.0000 \text{ J}} =$$

14.919% (or not return on the original energy investment)

In practical applications, the energy output (exergonic) of the *Component II System* can be parsed between the electrical energy required to power the Component I System, as an isothermal closed loop; while the surplus of approximately 15% can be sheared to an engine (heat) electrical, battery, etc.) that has a work load. Although this energy cost accounting represents an ideal model, it is believed that there is enough return (app. 15%) on the capital energy investment to yield a net energy profit that can be used to do useful work.

Conclusion

From the foregoing disclosure it will be appreciated that the achievement of efficient water splitting through the application of complex electrical waveforms to energized water molecules, i.e. tetrahedral molecules having bonding angles of 109° 28', in the special apparatus described and illustrated, will provide ample and economical production of hydrogen gas and oxygen gas from readily available sources of water. It is to be understood, that the specific forms of the invention disclosed and discussed herein are intended to be representative and by way of illustrative example only, since various changes may be made therein without departing from the clear and specific teachings of the disclosure. Accordingly, reference should be made to the following appended claims in determining the full scope of the method and apparatus of the present invention.

I claim:

1. A method for splitting water molecules into hydrogen and oxygen comprising
(a) generating complex electrical wave forms matching the complex wave form resonant frequencies of tetrahedral water molecules;
(b) applying said generated wave forms in resonance to said water molecules to shatter said molecules, thereby liberating hydrogen and oxygen.

2. The method of claim 1, in which
(a) the bond angles of said tetrahedral water molecules are approximately 109°.

3. The method of claim 1, in which
(a) said water molecules are saline water molecules.

4. The method of claim 1, in which
(a) the bond angles of said tetrahedral water molecules are 109° 28'.

5. The method of claim 1, in which
(a) the applied complex wave form is a signal in the form of an audio-frequency, amplitude modulated carrier wave;
(b) the water molecules are supplied to a cell during electrolysis;
(c) the impedance of said signal is matched continuously with that of said cell during the electrolysis of said molecules.

6. The method of claim 5, in which
(a) the audio frequency is in the range of 20 to 200 Hz.;
(b) the carrier wave is in the range of 200-100,000 Hz.

7. Apparatus for splitting water molecules into hydrogen and oxygen comprising
(a) water cell means including a pair of electrode means;
(b) means for supplying water molecules to said cell means;
(c) means for generating signals in the forms of complex electrical waves having resonant frequencies of tetrahedral water molecules;
(d) means for applying said generated signals to said electrode means;
(e) means to recover liberated hydrogen and oxygen from said cell means.

8. The apparatus of claim 7, in which
(a) said electrode means includes an outer cylindrical electrode of steel alloys coated on its inner surfaces with a nickel alloy and an inner coaxial hollow tubular electrode coated on its outer surface with a nickel alloy;
(b) said signal generating means, including means matching the impedance of said generated signal with that of said electrodes.

9. The apparatus of claim 8, in which
(a) said outer electrode includes integral fins;
(b) porous vitreous ceramic means, are disposed about said center electrode;
(c) a pair of spaced cylindrical glass tubes, one of which surrounds said vitreous ceramic means are disposed in said water cell means;
(d) the uppermost portion of said outer electrode is generally hemispherically shaped;
(e) the other of said glass tubes extends upwardly through said outer electrode and forms a gas vent for said cell means.

* * * * *

METHOD of SPLITTING THE WATER MOLECULE

according to the Theory of

Extremely Low Frequency (ELF)

PHONON-HYDRON AMPLIFICATION OF STIMULATED

EMISSION RADIATION

(Acronym = PHASER)

We have referred in the patent U.S. 4,394,230. p.3 to COMPONENT III as being the liquid water solution contained in COMPONENT II. In Fig. 15 we show the tetrahedral structure of water in the form in which the complex electromagnetic waves of COMPONENT I see the water molecule. The center of mass of this geometry is the oxygen atom, and as we will show later, it serves as a polarizing element very much like a diode (n-p) acts in a circuit. It is the geometry arrangement of the p electrons of oxygen that determine the vectors, $i(H_1)$ and $i(H_2)$; and $i(L_1)$ and $i(L_2)$ which in turn determines the tetrahedral architecture of the water molecule. The p electron configuration of oxygen is shown in Fig. 16. Reference to Fig. 15 shows that the diagonal of the right side of the cube has at its corner terminations the positive charge hydrogen (H^+) i(H) atoms; and that the left side of the cube diagonal has at its corners the lone pair electrons, i(L) (e^-, e^-). It is further to be noted that this

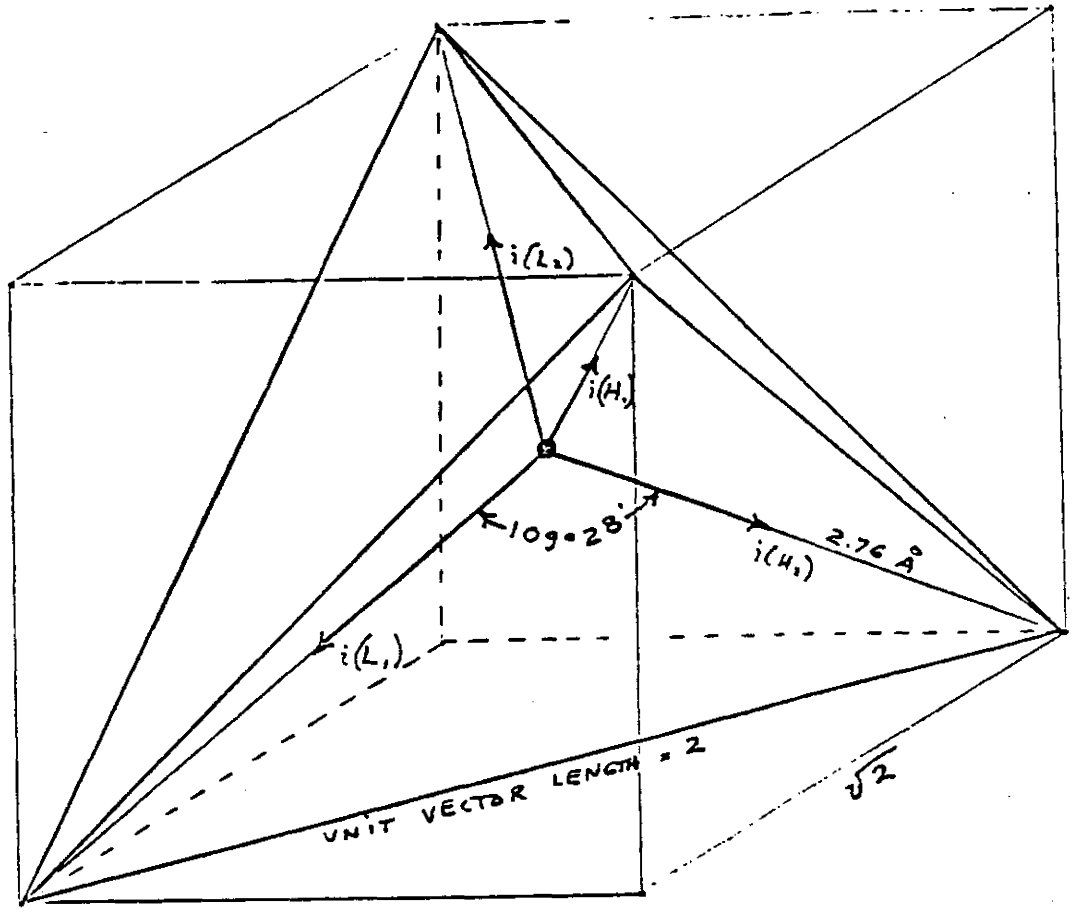

THE WATER MOLECULE IN TETRAHEDRAL FORM.

Hydrogen bonding occurs only along the four vectors pointing to the four vertices of a regular tetrahedron, and in the above drawing we show the four unit vectors along these directions originating from the oxygen atom at the center. $i(H_1)$ and $i(H_2)$ are the vectors of the hydrogen bonds formed by the molecule i as a donor molecule. $i(L_1)$ and $i(L_2)$ denote the unit vectors along the direction of the bonds formed by molecule i, as an acceptor molecule. These are assigned to the lone pair electrons. Molecules i are the neighboring oxygen atoms at each vertex of the tetrahedron.

FIG. 15

diagonal pair has an orthonormal relationship (90). This angle will also become important in the development of the theory. Basic to this theory is to give the diagonals, or tetrahedron edge length, the unit vector length of 2, independent of the actual metric employed, and the cube edge length the value, $\sqrt{2}$ = 1.4142135.

We will now present the complex E.M. wave as the tetrahedral water molecule sees it. The first effect felt by the water molecule is in the protons of the $i(H_1)$, $i(H_2)$ vector. These protons feel the 3.8 to 2.8 second cycling of the amplitude of the carrier frequency and its associated side bands. See Fig. 5. This sets up a rotation of the proton magnetic moment which we can clearly see on the X-Y plot of an oscilloscope as a hysteresis loop figure. However, it is to be noted that this hysteresis figure loop does not appear out of the liquid water sample - until all the parameters of the three COMPONENTS have been adjusted to the configuration which is the basis of this invention. The hysteresis loop gives us a vivid portrayal of the Nuclear Magnetic Relaxation cycle of the proton in water. We have found that the characteristic NMR rate, 1/T, in our experiment, is the 3rd subharmonic of 2, i.e. 0.25 secs.

Sheet 1 of 11, p. 2.

The next important effect felt by the water molecule is the COMPONENT I resonant frequency, f_o. At peak efficiency of electrolysis the value of f = 600 Hz (±5 Hz). This resonance however, is achieved through the control of two other factors. The first is the molal concentration of salt in the water. This is controlled in the following manner. The conductivity of the water is measured through the built-in current meter of COMPONENT I, and the built-in voltmeter. These two data points are fed to a microprocessor which measures the ratio I/E. The microprocessor then adds pure water if the salinity is

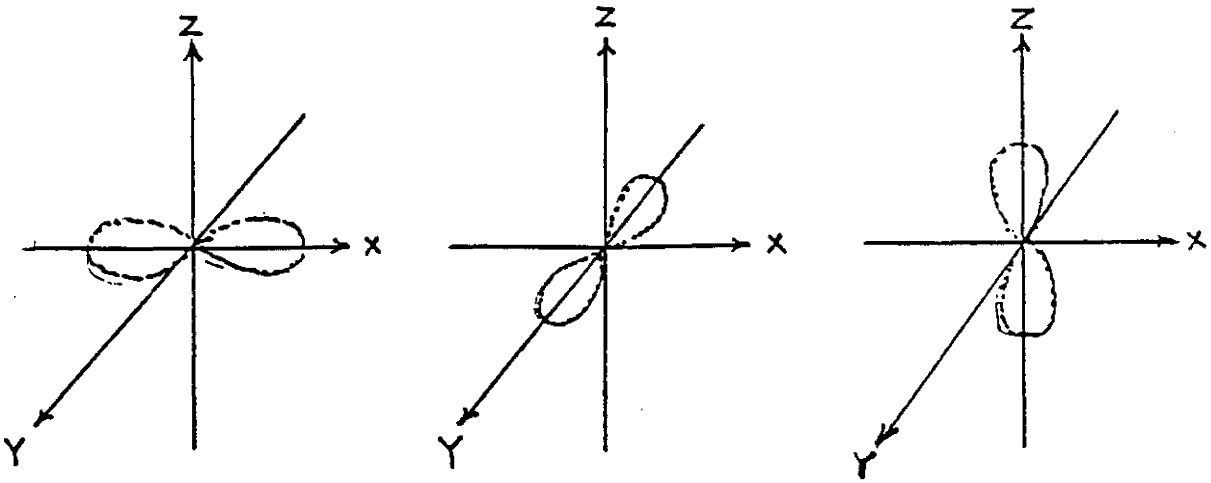

P_x P_y P_z

ELECTRON ORBITALS

Element	Electron Configuration
H	$1s^1$ (↑)
O	$1s^2$ (↑↓) $2s^2$ (↑↓) $2p^4$ (↑↓)$_{(2p^2)_x}$ (↑)$_{(2p^1)_y}$ (↑)$_{(2p^1)_z}$

Arrows indicate pairing of electrons in spin

FIG. 16

too high, or/and adds salt if the salinity is too low. The ideal ratio that the microprocessor maintains in the solution of COMPONENT III is I/E = 0.01870 which is equal to a salt solution = 0.1540 molar concentration.

The second factor holding the resonant frequency at 600 Hz is the gap distance, γ between the center electrode, and the rim electrode of COMPONENT III. This gap distance will vary depending on the size of COMPONENT II, but again it is found by the microprocessor adjustment of γ when the voltage reads between 2.30 (RMS) to 2.46 (RMS), at resonance, f_o, and at molal concentration, 0.1540 M. The molal concentration of the water is thus seen to represent the electron term of the water molecule, and hence its conductivity. Now it will be recalled that the carrier frequency wave is being amplitude modulated by audio frequencies sweeping over the range 20 Hz to 200 Hz, and this gives rise to a set of side bands in the power spectrum of the carrier frequency. It is these side bands which give rise to an acoustic vibration of the liquid water, and the tetrahedral water molecule, and hence to the <u>phonon</u> term - a quantum unit of vibration, and to the <u>hydron</u> term - a tetrahedral unit of water (from the Greek word <u>Hydro</u>).

The importance of the phonon effect - the acoustic vibration of water in electrolysis was discovered in a round-about way. Research work with COMPONENT I had earlier established that it could be used for the electrostimulation of hearing in humans. When the output of COMPONENT I is comprised of that flat circular metal plates - dielectric coated (mylar film) - applied to the head, normals could hear pure tones and speech. Acoustic vibration could also be heard by an outside observer with a stethoscope placed near one of the COMPONENT I electrodes on the skin.

We now examine this phonon effect in greater detail by first calculating the electric pressures generated under various electrode conditions.

Elementary electric pressure theory of forces acting on the skull is derived from the simple two-plate capacitor. In the ideal case, the dielectric between the plates of a capacitor is considered to be uniform and homogenous and the plates are considered plane, parallel, and infinite in area.

The force existing between the plates of a parallel plate capacitor is:

$$F = \frac{V^2 A \varepsilon}{2d^2} \tag{32}$$

where F is the force in Newtons;
V is the potential difference between the plates in volts;
A is the area of the plate in square meters;
ε is the permittivity of the dielectric between the plates in farads per meter;
d is the distance between plates in meters.

Since pressure is force divided by area:

$$p = \frac{F}{A} = \frac{\varepsilon}{2d^2} V^2 = 1/2\varepsilon \frac{V^2}{d^2} \quad 1/2\varepsilon E^2 \tag{33}$$

where:

$$E = \frac{V}{d}$$

and p is in Newtons per square meter.

When an amplitude-modulated carrier signal is applied between the plates of the capacitor, the voltage is:

$$V = V_c \quad (1 + \xi \cos \omega_m t) \quad \cos \omega_c t \tag{34}$$

where V_c is the carrier voltage in volts;
ξ is the modulation index;
ω_m is the modulation frequency;
t is time;
ω_c is the carrier frequency.

To derive the alternating pressures due to the audio frequency modulation component, terms are squared and, considering $\xi < 1$, the expression becomes:

$$V^2 = V_c^2 \xi \cos \omega_m t \quad (35)$$

The expression for electric pressure has two solutions:

$$p = \varepsilon E^2 (1/2 + \xi \text{ Sin } \omega_m t) \quad (36)$$

$$p = 1/2\ \varepsilon E^2 (1/2 + \xi \text{ Cos } \omega_m t) \quad (37)$$

These expressions for pressure can be applied to electric pressure on the skull in a straight-forward manner if the body is grounded as one plate of a capacitor and the other plate is the high side of the applied voltage separated from the body by a medium such as air or other dielectric. Such an application has been made by Sommer and von Gierke[2].

However, the situation becomes more complex when the head is placed between small conducting plates, and the head and/or body is the dielectric medium. We consider first the simplest condition, Case IB; the measurements are derived for threshold hearing in a normal for a pure tone of 1,000 Hz with a modulation index, ξ = 0.85, carrier frequency at resonance = 14.0KHz. See Table 13 (BF).

The electrodes are 4.0 cm in diameter and the area, $1.256 \times 10^{-3} M^2$. By bridge measurement at 14KHz, the absolute permittivity of the head between stationary electrodes is $C = 0.2 \times 10^{-6} F$ and can only take smaller values during stroking. The distance between the electrodes is 0.18 M. The hearing threshold for 1000 KHz is measured as 30 v (p-p) reactive voltage across the head electrodes.

The permittivity of air is 8.85×10^{-12} farad per meter, and for a distance of 0.18 meter, it is 49.16×10^{-12} farad. The relative dielectric constant of the head is:

$$\varepsilon_r = \frac{\varepsilon h}{\varepsilon o} = 4068.$$

The absolute permittivity of the head is $\varepsilon h = 3.6 \times 10^{-8}$ farad per meter. With stroking, εh assumes smaller values, but our calculations are carried out with the maximum value in order to establish the maximum value of electric pressure generate See Table 13 (BG) for minimum value. The force of the amplitude modulated carrier voltage driving the surface of the head is: $F = 1/2\ \varepsilon h A E^2$; where:

$$A = \text{area of plate electrode}$$
$$E = E_c (1 + \xi \text{ Cos } \omega_m t) \text{ (Sin } \omega_c t) \quad (38)$$

The calculated force exerted on the head at the electrodes is 6.2798×10^{-7} Newton, and the pressure under the electrodes is 5×10^{-4} Newton/M^2. The head between the electrodes can be considered as a spherical dielectric, and because of its inhomogenous structure, it becomes extremely difficult to calculate the distribution of electric pressures and forces within it. The force exerted between the electrodes has both radial and normal components which can be monitored. These undergo different resonant and damping effects. Von Bekésy has analyzed this problem for bone conduction by considering the mass of the head as a spherical model, and gives the following expression as an approximate solution[3]:

$$F = 4\pi R^2 p \left[\frac{\lambda}{2\pi R} \cos \frac{2\pi R}{\lambda} - \left(\frac{\lambda}{2\pi R} \right)^2 \sin \frac{2\pi R}{\lambda} \right] \quad (39)$$

here: R = radius of sphere;
p = pressure on skull (free field);
λ = wave length of sound.

he displacement amplitude of the skull is:

$$A = \frac{F}{(2\pi f)^2 m} \qquad (40)$$

where: F = force acting on the sphere;
M = mass of the sphere;
f = frequency of the sound.

hus, by calculation, the force distributed over the skull $F = 1.70 \times 10^{-5}$ Newton, and the displacement amplitude $A = 1.1 \times 10^{-13}$M.

e can summarize the 1000 KHz threshold for a normal expressed as electric force, lectric pressure, and displacement amplitude acting on the skull in Case IB.

$F = 1.70 \times 10^{-5}$ Newton (over skull);
$p = 3.50 \times 10^{-3}$ dyne/cm^2 (under electrodes);
$A = 1.10 \times 10^{-11}$ cm (over skull).

Von Bekesy[4] states that the absolute amplitude of the skull for threshold hearing of a 1000 KHz tone by bone conduction is 10^{-10} cm, and the pressure is 2 dyne/cm^2. It is apparent that the driving forces are above the air conduction thresholds, and below the bone conduction thresholds for normals in Case IB.

Furthermore it has been calculated by VON BEKESY, and others that at the absolute threshold of human hearing the amplitude of displacement of the eardrum is of the order of 10^{-11} meters, and the corresponding amplitude of the cochlear basilar membrane is 10^{-13} meter.

I then was able to achieve the absolute reversible threshold of electrolysis at a power level,

$$P = IE = 0.4 \text{ mA (RMS)} \times 0.4 \text{ V (RMS)} = 0.16 \text{ mW.}^{(RMS)}$$

By carrying out new calculations, I was able to prove that the water solution in COMPONENT II was being vibrated with a displacement of the order of $1\text{Å} = 10^{-10}$ M which is the diameter of the smallest atoms - such as hydrogen. Thus the acoustic phonons generated by audio side bands of the carrier were able to vibrate particle structures inside the tetrahedron. The harmonic oscillation between the acoustic side bands of the resonant carrier frequency - the phonons, entrained the water tetrahedron during electrolysis - the hydron. This is the meaning of the term PHONON-HYDRON.

We now turn to the effects observed during 100% efficient electrolysis of water. It was discovered during such high eficiency production of H_2 and O_2 at 0.16 mW power that electromagnetic noise was being radiated from COMPONENT II in the 20 to 40 Gigahertz E.M. radio band. At first this effect was thought to be due to the width of the resonant cavity in COMPONENT II = 14.0 mm = the wavelength of 22.3 GHz = a frequency known for water resonance. Then we went back to our earlier work on hearing and found that a similar phenomenon had been observed in the use of COMPONENT I in electrostimulation of hearing at high power levels. What we had found was that there was an interaction of side bands with the carrier frequency associated with

better hearing in hearing-impaired humans - and that this interaction was characterized by stationary harmonic waves on the X-Y plot of an oscilloscope. We also observed pulse generation, during peaks of AM, at higher levels of applied power.

Good Ear Subject's Thresholds As A Function of Electrode Condition

Pure tone threshold pressure in DB. Referenced to 0.0002 dyne per square centimeter.	54	54	25	0	68	56	74	16	26	26		
Electric pressure threshold across head, p (RMS), in dyne per square centimeter.	0.08	0.08	0.0035	0.0002	0.40	0.090	1.07	0.001	0.004	0.004		
Power, P_L, electrode:head system, in milliwatts.	4.8	2.4	0.18	0.16	1.4	2.6	3.2	0.72	0.45	0.50		
Quality Factor, Q.	4	3	50	15	57	4.6	65	5	50	45		
Electrode:head impedance at resonance, Z in ohms.	2400	7500	1000	500	700	1300	625	1000	900	1000		
Electric field strength, E_o, across head, V_r/d in volt/cm.	1.3	1.3	1.5	0.4	5.3	0.8	8.6	0.4	3	3		
Modulation factor, ξ, = E_m/E_c.	.85	.85	.85	.85	.85	.85	.85	.85	.85	.85		
Reactive voltage across head, V_r (p-p) in volts.	20	20	30	6	80	12	130	6	45	45		
Volts at resonance in one electrode, V_a (RMS) in volts.	2.4	3.0	0.3	0.2	0.7	1.3	1.0	0.6	0.45	0.50		
Current at resonance in one electrode, I_a (RMS) in ma.	1.0	0.4	0.3	0.4	1.0	1.0	1.6	0.6	0.5	0.5		
Sine wave modulation frequency, f_m, in KHz.	1	1	1	1	1	1	1	1	1	1		
Series LC resonant carrier frequency, f_o, in KHz.	22	14	14	22	31	31	30	27	55	55		
ELECTRODE CONDITION: F = Subject floating. G = Subject grounded. STA = elect. stationary. STR = elect. stroked. Dielectric = 0.25 mil mylar film.	Case IA, F. Sta.	Case IA, G. Sta.	Case IB, F. Str.	Case IB, G. Str.	CaseIII, F. Sta.	CaseIII, G. Sta.	CaseIII, F. Str.	CaseIII, G. Str.	Case II, F. Sta.	Case II, G. Sta.		
CODE, GE	AF	AG	BF	BG	CF	CG	DF	DG	EF	EG		

TABLE 1

The presence of stationary harmonic waves controlled by (1) stroking of a ..re metal electrode, and (2) resonance detuning to $+f_o$ strongly suggested ..e presence of resonance absorption in the skin and deeper tissues. This possibility was analyzed by the method outlined by von Hippel[3] for anomalous ..spersion and resonance absorption in dielectrics. Not knowing what would .. found in the skin-tissue dielectric in precise detail, we oriented ourselves to the problem by analyzing a simple model of electrons quasielastically ..ound to equilibrium positions and reacting to external field changes much ..ke linear harmonic oscillators.

.. consider first the transient response, and later, as more directly applicable to our problem, the steady state response.

..uch an oscillator when displaced from its equilibrium position in the Z direction by a length, Z_o, and then released to return to its original position is ..escribed by the force equation:

$$m \frac{d^2z}{dt^2} + F_s + fz = 0 \qquad (58)$$

..n the absence of a friction force, F_s, the electron would follow an undamped oscillation,

$$Z = Z_o \cos \omega_o t \qquad (59)$$

..of the resonance frequency:

$$\omega_o = \sqrt{f/m} \qquad (60)$$

Since a friction force is present according to classical theory by radiation of the linear oscillator, the friction force, F_s, exerted on an electronic dipole of the charge $Q = e$ by the emission of electromagnetic radiation of the phase velocity $V = c$, can be approximated by:

$$F_s = \frac{\mu_o e^2 \omega_o^2}{6\pi c} \cdot \frac{dz}{dt} \qquad (61)$$

By defining a friction factor, α ,

$$2\alpha = \frac{\mu_{oe}^2 \omega_o^2}{m6\pi c} \tag{62}$$

Equation (58) can be rewritten:

$$\frac{d^2Z}{dt^2} + 2\alpha \frac{dZ}{dt} + \omega_o^2 Z = 0 \tag{63}$$

And its solution is:

$$Z = Z_o e^{-\alpha t} \cos \omega_o^1 t \tag{64}$$

where:

$$\omega_o^1 = \omega_o^2 - \alpha 2$$

designating the reduced frequency of the damped oscillator. Without attenuation, the classical electronic oscillator would emit a monochromatic radiation of the wave length,

$$\lambda_o = \frac{Z\pi c}{\omega_o} \quad (m) \tag{65}$$

However, radiation damping and other causes broaden this spectral line over an infinite range of frequencies, as is seen when the oscillator amplitude is expressed by Fourier integrals.

In view of these classical considerations, an appropriate first test for the hypothesis of resonance absorption in the skin and head dielectric would be to look for the presence of an oscillation bandwidth broader than the harmonics observed thus far.

If negligible attenuation were present, we would expect to find a monochromatic radiation from the hypothetical tissue dipoles, and if a larger attenuation, α, were present, we would expect to find some kind of broad band radiation and/or oscillation.

We have already described the entrained oscillation centered around the carrier resonance frequency whose harmonics are controlled by the modulation frequency. Because of pulse generation observed earlier, we looked for broad band radiation in the radio frequency spectrum by monitoring the electromagnetic field of the body with a field strength detector (Empire Devices Model NF-105) and a

P noramic spectral analyzer (Model No. SPA-3). All the monitoring was done w-thin a shielded room (Shielding, Inc., New Jersey).

C_ntrol monitoring was carried out within the shielded room with (1) TD system not powered, (2) TD system powered and not placed on the human head, and (3) ? system powered and placed on the human head. Condition (1) showed no spurious e_ectromagnetic radiation in the shielded room. Condition (2) showed the presence of the carrier frequency (50KHz) and 1KHz modulated side bands (49KHz and 51KHz). C ndition (3) showed no electromagnetic radiation in the shielded room other than c_served in (2) until a threshold of 105 volts (p-p) from one electrode to ground was reached. Above this threshold the tuned antennas of the two detector ?vices placed a few feet from the human subject detected broad band electro- ı gnetic radiation. Having established these controls, a formal study was carried out.

Case III electrodes (one bare and one mylar) were used in this study. When the two electrodes are held face to face (not on the body) and a 1KHz modulated ırrier is tuned to resonance at a threshold of 900 volts (p-p) and 10 ma current, there is observed a bluish corona discharge in the dielectric between the electrodes. When the electromagnetic radiation from the corona is)nitored, there is found an irregular spectrum of radiation from about 1 MHz ..) about 1,000 MHz (See Figure 69I and 69II)

_ıen the TD input to the electrodes was observed on an oscilloscope, it was found that the EM radiation originated in a pulse discharge at the peak oltage of each cycle of the 1KHz modulation envelope, and not in the peak oltage of each cycle of the carrier wave.

hen one electrode (mylar covered) was held against a flat conductor connected to ground and the TD carrier tuned to resonance, a bluish corona discharge was again generated across the mylar dielectric at a threshold of ,200 volts (p-p) and 11 ma current. Again, the corona discharge originated ın the peak voltage of each cycle of the 1KHz modulation envelope and not in the carrier wave peaks. These control studies established the origin of broad and electromagnetic radiation in the TD system as an audio envelope corona pulse discharge across the mylar dielectric at a critical voltage threshold.

Ve then placed the Case III electrodes on the skin of the head to find out what would happen to the electromagnetic radiation as observed by the field strength detector antenna. First, it was observed that the corona discharge electromagnetic radiation was not damped out nor absorbed by the human body. Second, it was found that the corona discharge electromagnetic radiation could be detected from the human body at lower voltages and current than were obtained when the electrodes were face to face, or with one electrode coupled to ground. Third, it was found that in spite of the lowered corona threshold on the body, there was a gain of the electromagnetic radiation from the body. For example, Figure 69V shows a 5 db (reference 2 μv) level of electro- magnetic radiation at threshold for Case III electrodes held face to face, while Figure 69VI shows a 15 db level of electromagnetic radiation at threshold for Case III electrodes in dermal contact across the head. Fourth, it was found that the lowest threshold for corona discharge electromagnetic

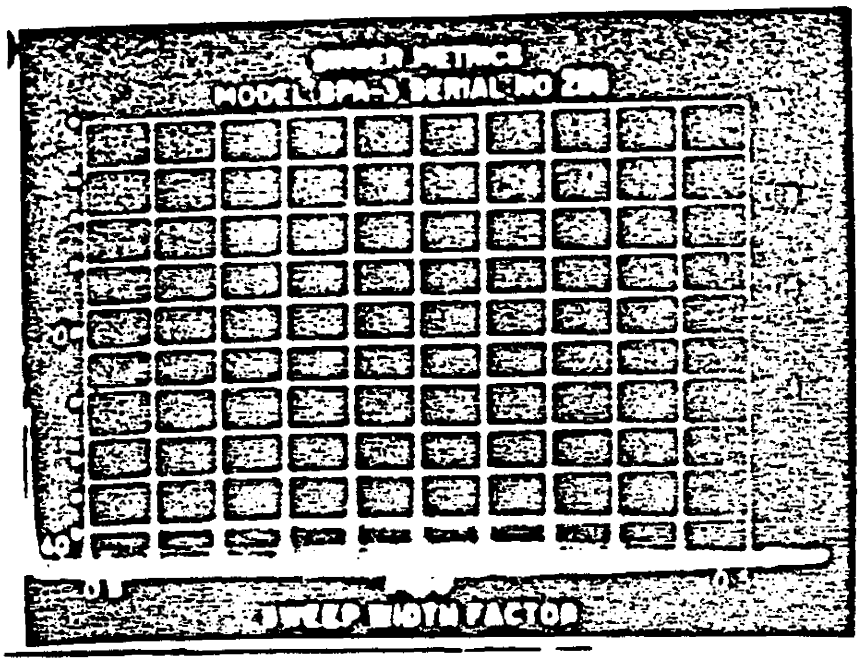

17 I

FIG. TWO ELECTRODES SEPARATED BY I MIL THICK MYLAR HELD FACE TO FACE. POWER SPECTRUM RECORDING BELOW CORONA RADIATION THRESHOLD. CARRIER AT RESONANCE WITH I KHz AM, 900 VOLTS p.p AT 9 mA. SPECTRUM ANALYSER: 3.4 MHz CENTER FREQUENCY; 3 MHz BANDWIDTH SWEEP; O DB ATTENUATION LOG.

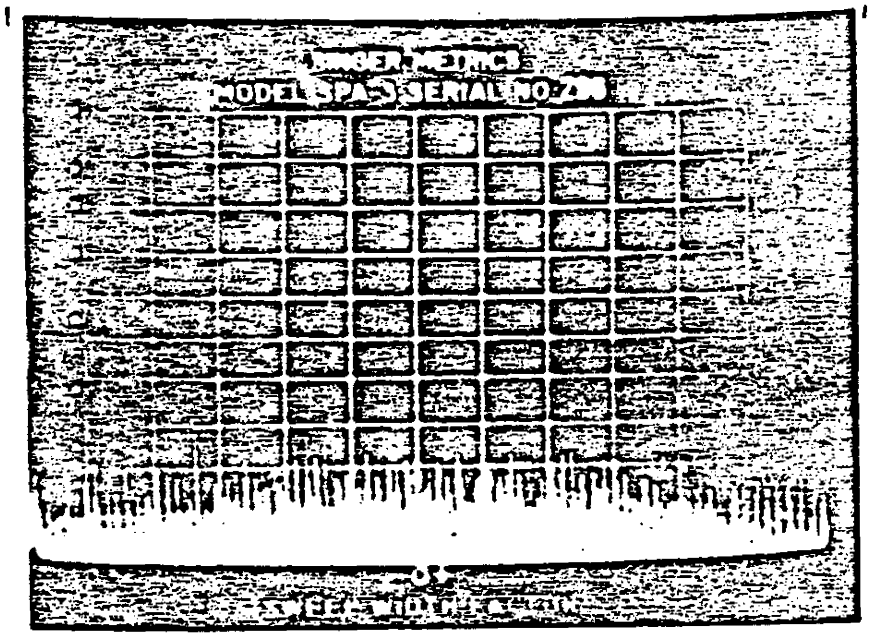

17 J

FIG. TWO ELECTRODES SEPARATED BY I MIL THICK MYLAR HELD FACE TO FACE. POWER SPECTRUM RECORDING ABOVE CORONA RADIATION THRESHOLD. CARRIER AT RESONANCE WITH I KHz AM, 900 VOLTS p-p AT 10 mA.
SPECTRUM ANALYSER: 3.4 MHz CENTER FREQUENCY; 3 MHz BANDWIDTH SWEEP; O DB ATTENUATION LOG.

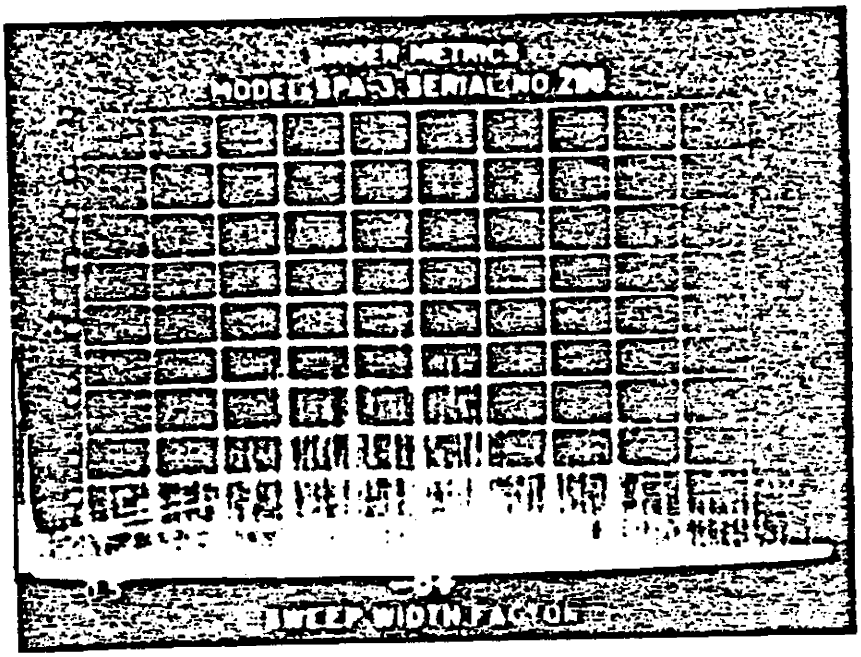

17

CASE III ELECTRODES PLACED ON SKIN. THE FIRST ELECTRODE IS COATED WITH 1 MIL MYLAR FILM, THE SECOND ELECTRODE IS OF BARE METAL. CARRIER IS AT RESONANCE WITH 1 KHz AM, 150 VOLTS p-p AT 10 mA. SPECTRUM ANALYSER: 3.5 MHz CENTER FREQUENCY, 3 MHz BANDWIDTH SWEEP, 0 DB ATTENUATION LOG SCALE.

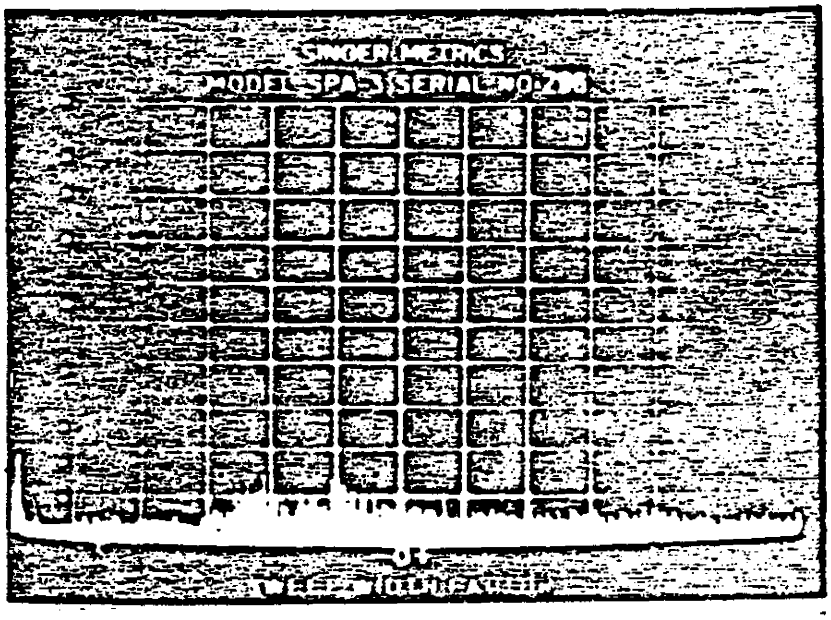

17

CASE III ELECTRODES PLACED ON GROUNDED CONDUCTOR. CARRIER IS AT RESONANCE WITH 1 KHz AM, 1200 VOLTS p-p AT 11 mA. SPECTRUM ANALYSER: 3.5 MHz CENTER FREQUENCY; 3 MHz BANDWIDTH SWEEP;

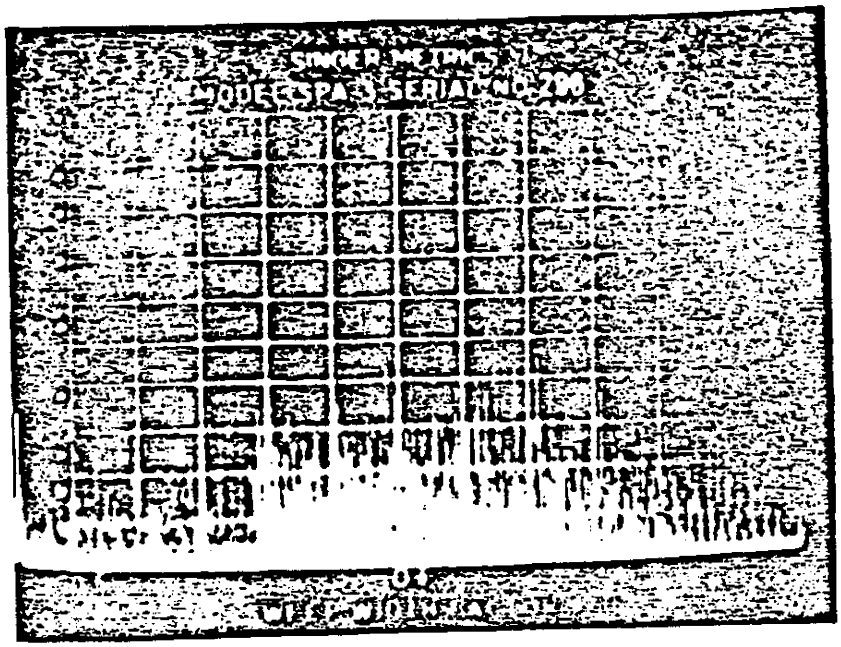

FIG. 17 V. TWO ELECTRODES SEPARATED BY 0.5 MIL TEFLON (TEP) HELD FACE TO FACE. POWER SPECTRUM RECORDING ABOVE THRESHOLD OF CORONA RADIATION. CARRIER AT RESONANC WITH 1 KHz AM; 1500 VOLTS p-p AT 10 mA. SPECTRUM ANALYSER: 3.4 MHz CENTER FREQUENCY; 3 MHz BANDWIDTH SWEEP; 5 DB ATTENUATION LOG.

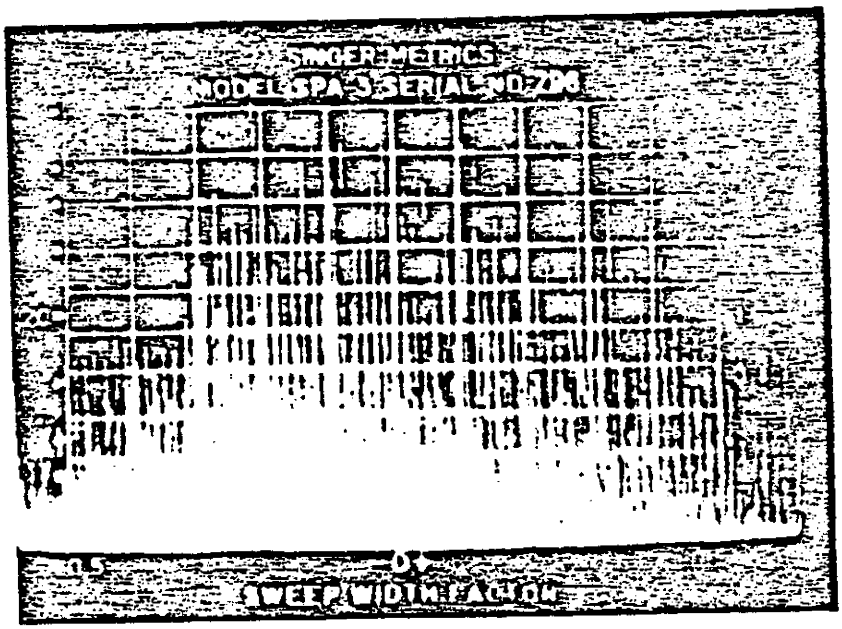

FIG 17 VI. CASE III ELECTRODES PLACED ON SKIN. THE FIRST ELECTRO IS COATED WITH 0.5 MIL TEFLON (TEP), THE SECOND ELECTRODE IS OF BARE METAL. CARRIER IS AT RESONAN WITH 1 KHz AM, 150 VOLTS p-p AT 10 mA. SPECTRUM ANALYSER: 3.4 MHz CENTER FREQUENCY; 3 MHz BANDWID

r iiation across the head occurred at the detuned $+f_o$ condition. Fifth, it was found that the greatest gain for the corona electromagnetic radiation at threshold occurred with the detuned $+f_o$ condition and skin stroking of the bare electrode. F gure 69 VII shows that this latter condition produces a gain of 30 db electromagnetic radiation when compared to Figure 69 V. Figure 69 VII shows a pattern of stationary waves comparable to those already seen for harmonic entrainment at m ch lower frequencies. This is evidence of a very high frequency complex harmonic entrainment as a result of the stroking mechanism.

Any electromagnetic radiation observed from the body has to be evaluated against the frequency distribution and power spectrum observed in the control condition illustrated in Figure 69 II. There was a fairly close correlation observed in e frequency distribution between the control condition Figure 69 II and the test condition Figure 69 III over the range from 1MHz to 1000 MHz (the upper limits of our detection equipment). We conclude that the electromagnetic radiation is given from the external source, the corona discharge mechanism.

ie fact that gain is observed as a result of such corona electromagnetic radiation exciting tissues increases confidence in the possibility that a resonance effect is being observed, particularly when gain is observed with lowered orona discharge thresholds. This is strong evidence for the presence of a large attenuation factor α both in the mylar dielectric and in the tissues. Considerably more work will have to be done in order to more precisely quantify ie attentuation factor. It would appear that this attentuation factor is a property of biological response mechanisms in the audio frequency range as surmised from the low frequency origin of the corona discharge. The circular ocus of Figure 35 has an angle of 60° equal to $(1 - \alpha)\ \pi/2$ which yields a value = 0.33 for the attenuation factor.

n the above case we are dealing not with a free electronic oscillator, but one subject to a driving force, eE' (where E' represents the externally acting electric field) and the law of motion (equation 63) changes to:

$$\frac{d^2H}{dt^2} + 2\alpha \frac{dz}{dt} + \omega_o{}^2 z = \frac{e}{m} E'$$

This equation can be written in the form of a differential equation for the polarization, P, by assuming that the dielectric is composed of N oscillators per unit volume, each of them contributing an induced electric moment:

$$\mu = ez \tag{66}$$

then:

$$P = Nez \tag{67}$$

In addition, it is assumed that the locally acting field E' can be described by the Mossotti approximation as:

$$E' = E + \frac{P}{3\varepsilon_o} \tag{68}$$

The differential equation becomes:

$$\frac{d^2P}{dt^2} + 2\alpha \frac{dP}{dt} + \left(\omega_o^2 - \frac{Ne^2}{3m\varepsilon_o}\right) P = \frac{Ne^2}{m} E \tag{69}$$

The effect of the polarization of the surrounding is to lower the resonance frequency of the individual oscillator from ω_o to:

$$\omega_o = \omega_o^2 \frac{-Ne^2}{3me_o} \tag{70}$$

The steady-state solution of equation (69) for an external sinusiodal driving field:

$$E = E_o e^{j\omega t} \tag{71}$$

is,

$$P = P_o e^{j(wt + \psi)} = \frac{Ne^2/m}{\omega_o^2 - \omega^2 + j\omega 2\alpha} E \tag{72}$$

The friction factor 2 α causes a phase shift ψ between the driving field and the resultant polarization; P becomes complex. The ratio $P/\varepsilon_o E$ determines the complex relative permittivity of the medium in molecular terms as:

$$K^* = 1 + \frac{P}{\varepsilon_o E} = 1 + \frac{Ne^2/\varepsilon_o m}{\omega_o^2 - \omega^2 + j\omega 2\alpha} \tag{73}$$

In the more general case where the dielectric contains oscillator types which contribute to K* without mutual coupling, the equation is generalized as:

$$K^* = 1 + \sum_s \frac{N_s e^2/\varepsilon_o ms}{\omega_s^2 - \omega^2 + j\omega 2\alpha} \tag{74}$$

N_s designates the number of dispersion electrons per unit volume for the oscillator type s.

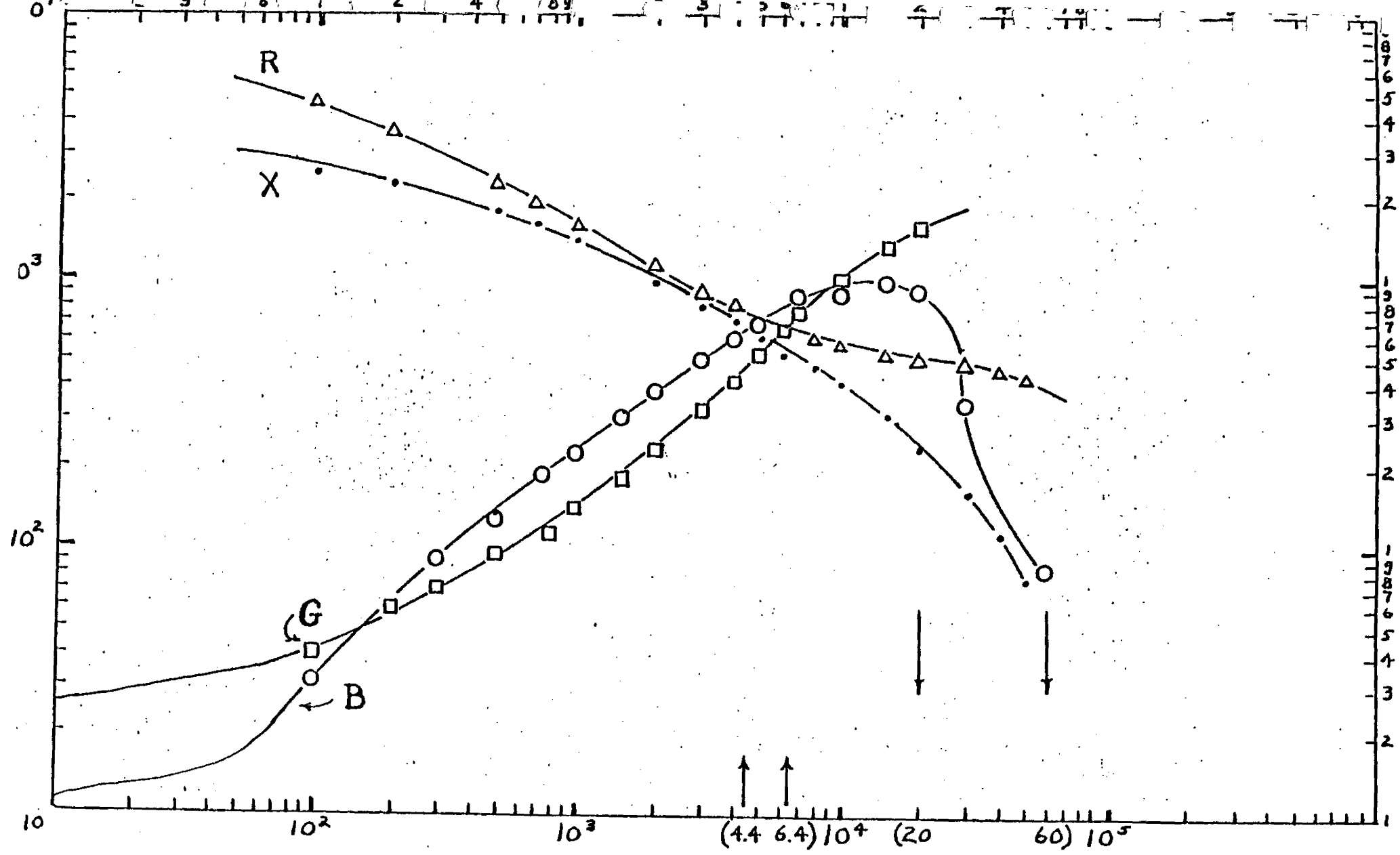

FREQUENCY IN Hz.

18

IG. IMPEDANCE AND ADMITTANCE OF TWO BARE METAL ELECTRODES (CASE IA) (D=2.5 cm) ACROSS HEAD TRAGAL AREAS (d = 18 cm)

Fig. 34 shows the measurement of impedance (X and R) and Admittance (G and B)

of the head between two bare electrodes as a function of carrier frequency. Both X and R decrease with increasing frequency, and G and B increase with increasing frequency.

The slope of these curves with respect to frequency can best be explained by reference to relaxation theory. We have observed in Figures 29, 30, and 32, the non-linear response of the polarization to a pulsed step function potentials. Assume that the sum of different polarization contributions due to different step function potentials as for example: from the half-wave rectified signal of Figure 1B, gives the total polarization. This superpositioning principle has been shown by Schwan to be equivalent to linear behavior. Schwan has shown that the complex dielectric constant is:

$$e^* = e_\infty + \frac{e_o - e_\infty}{1 + j\omega T} \tag{30}$$

which separates into:

$$e = e_\infty + \frac{e_o - e_\infty}{1 + (\omega T)^2} \tag{31}$$

$$K = K_o + (K_\infty - K_o) \frac{(\omega T)^2}{1 + (\omega T)^2}$$

The conductivity term includes a component, K_o, not related to the dielectric losses due to the assumed transient behavior of the dielectric material. It summarizes any additional conductance term that may arise. For example, from ionic conductance contributions. The frequency dependence given by the above equation is graphically summarized in Figures 32C and 32D. Analysis of data from Figure 34 shows a relaxation process, $T = C/G = 6.45 \times 10^{-5}$ second, where the characteristic frequency $f_{o_c} = 15.5$ KHz

The impedance plot, Figure 35, for Case IA electrodes shows good agreement between the experimental data and the circular plot for frequencies from 0 Hz to 50 KHz. This data can be interpreted by a polar relaxation mechanism (Debye) where molecules which carry a distribution of charges that can be simulated by a dipole will appear to rotate in an alternating current field. This rotation, whether virtual or real, is subject to viscous losses and, therefore, establishes a mechanism for conductance. The characteristic frequency, f_{o_c}, of dispersion decreases with increase in molecular size and weight.

For molecules as small as those of water, $f_{o_c} = 20{,}000$ MHz, and molecules of the size of proteins, $f_{o_c} = 1$ MHz. Therefore, the characteristic frequency, f_{o_c}, 15.5 kHz found for the head and the TD carrier range associated with hearing in the deaf leads us to look for a dipole structure that is

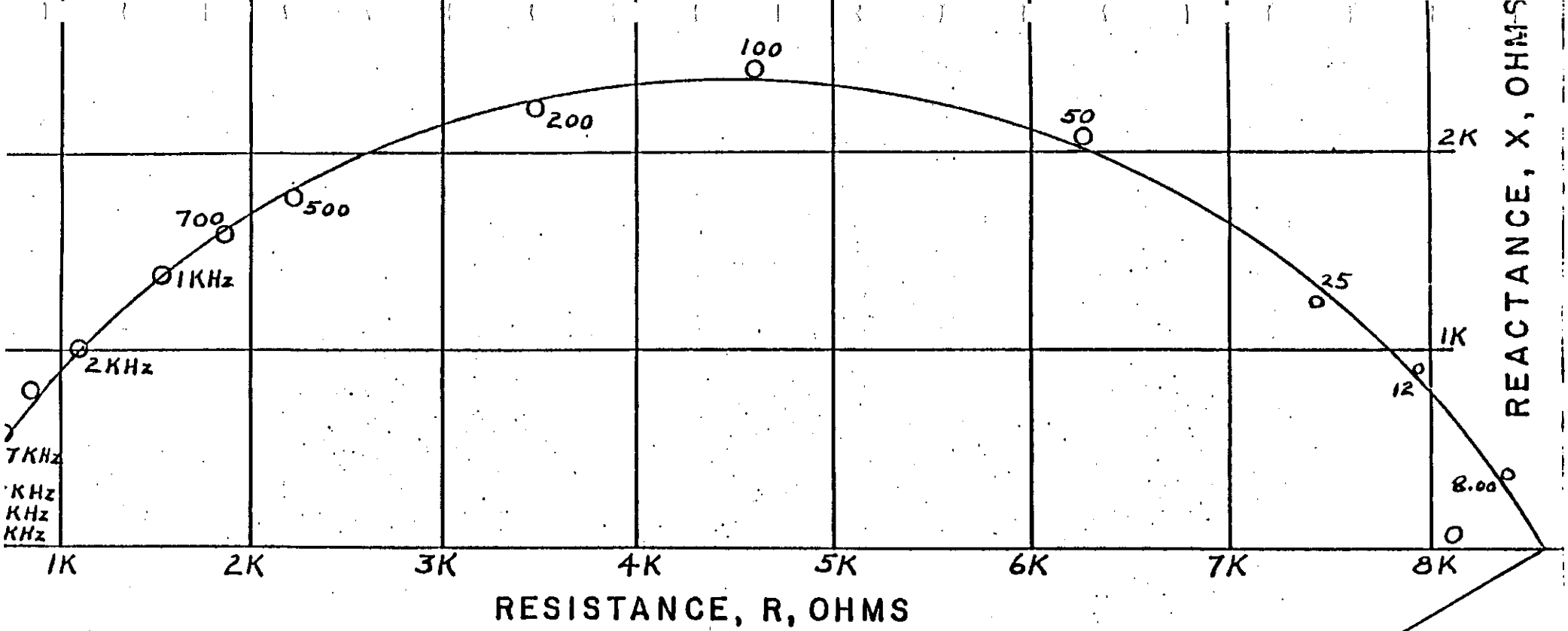

19

IG. COLE-COLE DIAGRAM OF IMPEDANCE LOCUS FOR CASE IA ELECTRODES ACROSS HUMAN HEAD. DRY ELECTRODES ON TRAGAL SKIN AT CONSTANT PRESSURE.



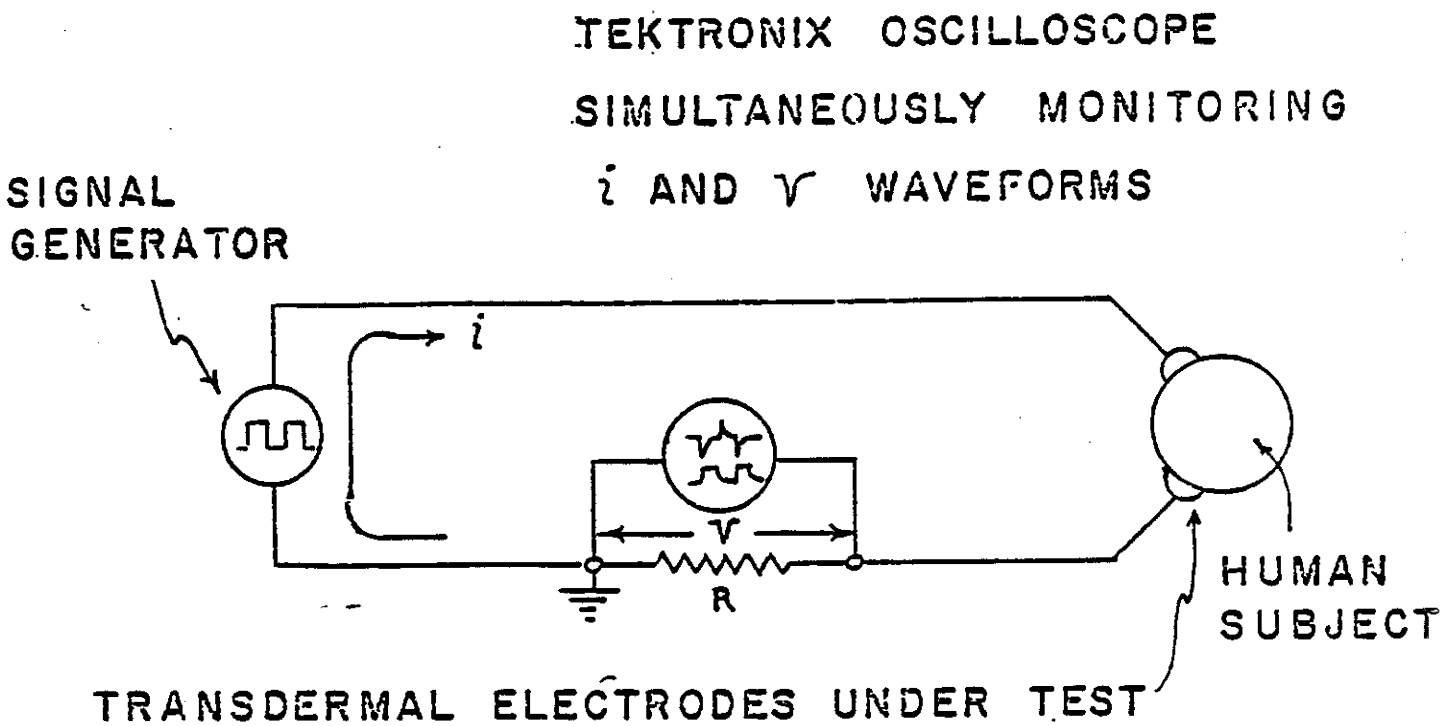

FIG. 20. TEST CIRCUIT TO MEASURE CURRENT AND VOLTAGE DECAY CURVES IN SQUARE WAVE SPECTROSCOPY OF ELECTRODE-HEAD CONFIGURATION.

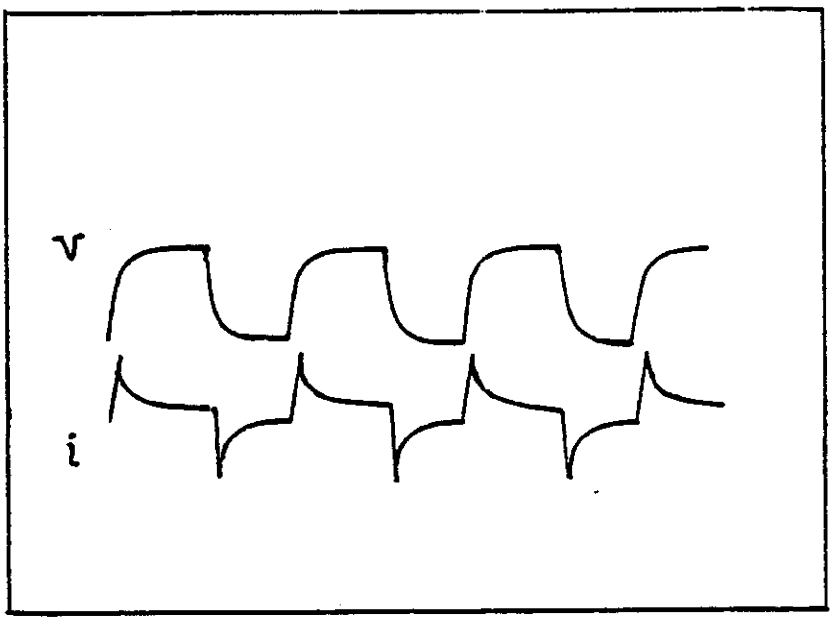

FIG. 21 CASE 1A ELECTRODES. 10 OHM SERIES RESISTANCE
SEE FIG. 28.
SQUARE WAVE PULSE INPUT ACROSS CHEEK TISSUES.
20 μscc/cm TIME BASE
UPPER TRACE: VOLTAGE DECAY CURVE
LOWER TRACE. CURRENT DECAY CURVE
LOWER TRACE. CURRENT DECAY CURVE

In the Equal Temperament scale the intervals are based on the ratio, $\sqrt[12]{2}$ = 1.059 463 094.

It is assumed that this dispersion is the result of phonon vibrations between the four vertices of the tetrahedron water molecule. The number of vibratory modes can be represented by the four vertices:

$$\frac{4!}{2} = \frac{24}{2} = 12 \text{ modes}$$

It is to be noted that the intervals in the 360 : 720 Hz octave are twelve (semitones) based on the $\sqrt[12]{2}$.

The mechanism behind these ratios must be due to the perturbations of the 4 vertices, i.e., two sets of lone pair electrons , and the two hydrogen protons , H^+. The electron and the proton have certain textbook classical relations which we will briefly review.

The precession of a proton (in water) in a fixed magnetic field value, called the gyromagnetic ratio of the proton is:

$\gamma_p'/2\pi$ = 4.257602 x 10^7 Hz per Tesla, or

x 2π = 2.675130 x 10^8 ω per Tesla.

The frequency of an electron orbiting the precession of the proton is denoted by:

e/me = 1.758 8047 x 10 Hz.

The ratio between the two frequencies is usually denoted by the formula,

$\mu_B / \mu_p = \frac{\text{left}}{2} / m_e \mu_p'$, and numerically,

$$= \frac{1.758\ 8047 \times 10^{11}\ \text{Hz}}{2.675\ 130 \times 10^{8}\ \text{Hz}} = 657.465$$

Now the difference between these two frequencies can also be considered legitimately as a "beat" effect giving rise to a frequency which would be ca. 657 Hz. Now these are classical values from studies and measurements on pure water. (1)We would expect some lowering of these values due to the lowering effect of the conductivity on the dielectric constant. This would bring the ratio down close to 600 Hz. Following this line of thought we can begin to test the power of our theory and extrapolate from classical data to our observations.

($\gamma_p = 2.675\ 1301 \times 10^{8}\ \text{Hz T}^{-1}$)

NOTE THAT $\gamma_p = 2^{28}$,

($\gamma_s = 2.684\ 35436 \times 10^{8} = 2^{28}$)

Note that $e_\nu = 1.758,8047 \times 10^{11}$ Hz, as above.

If we lower this frequency by the closest $\log_2$ periodic function, namely,

$2^{37} = 1.374\ 3895 \times 10^{11}$ Hz, we get,

$$\frac{2^{37}}{2^{28}} = 512\ \text{Hz} = 2^{9}$$

Since in the tetrahedron water molecule we have the orthonormal relationship between the proton i(H_1) and the lone pair

(1) FRITZ-ALBERT POPP, Editor; Electromagnetic Bio-information ; Urban & Schwarzenberg, Baltimore, 1979.

electons, $i(L_1)$, we would expect them to strongly influence each other, due to charge polarity, spin polarity, and resonance and dispersion interactions. These effects all add up to a phonon-pumping mechanism working on the unit hydron. We would expect that the end product of this action (before splitting of the water molecule occurs) is to stimulate the emission of photons, or a true PHASER effect. There is reason to believe that true photon emission occurs in many cellular living systems, but why or how this occurs is unknown.

Since alternating current perturbation of a saline water solution electrolyses a proven and measurable amount of hydrogen and oxygen gases, we can be certain that bond breakage has occured in, at the very least, the $i(H_1)$ and $i(H_2)$ intramolecular vectors. We begin our exploration of the nature of the bond-breaking mechanism by considering classical neutron-scattering by the nuclei in water.

We first consider the energy transfer, ΔE, and the momentum transfer, $\hbar\chi$ by

$$\hbar\omega = E_o - E = \Delta E \qquad (\chi \text{ is a reversed aleph})$$
$$= (\hbar^2/2m_n)\,(K_o^2 - K^2) \qquad (15)$$

K_o and K are respectively the initial and final wave vectors of the scattered neutron, corresponding to E_o and E. $\chi = K_o - K$, the wave vector.

$$\hbar^2\chi^2/2m_n = E_o + E - 2(E_oE)^{\frac{1}{2}} \cos\theta$$

These relations lead to scattering laws,

$S_s(\chi, \omega)$ for incoherent scattering, and

$S(\chi, \omega)$ for coherent scattering

for the system. The scattering law is independent of the properties of the neutron and the details of the scattering process , and depends only on the properties of the scattering system. In our case, we consider the tetrahedral water molecule, the HYDRON, as the scattering system, perturbed by phonon packets of energy.

D.I. Page has brought our attention to the role of Fourier transformation of the scattering law which brings to light the correlation between the spacings between nuclei, and incident radiation. He develops his analysis somewhat along the following lines. (1)

He considers just the simple case of radiation that is Bragg-reflected by a crystal. Bragg's law relates the wavelength of the radiation λ to the spacing, d, of the lattice planes in the crystal:

$$\lambda = 2d \sin (\theta/2)$$

This equation is compared to Eq.15 for elastic scattering ($\omega = 0$) and $(K - K_o)$ which gives

$$\chi = 2K \sin (\theta/2) = (4\pi/\lambda) \sin (\theta/2)$$

The variable χ behaves like the reciprocal of the spacing d ($1/d = 1/L = L^{-1}$), and this leads one to try Fourier-transforming with respect to χ in order to seek information about the spacing between atoms in the scattering system.

(1) WATER, VOL.I, Chapter 9, Ed Franks, Plenum Press, N.Y. 1972

Similarly, the variable ω behaves like the reciprocal of a time ($1/T = T^{-1}$). If we use a harmonic oscillator of frequency ω, and a period of oscillation T, a Fourier-transform of the oscillator (i.e. the function $\cos \omega t$), there is obtained a sharp peak at a frequency $\omega = 1/\tau$. In the case of water this would be $\omega_o = f_o = 600$ Hz. The Fourier transform represents the atom's modes of motion. The double Fourier-transform of the scattering law gives information about the position of the atoms as a function of time. This theorem was just developed and proved in 1954 by Van Hove (2)who showed:

$$S(\chi, \omega) = (\tfrac{1}{2}\pi) \int_V dr \int_{-\infty}^{\infty} d\tau \left[G(r,t) - \rho \right] \exp\left[i(\chi - r - \omega t) \right] \qquad (18)$$

where ρ is the average density of the scattering nuclei. The function G(r,t) is the space-time correlating function, and for a classical system has a simple meaning. If there is a proton of position r, at a time t, then G($\mathbf{r}$,t) is the probability of finding an atom at position $\mathbf{r}_2$ at a time t . The quantities $\mathbf{r}$ and t are the space and time differences. G($\mathbf{r}$,t) can be divided into two parts, $G_s(\mathbf{r},t)$, which measures the probability of finding the same atom each time, and G_d ($\mathbf{r}$,t), which is the probability of finding a different atom each time.

$$G(\mathbf{r},t) = G_s(\mathbf{r},t) + G_d(\mathbf{r},t) \qquad (19)$$

Notice that G ($\mathbf{r}$,t) describes the motion of a single atom, while the total function describes the dynamic behavior of all the

(2) L. Van Hove, Phys. Rev. 95:249, 1954

function, $S(\chi,\omega)$ are computed out for light water, the qualitative form of these two functions is seen in the next Figure. (1)

The uppermost curve shows the structure factor form $S(\chi)$.

(1) Fig.3, p.342 from D.I. Page, WATER , VOL. I, Chap.9

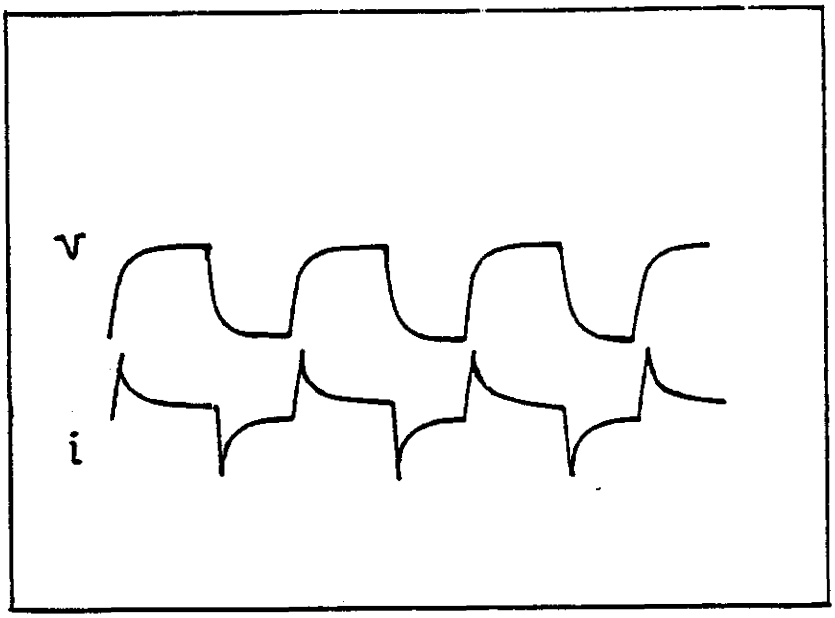

FIG. 21 CASE I A ELECTRODES. IC OHM SERIES RESISTANCE
SEE FIG. 28.
SQUARE WAVE PULSE INPUT ACROSS CHEEK TISSUES.
20 μscc / cm TIME BASE
UPPER TRACE: VOLTAGE DECAY CURVE
LOWER TRACE . CURRENT DECAY CURVE

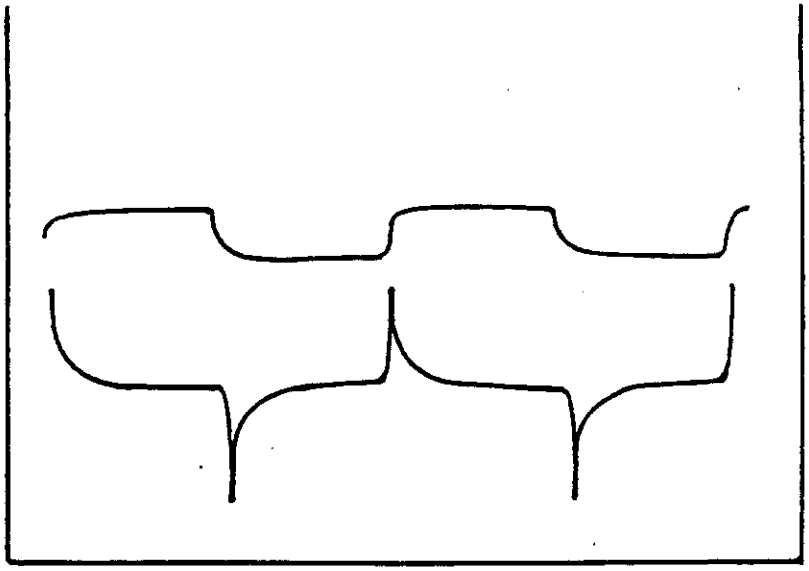

FIG. A. CASE IA ELECTRODES ACROSS HEAD.
15 OHM SERIES RESISTANCE. SEE FIG. 28.
20 μsec PULSE WIDTH
UPPER TRACE: VOLTAGE DECAY CURVE
LOWER TRACE: CURRENT DECAY CURVE

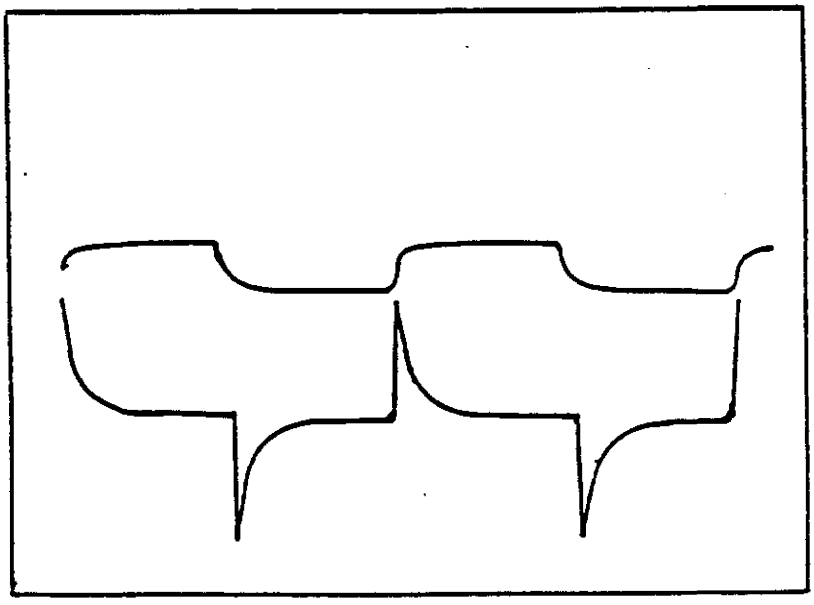

FIG. B. CIRCUIT SYNTHESIZED (SEE FIG. 31 CASE IA)
EQUIVALENT CIRCUIT OF HEAD.
UPPER TRACE: VOLTAGE DECAY CURVE
LOWER TRACE: CURRENT DECAY CURVE

ELECTRODE: HEAD

CONFIGURATION

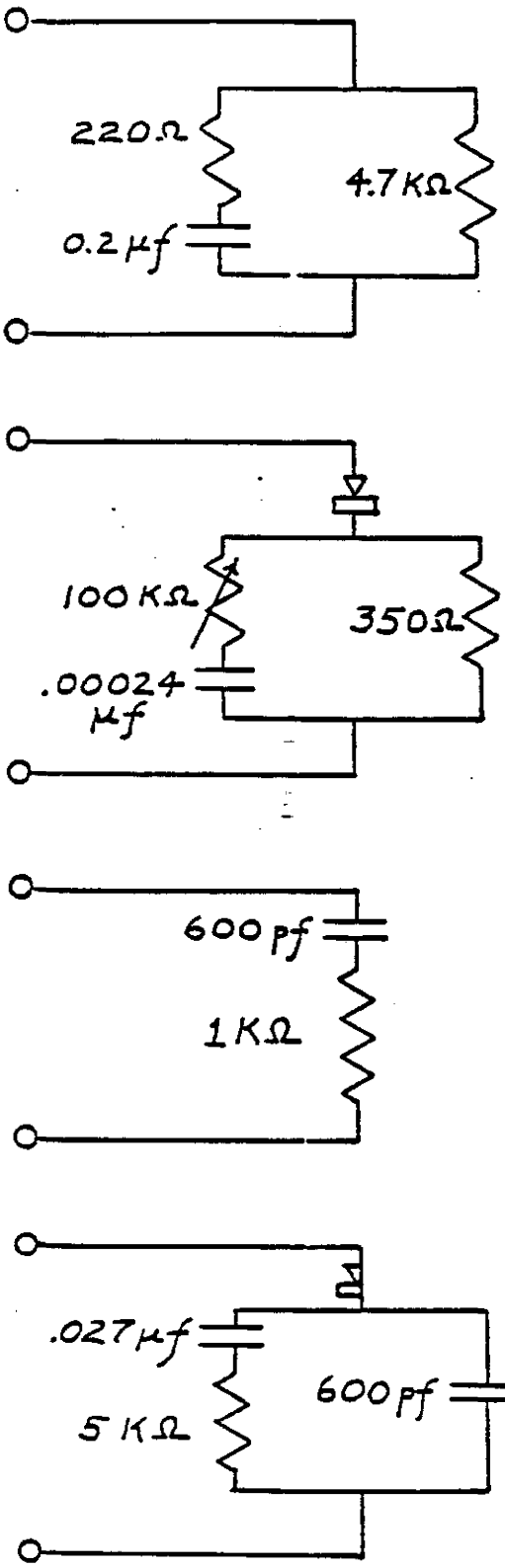

CASE IA

BARE METAL ELECTRODES STATIONARY ON THE SKIN ACROSS THE HEAD.

CASE IB

BARE METAL ELECTRODES STROKED ON THE SKIN ACROSS THE HEAD.

CASE II

MYLAR (0.25 MIL) COVERED ELECTRODES STATIONARY ON THE SKIN ACROSS THE HEAD.

CASE III

ONE BARE METAL ELECTRODE AND ONE MYLAR (0.25) COVERED ELECTRODE STATIONARY ON THE SKIN ACROSS THE HEAD.

FIG.23 . EQUIVALENT CIRCUITS OF ELECTRODE-HEAD CONFIGURATIONS

Far below its resonance frequency ($\omega << \omega_s$) each oscillator type adds a constant contribution.

$$\frac{N_s e^2/\varepsilon_o m s}{\omega_s^2} \tag{75}$$

to the static dielectric constant of the medium, whereas far above the resonance frequency its contribution vanishes. To follow the behavior of the lowest oscillator type, r, through its resonance region, the effect of vacuum and the remaining resonator types is lumped into a constant contribution.

$$A = 1 + \sum_{s} \frac{N_s e^2/m_s}{\omega_s^2} \quad \text{for } s \neq r \tag{76}$$

In place of ω, we introduce the deviation from resonance:

$$\Delta\omega \equiv \omega_r - \omega, \text{ as the variable, approximate} \tag{77}$$

$$\omega_r + \omega \simeq 2\omega_r$$

$$\frac{\omega}{\omega_r} \simeq 1$$

and thus equation 74 is rewritten as:

$$K^* = \eta^{*2} = A + \frac{B}{\Delta\omega + j\alpha} \tag{78}$$

where the factor B stands for:

$$B = \frac{N_r e^2/\varepsilon_o m_r}{2\omega_r} \tag{79}$$

The frequency dependence of the real part of the relative permittivity:

$$K' = m^2 (1 - K^2) = A + \frac{B\Delta\omega}{\{\Delta\omega\}^2 + \alpha^2} \tag{80}$$

describes the dispersion characteristic of the dielectric medium near resonance. These changes are plotted in Figure 70, K' rises hyperbolically from the low frequency value $A + \frac{2B}{\omega_r}$ to a maximum:

$$K' \max = A + \frac{B}{2\alpha} \tag{81}$$

at $\Delta\omega = +\alpha$, falls with a linear slope $-B/\alpha^2$ through the value A at the resonance frequency ($\Delta\omega = 0$), reaches a minimum:

$$K' \min = A - \frac{B}{2\alpha} \tag{82}$$

at $\Delta\omega = -\alpha$, and then rises again asymptotically to the constant value A for very high frequencies ($\omega >> \omega_r$).

The absorption characteristic of the dielectric, identified near resonance by the relative loss factor,

$$K'' = 2\eta^2 K = \frac{B\,\alpha}{\{\Delta\omega\}^2 + \alpha^2} \tag{83}$$

starts from zero at low frequencies, traverses its maximum B/α at resonance, and falls again symmetrically to zero at high frequencies. The half-value points $B/2\alpha$ of this bell-shaped absorption characteristic are reached at the deviation from resonance $\Delta\omega = \pm\alpha$.

For the phase relation between applied field and induced dipole moment near resonance, the relation,

$$\tan\psi = \frac{K''}{K' - A} = \frac{\alpha}{\Delta\omega} \tag{84}$$

at low frequencies ($\omega << \omega_r$) the moment follows in phase, at resonance it lags by $\pi/2$, and at very high frequencies by π.

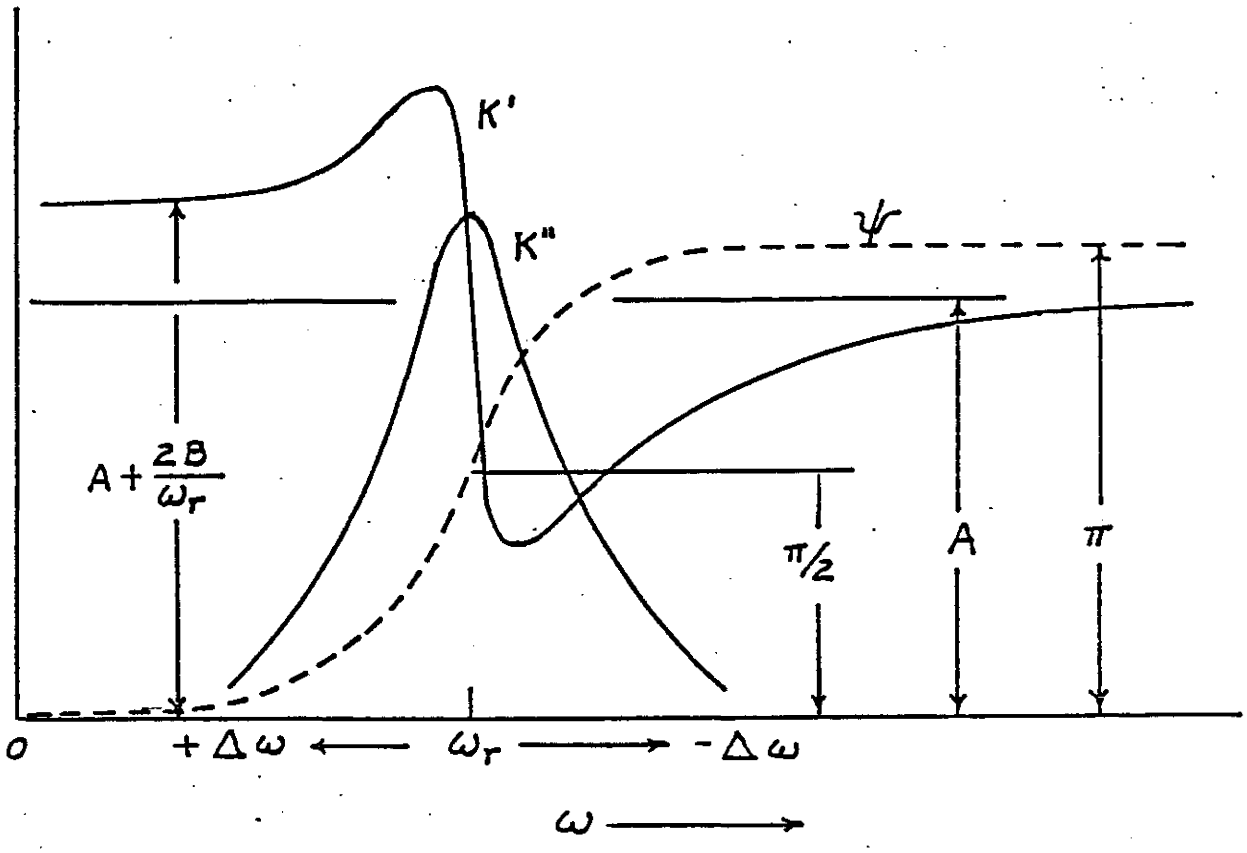

24

FIG. ANOMALOUS DISPERSION AND RESONANCE ABSORPTION. (after von Hippel)[3]

REFERENCES

1. Schwan, H.P., Electrical Properties of Tissue and Cell Suspensions, Proceedings Fourth Annual Tri-service Conference on the Biological Effects of Microwave Radiation, New York, 1960.

2. Sommer, H.C., and von Gierke, H.E., Hearing Sensations in Electric Fields, Aerospace Medicine, Volume 35, No. 9, September, 1964, pages 834-839.

3. von Bekèsy, Georg, EXPERIMENTS IN HEARING, McGraw-Hill, New York, 1960, equations 6 and 7, page 169.

4. Ibid., equation 8, page 170.

5. Bennett, M.V.L., Physiology of Electrotonic Junctions in Biological Membranes, Annals of the New York Academy of Sciences, Volume 137, Article 2, pages 509-539 (see equation 28 and figures 4 and 5 for $\alpha = 0$).

In our water electrolysis studies the curve of K´ was found to intercept K" at a frequency close to 2 = 512 Hz, but showed an interesting pattern of dispersion. As stated before, measured resonance, $f_o = \omega_r$, centered at 600 Hz. In examining the side bands around this frequency, it was found that $+\Delta\omega$= 360 Hz, and that $-\Delta\omega$= 720 Hz. Within this octave, the dispersion pattern was found to correspond to small peaks which closely mimicked the equal temperament scale:

OBSERVED, Hz			EQ. TEMP.Hz	PYTHAGOREAN SCALE	MUSICAL NOTES (Rising scale)
360	$+\Delta\omega$		360	D = 360 HZ	D
		1/3	384		e^b
			400	E = 405 Hz	e
420		OCTAVE	432		f
			450		$f^\#$
480			480	G = 480 Hz	G
540		1/3	540	A = 540 Hz	A
		OCTAVE	576		b^b
f_o=600= ω_r			600		b
			648	C = 640 Hz	C
660		1/3	675		$C^\#$
720	$-\Delta\omega$	OCTAVE	720	D = 720 Hz	D

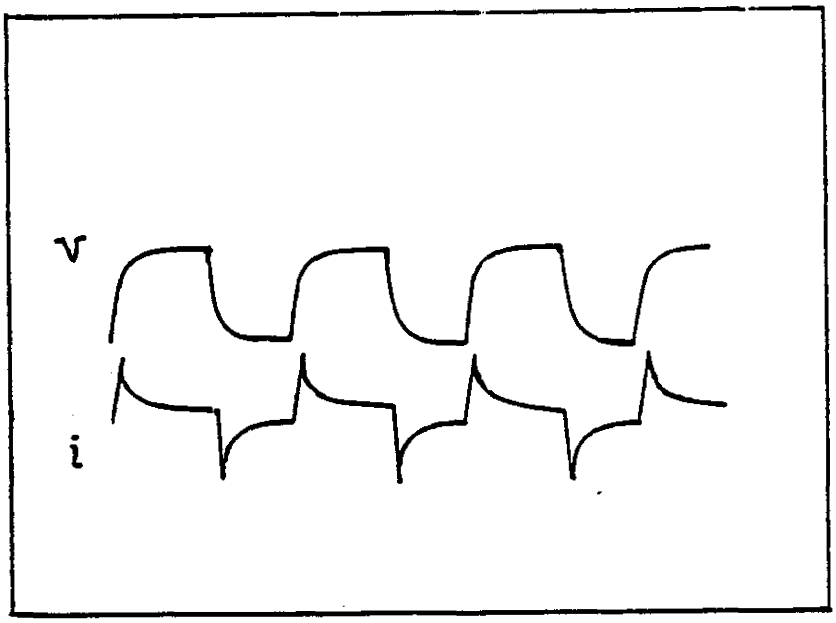

FIG. 21 CASE I A ELECTRODES. IO OHM SERIES RESISTANCE SEE FIG. 28.
SQUARE WAVE PULSE INPUT ACROSS CHEEK TISSUES.
20 μscc / cm TIME BASE
UPPER TRACE: VOLTAGE DECAY CURVE
LOWER TRACE. CURRENT DECAY CURVE
LOWER TRACE: CURRENT DECAY CURVE

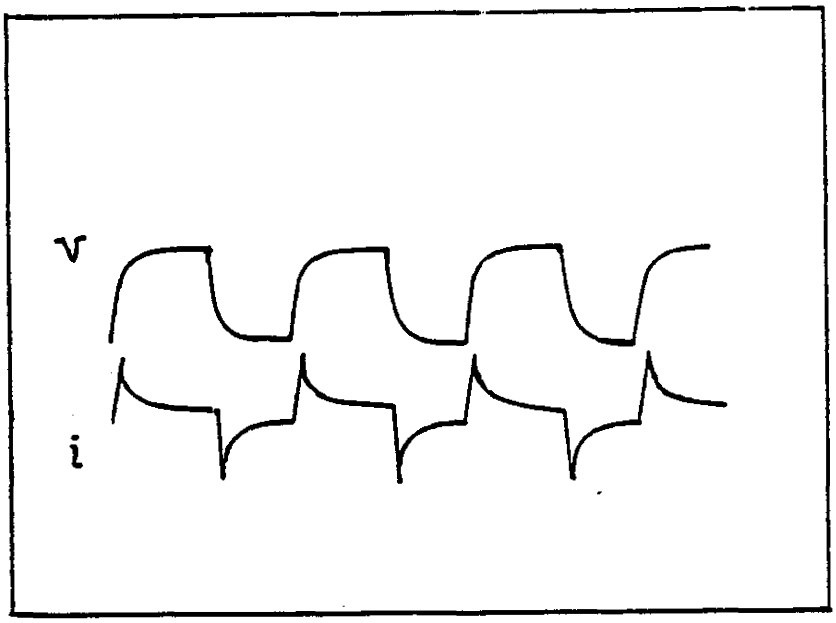

FIG. 21 CASE I A ELECTRODES. IO OHM SERIES RESISTANCE SEE FIG. 28.
SQUARE WAVE PULSE INPUT ACROSS CHEEK TISSUES.
20 μscc / cm TIME BASE
UPPER TRACE: VOLTAGE DECAY CURVE
LOWER TRACE. CURRENT DECAY CURVE
LOWER TRACE: CURRENT DECAY CURVE

In the Equal Temperament scale the intervals are based on the ratio, $\sqrt[12]{2}$ = 1.059 463 094.

It is assumed that this dispersion is the result of phonon vibrations between the four vertices of the tetrahedron water molecule. The number of vibratory modes can be represented by the four vertices:

$$\frac{4!}{2} = \frac{24}{2} = 12 \text{ modes}$$

It is to be noted that the intervals in the 360 : 720 Hz octave are twelve (semitones) based on the $\sqrt[12]{2}$.

The mechanism behind these ratios must be due to the perturbations of the 4 vertices, i.e., two sets of lone pair electrons , and the two hydrogen protons , H^+. The electron and the proton have certain textbook classical relations which we will briefly review.

The precession of a proton (in water) in a fixed magnetic field value, called the gyromagnetic ratio of the proton is:

$\gamma_p'/2\pi$ = 4.257602 x 10^7 Hz per Tesla, or

x 2π = 2.675130 x 10^8 ω per Tesla.

The frequency of an electron orbiting the precession of the proton is denoted by:

e/me = 1.758 8047 x 10 Hz.

The ratio between the two frequencies is usually denoted by the formula,

$\mu_B / \mu_p = \frac{\text{left}}{2} / m_e \mu_p'$, and numerically,

$$= \frac{1.758\ 8047 \times 10^{11}\ \text{Hz}}{2.675\ 130 \times 10^{8}\ \text{Hz}} = 657.465$$

Now the difference between these two frequencies can also be considered legitimately as a "beat" effect giving rise to a frequency which would be ca. 657 Hz. Now these are classical values from studies and measurements on pure water. (1)We would expect some lowering of these values due to the lowering effect of the conductivity on the dielectric constant. This would bring the ratio down close to 600 Hz. Following this line of thought we can begin to test the power of our theory and extrapolate from classical data to our observations.

($\gamma_p = 2.675\ 1301 \times 10^{8}\ \text{Hz T}^{-1}$)

NOTE THAT $\gamma_p = 2^{28}$,

($\gamma_s = 2.684\ 35436 \times 10^{8} = 2^{28}$)

Note that $e_\nu = 1.758,8047 \times 10^{11}$ Hz, as above.

If we lower this frequency by the closest $\log_2$ periodic function, namely,

$2^{37} = 1.374\ 3895 \times 10^{11}$ Hz, we get,

$$\frac{2^{37}}{2^{28}} = 512\ \text{Hz} = 2^{9}$$

Since in the tetrahedron water molecule we have the orthonormal relationship between the proton i(H_1) and the lone pair

(1) FRITZ-ALBERT POPP, Editor; Electromagnetic Bio-information ; Urban & Schwarzenberg, Baltimore, 1979.

electons, $i(L_1)$, we would expect them to strongly influence each other, due to charge polarity, spin polarity, and resonance and dispersion interactions. These effects all add up to a phonon-pumping mechanism working on the unit hydron. We would expect that the end product of this action (before splitting of the water molecule occurs) is to stimulate the emission of photons, or a true PHASER effect. There is reason to believe that true photon emission occurs in many cellular living systems, but why or how this occurs is unknown.

Since alternating current perturbation of a saline water solution electrolyses a proven and measurable amount of hydrogen and oxygen gases, we can be certain that bond breakage has occured in, at the very least, the $i(H_1)$ and $i(H_2)$ intramolecular vectors. We begin our exploration of the nature of the bond-breaking mechanism by considering classical neutron-scattering by the nuclei in water.

We first consider the energy transfer, ΔE, and the momentum transfer, $\hbar\chi$ by

$$\hbar\omega = E_o - E = \Delta E \qquad (\chi \text{ is a reversed aleph})$$
$$= (\hbar^2/2m_n)\,(K_o^2 - K^2) \qquad (15)$$

K_o and K are respectively the initial and final wave vectors of the scattered neutron, corresponding to E_o and E. $\chi = K_o - K$, the wave vector.

$$\hbar^2\chi^2/2m_n = E_o + E - 2(E_oE)^{\frac{1}{2}} \cos\theta$$

These relations lead to scattering laws,

$S_s(\chi, \omega)$ for incoherent scattering, and

$S(\chi, \omega)$ for coherent scattering

for the system. The scattering law is independent of the properties of the neutron and the details of the scattering process , and depends only on the properties of the scattering system. In our case, we consider the tetrahedral water molecule, the HYDRON, as the scattering system, perturbed by phonon packets of energy.

D.I. Page has brought our attention to the role of Fourier transformation of the scattering law which brings to light the correlation between the spacings between nuclei, and incident radiation. He develops his analysis somewhat along the following lines. (1)

He considers just the simple case of radiation that is Bragg-reflected by a crystal. Bragg's law relates the wavelength of the radiation λ to the spacing, d, of the lattice planes in the crystal:

$$\lambda = 2d \sin (\theta/2)$$

This equation is compared to Eq.15 for elastic scattering ($\omega = 0$) and $(K - K_o)$ which gives

$$\chi = 2K \sin (\theta/2) = (4\pi/\lambda) \sin (\theta/2)$$

The variable χ behaves like the reciprocal of the spacing d ($1/d = 1/L = L^{-1}$), and this leads one to try Fourier-transforming with respect to χ in order to seek information about the spacing between atoms in the scattering system.

(1) WATER, VOL.I, Chapter 9, Ed Franks, Plenum Press, N.Y. 1972

Similarly, the variable ω behaves like the reciprocal of a time ($1/T = T^{-1}$). If we use a harmonic oscillator of frequency ω, and a period of oscillation T, a Fourier-transform of the oscillator (i.e. the function $\cos \omega t$), there is obtained a sharp peak at a frequency $\omega = 1/\tau$. In the case of water this would be $\omega_o = f_o = 600$ Hz. The Fourier transform represents the atom's modes of motion. The double Fourier-transform of the scattering law gives information about the position of the atoms as a function of time. This theorem was just developed and proved in 1954 by Van Hove (2)who showed:

$$S(\chi, \omega) = (\tfrac{1}{2}\pi) \int_V dr \int_{-\infty}^{\infty} d\tau \left[G(r,t) - \rho \right] \exp\left[i(\chi - r - \omega t) \right] \qquad (18)$$

where ρ is the average density of the scattering nuclei. The function G(r,t) is the space-time correlating function, and for a classical system has a simple meaning. If there is a proton of position r, at a time t, then G($\mathbf{r}$,t) is the probability of finding an atom at position $\mathbf{r}_2$ at a time t . The quantities $\mathbf{r}$ and t are the space and time differences. G($\mathbf{r}$,t) can be divided into two parts, $G_s(\mathbf{r},t)$, which measures the probability of finding the same atom each time, and G_d ($\mathbf{r}$,t), which is the probability of finding a different atom each time.

$$G(\mathbf{r},t) = G_s(\mathbf{r},t) + G_d(\mathbf{r},t) \qquad (19)$$

Notice that G ($\mathbf{r}$,t) describes the motion of a single atom, while the total function describes the dynamic behavior of all the

(2) L. Van Hove, Phys. Rev. 95:249, 1954

function, $S(\chi,\omega)$ are computed out for light water, the qualitative form of these two functions is seen in the next Figure. (1)

The uppermost curve shows the structure factor form $S(\chi)$.

(1) Fig.3, p.342 from D.I. Page, WATER , VOL. I, Chap.9

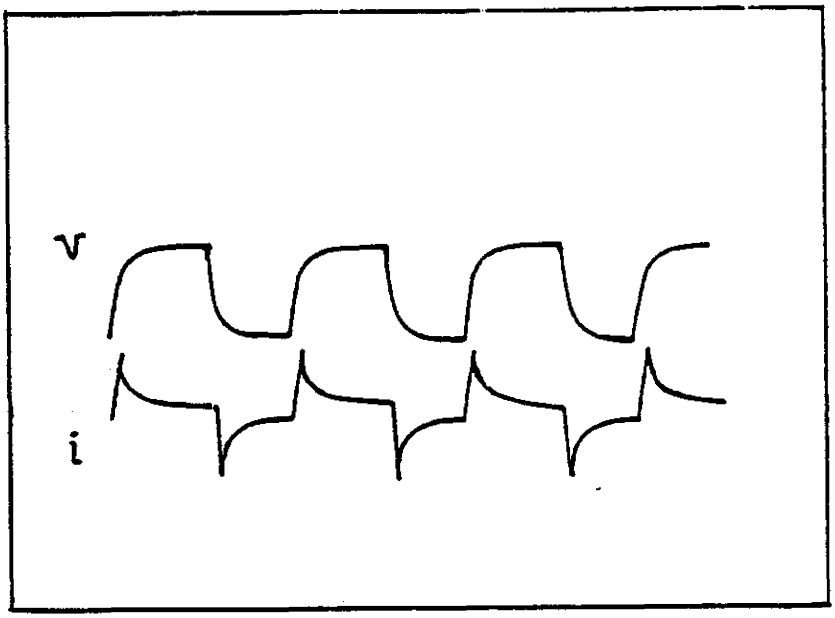

FIG. 21 CASE I A ELECTRODES. IC OHM SERIES RESISTANCE
SEE FIG. 28.
SQUARE WAVE PULSE INPUT ACROSS CHEEK TISSUES.
20 μscc / cm TIME BASE
UPPER TRACE: VOLTAGE DECAY CURVE
LOWER TRACE . CURRENT DECAY CURVE

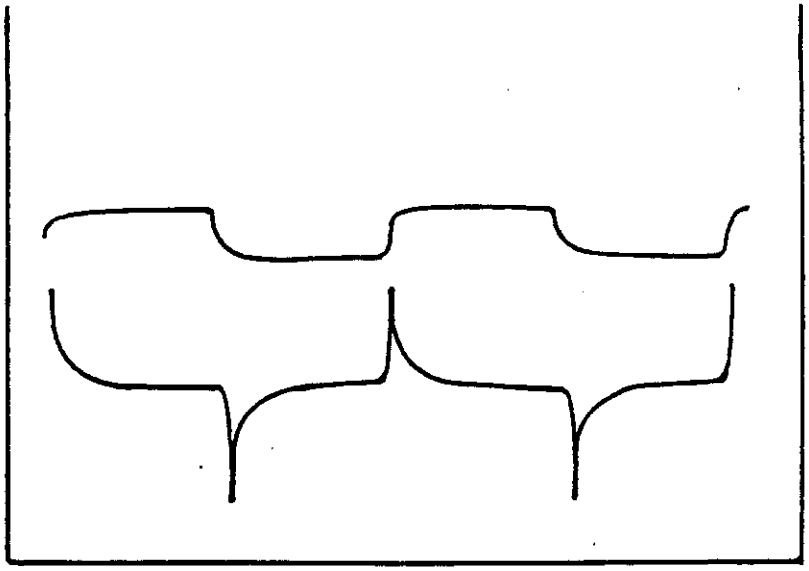

FIG. A. CASE IA ELECTRODES ACROSS HEAD.
15 OHM SERIES RESISTANCE. SEE FIG. 28.
20 μsec PULSE WIDTH
UPPER TRACE: VOLTAGE DECAY CURVE
LOWER TRACE: CURRENT DECAY CURVE

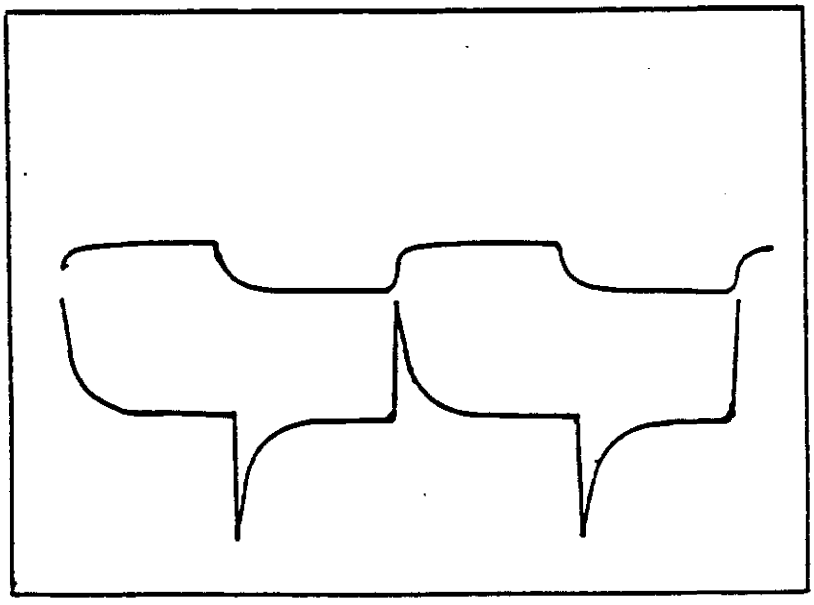

FIG. B. CIRCUIT SYNTHESIZED (SEE FIG. 31 CASE IA)
EQUIVALENT CIRCUIT OF HEAD.
UPPER TRACE: VOLTAGE DECAY CURVE
LOWER TRACE: CURRENT DECAY CURVE

ELECTRODE: HEAD

CONFIGURATION

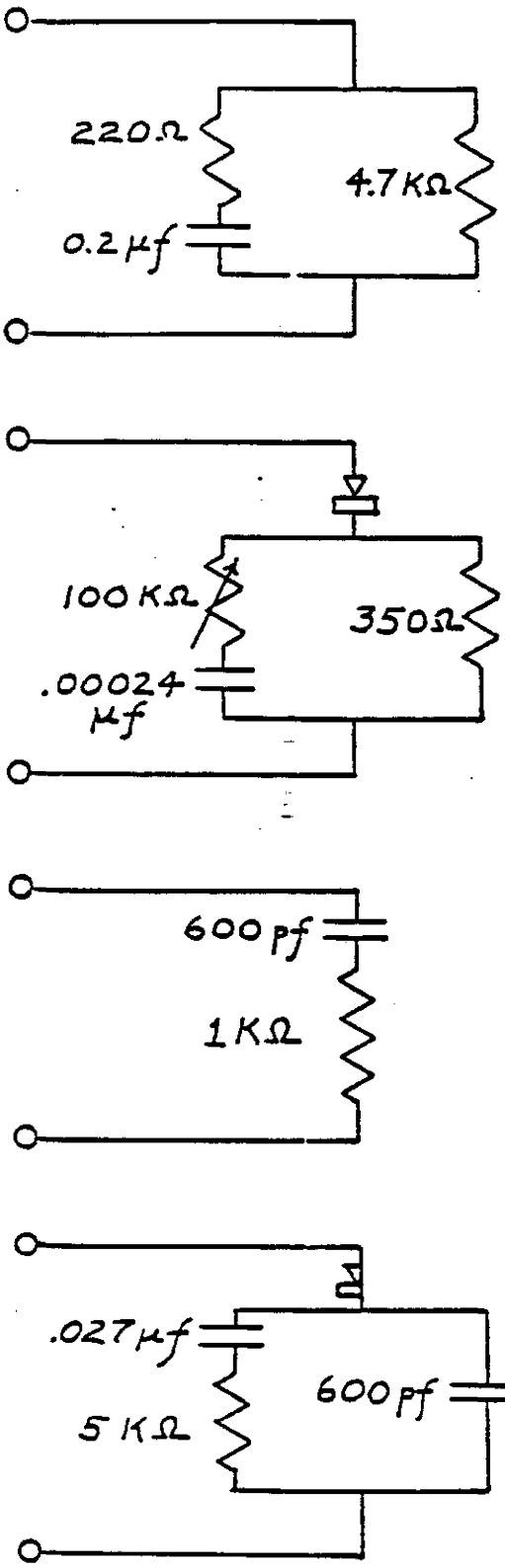

CASE IA

BARE METAL ELECTRODES STATIONARY ON THE SKIN ACROSS THE HEAD.

CASE IB

BARE METAL ELECTRODES STROKED ON THE SKIN ACROSS THE HEAD.

CASE II

MYLAR (0.25 MIL) COVERED ELECTRODES STATIONARY ON THE SKIN ACROSS THE HEAD.

CASE III

ONE BARE METAL ELECTRODE AND ONE MYLAR (0.25) COVERED ELECTRODE STATIONARY ON THE SKIN ACROSS THE HEAD.

FIG.23 . EQUIVALENT CIRCUITS OF ELECTRODE-HEAD CONFIGURATIONS

Far below its resonance frequency ($\omega << \omega_s$) each oscillator type adds a constant contribution.

$$\frac{N_s e^2/\varepsilon_o m s}{\omega_s^2} \tag{75}$$

to the static dielectric constant of the medium, whereas far above the resonance frequency its contribution vanishes. To follow the behavior of the lowest oscillator type, r, through its resonance region, the effect of vacuum and the remaining resonator types is lumped into a constant contribution.

$$A = 1 + \sum_{s} \frac{N_s e^2/m_s}{\omega_s^2} \quad \text{for } s \neq r \tag{76}$$

In place of ω, we introduce the deviation from resonance:

$$\Delta\omega \equiv \omega_r - \omega, \text{ as the variable, approximate} \tag{77}$$

$$\omega_r + \omega \simeq 2\omega_r$$

$$\frac{\omega}{\omega_r} \simeq 1$$

and thus equation 74 is rewritten as:

$$K^* = \eta^{*2} = A + \frac{B}{\Delta\omega + j\alpha} \tag{78}$$

where the factor B stands for:

$$B = \frac{N_r e^2/\varepsilon_o m_r}{2\omega_r} \tag{79}$$

The frequency dependence of the real part of the relative permittivity:

$$K' = m^2 (1 - K^2) = A + \frac{B\Delta\omega}{\{\Delta\omega\}^2 + \alpha^2} \tag{80}$$

describes the dispersion characteristic of the dielectric medium near resonance. These changes are plotted in Figure 70, K' rises hyperbolically from the low frequency value $A + \frac{2B}{\omega_r}$ to a maximum:

$$K' \max = A + \frac{B}{2\alpha} \tag{81}$$

at $\Delta\omega = +\alpha$, falls with a linear slope $-B/\alpha^2$ through the value A at the resonance frequency ($\Delta\omega = 0$), reaches a minimum:

$$K' \min = A - \frac{B}{2\alpha} \tag{82}$$

at $\Delta\omega = -\alpha$, and then rises again asymptotically to the constant value A for very high frequencies ($\omega >> \omega_r$).

The absorption characteristic of the dielectric, identified near resonance by the relative loss factor,

$$K'' = 2\eta^2 K = \frac{B\,\alpha}{\{\Delta\omega\}^2 + \alpha^2} \tag{83}$$

starts from zero at low frequencies, traverses its maximum B/α at resonance, and falls again symmetrically to zero at high frequencies. The half-value points $B/2\alpha$ of this bell-shaped absorption characteristic are reached at the deviation from resonance $\Delta\omega = \pm\alpha$.

For the phase relation between applied field and induced dipole moment near resonance, the relation,

$$\tan\psi = \frac{K''}{K' - A} = \frac{\alpha}{\Delta\omega} \tag{84}$$

at low frequencies ($\omega << \omega_r$) the moment follows in phase, at resonance it lags by $\pi/2$, and at very high frequencies by π.

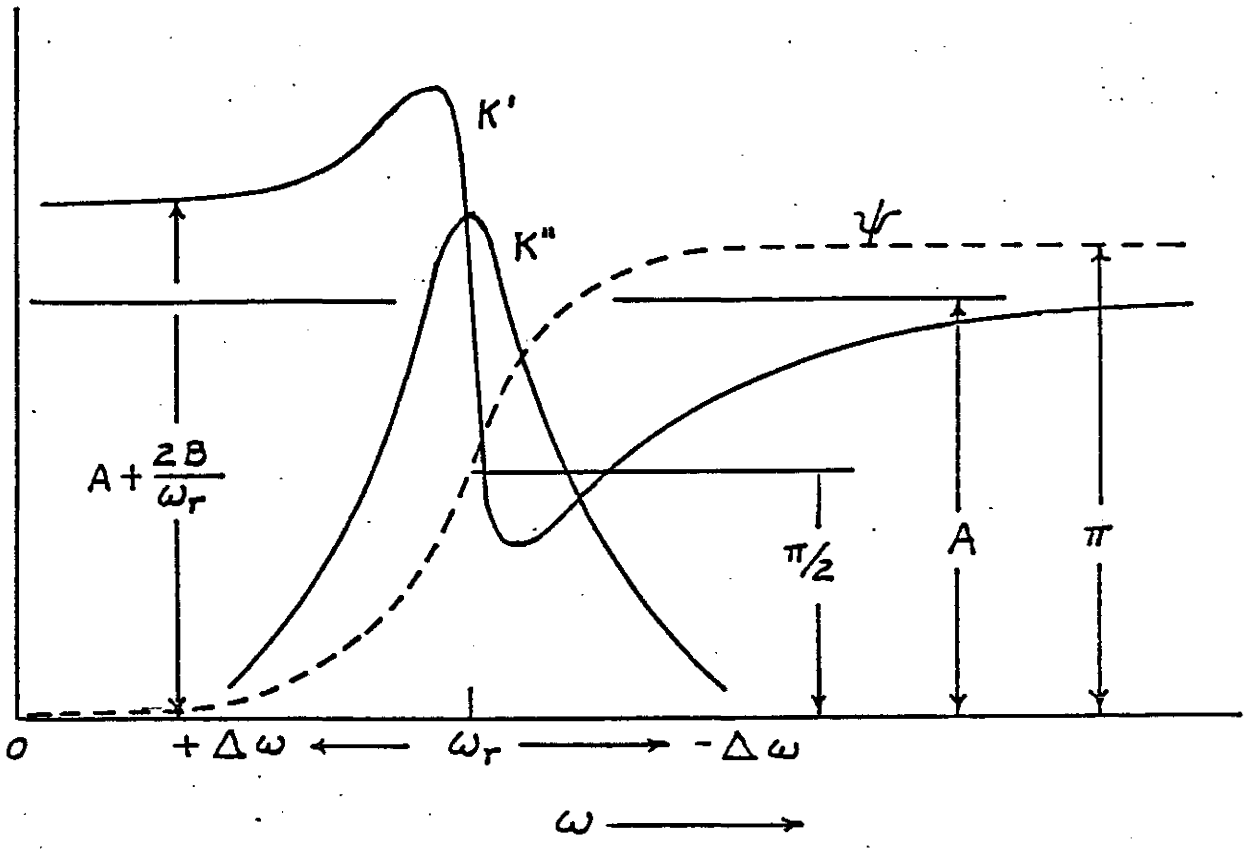

24

FIG. ANOMALOUS DISPERSION AND RESONANCE ABSORPTION. (after von Hippel)[3]

REFERENCES

1. Schwan, H.P., Electrical Properties of Tissue and Cell Suspensions, Proceedings Fourth Annual Tri-service Conference on the Biological Effects of Microwave Radiation, New York, 1960.

2. Sommer, H.C., and von Gierke, H.E., Hearing Sensations in Electric Fields, Aerospace Medicine, Volume 35, No. 9, September, 1964, pages 834-839.

3. von Bekèsy, Georg, EXPERIMENTS IN HEARING, McGraw-Hill, New York, 1960, equations 6 and 7, page 169.

4. Ibid., equation 8, page 170.

5. Bennett, M.V.L., Physiology of Electrotonic Junctions in Biological Membranes, Annals of the New York Academy of Sciences, Volume 137, Article 2, pages 509-539 (see equation 28 and figures 4 and 5 for $\alpha = 0$).

In our water electrolysis studies the curve of K´ was found to intercept K" at a frequency close to 2 = 512 Hz, but showed an interesting pattern of dispersion. As stated before, measured resonance, $f_o = \omega_r$, centered at 600 Hz. In examining the side bands around this frequency, it was found that $+\Delta\omega$= 360 Hz, and that $-\Delta\omega$= 720 Hz. Within this octave, the dispersion pattern was found to correspond to small peaks which closely mimicked the equal temperament scale:

OBSERVED, Hz			EQ. TEMP.Hz	PYTHAGOREAN SCALE	MUSICAL NOTES (Rising scale)
360	$+\Delta\omega$		360	D = 360 HZ	D
		1/3	384		e^b
			400	E = 405 Hz	e
420		OCTAVE	432		f
			450		$f^\#$
480			480	G = 480 Hz	G
540		1/3	540	A = 540 Hz	A
		OCTAVE	576		b^b
f_o=600= ω_r			600		b
			648	C = 640 Hz	C
660		1/3	675		$C^\#$
720	$-\Delta\omega$	OCTAVE	720	D = 720 Hz	D

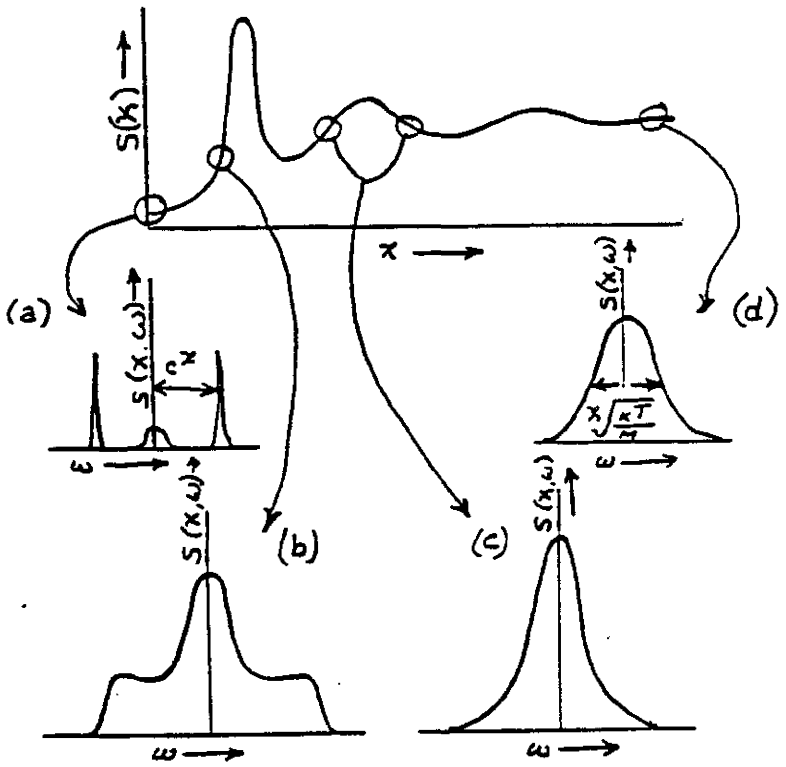

QUALITATIVE BEHAVIOUR of $S(x,\omega)$ FOR SEVERAL VALUES of x.
THE UPPER CURVE IS THE STRUCTURE FACTOR $S(x)$ AND THE REMAINING CURVES SHOW THE SPECTRAL SHAPE AT SEVERAL FIXED VALUES of x. AT LOW AND HIGH VALUES OF x THE WIDTHS CAN BE CALCULATED.

FIG. 25

In the table of PHASER PARAMETRIC HARMONICS my attention now focused on the 7th harmonic of 0.125 Hz, i.e. 8.00 Hz. It is known that there is a spin/spin: proton/proton magnetic coupling of 8 Hz which is a fundamental constant. I began to wonder what role this magnetic 8 Hz frequency played in water splitting? First I developed methods of measuring such extremely low frequency (magnetic) fields. This ELF magnetic detector had a bandpass of 1-40 Hz. When I measured the ELF output of the COMPONENT I (U.S. Patent Sheet 1 of 11). There was the usual AM carrier signal which I have described. I was most surprised to find that the ISOLATION TRANSFORMER and LC series resonant output showed a strong 8.00 Hz subharmonic signal which I had not seen before. I repeated many of my experiments in the light of this new finding. These I will briefly review.

The author now repeated his experiments in splitting water molecules (H_2O) into hydrogen (H_2) and oxygen (O_2) with the usual weak alternating current electric fields. The electric field was found to have a fundamental magnetic (B Field) oscillation of 8 Hz with higher harmonics, 2^n, where n represents the higher harmonics. The products of electrolysis were measured with the mass spectrometer. The starting composition of the water was made up of:

H_2O (water)

NaCl (salt)

Cu^{++} (copper ions)

Table 3.

$$ {}_{8}O^{16}_{8} \longrightarrow {}_{7}N^{14}_{7} \longrightarrow {}_{6}C^{12}_{6} $$

$p' + n + \nu$ $\qquad$ $p + n + \nu$

INITIAL VOL. %		AFTER 120 min. ELECTROLYSIS.		AFTER 240 min. ELECTROLYSIS.
H_2 - 21%	① →	H_2 - 89%	→	H_2 - 89%
O_2 - 18.7%	② →	O_2 - 0.87%	→	O_2 - 1.53%
N_2 - 59%	④ →	N_2 - 9.6%	→	N_2 - 8.7%
A_R - 0.87%		A_R - 0.3%		A_R - 0.199%
CO_2 - Not Detectable		CO_2 - 0.0137%	⑤ →	CO_2 - 0.062%
pH - 3.2	③ →	pH - 13.0	→	pH - 13.0
Na^+ - trace		Na^+ - trace		Na^+ - trace
Cl^- - tr.		Cl^- - tr.		Cl^- - tr.
Cu^{++} - tr.		Cu^{++} - tr.		Cu^{++} - tr.
Fe^{+++} - tr.		Fe^{+++} - tr.		Fe^{+++} - tr.

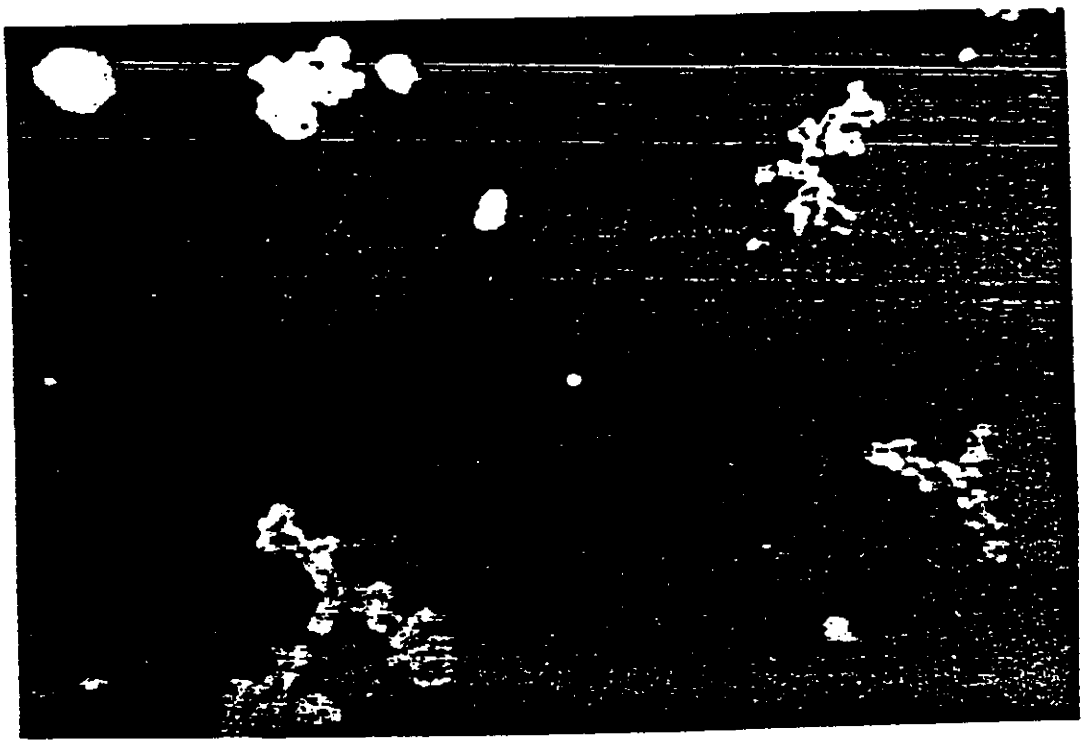

FIG. 27. PRIMITIVE LIFE FORMS CREATED DURING ELECTROLYSES OF STERILE WATER.

Fe^{+++} (iron ions)

plus dissolved air, N_2 and Ar,

and it was electrolysed. The resulting composition of the solution was: See Table 1. The significant changes are marked by arrows:

1) H_2 increased as a result of electrolysis from 21% to 89%.
2) O_2 decreased from 18.7% to 1.53% as a result of two mechanisms (a) hydroxyl formation with Na and Cu, and Fe, as reflected in pH (3) change from 3.0 to pH 13.0, and (b). appearance of CO_2 in the solution.
3) Before electrolysis the N_2 content of air was 59% and by vacuum pumping was being reduced to 9.6%; the CO went from a non-detectible level to 0.062 vol% in four hours. No artifact cause could be found for the appearance of CO_2. It was concluded that we were observing the weak transmutation of Kevran as shown on the top of Table 1.

Note that in O^{16} -N^{14} there is a loss of a proton (p) and a neutron (n) plus a neutrino to account for the mass loss. The same reaction is found in N^{14} to C^{12}.

This experiment was replicated many times with the same results. As time went on it was found that many carbon-based organic molecules including amino-acids were being produced during the electrolysis reaction, and that these were formed into arboreal-patterned life forms. Fig. 27. Note the fractal geometric forms of the bodies. This phenomenon leads us to argue for the presence of an organizing principle corollary to the Kevran weak transmutation.

A separate quest was initiated to discover the basis of this hypothetical organizing, or morphogenic principle.

New and more sophisticated equipment was designed and built to measure extremely weak ELF magnetic fields > 10 nanotesla (10^{-}

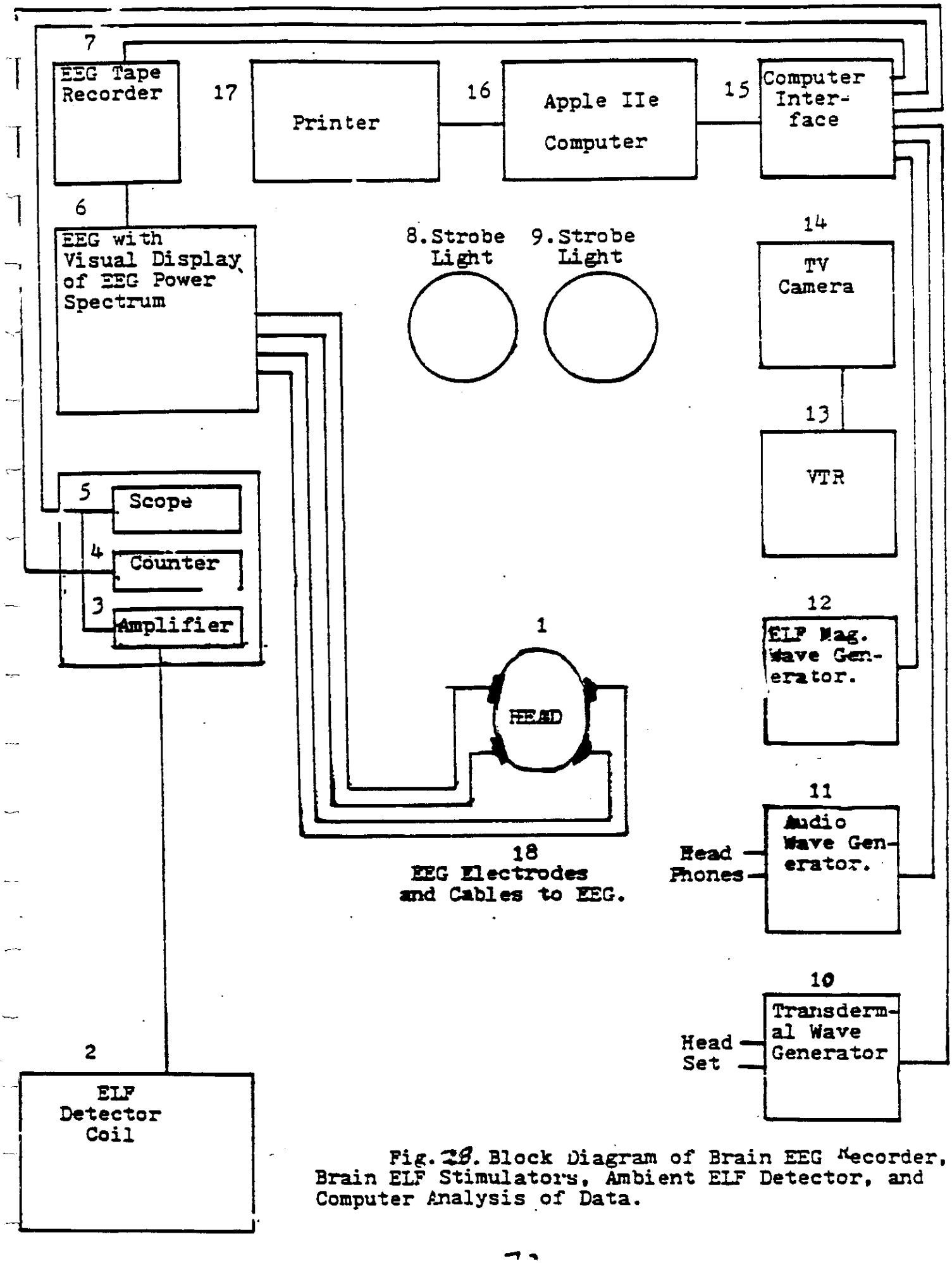

Fig. 28. Block Diagram of Brain EEG Recorder, Brain ELF Stimulators, Ambient ELF Detector, and Computer Analysis of Data.

extremely weak ELF magnetic fields > 10 nanotesla (10^{-9} T, where 1 Tesla = 10,000 gauss) over the frequency range from 1 to 38 Hz. See Fig. 28.

The first basic finding was made during measurements of persons who had a high record of success in treating (by laying-on of hands) organic diseases in humans. Such people are called healers. I studied healers from different age groups (19 to 70 years); different cultural groups (U.S.A., Brazil, Costa Rica, Great Britain, India, Israel, etc); and of different religous backgrounds. In spite of the vast range of differences between such individuals they all had one scientific factor in common between them: When they operated as healers-each, and all, radiated an 8 Hz ELF magnetic field from their hands. When not healing, these persons could charge tap water in glass bottles with their hands, and produce a remanent 8 Hz ELF magnetic field in the water for weeks after their hands were removed. This appears to be a universal repeatable effect in all healers examined. Since healing is an organizing and repair operation on biological systems, and it occurs as an effect of an 8 Hz ELF magnetic field, we wanted to find out what is the physics of this phenomenon? First, the foundation of this effect lies in the nuclear magnetic resonance (NMR) of each atom, molecule, or compound in the human body. This NMR phenomenon is illustrated in Table 3.1. It shows that proton-proton coupling constants (in H_2) between

ΓON AND CARBON-13
MR SPECTROSCOPY
AN INTEGRATED APPROACH

R. J. Abraham
University of Liverpool

and

P. Loftus
Merchant Taylors' School, Crosby

HEYDEN
London · Philadelphia · Rheine

TABLE 4.

Table 3.1

Characteristic Proton–Proton Coupling Constants (Hz)

System	Coupling range	System	Coupling range
OPEN CHAIN			
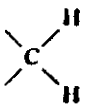	−10 to −18	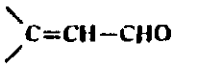	7 to 9
			6 to 8
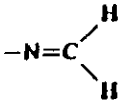	8 to 16	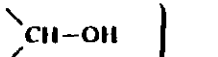	4 to 8
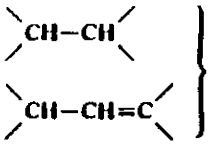	5 to 10	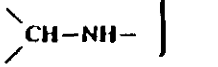	0 to 1
$CH_3.CH_2-$	7 to 8	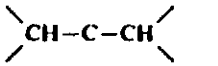	0 to −2
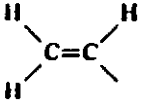	J_{gem} −3 to +7 J_{cis} 3 to 18 J_{trans} 12 to 24	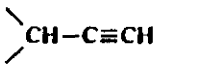	−2 to −3
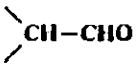	1 to 3	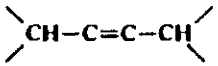	0 to 2
		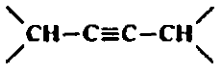	2 to 3

CYCLIC

Aromatic and olefinic	*ortho*	*meta*	*para*
Benzene derivatives	5–9	2–3	0–1

	J_{12}	J_{34}	J_{24}	J_{25}
Furan	1.8	3.5	0.8	1.6
Pyrrole	2.6	3.4	1.4	2.1
Thiophene	5.2	3.6	1.3	2.7
Cyclopentadiene	5.1	1.9	1.1	1.9

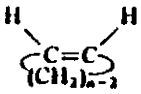

n =	3	4	5	6	7	8	9
cis	ca. 1	2.7	5.1	8.8	10.8	10.3	10.7

Saturated	J_{gem}	J_{cis}	J_{trans}
Cyclopropane	−4.5	9.2	5.4
Ethylene oxide	+5.5	4.5	3.2 CARCINOGEN
Ethylene imine	+2.0	6.3	3.8
Ethylene sulphide	ca. 0	7.1	5.6
Cyclobutane derivatives	−11 to −15	6 to 11	3 to 9
Cyclopentane derivatives	−11 to −17	7 to 11	2 to 8
Cyclohexane derivatives	−12 to −15	J_{ax} 2 to 5	J_{ax} 8 to 13 J_{eq} 1 to 4

adjacent hydrogen atoms (H) in a molecule all fell within the frequency range of ELF magnetic fields. Many of the common proton-proton bonds such as $-N=C\begin{matrix}H\\H\end{matrix}$ fall in the 8 Hz range; See Col. 1, molecule in 2nd row (8-16 Hz). Other molecules which are known to be carcinogenic , such as ethylene Oxide (col. 1, 6th row from bottom of page) show a 3.2 Hz resonance in the J trans mode. This same frequency of ELF when used to irradiate a mouse produces skin cancer within 24 hours. Thus, the NMR properties of each molecule, or a part thereof reveals the origin of the ELF magnetic waves that emanate from the human body. When these emissions are coherent around 8 Hz (as a center frequency) a person can be defined as being in a healthy state, or may be a healer-potential, or actual. When the NMR coupling constants are widely dispersive around the center frequency of 8 Hz, we can look for pathological mechanisms at work. See . Note that a frequency as close as is 3.2 Hz to the 8.00 Hz center frequency can cause skin cancer in mice.

In order to double check the role of 8.00 Hz ELF magnetic fields as an organizing principle for biochemical molecules leading to life forms, we shifted the 8.00 Hz fundamental of the electrolysis generator current to 5.00 Hz. This new fundamental frequency did not produce complex biochemicals, and did not produce life forms. This finding was further tested by irradiati

Figure 29.

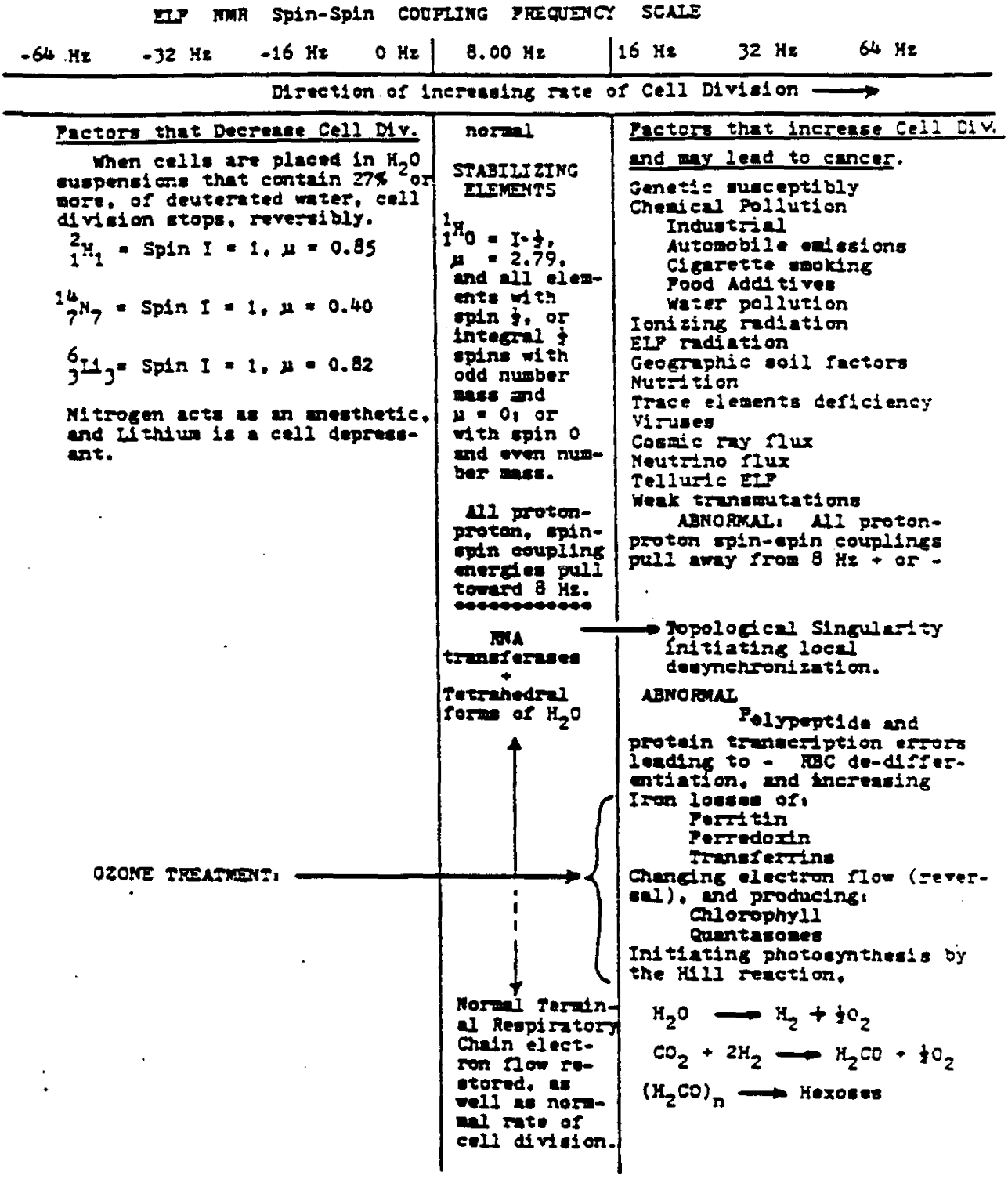

FLOW CHART RELATING NUCLEAR SPIN PROPERTIES, MAGNETIC MOMENT PROPERTIES TO THE RATE OF CELL DIVISION, AND TO ELF NMR COUPLING ENERGIES

cells, and organisms with a wide range of frequencies other than 8 Hz. As an example of our findings- irradiating humans with 6.66 Hz produced brain wave entrainment, and depression. Irradiating humans with 13.00 Hz produced brain wave entrainment, and agitated excitatory states leading to riotous behavior. Other workers have found that harmless lymphotrophic viruses can be switched with specific ELF frequencies to become the HLTV III virulent forms. Another ELF frequency can switch the HLTV III virus back to an inocuous form.

Thus we may conclude that man has found the key with which to open Pandora's box. The good side of the story is that 8.00 Hz ELF magnetic fields can be used to stimulate reparative and normalizing functions in the human. The down side of the story is that our planet has been ravaged by ELF warfare since 1976 between the superpowers. All living things in the path of ELF emissions are subject to degrading influences in such warfare. As if this is not bad enough, our research has uncovered spontaneous and spurious ELF emissions from all types of common household appliances from TV sets to motors. These ELF frequencies all have long term deleterious and degrading effects. Humanity has a task of at least two generations to clean up the ELF ecological mess. We also have an opportunity to learn how life can be individually balanced and optimize In the meantime, as a stop gap against the pollution

Curve (a) shows the behavior of $S(\chi,\omega)$ at low values of χ. This curve is of the greatest importance for our understanding of both the sense of hearing, and water electrolysis . At threshold levels, both of these effects show vector displacements, χ , of the order of 10^{-8} cm, or less, (or 10^{-10}M) which is 1Å. This is of the order of distances for the O-H vector, and in the intramolecular O-O distances of 2.80Å to 3.24Å in water. Of outmost importance is the splitting of $S(\chi,\omega)$ into these three components at low values of χ. (1)

This would correspond to a center frequency ω_o, and an upper and lower side band $\omega_o \pm$. In curve (b) the center frequency and the side bands are true (phonon) sound wave modes where size and shape can be described by simple hydrodynamic theory. The center frequency, ω_o [$S(\chi,\omega)$] height varies with the entropy fluctuation in the system, and is usually interpreted as corresponding to the thermal damping of the sound waves.

Curve (b) shows the blurring of the side bands with a slightly higher value of χ than that of (a). Curves (c) and (d) shows shapes more appropriate to an ideal gas.

There is a discrepancy however in the level of energy transfer from neutrons to nuclei (of the order of 10^6 eV), and that found in threshold electrolysis of water at a threshold of the order of a few electron Volts.

This could be explained by spectra where there is a large quasi-elastic peak around a region of zero energy transfer which indicates the long time behaving atoms as seen in proton relaxation; and an inelastic region extending outward from this peak where the energy transfer peaks at 50 to 100 Mev. This inelastic region

(1) WATER VOL.I, p.120

of ELF in our environment, we have developed a circuit housed in a bracelet that can adequately protect people against personal pollution from negative ELF sources in our immediate environment.

REFERENCES

1. Puharich, Andrija. TMT, The Magnetic Threat. Unpublished manuscript under contract with Dell Publishing Co. One Dag Hammarskold Square, New York, N.Y. 10022.

2. Liboff, A.R., T. Williams, Jr., D.M. Strong, and R. Wistar, Jr. Time-varying Magnetic Fields: Effect on DNA Synthesis. Naval Medical Research Institute. SCIENCE, Vol. 223, February 24, 1984.

3. Baker, C.B. The Weatherwar Devastation of America. YOUTH ACTION NEWS, February 1981.

4. Bearden, Thomas E. STAR WARS NOW, The Bohm-Aharonov Effect, Scalar Interferometry, and Soviet Weaponization. Tesla Book Company, Millbrae, California, 1984.

5. Puharich, J.H., Successful Treatment of Neoplasms in mice with gaseous superoxide anion (O_2^-) and Ozone (O_3); with a rationale for the effect. Yearbook of the Sixth World Congress, of the International Ozone Association, Zurich, Switzerland, 1983.

6. Bearden, Thomas E. Toward a New Electromagnetics, Part III: Clarifying the Vector Concept. Tesla Book Company, Millbrae, California, 1983.

7. Abraham, R.J. and P. Loftus. Proton and Carbon-13 NMR Spectroscopy. Pages 34-59. Heyden, London, 1981.

represents the neutron interaction with the vibrational modes of the system. It is obvious that in H_2O electrolysis we do not deal with this inelastic energy transfer system.

The origin of these two regions in the scattering spectra are explained by reference to events occurring in a solid. At time zero, the position of an atom is given by definition, and on the average it is moving with substantially the velocity it would have as a gas atom. Because such an atom is "bound", there is rapidly built-up around it a "thermal cloud". The formation and fluctuations of the cloud give rise to the inelastic component ; the scattering from the cloud as a form factor gives rise to the elastic component, and it is stated that it is elastic because the cloud endures for a long time. These two energy components reflect the quick formation of the thermal cloud, and its long life once and when formed.

If we consider a liquid, by analogy to the solid, the two components in the liquid energy distribution refer to the formation of a "thermal cloud" in the liquid and the subsequent duration of the cloud which now has a finite lifetime. The quasi-elastic region is usually related to the long-time behavior of hydrogen in water which is the scattering atom (incoherent scattering).

The fall-off with neutron angle of the intensity of the quasi-elastic component measures the spatial extent of the thermal cloud associated with the vibrating hydrogen atom. The angular variation of the quasi-elastic intensity has been measured for water at room temperature by several workers (128, 365, 632, 656), and the results are given as the root mean square (RMS) displacement, $\overline{u}$, of the hydrogen atoms in light water. These measurements indicate that the probable value of $\overline{u}$ is between 1.0Å and 1.5Å. Thus we can conclude

that the physical basis of threshold sensory activation, and reversible threshold of water electrolysis is due to quasi elastic perturbations of the thermal cloud surrounding the hydrogen atom. Although the displacements, $\bar{\alpha}$, center on approximately 1Å - the actual energy transfer involved is less than 1eV. The thermal cloud mechanism is useful in understanding the thermal, or heat flow coupling between electricity and the Gibbs function ΔG.

When we consider how the quasielastic perturbation of the thermal cloud leads to an actual bond-breakage. In the following figure we show the tetrahedral water molecule, and above it the equivalent circuit of the PHASER mode of action.

On the left we have the COMPONENT I driver of the molecular oscillation, as already defined. A barrier potential will build up, as already described, to give a D.C. source, E, with poles as shown made up from the energized lone pair electrons, e^-, e^- and the H^+ atom pumped up to the full energy level giving the $109^o 28'$ tetrahedral angle.

On the right we have the ferroelectric capacitor element made up of the e^- and H^+ pair. And to the far right we have the load which is the next tetrahedral molecule in a chain of water molecules.

In the top center of the equivalent circuit is the non-linear polarizing element shown as an n-p diode, and whose function is that of the oxygen atom at the center of the tetrahedron. These are the elements of the "circuit".

First, the oxygen atom will be clamped by the electron-proton gyromagnetic frequency ratio, the resonant frequency, f_o = 600 Hz. This, plus the side band distribution of the audio

FIG. 26

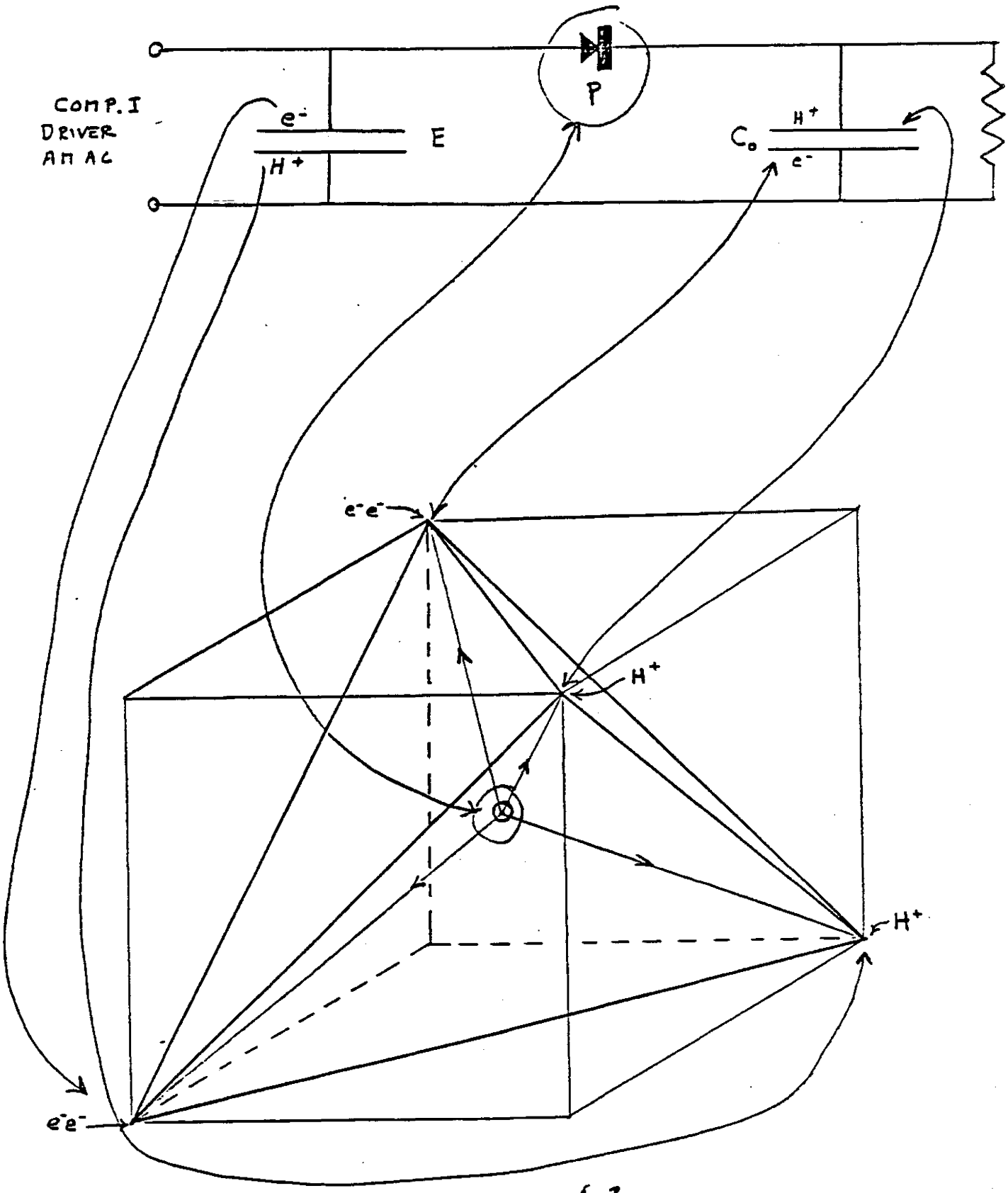

frequencies distributed according to the $\sqrt[12]{2}$ rule, will set up the phonon mechanism. The phonon mechanism is the direct cause for stimulating photon emission. We will describe in more detail later how this occurs, but suffice to say that it brings about coherent infra-red emission - the cause of the O-H bond-breakage.

First with reference to the ferroelectric capacitor, C, mechanism made up of proton and electron dipoles. C will charge up from E at the left, where Q is charge; C_o is the capacitance, and V is Volts,

$$Q = C_oV$$

As Q builds up there will be a build up of heat (infra-red photons) in the thermal cloud. This heat will cause a decrease in the charge Q of C, and current will flow to the load. The current will flow to the load because the oxygen atom is 180° out-of-phase with the potential of the charge and it will act as a block to current flow through it, and will shunt the current to the load. The capacitor will then fully discharge and release more heat and a population inversion into the load, and this heat will be a coherent beam of infra-red due to the phonon pulsing.

Then the ferroelectric will go through a negative heat phase, i.e., act as a heat sink - a well-known property of ferroelectrics.

This negative heat phase leads to polarization of the ferroelectric dipoles and an increase in the capacitance, C_o. This in effect reverses the current flow through the load, and releasing charge from E to build up capacitor charging. The outcome of this process is that an alternating current is produced at the output, and this alternating current controls the heat output in quantal photons -

at the cycling rate of the NMR rate of the proton at the IIIrd subharmonic of 2. The bond-breakage occurs at each peak of the current and heat output due to a dipole disordering effect that looks like a Curie point temperature - and in fact the spin temperature may look like $374^{\circ}K$ in the small regions of space in the tetrahedron.

It is to be noted that the elements of this PHASER MECHANISM are simple:

E, looks like a fuel call

P, (the O atom) looks like a diode

C, looks like a ferroelectric capacitor

R_L, looks like a link in a chain of molecules.

The principal phaser parametric harmonics involved in the bond-breakage processes as integer powers of Log_2 are given in the following table.

TABLE 2.

PRINCIPAL PHASER PARAMETRIC HARMONICS

INVOLVED IN SPLITTING THE WATER MOLECULE

FREQUENCY, HZ	TARGET
0.125 Hz (3) 0.125 Hz x 7th Harmonic = 8.00 Hz	PROTON, NMR
$0.125 \times 2^{12} = 2^{9}$ Hz (2)	PHONON-HYDRON = f_o (Conductivity term)
$2^{9} \times 2^{(12+1)} = 2^{22}$ Hz (1)	ELECTRON (DIELECTRIC TERM)
3×10^{14} Hz TO 4×10^{14} Hz	PHOTONS - IR (Coherent)
8×10^{14} Hz to 3×10^{17} Hz	PHOTONS - UV (Coherent, Hα line

(1) Harmonic RF Bands are continuous from 2^{10}, 2^{11} ..., etc to 2^{21} Hz.

(2) Dispersion around these and the other bands will follow the $\sqrt[12]{2}$ rule for side band intervals.

(3) 1/.125 is the phase velocity difference between the velocities of the orbits of the proton vs. the electron. The first and second harmonics [(0.25 Hz) and (0.5 Hz)] of this fundamental are used in the cycling of the amplitude modulation during peak efficiency hydrolysis.

Paper 4.

PROTOCOMMUNICATION II

Universal Information/Action Transfer

Theory

and

An experimental model designed to test the theory: Project TESLAR

nervous system. Let us look deeper into this phenomenon.

In many experiments carried out with healers during the ast 20 years, it has been found, repeatedly, in bona fide healers, that their hands radiate an 8.00 Hz ELF magnetic field. As already xplained, the target of the 8.00 Hz signal, is the DNA of the healee. What is important to note is that the 8.00 Hz ELF field carries pecific instruction to the DNA to carry out, very specifically, the egeneration of diseased cells, and tissues. This leads us to believe, as in the case of TD electrostimulation of hearing that very precise nformation is carried by ELF waves to DNA, and even to higher complex information systems.

During many experiments over the past 37 years with the henomenon of psychometry, I found that there was an incredible recovery of information about a person from present time, past time, nd future time by this method. Psychometry is the art of giving a "psychometrist" an object from a person, and by touch contact with the object, the practitioner recovers much information. A case in point will illustrate the effects. A person can be photographed. Here visible light bounces off of the person, enters the lens of a camera, and the light differentially activates molecules in the film emulsion to create a portrait - either in color, or in black and white. Without ever seeing the person photographed, the psychometrist can recover any information desired about the photographee. What is most remarkable is that the psychometrist can transcend the limitations of time in recovering information. Peter Hurkos is the best practitioner of psychometry that I know of.

There is a postulate by John Bell, often called Bell's Theorem which states that every particle (in our case, proton) is

correlated with every other particle (proton) in the Universe by supra-luminal signals. One could argue that the case of psychometry lends support to Bell's postulate. There are other experiments which I have carried out beginning in 1950 which may help to clarify our problem with the proton, and ELF magnetic fields. The basic question that I raised is: why do ELF fields pass through perfect copper-shield rooms without signal distortion?

See Fig.4, p.9 for the design of the double shielded room wherein the test subject worked, Photo Fig.6, p.10. Fig.6, p.11 shows the distance relation between the two sets of shielded rooms. The second set of shielded rooms is shown as LAB 2 containing a pure random switch triggered only by big cosmic ray pulses. See Fig.7, p.12. The task of the test subject was to determine <u>when</u> the cosmic ray switch was triggered by a big cosmic ray pulse. Fig.11, p16 shows the statistical analysis with a critical ratio 4.87, or odds against a chance result of a million to one. Fig.8.b., p.13 shows the clustering of the test subject's calls around the arrival time (ϑb) at 0 of the C.R. pulses. We became curious about the calls of target arrival mode <u>before</u> the C.R. arrival at the switch. We ran a separate set of experiments to evaluate a possible precognition accuracy. Note (p.18, Table 1) that Column Group 2, Col. Group 3, and Col. Group 4, showed a probability of precognition hits significally in excess of chance. See Part 1, p.36, for the test subject's description of a cosmic ray event long before it hit the earth, and the C.R. experiment. This experiment proved that the test subject could perceive and interact with a high energy, proton, or muon, (we know not which), long before being registered on earth by a detector.

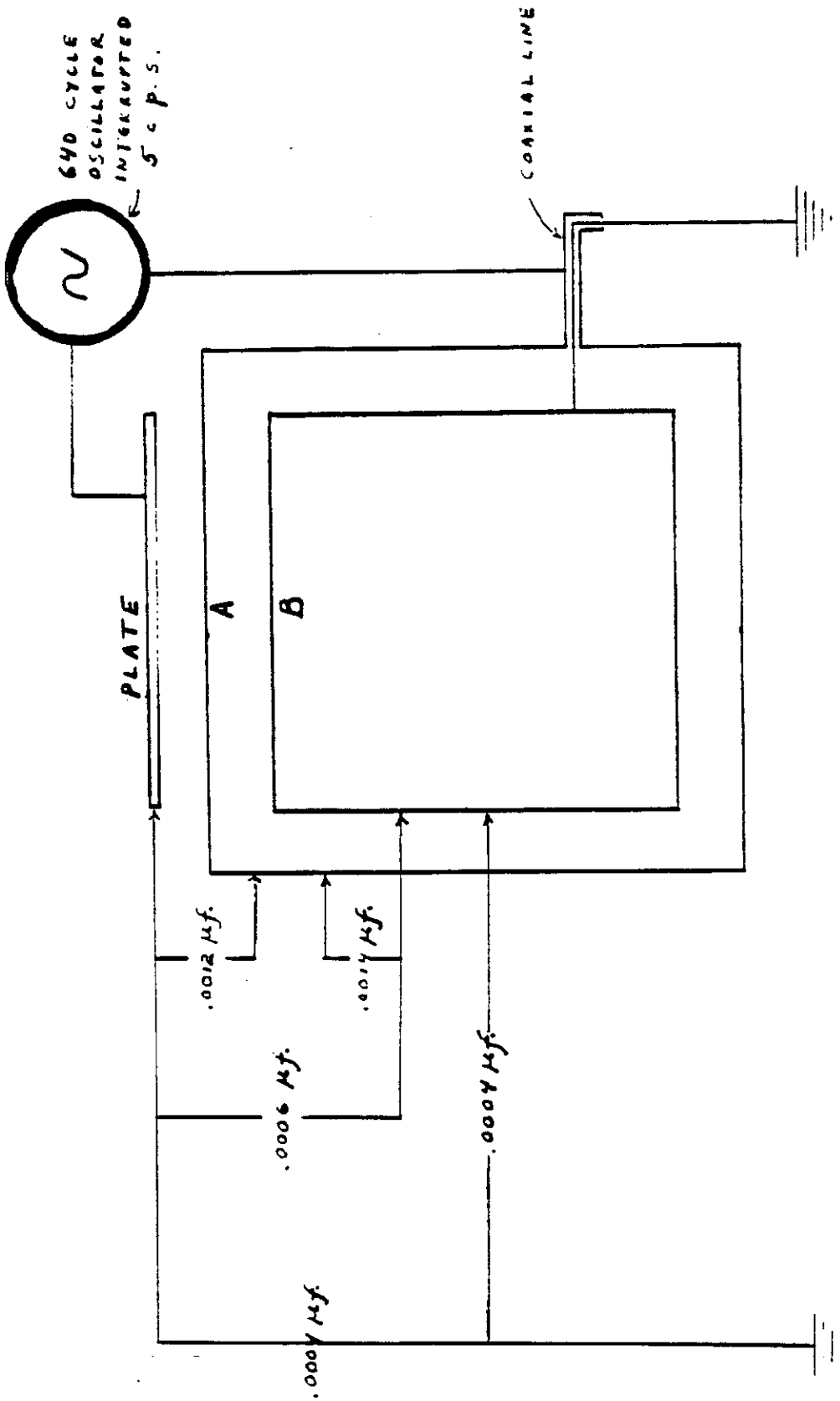

FIG. 4. TREATED FARADAY CAGE.

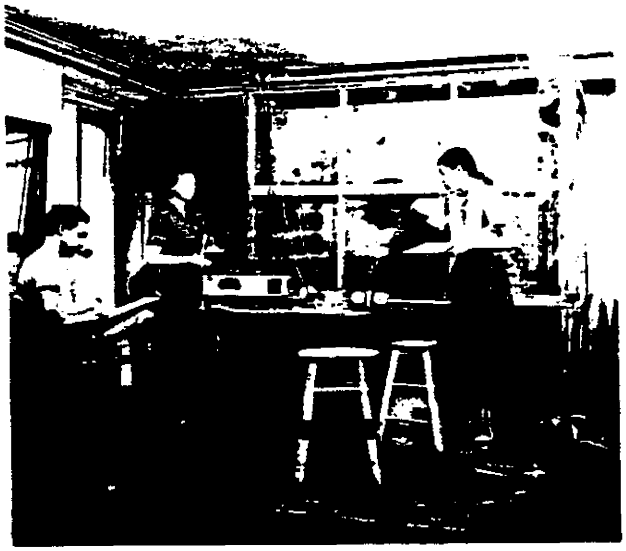

FIG. 5. DOUBLE FARADAY CAGE IN LAB 1, GLEN COVE, MAINE, 1952.

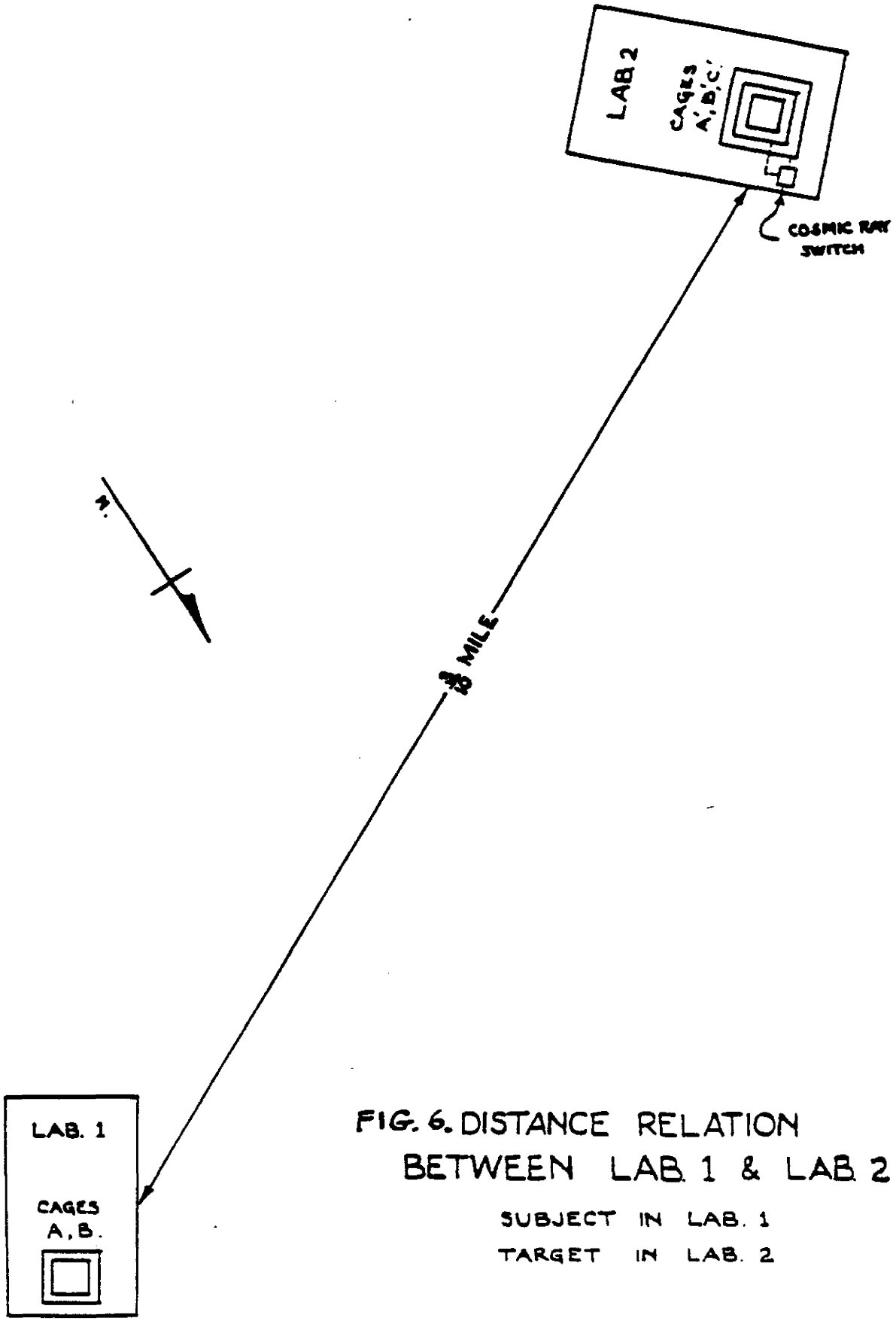

FIG. 6. DISTANCE RELATION BETWEEN LAB 1 & LAB 2

SUBJECT IN LAB. 1

TARGET IN LAB. 2

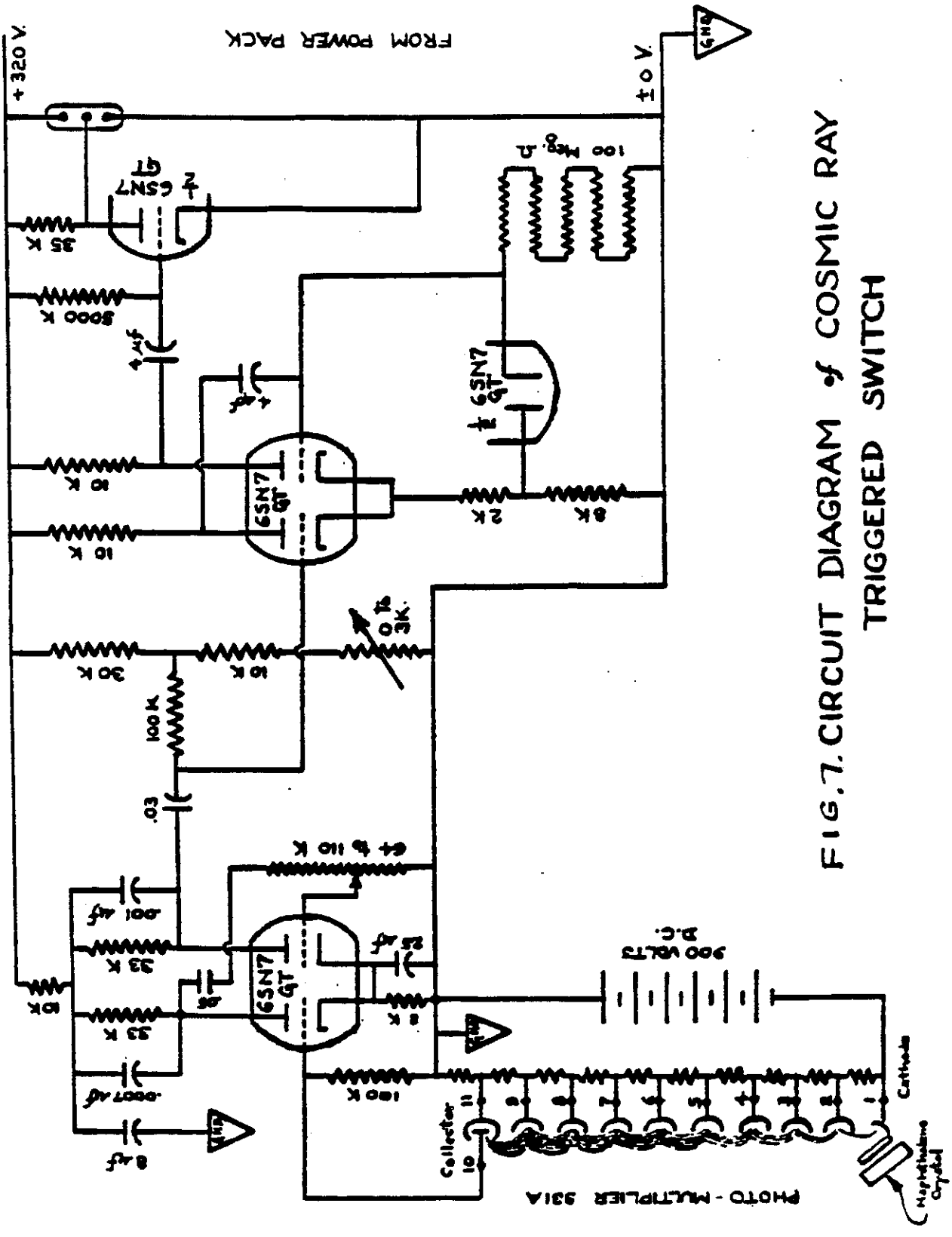

F I G. 7. CIRCUIT DIAGRAM of COSMIC RAY TRIGGERED SWITCH



Fig. 8a. Graph of Target Frequency Distribution. Project IV, Groups 5, 7, 8. Zero time in x-axis represents preceding target.

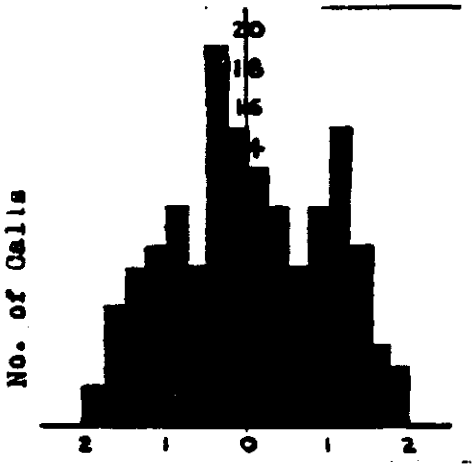

Fig. 8b. Graph showing calls made in relation to above targets within two minutes of a target, and their distribution around target axis 0. This represents 76.5% of the calls made in Group 5, 7, 8 of Project IV.

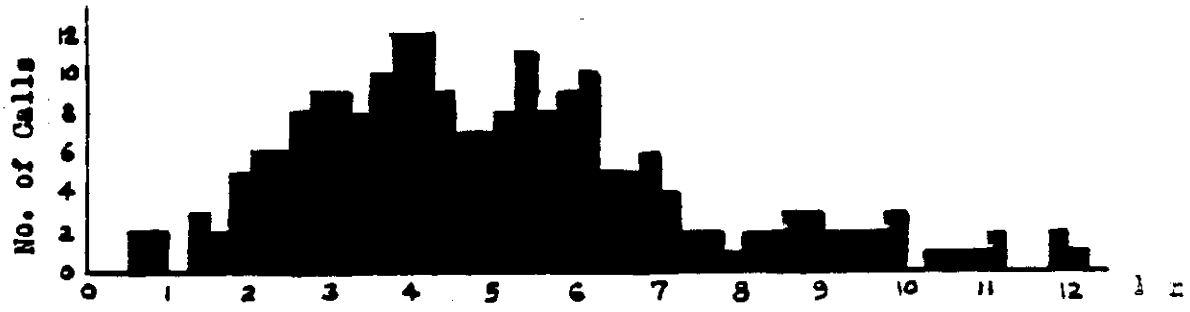

Fig. 8c. Graph of Call Frequency Distribution. Project IV, Groups 5, 7, 8. Zero time in x-axis represents preceding call.

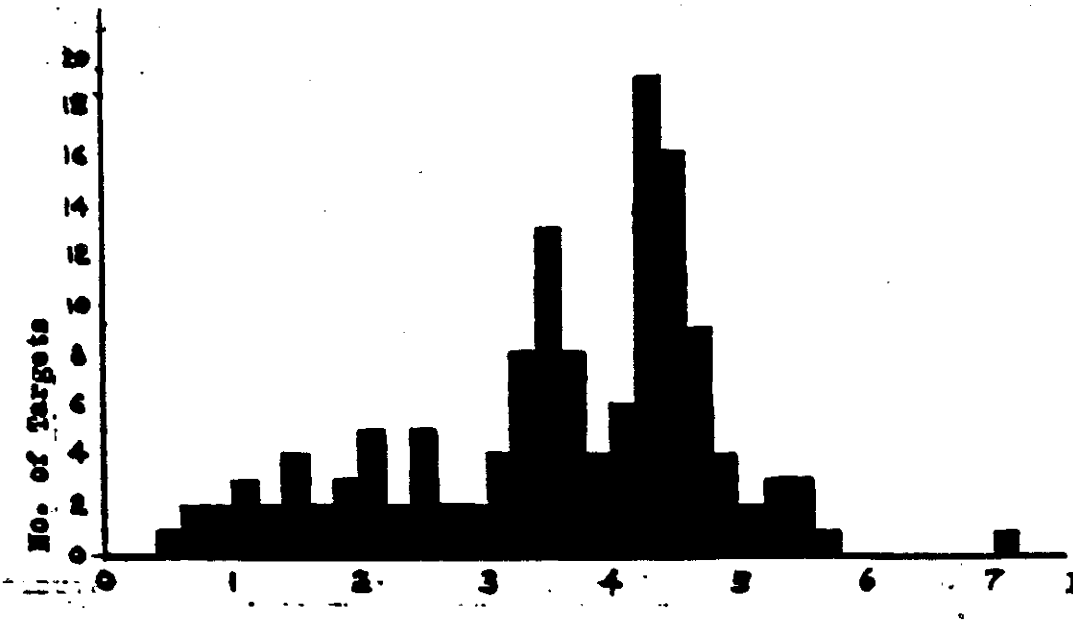

Fig. 9a. Graph of Target Frequency Distribution. Project III. Zero time in x-axis represents preceding target. Targets distributed by frequency according to time interval after preceding target.

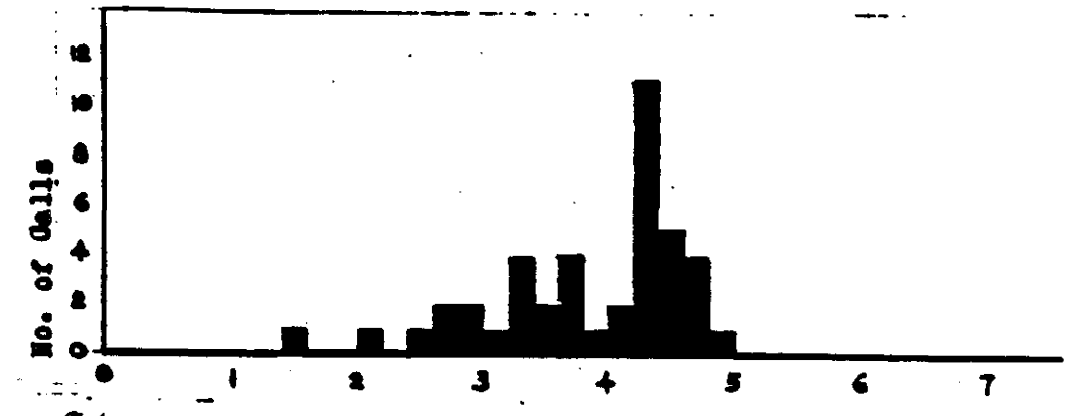

Fig. 9b. Graph of Hit Target Frequency Distribution. Project III. Standard for a hit is a call made within twelve seconds of a target. It can be seen by prima facie inspection that the frequency of hits corresponds to the target frequency distribution.

Exp. No.	43	44	46	47	51	52	54	59	45	49	50	55		
43	.32	.32	.32	.45	.38	.32	.32	.25	.19	.25	.25	.38		
44	.39	.39	.39	.55	.47	.39	.39	.32	.24	.32	.32	.47		
46	.47	.47	.47	.67	.57	.47	.47	.38	.29	.38	.39	.57		
47	.55	.55	.55	.78	.67	.55	.55	.45	.33	.45	.45	.67		
51	.47	.47	.47	.67	.57	.47	.47	.38	.29	.38	.38	.57		
52	.39	.39	.39	.55	.47	.39	.39	.32	.24	.32	.32	.47		
54	.32	.32	.32	.45	.38	.32	.32	.25	.19	.25	.25	.38		
59	.47	.47	.47	.67	.57	.47	.47	.38	.29	.38	.38	.57		
45	.39	.39	.39	.55	.47	.39	.39	.32	.24	.32	.32	.47		
49	.39	.39	.39	.55	.47	.39	.39	.32	.24	.32	.32	.47		
50	.39	.39	.39	.55	.47	.39	.39	.32	.24	.32	.32	.47		
55	.24	.24	.24	.33	.29	.24	.24	.19	.14	.19	.19	.29		
												$\Sigma N_i' = 56.85$		

Fig. 10 Chance Expected hits in each cell.
Group 5, Project I7.

$(N - N_D)\ 12/11\ P_i$ equals chance expected hits in each cell.

$= 57 \times P_i$

As a check: The sum of chance expected hits in each cell should equal 57.

Exp. No.	43	44	46	47	51	52	54	59	45	49	50	55	
43	2.922	.102	2.922	.203	.384	.102	.102	.063	.036	.063	.063	.144	4.084
44	.152	2.592	.152	.203	.221	.372	.152	.102	.578	.462	.102	.221	2.717
46	.221	.285	2.341	.449	.325	.28	.221	.144	.504	.384	.384	.449	3.647
47	.303	.303	.303	1.488	.109	.303	.303	.303	2.787	2.403	.303	.449	7.871
51	.221	.221	.221	.449	.325	.221	.285	.144	.504	2.624	.144	.325	5.359
52	.152	.152	.152	2.103	.285	.152	.372	.102	.578	.462	.462	.221	5.041
54	.462	.462	.102	.203	2.624	.102	.462	.063	.036	.063	.063	2.624	6.804
59	.221	.221	.221	.449	.325	.221	.221	2.624	.504	.144	.144	.325	2.996
45	.152	.152	.152	.303	.221	.152	.152	.152	.578	.102	.102	.221	1.861
49	.152	.152	.152	2.103	.221	.152	.152	.102	.578	.102	.102	.221	4.087
50	.152	.152	.372	.303	.221	.372	.372	.102	.578	.102	2.822	.281	3.007
55	3.698	.578	.058	.109	.084	.058	.578	.036	.020	3.276	.656	2.924	9.551
									Excluding		Σx_1^2 -	Σx_1^2	= 56.025

Fig. 11. Square of Deviation from chance expected, x_1^2
Group 5, Project IV.

Mean Square Deviation is found by adding the x_1^2 values for each cell, excluding those of the leading diagonal, and dividing by the total number of cell minus those in the leading diagonal minus one.

$$= \frac{56.025}{144-12-1} = \frac{56.025}{131}$$

$$= .4277$$

Standard Deviation^2 = Number of Experiments X .4277
= 12 X .4277
= 5.1324

Standard Deviation = Square root of 5.1324

S.D. = 2.26

x = The deviation in the normal distribution in terms of the standard deviation.

= Actual deviation divided by the standard deviation
= 11/2.26
x = 4.87

P value for 4.87 is .000,001, or odds that such a result will occur by chance alone once in a million times.

PAPER 4 CONTENTS

A. Brief synopsis of the Nature of the Universe. 1

B. The Nature of Man. 3
Artificial Stimulation of hearing in the deaf. Researches with healers. Researches in psychometry. Researches of ESP in Faraday Cages. Precognition of Cosmic Ray Pulses coming to earth.

C. The quantum nature of ultimate physical particles - preons, and their guage fields. Clairvoyant vision of quarks and preons in 1895 by Besant & Leadbeater. This work anticipates quarks and preons. Super-string theory. 16

D. What can the theory predict? 27
It predicts the nature and solution of 22 problems of science. It predicts that a device can be built that will duplicate the normalizing effects of healers in disease.

E. A device is built that duplicates some of the healing effects of healers. It is called the TESLAR , and is packaged as a wrist watch. 35

SUMMARY 45

APPENDIX A 48

C. The quantum nature of ultimate physical particles - preons, and their guage fields.

Our discussion of this question begins both with the advent of recent string theory, 1982 (Scwartz and Green); and experiments done in in 1895 by Besant and Leadbeater by peering into the inner structure of matter by clairvoyance. In this late Victorian period of history, man had, since the time of Democritus in Ancient Greece, the idea of an atom. But in 1895 no one on earth knew the nature and constitution of the atom. The electron was unknown, the proton was unknown, the photon had to await Einstein's paper of 1905 to be announced. In spite of the prevailing ignorance of Victorian science, these two brave souls, Annie Besant, and Charles W. Leadbeater, set out to explore the mysteries of the atom through clairvoyance.

Here is what they observed. They peered into a vial of hydrogen gas. In (Fig. 1.6), p.20, Fig.12) , they saw the hydrogen atom whirling around as an ovoid shimmering globule. Somehow they learned to stop the whirling atom, and "stop-framed" it, to observe an inner set of structures, labelled micro psi atom (M.P.A.). The arrangement of the two triangles was not actually seen as drawn in (Fig.1.6.) of Fig. 12, but rather was the impression of the viewers of what they were looking at. The relationship of the two triangles was a puzzle to all, until Stephen Phillips, Ph.D. published his commentary on this 1895 work in "ESP of QUARKS" Theosophical Publishing, Wheaton, ILL. in 1982. In this work he made a meticulous analysis of the work of Besant and Leadbeater, and concluded that they

TABLE 1.

Results - Project III

A. Percentage Tabulation

	Circuit I Group 1	Circuit II Group 2	Circuit III Group 3	Circuit IA (3 cages) Group 4	Project III Totals
NUMBER OF TARGETS	38	30	49	45	162
TOTAL TRIAL CALLS	62	40	59	47	208
less redundant calls	8	9	12	3	32
NET TRIALS	54	31	47	44	176
NUMBER OF RESPONSE HITS	21	30	43	35	129
% OF HITS TO TARGETS	55%	100%	87%	77%	80%
% OF HITS TO NET TRIALS	38%	96%	91%	79%	73%
PRECOGNITION RESPONSES	11	26	34	13	84
% OF HITS AS PRECOGNITIONS	52%	86%	79%	37%	65%

B. 15 Second Standard Contingency Analysis

STANDARD DEVIATION	1.71	1.40	1.89	1.54
EXCESS HITS	-1.00	+6.00	+13.00	+11.00
CRITICAL RATIO (X)	0.58	4.3	6.86	7.1
PROBABILITY	P = CHANCE	P = .0000085	-log Q(X) 9.00586	-log Q(X) 11.89285

	Group 5	Group 6	Group 7	Group 8	Group 9
Subject	Garrett	Marchesi	Garrett	Garrett	Marchesi
Position of Subject. Cage —	Lab. 1 Treated	Lab. 2 Untreat.	Lab.1 Untreat.	Lab. 2 Untreat.	At Home No Cage
Position of Target	Lab. 2	Lab. 2	Lab. 2	Lab. 2	Lab. 2
Length of Experiments	31 min.	31 min.	31 min.	31 min.	20 min.
Number of Targets	59	58	55	66	33
Number of Calls	61	92	51	84	48
N - Nexp.	11	1	-2	6	0
Standard Deviation	2.26	2.20	1.86	2.39	
Critical Ratio - x	4.87	0.46	1.08	2.51	
Significance - P *	.000,001	.64	.28	.01	
Critical Ratio of Difference	4.43 3.17				

* R. A. Fisher, STATISTICAL METHODS FOR RESEARCH WORKERS Hafner, New York, 1950 p. 77, Tables I and II.

TABLE 2. Summary of the Statistical Analyses of the various Groups in Project IV.

FIG. 12.

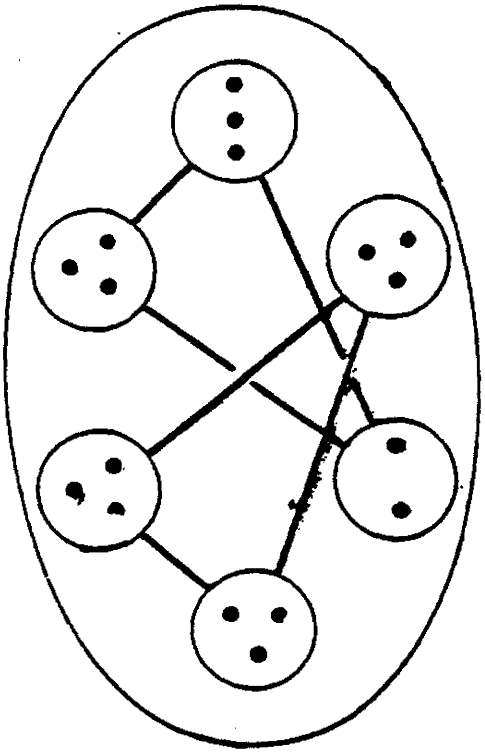

Fig. 1.6. M.P.A. of hydrogen

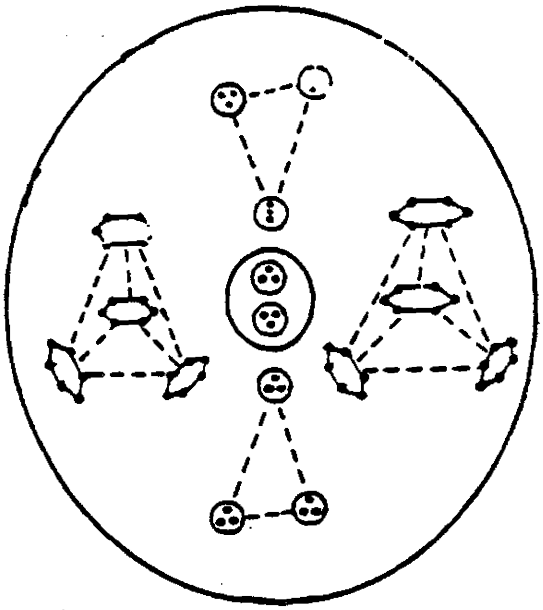

Fig. 1.7. M.P.A. of helium

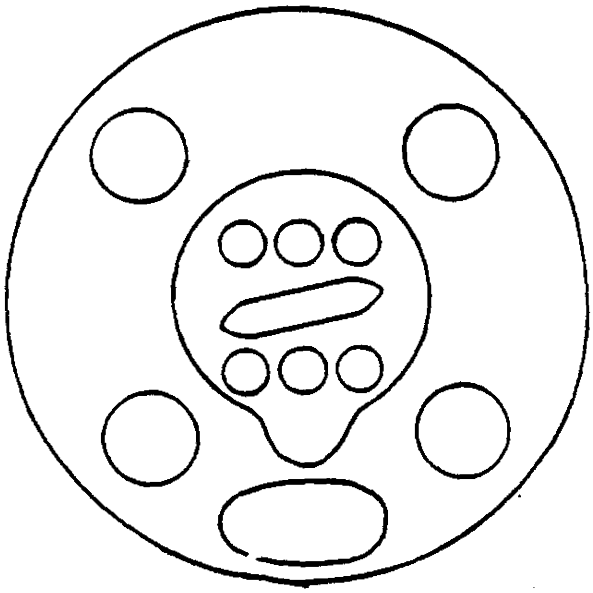

Fig. 1.8. M.P.A. of nitrogen

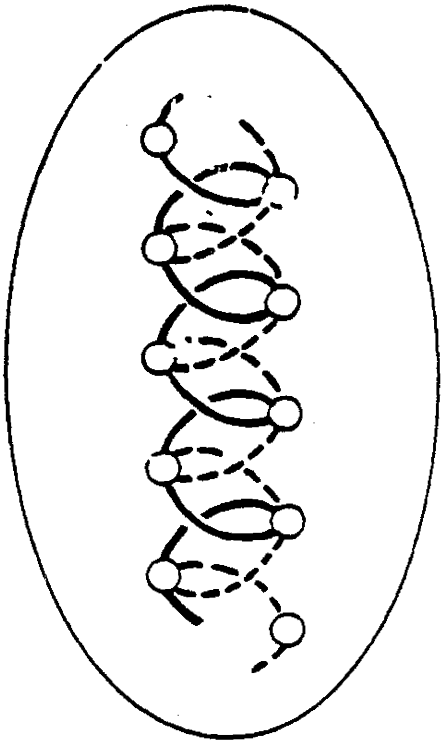

Fig. 1.9. M.P.A. of oxygen

had anticipated in minute detail both quark theory, and string theory. e identified the three circles (Fig.12) inside the bag model of the proton, as being quarks. He identified the three particles inside the quark as the ultimate physical atoms (U.P.A.) which he named OMEGONS, and named PREONS by others.

Phillips interpreted the two triangles as being two hydrogen protons brought together by the act of observation. This accords well with the principle of uncertainty (during observation) of quantum mechanics.

With repeated and great effort they slowed down and held fixed for observation the U.P.A., the preon. In (Fig.1.10), p.23, Fig.23, we see the two forms (chiral) of the U.P.A. which appear as a wave-function. It would be well for the reader to read Phillips' original paper, and its mathematical argument, and proof that Besant and Leadbeater were indeed observing the ultimate physical atom which he identifies with modern super-string theory. Phillips identifies the preons as being the long sought for (35 years) magnetic monopoles predicted to exist by P.A.M. Dirac in 1932.

According to Phillips (and Besant and Leadbeater) the proton of hydrogen contains within each quark, 3 preons, or a total of 9 bound preons per proton, plus one free preon. It is possible to derive a very complex communication system between protons when each has a set of 10 preons. We assume that each preon has a distinct quality (frequency, charge, or spin, etc.). This would form a combination set of 10 comparable to a number set from 1 to 10. In Figs.24 and 25 on pp.25,26 we present a graphic display of such a set. I have used this set for many years as a simple test for extra-sensory perception (ESP) where the test subject arranges the top row of numbers manually to match the lower set. Both rows of numbers are randomized before each test. The total number of possible combinatorial matching sets is 10!, or 3, 628, 800, or 3.6288×10^6. This provides nature with a huge switching and information storage system, based on magnetic monopoles comparable to a magnetic bubble memory system.

Super-string theory states that there are 506 dimensions to the known universe. Of course, it is impossible to do computations with so many dimensions. So theoreticians have reduced the 506

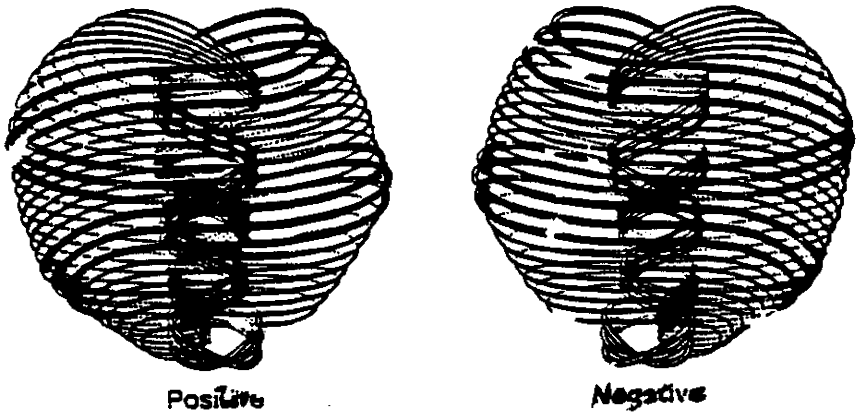

Fig. 1.10. The two chiral forms of the "ultimate physical atom"

FIG. 23.

dimensions to only ten dimensions where four dimensions are AND THE REMAINING 6-D ARE COMPACTIFIED.
Einsteinian 4 dimensions, These ten dimensions are best represented, not by classical "points", but by strings. The original drawing by Besant and Leadbeater in Fig.5.5.16, 5.15a, 5.15b and 5.11 on pp.28-3 , Figs.26-29 show how they observed such "strings" in 1895. In modern theory, one calculates the end of a string as being a quantum of energy connected by a string (gluon) to another quantum of matter-energy. This describes the essence of the modern "super-string" theory.

FIG. 24. MATCHING ABACUS TEST

FUNDAMENTAL PROBABILITY SET OF TEN

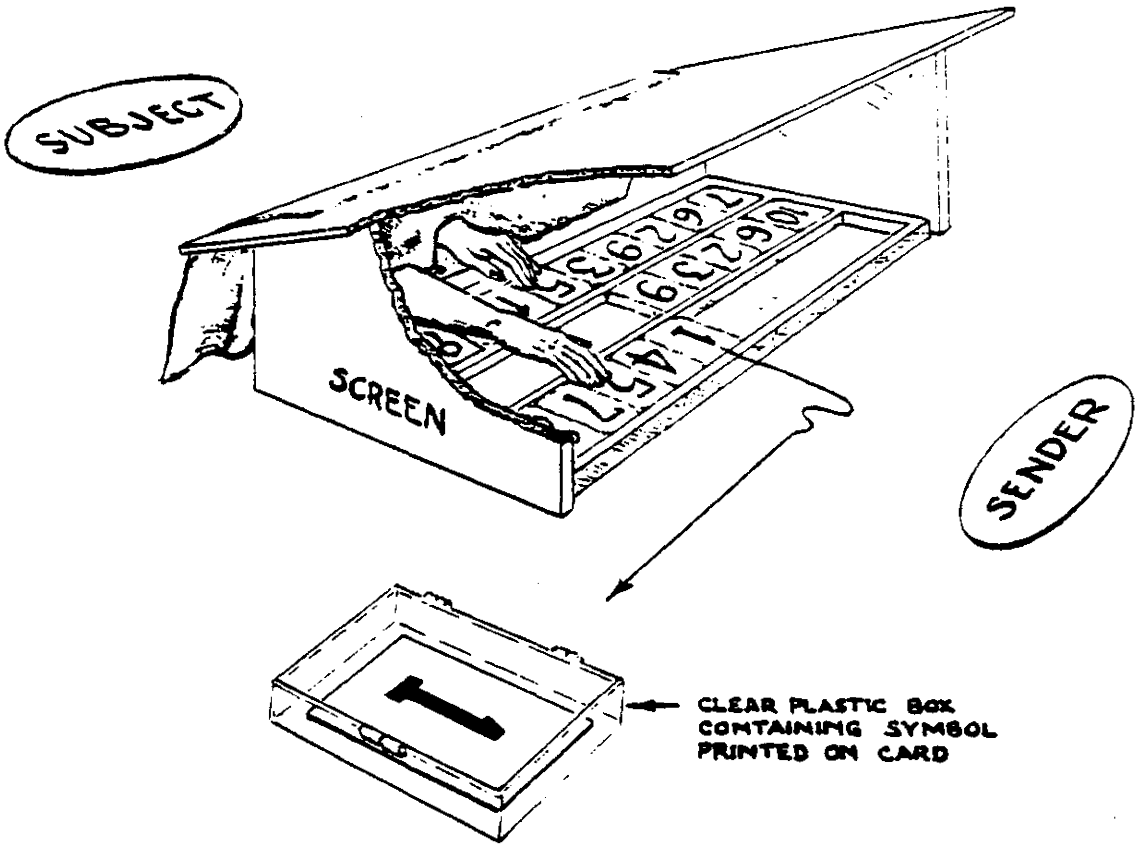

The MATCHING ABACUS TEST consists of 20 identical transparent plastic boxes which contain printed SYMBOLS (numbers, pictures, or playing cards, etc..) The plastic boxes are arranged in 2 Rows; each Row contains an identical set of 10 SYMBOLS. Before each run, each Row of SYMBOLS is randomized.

Sensory clues that might arise due to irregularities in the Plastic Boxes are eliminated by inter-changing SYMBOLS from one box to another before each test run.

The SUBJECT attempts to match up the randomized SYMBOLS without the help of any sensory clues. The illustration above shows the SUBJECT (who is blindfolded) sitting behind a Screen which covers the Matching Abacus Test. Directly opposite the SUBJECT sits the SENDER who visually observes the location of the correct matching SYMBOL or 'TARGET'. The SENDER then concentrates on the correct matching SYMBOL and tries to transmit this information to the SUBJECT telepathically.

FIG. 25, DETAILS of MATCHING ABACUS TEST

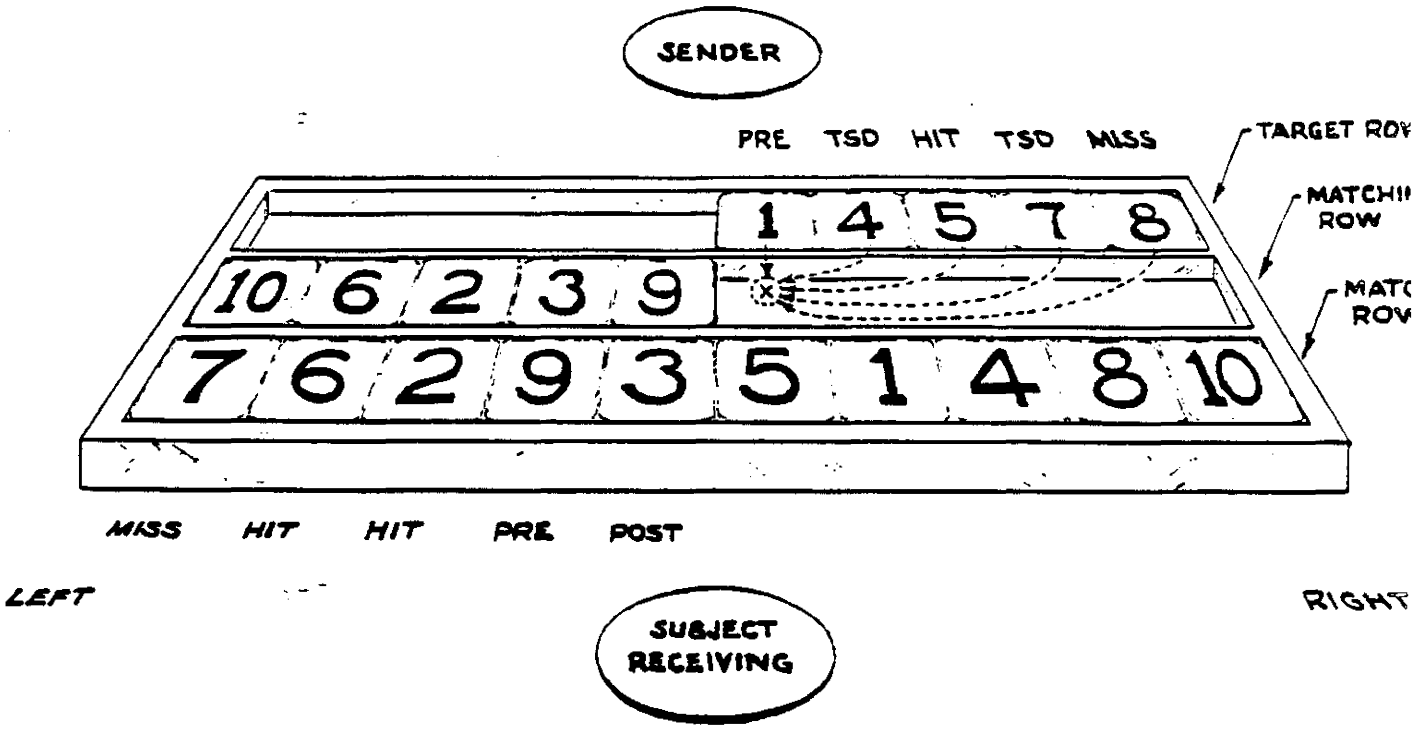

HIT is a Correct Match

MISS is an Incorrect Match

PRE stands for PRE-Positional Displacement

POST stands for POST-Positional Displacement

TSD stands for Target Selection Displacement

The Matching Abacus Test Run illustrated above has been half completed. The Subject began Matching Symbols (numbers) from the left and is working toward the right. Note that the next Symbol to be matched in the MATCH ROW is #5, while the TARGET ROW shows a selection of five possible choices available for movement into position (x) in the MATCHING ROW.

The SENDER visually observes and concentrates on #5 in the TARGET ROW while the SUBJECT (blindfolded by a mask moulded to the face) attempts to receive the location of #5 in the TARGET ROW telepathically. If the SUBJECT selects the Symbol on either side of the correct TARGET in the TARGET ROW, namely #4 or #7, the choice is significant and recorded as a TSD (Target Selection Displacement.) If #1 in the TARGET ROW is moved into position (x) as a match for #5, the choice would be recorded as a PRE (PRE-Positional Displacement) --- and NOT as a MISS. However, if #8 were selected and moved into position (x), the choice would constitute a MISS and be recorded as such.

A. Brief synopsis of the nature of the Universe,
as now known (Feb. 1987)

Physics now knows that nature is "quantal", i.e. all matter is made up of bits and pieces (particles) bound together by fields. See Figure 1, p.2 for a list of particles as now known, and the fields that bind them.

Furthermore, the true language of nature can be written precisely with mathematics. This simple fact has yet to be fully appreciated.

At the moment it is believed that the ultimate particle is the quark. A proton, for example, is made up of three quarks. The quark, however, is made up of a fractal electric and magnetic charge. The three quarks in a proton are each made up of qualities called "flavors" and each quark has 6 such flavors. This multiplicity of "qualities" has led some physicists to theorize that the quark is <u>not</u> a fundamental particle, but state that each quark is made up of <u>three</u> more fundamental particles, called either omegons, or preons. In this paper I shall use the term preons. Later in this paper I will show how preons can be considered to be the universal carrier of information/ACTION transfer, per se.

FIG. 1.

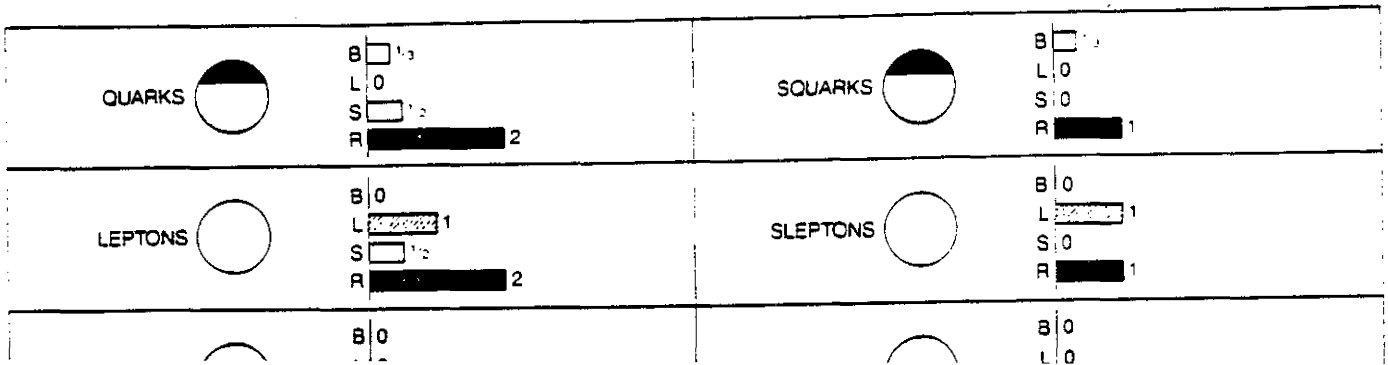

WHAT CAN THE THEORY PREDICT?

The Elf field theory presented is expected to make rational observation possible, and scientifically explain the following effects. In the left hand column we list the phenomenon that needs explanation; and in the right hand column we present a hypothesis of scientific explanation predicted by the theory, i.e. a plasmon microstructure made up of magnetic bubbles, and magnetic monopoles organized according to the fractal geometry of Mandelbrot.

Phenomenon	Scientific Hypothesis
1. Origin of biochemical life with build-up of biochemistry to DNA molecules.	1. Self-organizing 8 Hz magnetic soliton with Kervran transmutation. Note: Earth's magnetic field is 7.8 Hz. This pulsation plus heat energy produces life forms at thermal vents.
2. Control of go, no-go functions of DNA including go, no-go signals for cancer.	2. Each genetic segment of DNA has a specific ELF go, no-go frequency control operating in the form of magnetic bubbles.
3. Muscular chemistry - propulsion and motor action.	3. Circularly polarized molecules contracted and relaxed by respectively, plasmon microbubble build up and collapse.
4. Sensory detection.	4. Phototonic-electronic plasmon microbubble events as in 3.
5. Coordination of information leading to intelligence.	5. Bell interconnectness principle of a non-local nature similar to 6.

FIG.26.

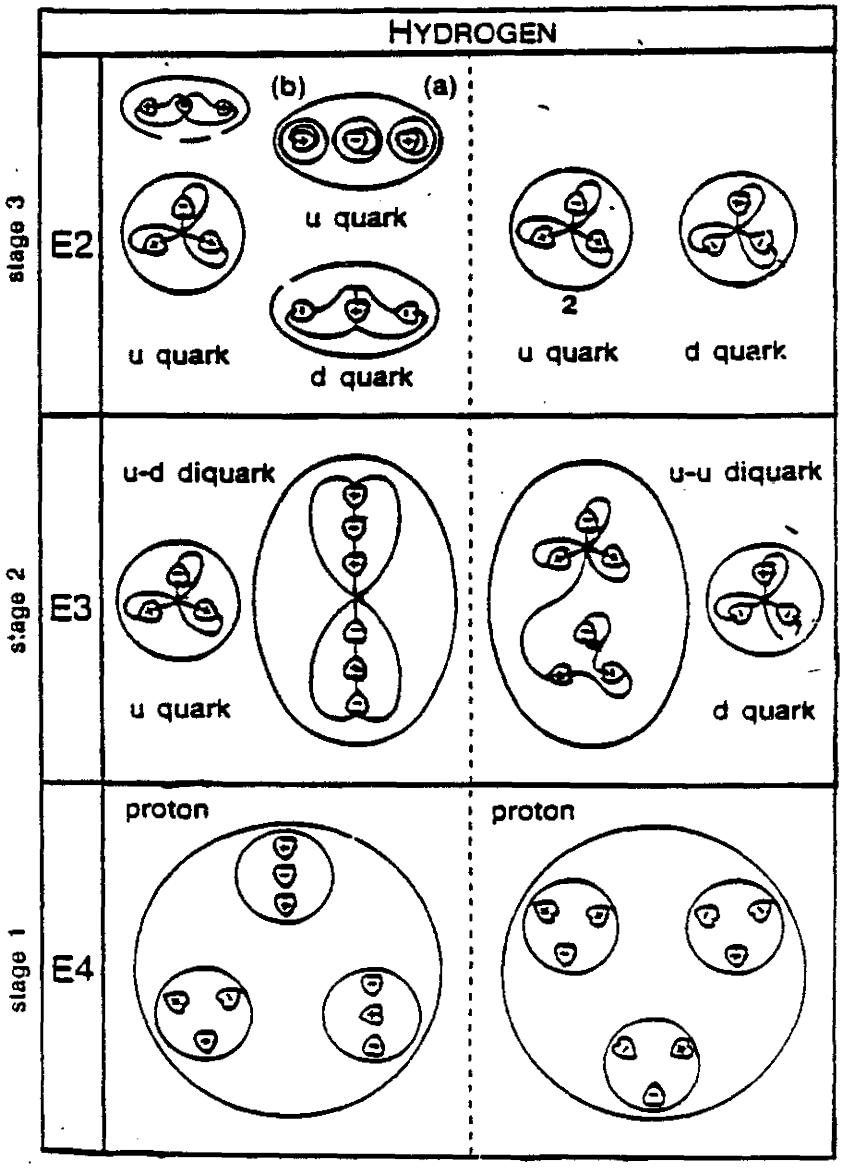

Fig. 5.16. Disintegration of the hydrogen M.P.A.

FIG. 27

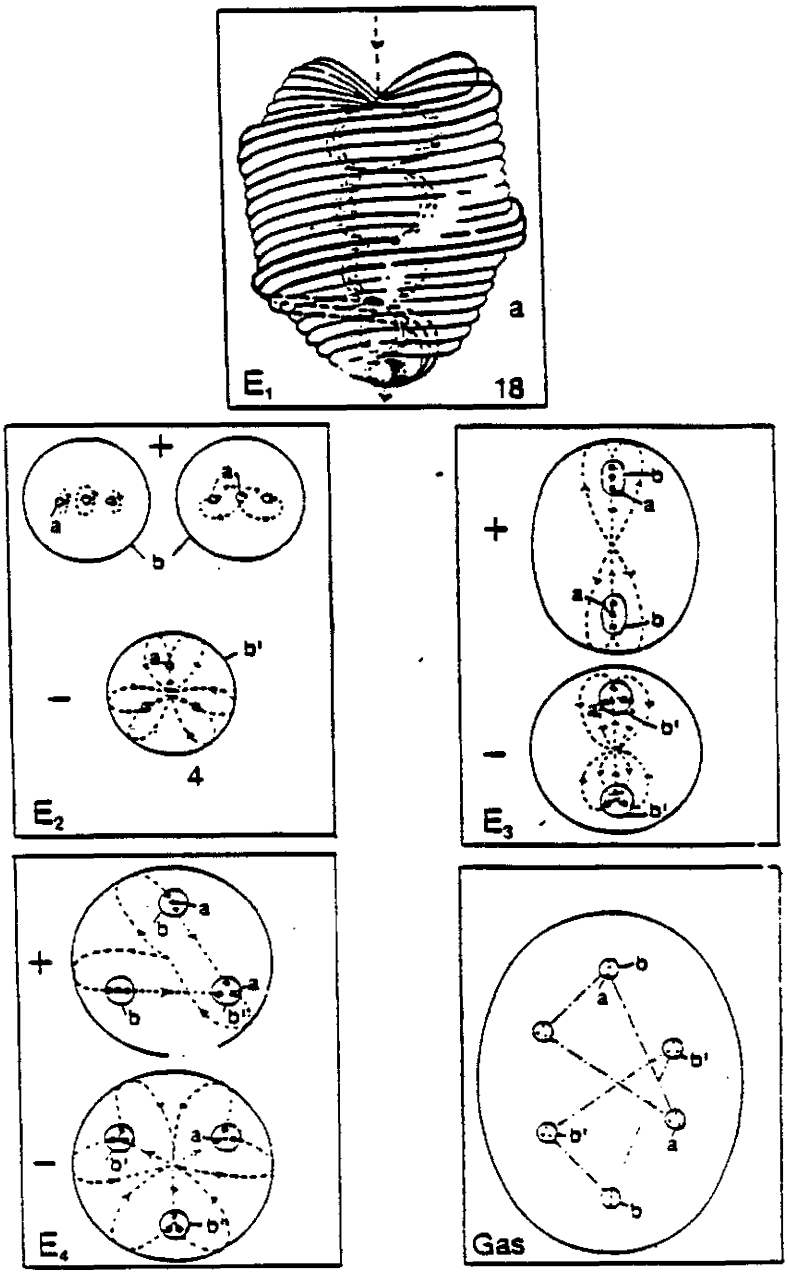

Fig. 5.15a. Micro-psi observation (1895) of hydrogen

FIG. 28.

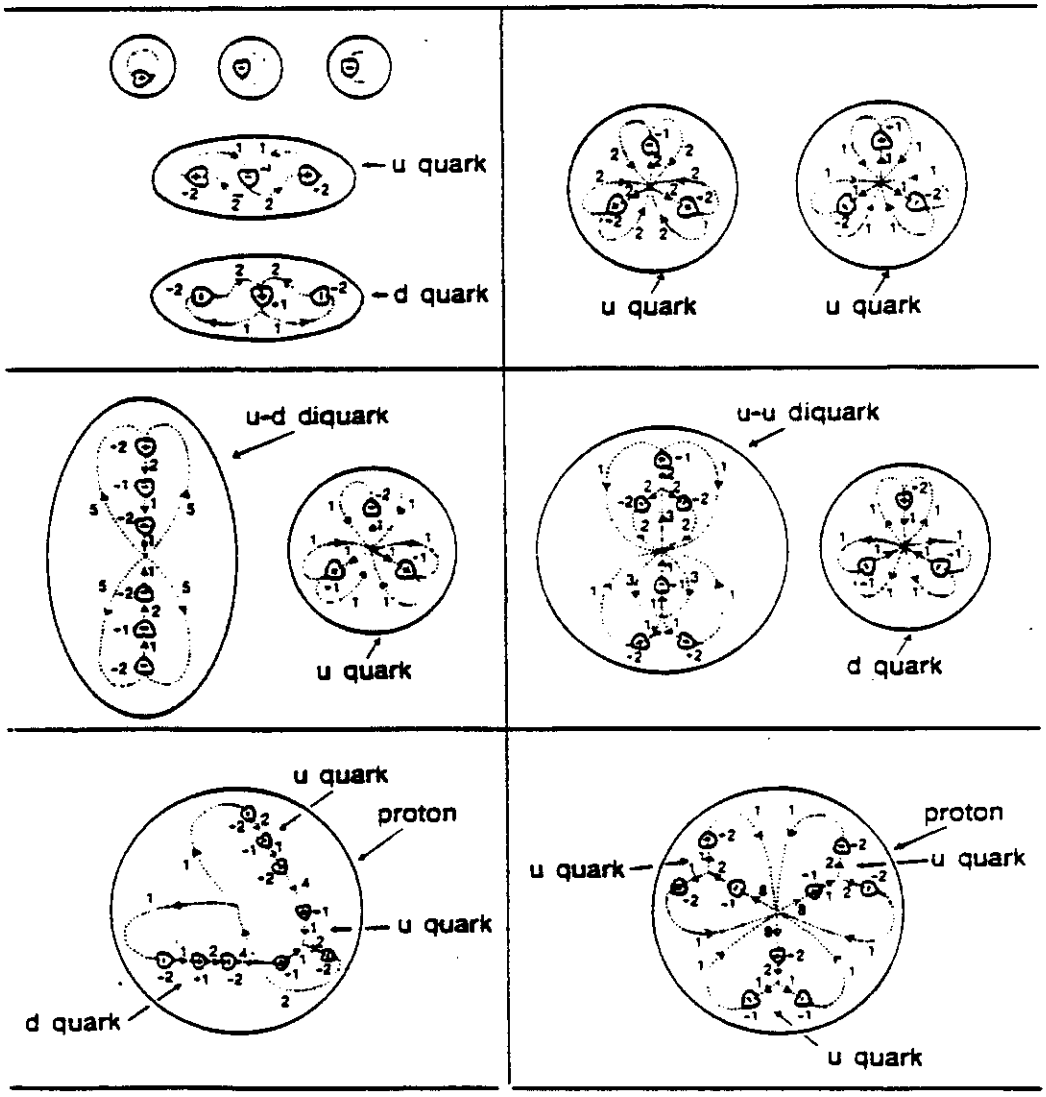

Fig. 5.15b. Configuration of gluon flux lines inside proton

FIG. 29.

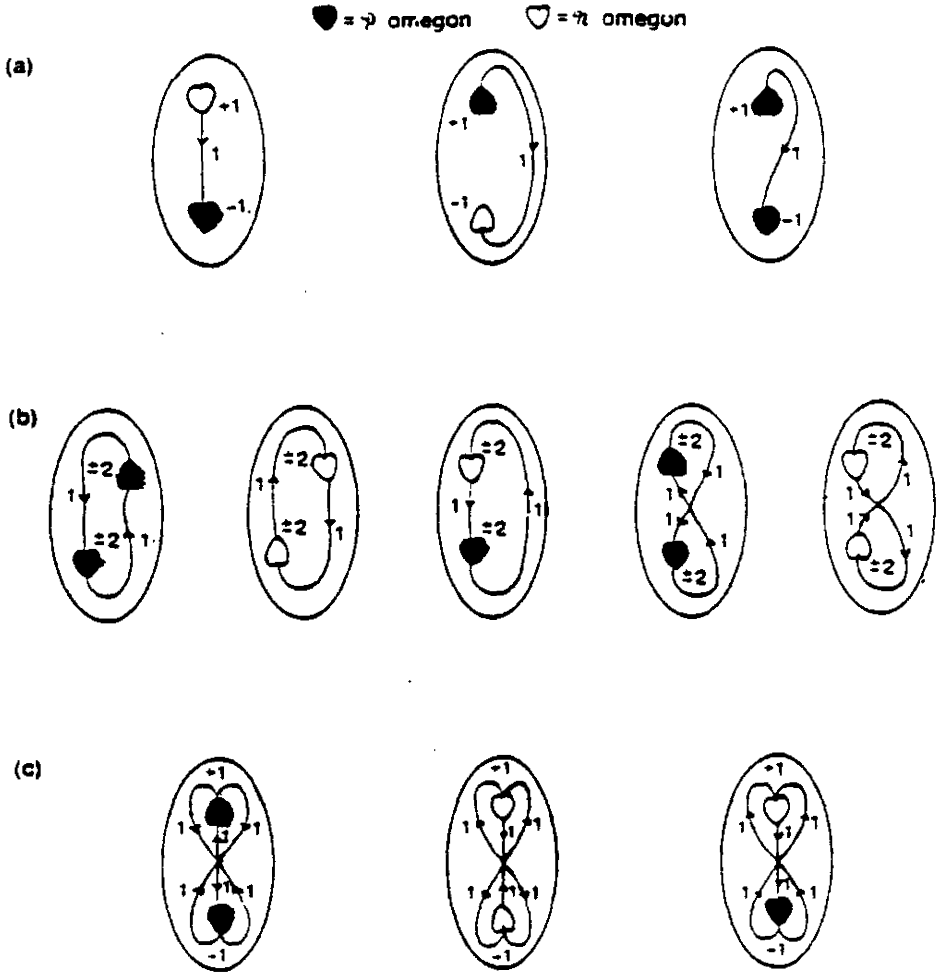

Fig. 5.10. Observed pairs of U.P.A.'s bound by 1, 2, or 3 strings

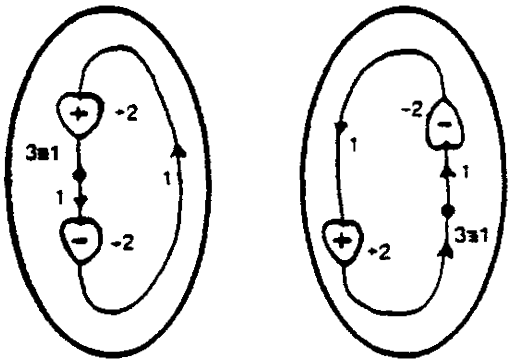

Fig. 5.11

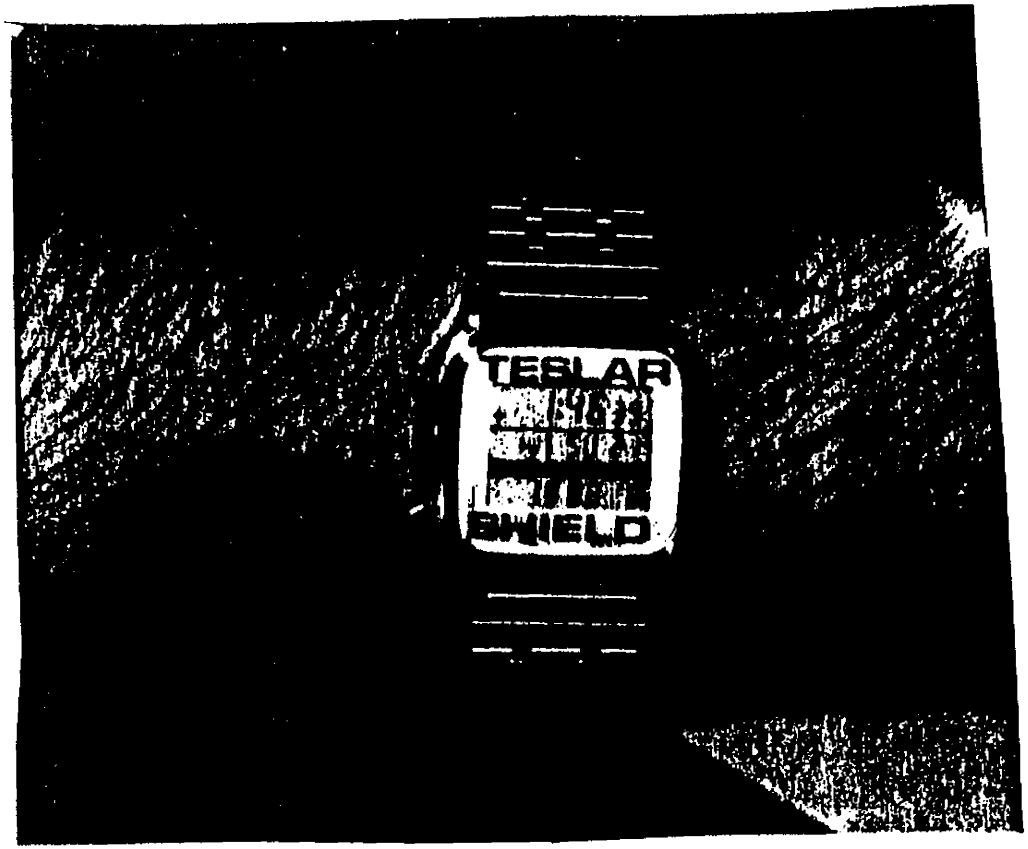
TESLAR
SHIELD

6) Telepathy. The better a telepathist is shielded by a Faraday Cage, the higher the scores.	6. ELF fields at 8 Hz will pass through a Faraday Cage as will quark, neutrino and monopole fields. Non-local fields. Transmission of information through a tubular plasmon world line.
7) Psycho-kinesis.	7. Quark domain polarization in n-dimensional axes.
8) Mobile center of consciousness. (Mind out of body experience.) Can be induced by 8 Hz light pulses to eyes.	8. Self-organizing macrosolitons of body, can decouple from fundamental particles.
9) Teleportation of a person, or an object.	9. Hyperdimensional orthorotation of quark polarities.
10) Precognition and clairvoyance.	10. Hyperdimensional orthorotation of quarks, to yield advance waves.
11) Aura as viewed in medical diagnosis.	11. Magnetic bubbles as a quantum plasmon where optical coupling occurs, and governing equation [6] is: $E = hf_p / \sqrt{2\varepsilon_o + 1}$
12) Healing by laying on of hands.	12. ELF: DNA resonance which is frequency specific (8 Hz).
13) Rooting effect - where a trained person cannot be picked up by another person.	13. Increase in gravitational constant by an act of will in positive polarization of quarks.
14) Levitation of a person.	14. Decrease in gravitational constant by negative polarization of quarks, and preons
15) a. Dematerialization, and b. the converse effect.	15. a. Orthorotation of quarks into hyperspace and b. reverse orthorotation into 4D normospace.
16) Fire walking.	16. ELF micro-magnetic bubbles organized into a soliton-plasmon on surfaces of skin and on coals, where the

governing equation is [7]:
$f = f_p \sqrt{Ka/(2Ka+1)}$

This is a dispersion relation

17. Metal-bending, and metal-fracture.	17. Warping of electronic/proton domain plasmon polarization.
18. Hypnosis, trance.	18. ELF soliton-plasmon hyper-polarization at synapses.
19. Phantasmagoria, monsters, tulpas, and ectoplasm.	19. Dispersion of normal self-organizing ELF bubble soliton plasmon.
20. Geopathic zones which induce cancer.	20. Due to beat-frequency difference between two underground water streams, each one of which is off of 8 Hz resonance. Ex. 7 Hz + 10 Hz = 3 Hz.
21. Paranormal photos.	21. High resolution of domain formation of plasmons - guided by telepathy.
22. Memory in living; and non-living objects. PSYCHOTRONIC SYSTEMS.	22. Stationary field magnetic bubbles at resonance, and polarization of quarks and preons.

A new concept is presented which integrates all biological effects under one general theory. The theory is testable for each of the mysterious phenomena of life. It is expected that within two years of field, clinical, and laboratory research, enough data will be accumulated, and the theory tested, to lay the foundations for a revolution in the scientific understanding of the living process, including healing.

The first test of the theory is to design, build, and test a device to mimic the effects of a healer's 8.00 Hz magnetic field radiation. Such a device should be capable of performing some primitive form of healing. This is the subject of the following section.

This 3 year old theory of Schwartz and Green is the most profound theory of nature developed by man, and is causing intense interest and excitement in the world of physics. It has been dubbed "The Theory of Everything". In this theory, troublesomes "infinities" vanish in the equations, anomalies do not exist, and it is believed that the four fundamental forces of nature can be unified.

We can now present the essence of our theory of protocommunication.

Preons (10 in number) are the ultimate physical particles that carry information using a basic alphabet of distinct units. This alphabet is expressed as magnetic fields with a frequency range from 10^{-3} Hz to 10^{3} Hz. The preons plus the gluons generate the ELF magnetic field through string vibrations.

In order to send precise signals to protons in DNA, the ELF magnetic fields must be tuned accurately to 10^{-2} to 10^{-3} parts of a cycle per second. One frequency, and one frequency only, keeps the DNA perfectly tuned for health, and that is 8.00 Hz. Protons are the senders and receivers of information in biological systems as bound in water and DNA. Protons are changed through preon information and action to carry out the Kervran weak transmutation of atoms.

. Development of a device to mimic the effects of a healer's 8.00 Hz magnetic field radiation. Such a device was developed, and it is called the <u>TESLAR.</u>

We will try to briefly summarize the results of eight years of research. The initial goal was to develop a device that would

protect an individual human being from the effects of ELF magnetic fields that were dangerous to health.

The first advance came when an iron bracelet was wrapped with Fe_2O_3 (iron oxide) impregnated mylar tape. The wrapping was such that with each 360° turn of the tape around the bracelet circle, the flat audio tape was rotated 180° to form a Mobius loop with each turn. It was found that such a bracelet worn on the wrist neutralized ambient ELF fields in the range 1 to 38 Hz, and protected the wearer from the harmful effects of certain ELF fields.

The next step was to try to drive such an audio tape, Fe_2O_3, Mobius coil with an E field in order to find out if this field would produce a B field in the Fe_2O_3 tape. I first used a cheap quartz clock made by NELSONICS, Inc. as a source of an E field. The E field of this clock was 2.0 Hz.

When the clock was brought in contact with the mobius loop tape, and the output from the tape measured with an ultrasensitive B field detector - it was found that a 2.00 Hz weak B field was present coming from the tape. When the clock was mounted on a bracelet and placed on the wrist of a person - the B field was amplified by a factor of 3-4 x. This device was quite large and clumsy to wear, and therefore had to be miniaturized.

First a Mobius coil audio tape, Fe_2O_3, was miniaturized until it could be fitted outside of a quartz electronic wrist watch. Then a long search was initiated to find a quartz watch whose oscillator RC network output produced E pulses at 8.00 Hz. The search was successful when I found the Lorus GN003, quartz electronic clock with a basic beat of 8.00 Hz. Furthermore, this clock had a 10 year lithium battery with a 3.0 D.C. volt output. Such power was necessary

A. Brief synopsis of the nature of the Universe,
as now known (Feb. 1987)

Physics now knows that nature is "quantal", i.e. all matter is made up of bits and pieces (particles) bound together by fields. See Figure 1, p.2 for a list of particles as now known, and the fields that bind them.

Furthermore, the true language of nature can be written precisely with mathematics. This simple fact has yet to be fully appreciated.

At the moment it is believed that the ultimate particle is the quark. A proton, for example, is made up of three quarks. The quark, however, is made up of a fractal electric and magnetic charge. The three quarks in a proton are each made up of qualities called "flavors" and each quark has 6 such flavors. This multiplicity of "qualities" has led some physicists to theorize that the quark is <u>not</u> a fundamental particle, but state that each quark is made up of <u>three</u> more fundamental particles, called either omegons, or preons. In this paper I shall use the term preons. Later in this paper I will show how preons can be considered to be the universal carrier of information/ACTION transfer, per se.

t drive the iron oxyde, Fe_2O_3 with sufficient voltage pulses to p oduce an ELF B pulse of at least 10 nanotesla. Then began a two year period of human experimentation to see if:

1) The Teslar protected a person against harmful ELF fields.

2) The Teslar promoted health, and corrected pathological states.

The last technical problem was to perfect the Mobius loop chip so that, 1) it would be thin enough to go inside of a watch case; a d 2) have it tuned to produce an 8.00 Hz B field. This problem was s lved with the help of Larry Kruser, an expert in magnetic materials.

Referring to Fig.5, Fig.30, p.38 we see an illustration of ie Meissner effect. (a) The normal state, at top shows the lines of magnetic (B) flux going through a magnetic material. In the s perconducting state the magnetic flux is expelled from the inside of magnetic material. (b) We made use of our knowledge of how ELF magnetic fields pass through all known materials without attenuation, distortion; and a knowledge of the Hall effect where a voltage applied in the plane of a magnetic material will cause a current to low. We coiled thin aluminium foil with magnetic material on each ide, and polarized the magnetic material on each side in a magnetic field so as to simulate the Mobius loop. By applying a D.C. bias on he side of this "magnetic chip", and then pulsing the chip with the RC network across the crystal of the watch we are able to produce a precision 8.00 Hz B field which radiated out from the chip as shown in ig. 5.2(b) and Fig.31 (4) p.41. The measured B field radiates from the human body in the form shown in the figure 31, "How the Teslar orks". The parameters of the Teslar are given in Fig.31, p.41.

FIG. 30.

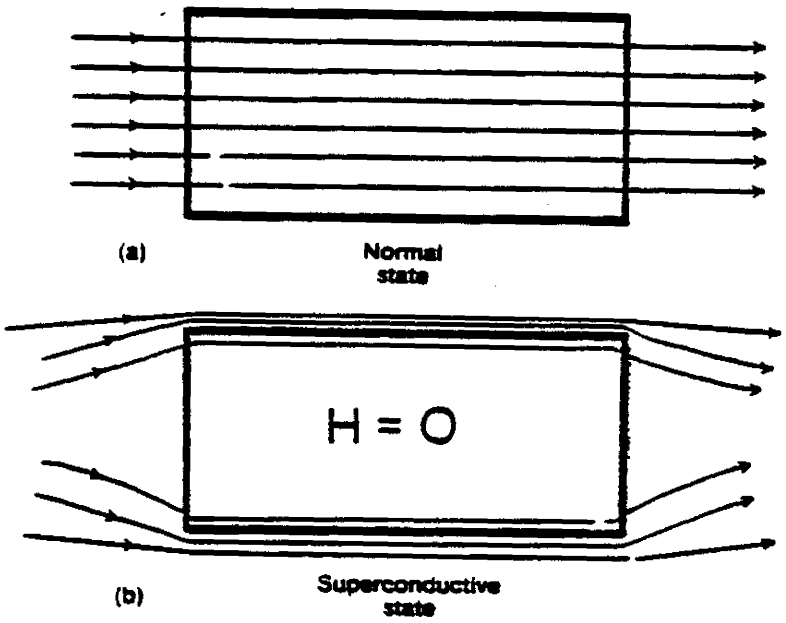

Fig. 5.1

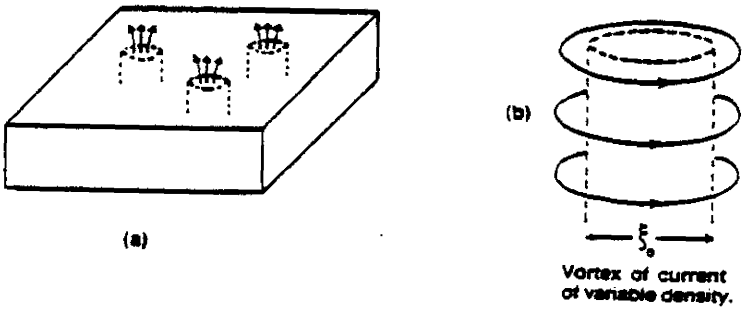

Fig. 5.2

100 subjects wore the TESLAR, on their left wrist for a year to test its efficacy as an ANTI-ELF shield. It was found to be efficacious in extensive laboratory measurements. A safety and hazard program was run concurrently, and no contra-indications for human use were found. See Table 3, p.42. We also ran into a series of beneficial health effects.

We then planned to market the TESLAR primarily as a personal shield to protect an individual from harmful ELF fields. Since in the U.S.A, one does not need FDA (Federal Drug Administration) approval for such a device, we went ahead with the sale of Teslars. Fig.32 shows the current form of the TESLAR. Table 4 gives the E field, and B field parameters of the Teslar both when worn on a human, and during bench tests.

HOW THE TESLAR WORKS

FIG. 31.

CRYSTAL IS PULSED AT 8 HERTZ BY A BATTERY AND RC NETWORK

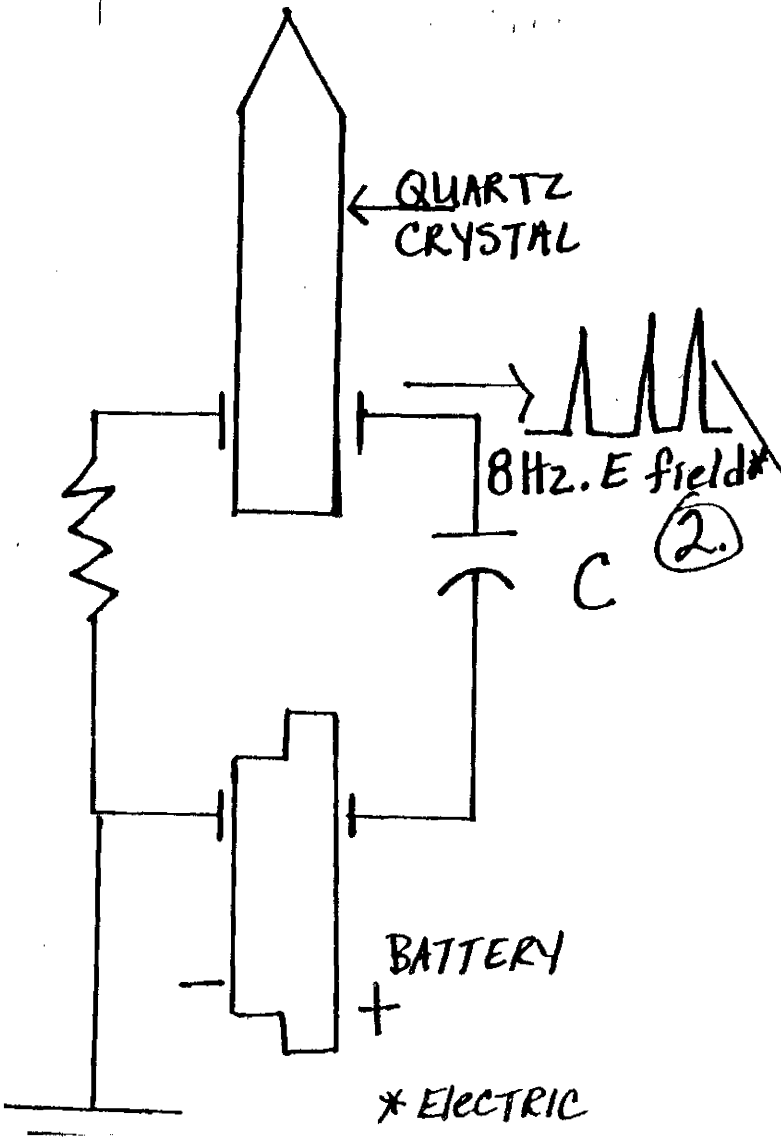

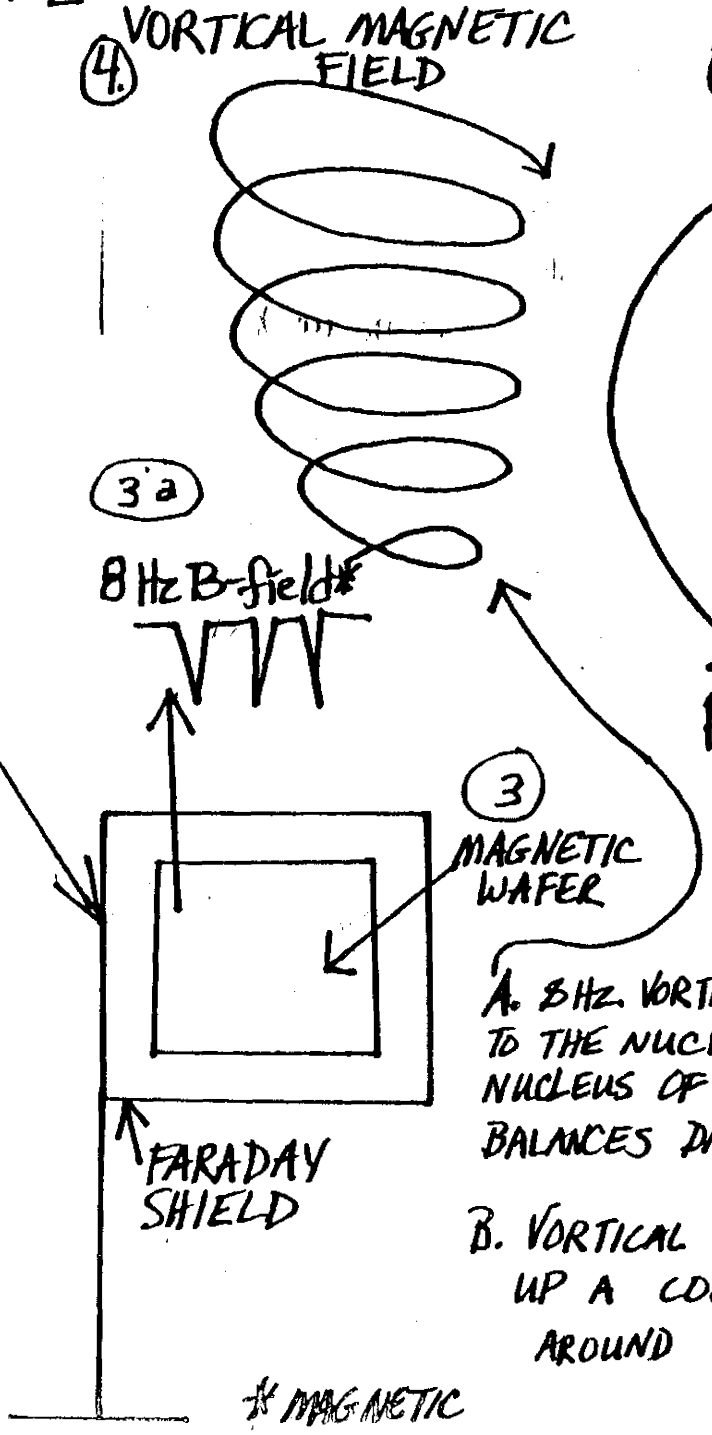

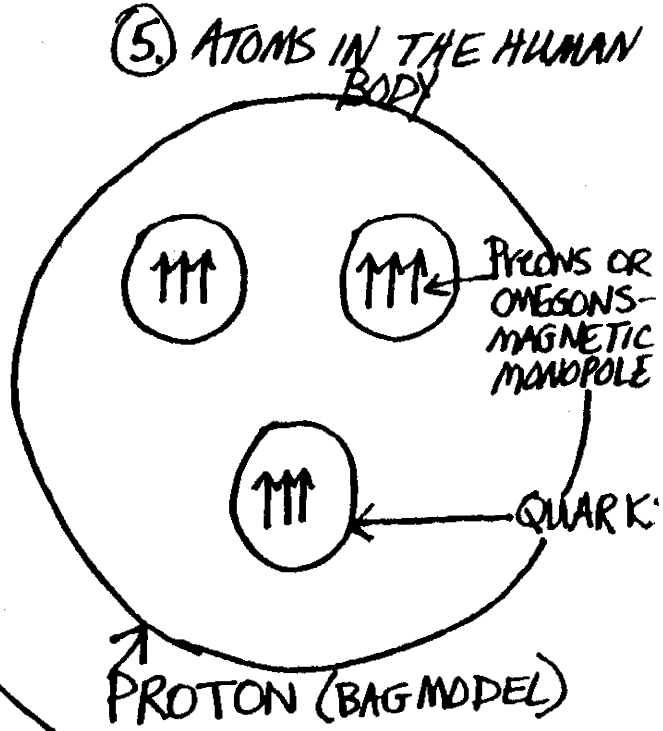

A. 8 Hz. VORTICAL MAGNETIC Field Penetrates TO THE NUCLEUS OF EVERY ATOM IN THE NUCLEUS OF EVERY CELL WHERE IT BALANCES DNA FUNCTIONS.

B. VORTICAL MAGNETIC FIELD BUILDS UP A COCOON-LIKE SHIELD AROUND THE HUMAN BODY.



FIG. 32

TABLE 3. SAFETY AND HAZARD DATA ON HUMAN SUBJECTS

(1) Measured photonic radiation in body with Teslar on:
Range: 50 MHz to 10 GHz
Results: 100% inc. in coherence of photonic radiation
s/n: up 80%

(2) Measured electronic radiation from brain - EEG, 1-40 Hz:
Results: 50% inc. in coherence of electronic radiation.
Entrainement occurs at 8.00 Hz.

(3) Measured Protonic Radiation.
Radionics: 100% inc. in energy level of a human.

(4) Measured E (Electric) field of body with Skilling Detector:
Watch and Body entrained @ 8.00 Hz E.

(5) Measured B (Magnetic) field of body with Beck Detector:
Watch and Body entrained @ 8.00 Hz B.

(6) Healers measured from all over planet earth:
All healers radiate 8.00 Hz B field and entrain the magnetic field of body of a patient @ 8.00 Hz.

(7) Kinesiology is a poor and unscientific method of measuring photonic, electronic, protonic, E and B Scalar fields, because it can easily be proven that the Testor can bias the

utcome

muscle strength measurements. We do not use this test.

) All above results were presented at the following meetings:
Psychophysics Conference at University of Oxford, Oxford England, Sept 1, 1985. Meeting presided over by Nobel Laureate, Brian Josephson.
International Association of Psychotronic Research, in Zagreb Yugoslavia, November 12-16, 1986. Teslar data and Theory approved by distinguished panel of physicists from 10 countries. Published in the proceedings as an abstract.

9) Over five thousand Teslars have been sold. Hundreds of Teslar wearers have reported dramatic rehabilitation of chronic diseases. This is the best testimony for the efficacy and safety of the Teslar.

TABLE 4.

LAB REPORT ON (LORUS GN003) TESLAR DIGITAL WATCH

	TEST I SKILLING E- FIELD DETECTOR		TEST II BECK B-FIELD DETECTOR	
	B. BENCH.	A. WRIST.	A. ON WRIST.	B. BENCH TEST
FREQUENCY:	8.00 Hz	8.00Hz	8.00 Hz	8.00 Hz
WAVE FORM:	sine wave	sine wave	impulse wave	sine wave
WRIST LOADING:	gain= 0	gain= 0	gain= x4	gain= 0
MAGNETIC FIELD:	not detectable	N.D.	9-10 nanotesla	N.D.

The above data denotes criteria, as shown in column Test II A , for efficacy of the Teslar and safety of the Teslar.

Andrija Puharich. M.D.. LLD.
Director of Research
E.C.C.O.

IN SUMMARY

We have sold over 5000 Teslars to date. In the course of people wearing the Teslars, reports started to report beneficial health effects. We began to check such reports and found that they were true. To date we have verified that the Teslar has a therapeutic effect on the following medical conditions:

a. accelerates bone fracture healing in elderly patients.
b. alleviates symptoms of pre-menstrual syndrome.
c. relieves menopausal symptoms.
d. eliminates jet-lag symptoms.
e. alleviates chronic rheumatic bone pain.
f. eliminates severe migraine headaches due to stress.
g. calms hyperactive children.
h. relieves symptoms of certain kinds of allergies.
i. has a dramatic effect on lowering essential hypertension both systolic and diastolic readings.
j. lowers the abortion rate of pregnant women who operate video display terminal of computers.
k. there is no hazard connected with the Teslar.

Now all of these reports were spontaneous and unsolicited both from the patients, and their doctors. We have made no medical claims for the Teslar. We shall have to make a decision as to whether we want to exploit these medical effects of the Teslar, and file an "investigatory new drug application" with the U.S.A. FDA. We have several M.D. doctors who are following these many medical effects of

the Teslar in order to compile a data base.

We can now review the essential data about the Teslar.

The Teslar has been shown to mimic some of the effects shown by natural healers on human pathology. In my opinion one of the most surprising effects of the Teslar is on the elimination of the symptoms of jet-lag. This gives us a profound insight into what happens inside the protons of the human body when one travels across the magnetic lines of force of the earth at high sonic, or supersonic speeds. It is obvious that the preons go from an ordered homeostatic state to a disordered state. I believe that we are now getting in a position to understand how a human being can be helped to maintain a normal healthy state; and how pathological states can be rectified. We may be on the threshold of a new, true science of medicine.

FIG. 1.

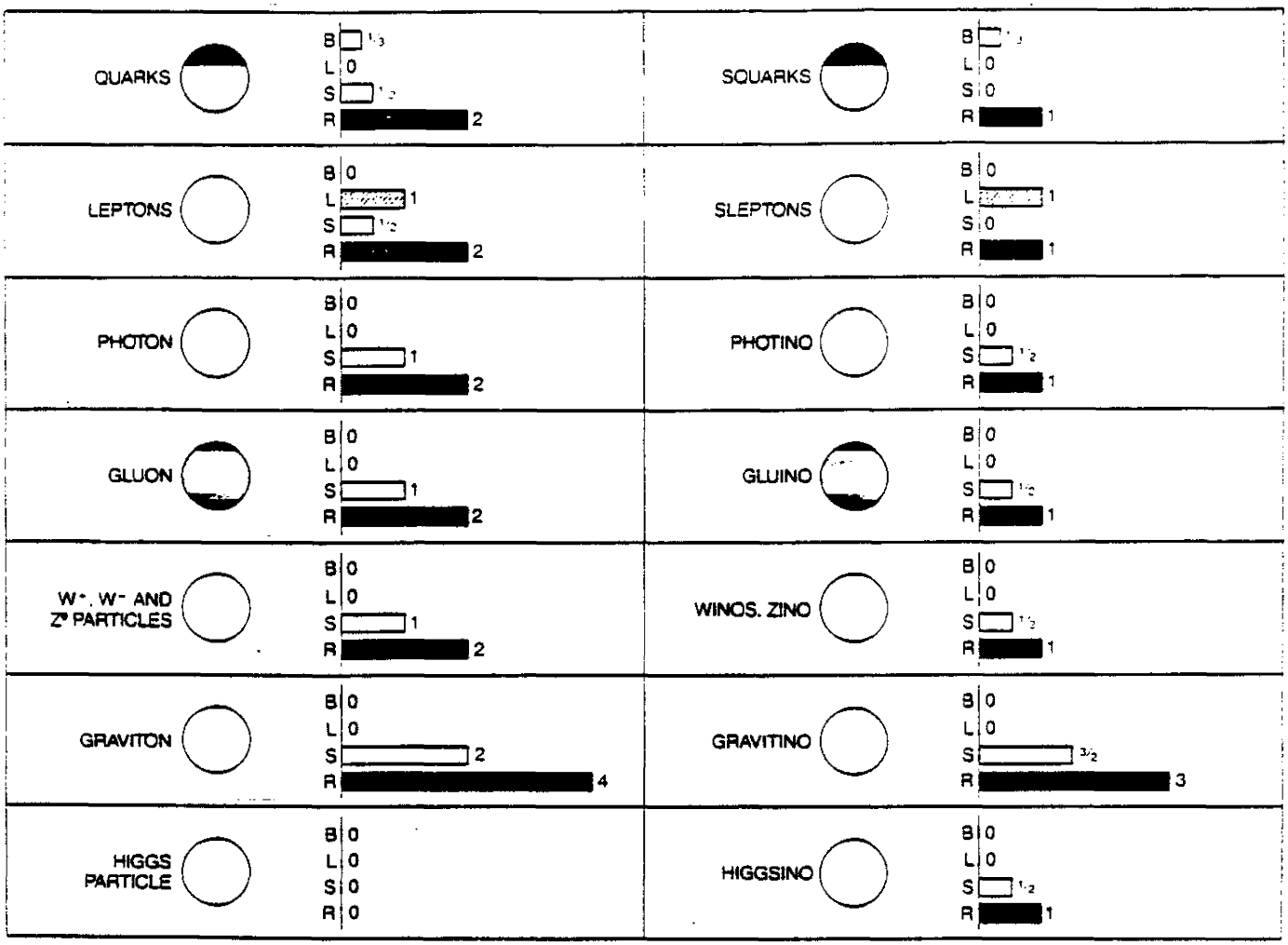

FUNDAMENTAL PARTICLES can be categorized by such quantities as baryon number (B), lepton number (L), spin (S) and R number (R). (The R number is given by the formula $R = 3B + L + 2S$.) Lepton number, baryon number and spin vary among the different particle types, but the R number is even for all ordinary particles (*left side of chart*) and odd for all predicted superpartners (*right side*). The pattern has important consequences. Specifically, one property of most supersymmetric theories is that the R number cannot change from even to odd (or from odd to even) during reactions among particles. If, for instance, protons are collided, supersymmetric particles must be produced in pairs or the R number would change from even to odd. Assuming that a supersymmetric particle is indeed produced, its decay products must contain an odd number of supersymmetric particles. As a consequence the least massive of all the supersymmetric particles must be stable, since there are no lighter supersymmetric particles into which it can decay.

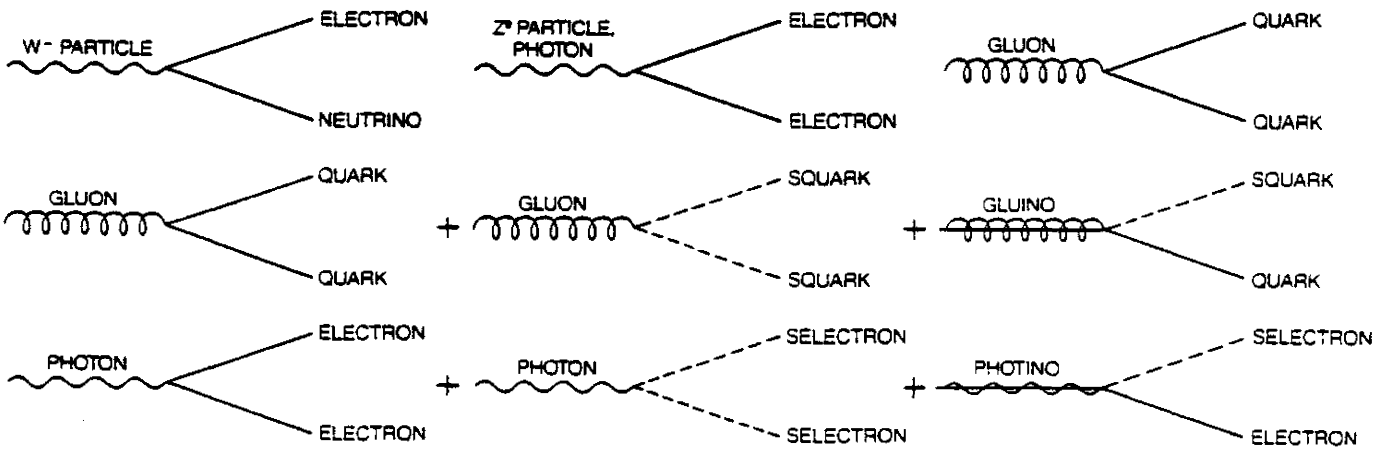

FEYNMAN DIAGRAMS offer a convenient method of illustrating reactions among elementary particles. The various lines (straight, wavy, curly, broken and combinations thereof) represent particular particles. The lines are joined to represent interactions, called scattering, that can take place among particles. Shown here are vertexes: building blocks of more complex reactions. The vertexes in the top row illustrate typical processes described in the prevailing theory, which is known as the standard model. The interactions of a supersymmetric theory are easily obtained by replacing any two lines of the vertexes of the standard model with the corresponding supersymmetric partners. Such replacements for the gluon-quark-quark vertex yield the vertexes in the middle row; replacements for the photon-electron-electron vertex yield the vertexes in the bottom row. Feynman diagrams are more than pictures; they are a shorthand for a well-defined mathematical procedure for determining the probability that any given scattering process will take place.

SCI. AM. OCT. 82.

REFERENCES

[1] Paper Presented at St. Edmund Hall College, Oxford University, Oxford, England on September 1, 1985.

[2] Puharich, H., Andrija. "Succesful treatment of neoplasms in mice with gaseous superoxide anion (O_2^-) and ozone (O_3); with a rationale for the effect". Sixth World Congress, of the International ozone association 1983. May 22-26, 1983. Washington, D.C., U.S.A.

[3] Kervran, Louis C. Transmutations biologique et physique moderne. Maloine, S.A.. Editeur, 27 Rue de l'ecole de Medicine, 75006 Paris, 1982.

[4] Puharich, Andrija, Ed. The Iceland Papers. Select papers on experimental and theoretical research on the physics of consciousness. With foreword by Brian D. Josephson, Ph.D. Nobel Laureate physics. Essentia Research Associates, Amherst, Wisconsin 54406. 1979.

[5] Byrd, Eldon. United States Navy Surface Weapons Center. "Biological effects of ELF fields". United States Psychotronic Association Annual Meeting. Atlanta, Georgia, June 29, 1984. Available as a videotape. Write to Robert Beutlich, secy-treas, U.S.P.A. 3459 Montrose Ave. Chicago, Ill. 60618. Price $ 40,00 (U.S.). Specify type of VCR.

[6] Ferrell, T.L., T.A. Callcot, R.J. Warmack. Plasmons and surfaces. American scientist, p. 344, vol. 73, no. 4, July-August 1985.

[7] Mandelbrot, Benoit B. The fractal geometry of nature. W.H. Freeman & Co. San Francisco, CA. 1983. A.K. Dewdney, Computer recreations, p. 16-24. Scientific American, August 1985, Vol. 253, no. 2.

This is the fundamental group of $SU(3)$, Z_3, which is triply connected and for which, therefore, two non-trivial types of vortices are defined—those whose end-points are monopoles of charge 1 (mod 3) and 2 (mod 3). In being colour $SU(9)$ monopoles, omegons are $SU(3)$, monopoles as well. As such, they are the ends of Y-shaped vortices carrying flux quanta defined modulo 3 (fig. 3.5). Consequently, omegons are the joint end-points of nine-legged $SU(9)$ vortices and Y-shaped $SU(3)$, vortices, that is, they cluster into three groups of three, bound externally by the former and internally by the latter. Figure 3.6 shows the proposed vortex configuration in a baryon.

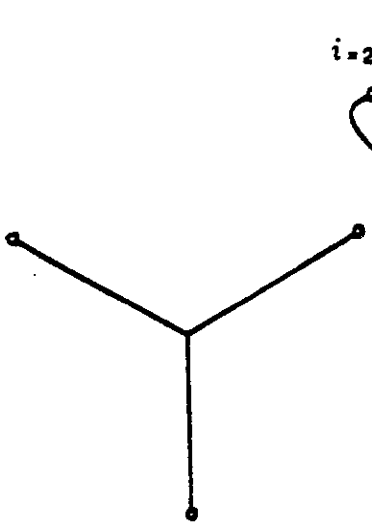

Fig. 3.5

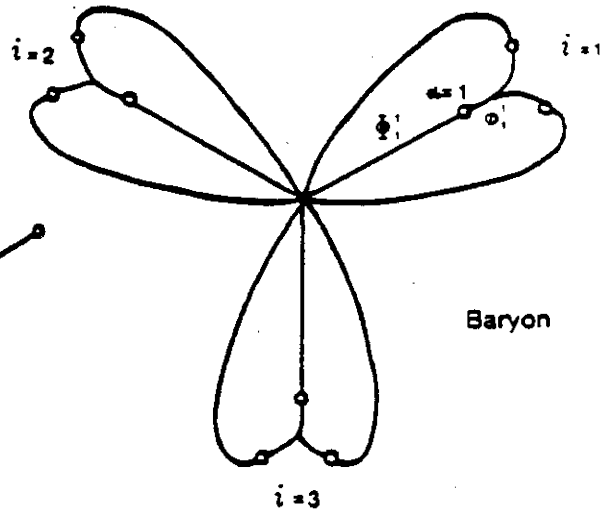

Fig. 3.6

The $SU(3)$, and colour $SU(9)$ vortices terminating on the αth omegon in the ith group carry flux

$$\phi_i^\alpha = m_i^\alpha \pmod 3 , \tag{18}$$

$$\Phi_i^\alpha = M_i^\alpha \pmod 9 , \tag{19}$$

respectively. The ith group is an $SU(3)$, singlet, provided that

$$\sum_{\alpha=1}^{3} m_i^\alpha = 0 \pmod 3 . \tag{20}$$

The total flux emanating from it is

$$\Phi_i = \sum_{\alpha=1}^{3} \Phi_i^\alpha = 3\bar{M}_i \pmod 9 , \tag{21}$$

APPENDIX A PART 4

These are a few pages from
S. Phillips´ work: "Extra-sensory
Perception of Quarks".
The interested reader may
profitably read these few pages
before ordering the book.

AP

This is the fundamental group of SU(3), Z_3, which is triply connected and for which, therefore, two non-trivial types of vortices are defined—those whose end-points are monopoles of charge 1 (mod 3) and 2 (mod 3). In being colour SU(9) monopoles, omegons are SU(3), monopoles as well. As such, they are the ends of Y-shaped vortices carrying flux quanta defined modulo 3 (fig. 3.5). Consequently, omegons are the joint end-points of nine-legged SU(9) vortices and Y-shaped SU(3), vortices, that is, they cluster into three groups of three, bound externally by the former and internally by the latter. Figure 3.6 shows the proposed vortex configuration in a baryon.

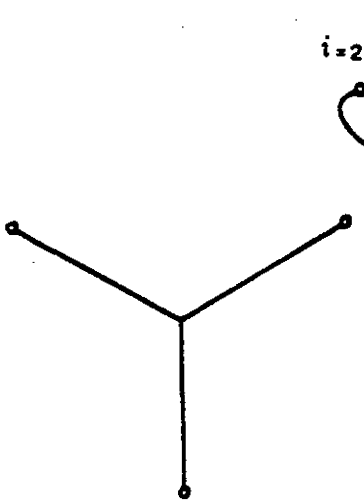

Fig. 3.5

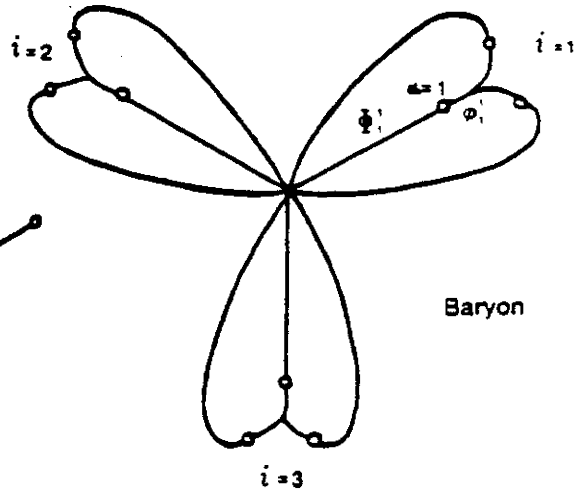

Fig. 3.6

The SU(3), and colour SU(9) vortices terminating on the αth omegon in the ith group carry flux

$$\phi_i^\alpha = m_i^\alpha \pmod 3 , \tag{18}$$

$$\Phi_i^\alpha = 3M_i^\alpha \pmod 9 , \tag{19}$$

respectively. The ith group is an SU(3), singlet, provided that

$$\sum_{\alpha=1}^{3} m_i^\alpha = 0 \pmod 3 . \tag{20}$$

The total flux emanating from it is

$$\Phi_i = \sum_{\alpha=1}^{3} \Phi_i^\alpha = 3\bar{M}_i \pmod 9 , \tag{21}$$

theory predicts that colour SU(3) is *not* a fundamental gauge symmetry that should be incorporated in "grand unified theories" with $U(1) \times SU(2)_L$ for electro-weak forces and with SL(2, C) for gravitation (although $SU(3)_c$ is the gauge symmetry of the superstrong interaction confining three omegons in a quark). Instead, colour SU(3) is an *effective* gauge symmetry of the total interaction between composite quarks, one that is actually mediated by the gauge fields of the primary colour SU(9) coupling between omegons.

MAGNETIC CHARGE COMPOSITION OF BARYONS

The condition that quarks are SU(3), singlet bound states of three SU(3), monopoles is

$$m_i \equiv \sum_{a=1}^{3} m_i^a = 0 \pmod 3 . \tag{41}$$

Since SU(3), monopole moments are defined by modulo 3, $m_i^a = \pm 1, \pm 2$, and $m_i = 0, \pm 3, \pm 6$. SU(3), monopoles couple to a gauge-invariant SU(3), scalar field tensor in an Abelian-like manner, obeying Dirac's equation for an Abelian monopole.[7] Omegons have an electric dipole moment of Dirac form. The corresponding operator for a non-relativistic system q_i ($i = 1, 2, 3$) of three Dirac monopoles of charge g_i^1, g_i^2, and g_i^3 in a bound state with zero orbital angular momentum is

$$P_i = -\sum_{a=1}^{3} (g_i^a \hbar / 2M_a c)\, q_a . \tag{42}$$

$\mathcal{P}$ and $\mathfrak{N}$ omegons in u and d quarks are bound in symmetric spin/unitary spin states, so that

$$\langle q | P_i^a | q \rangle = -(\hbar / 2Mc)\, g_i , \tag{43}$$

where

$$g_i = \frac{1}{3} \sum_{a=1}^{3} g_i^a , \tag{44}$$

and q = u or d ($\mathcal{P}$ and $\mathfrak{N}$ omegons are assumed to have the same mass M). The nucleon (N) electric dipole moment (E.D.M.) operator is

$$P = -\frac{\hbar}{2Mc} \sum_{i=1}^{3} q_i q_i . \tag{45}$$

Therefore,

$$\langle N | P | N \rangle = -(\hbar / 2Mc)\, q , \tag{46}$$

where

$$\bar{g} = \frac{1}{3}\sum_{i=1}^{3} g_i = \frac{1}{9}\sum_{i,a=1}^{3} g_i^a . \tag{47}$$

The experimental upper limits[8] for the nucleon are

$$\text{E.D.M.} \leq (7 \pm 9) \times 10^{-23} e \text{ cm} \quad \text{(proton)}$$

$$\leq 5 \times 10^{-23} e \text{ cm} \quad \text{(neutron)} .$$

The omegon mass would have to exceed 10^{10} GeV in order for the theoretical nucleon E.D.M. to be less than these upper limits. This would imply that quarks are massive, contrary to current estimates of about 350 MeV for the u and d. It is inferred that the E.D.M. is exactly zero, that is,

$$\sum_{i,a=1}^{3} g_i^a = 0 \tag{48}$$

or (in Dirac units)

$$\sum_{i,a=1}^{3} m_i^a = 0 , \tag{49}$$

which is the condition for magnetic neutrality of a system of nine Abelian monopoles. It may be written

$$m_1 + m_2 + m_3 = 0 . \tag{50}$$

There are three possibilities:

$$\text{(a) } m_1 = m_2 = m_3 = 0 ; \quad \text{(b) } m_1 = m_2 = \pm 3 , \; m_3 = \mp 6 ;$$

$$\text{(c) } m_1 = 3 , \; m_2 = 0 , \; m_3 = -3 .$$

SU(3), monopoles of charge $+1$ and -2 have topologically identical vortex strings; similarly for monopoles of charge $+2$ and -1. Hence, quarks with monopole configurations (1, 1, 1), (1, 1, -2), (1, -2, -2), and (-2, -2, -2) are allowed. These are topologically distinct from the configurations (2, 2, 2), (2, 2, -1), (2, -1, -1), and (-1, -1, -1). The configurations corresponding to the permitted values of m_i are

$$\text{(1) } m_i = 0\text{: } \quad \pm (1, 1, -2) ,$$

$$\text{(2) } m_i = \pm 3\text{: } \pm (1, 1, 1) \text{ or } \pm (2, 2, -1) ,$$

$$\text{(3) } m_i = \pm 6\text{: } \pm (2, 2, 2) .$$

They give rise to a variety of possible magnetic charge compositions for the nucleon (and for any baryon with zero E.D.M.). But, in terms of positive (+) and negative (−) magnetic charges, it is easily verified that cases

break up into free omegons (stage 4). Why the M.P.A. should contain two protons is explained in chapter 7.

The investigators claimed that they could distinguish between what they called "positive" and "negative" groups. They portrayed this distinction in diagrams by means of the following convention: "Speaking generally, positive groups are marked by the points of Anu being turned outward and negative groups by the points being turned inward towards each other and the centre of the group."[20] They did not elucidate what they meant by "positive" and "negative" but remarked only that "combinations of three or more Anu are positive, negative or neutral, according to the internal molecular arrangement: the neutral are relatively stable, the positive and negative are continually in search of their respective opposites, with a view to establishing a relatively permanent union."[21] The following consideration shows that the terms signify the sign of the total electric charge of a group of U.P.A.'s: the Hydrogen Triangle in figure 5.16 with four (+) and five (−) U.P.A.'s has two triplets with their U.P.A.'s pointing outward even though one has two (+) U.P.A.'s and one (−) U.P.A. and the other has two (−) U.P.A.'s and one (+) U.P.A. A "positive" triplet, therefore, cannot be one that has more (+) U.P.A.'s than (−) U.P.A.'s. But, if the terms refer to electric charge, then the Hydrogen Triangle should contain two positively charged triplets and one negatively charged triplet. The reader is reminded that the Quark Model predicts that a proton consists of two positively charged u quarks and one negatively charged d quark. Figure 5.16 is consistent with two features of the Quark Model: it shows the presence of three bodies in what has been identified in chapter 4 as a proton —a Hydrogen Triangle. It also indicates that two bodies are "positive" and one is "negative."

Unfortunately, similar considerations cannot be applied to the other Hydrogen Triangle because diagram *a* in figure 5.16 does not indicate clearly whether the linear triplet is positive or negative. But since, for this Hydrogen Triangle, the triangular triplet with its U.P.A. pointing outward must be a u quark and the linear triplet with its outside U.P.A. pointing inward must be a d quark, it may be inferred that *a* is a u quark, or, more accurately speaking, a u quark depicted *after* its disintegration into free omegons. It would appear that the diagram is one showing a linear Hydrogen Triplet (*b*) that was accidentally broken up by the investigators while they observed it. This is because, according to the investigators' own testimony on the appearance of free U.P.A.'s (given shortly), the U.P.A.'s are depicted in diagram *a* as being in the free state.

Figure 5.15*b* shows two different string configurations for the proton. In one of them, three lines of force connect each triplet to the centre of their

orbital motion. It is interpreted as follows: quarks are bound to one another in baryons by SU(9) Nielsen-Olesen vortices extending between their constituent omegons. The total flux emanating from the junction of the nine vortices is 0 (mod 9). Quarks are clusters of three SU(9) magnetic monopoles that are internally bound by Y-shaped SU(3) vortices carrying either one or two flux quanta. The flux emanating from the junction of a Y-shaped string is 0 (mod 3). Note that the trigonal symmetry of the sets of three SU(9) strings is identical with the symmetry of arrangement of the SU(3) strings between omegons in a free quark. This is because each quark contributes a net flux of three quanta to the junction of the nine SU(9) strings binding omegons together in a baryon, while each omegon contributes a net flux of one quantum to the junction of the nine SU(3) strings binding them in a free quark. The internal Y-shaped string structure of a bound quark is identical with current models of baryons as three SU(3) quark monopoles bound by Y-shaped strings.

It must be emphasized here that all drawings of groups of particles have only qualitative significance and are not even approximately correct in scale. This is because the micro-psi observer employs widely varying powers of magnification in order to discern and to examine objects of different size. Hence, he finds accurate comparison and depiction of their relative sizes to be quite impossible tasks: "It should be specifically noted that the diagrams are not drawn to scale, as such drawings would be impossible in the given space. The dot representing the Anu is enormously too large compared with the enclosures, which are absurdly too small; a scale drawing would mean an almost invisible dot on a sheet of many yards square."[22] Also: "It must be remembered that the bodies shown diagrammatically in no way indicate relative size; as a body is raised from one substate to the one immediately above it, it is enormously magnified for the purpose of investigation."[23] Still, Hydrogen Triangles were described as very large compared with their constituents, a feature that is consistent with experimental evidence for relatively small or pointlike quarks inside protons.[24]

DISINTEGRATION OF GROUPS OF U.P.A.'S

Besant and Leadbeater claimed not only that they could observe atoms but that they could also disintegrate them into their constituent bodies, and these in turn into smaller groups, until everything was finally broken up into free U.P.A.'s (or at least they could manipulate micro-psi images in this way). They stated: "The first thing that happens on removing a gaseous atom from its 'hole' or encircling 'wall' is that the contained bodies are set free, and, evidently released from tremendous pressure, assume spherical or ovoid forms, the Anu within each re-arranging themselves,

SUMMARY AND CONCLUSIONS (In Abstract form).

A B S T R A C T

MAGNETIC MODEL OF MATTER AND MIND

PHYSICAL FOUNDATION OF INFORMATION AND ACTION TRANSFER IN THE HEALING PROCESS

Quantum imaging of magnetic monopoles, massless scalars and gravitor

Andrija Puharich, M.D., & Sharron Jacobson,Q.I.

It is affirmed that ESP exists.
Is ESP based on electromagnetic transmission?

When ESP test subjects were sealed in EM super shielded rooms, ESP test scores rose significantly above controls. EEG measurements were made of test subjects during such tests: 8Hz readouts were found when ESP hits were made.

When healer and healee pairs worked together, the healer showed an 8Hz readout which then entrained the healee's EEG at 8 Hz. The same effect occurred when the healer and healee were separated by a super shielded room.

When normal test subjects (with EEG readout) were enclosed in a super shielded room, and then irradiated (randomly and double blind) from an ELF scalar transmitter instrument placed outside of the super shielded room, producing a frequency range from 1 to 15 Hz. There was found EEG entrainment of the test subject's brain inside the super-shielded room. This proved that ELF scalar fields will pass through the walls of a super shielded room.

A dry kidney bean was placed in a healer's hand which was then closed over it. The healer was instructed to make the bean 'sprout'. Within two minutes a three inch sprout appeared from the bean. This is called growth in forward time (G.I.F.T.)

B. The Nature of Man

Man's ultimate pattern of existence and being is encoded n his body giant macromolecular makeup whose building block unit is DNA. Each unit of this material contains some 3.6 billion base pair nstructions. Each of these instructions can be signalled for GO or O-GO action by a single ELF magnetic field pulse at an ultra-low intensity of the order of 10^{-9} TESLA. The two coils of the double elix of DNA are triggered for GO , or NO-GO , at the proton of the resonant hydrogen bond, binding the two coils of DNA by a single requency of the ELF field.

With respect to the origin of biomolecular life we will review the material covered in Part 2. To create such "life" requires nly 6 atomic elements. Of course, more elements are required for higher forms of life. Here we consider only proto-life forms. These elements are:

Fe, Cu, Na, Cl - as catalysts

Free H_2 and O_2 - freshly electrolysed in the form, O and H from water @ 8 Hz and higher harmonies.

C, N are produced by the Kervran transmutation process.

These elements in turn produce the biomolecular building blocks of life - as already described.

Then the healer was instructed to make the 'sprout' ;ow back into the bean. This is called growth into reversed time. (G.I.R.T.). This was accomplished in about two minutes. EEG read- igs, as well as the scalar wave detector showed 8.00 Hz radiated from the healer's hand, both in the GIFT and GIRT mode.

Test subjects working in a supershielded room were asked to detect when a cosmic ray pulse hit a cosmic ray detector id recorder housed in a separate super shielded room 0.3 miles away. The results were highly significant statistically for precognition, ; long as 120 seconds before the cosmic ray pulse hit the cosmic ray detector. This is proof for Time Reversal.

Many healer's hands from all over the world were measured during the act of healing a patient. All bona fide healers showed an 8.00 Hz ELF scalar field emanating from their hands.

Test subjects were found (starting with Uri Geller), who could bend metals without manual contact. It was found that ich hands put out a 7 Hz scalar field. This action affects the Fermi electron band of atoms resulting in bond weakening, or breaki ; me of this group could also make objects vanish (dematerialize), s well as teleport and materialize.

In 1972 a psychic was found, Sharron Jacobson, who could look at sub-atomic quantum dynamics, i.e., he observed:

) Hadrons (particularly protons) could be freeze-framed, and closely examined for internal dynamics, and described 3 quarks;

) Each quark contains 3 bound 'wave functions' identified as magnetic monopoles. Also, there is an additional free magnetic monopole confined in the bag model (described as a 'wall of light') of the proton;

) In the proton were 10 magnetic monopoles (MM), matched by 10 anti-monopoles ($\overline{MM}$). This makes a fundamental probability set of 10 MM coupled to 10 $\overline{MM}$. This appears to be the basic alphabet of the universe. When two single protons, at any distance apart

communicate, they can exchange 10! messages or 3,280,000 messages.

S.J. was asked to observe the origin of a healer's 8.00 Hz ELF scalar field, and the target of that field in a patient

a) The origin of the Healer's 8.00 Hz was in his double helix coupling-protons, which transferred an ELF scalar field to DNA in the nucleus of the cells of the healee by resonance;

b) The target hit by the ELF scalar field was a coupling-proton suspended between two single DNA helices which make up the double helix.

c) Resonance between the Healer's DNA 8.00 Hz proton ELF scalar field and the Healee's proton coupling the two DNA helices, a local separation between the 2 helices, which triggers a signal to the messenger RNA. This produces, or releases, a genome called RAD 6 which initiates the healing process.

An instrumented ELF scalar field generator was designed, and placed in production, to put out an 8.00 Hz ELF scalar field of strength 9 x 10 minus 9th Tesla. It was packaged in a wrist watch. Over 2,000 persons wore such a watch, called a TESLAR, for a period of two years. The study was triple blind . It was found that such an artificially generated 8.00 Hz ELF scalar field cured 27 different organic diseases, to date.

It was discovered only two years ago (1986) that quantum imaging observations of magnetic monopoles had been carried out some 90 years ago and published in London in 1895 by Annie Besant and Charles Leadbeater. In 1979, a British Physicist, Stephen Philips, analyzed the B & L observations, and drawings. He published his conclusion in, "Physics Letters", 1979 stating that he believed that they had observed magnetic monopoles and strings (now known as super-string theory).

In our sixteen years of quantum imaging we are able to confirm the B. & L. findings, and recognize their priority in this pioneering work. We also concur with Philips' mathematical model of hadron leptons.

CONCLUSIONS:

It is believed that MM and $\overline{MM}$ have been found in a adron existing in a 26-dimensional state. It is believed that MM and $\overline{MM}$ carry all the biological information to create life, rganize life for growth and repair, and to maintain health. All he evidence points to the Dirac-t'Hooft-Polyakov magnetic monopole string to be the long-sought for graviton. Two proton monopole ystems coupled over any distance by the magnetic monopole string produce the gravitational field. If this idea is proven, the four undamental fields can be unified out of one basic field. The unified theory will also explain why the Universal Action Principle, Ω, is so close to 1.

BERMUDA
April 15th, 1988

Temple University Conference
on Frontier Issues in Physics,
Biology, and Quantum Theory.

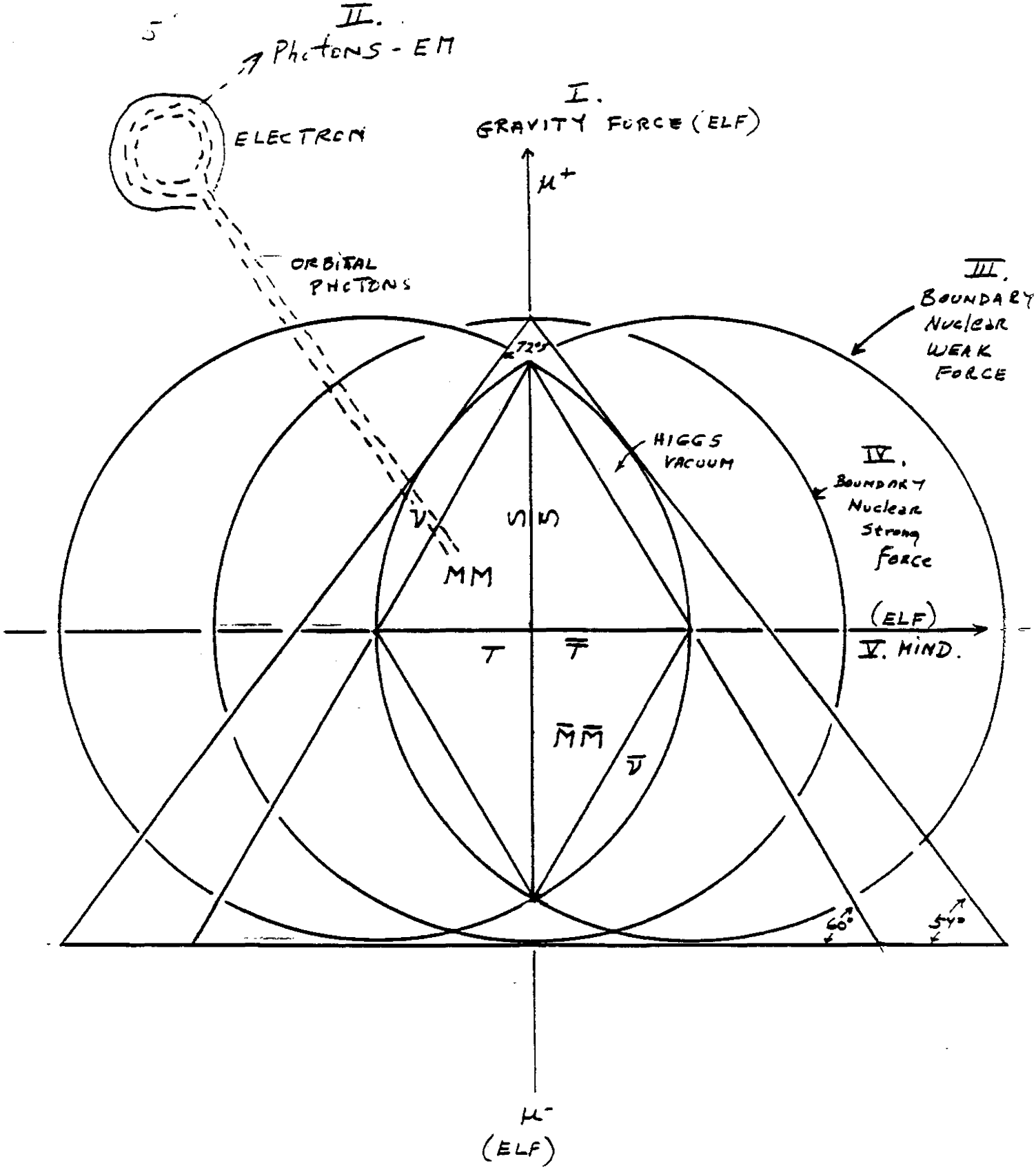

Fig.1. Schematic relationships between the five forces of Nature: I. Gravity, II.Electromagnetic, III. Nuclear Weak Force, IV. Nuclear Strong Force, V. The Mind - Universal as well as embodied in Bio-Systems.

FIGURES 2 a, b, c, etc.

Measurements of the ELF radiation coming

from the hand of a person.

a) Control reading on Tap Water. The time-averaged spectral analysis shows: 1) The random ELF noise coming from the water. 2) The inserted 8.6 Hz marker signal (two squares vertical deflection shows a 10 db gain. 3) The 12.2 Hz ELF signal emanating from the USSR. All measurements taken inside of a super-shielded Faraday Cage.

b) ELF spectrum emanating from the right hand of a test subject. Note sharp peaks of ELF at:

6.3 Hz
7.3 Hz
8.4 Hz

and, note that the Soviet ELF signal has vanished.

c) Spectral distribution of ELF fields emanating from the right hand of a "healer" into the control water sample. The ELF field distribution is:

3.1 Hz
6.2 Hz
7.0 Hz
7.7 Hz
8.75 Hz

Figures 3, 4, 5, 6

These figures clearly show the science behind the Teslar watch. The main point is that it shows how the "chip" integrates the separate ELF frequencies emanating from the hand (as in Figure 2 (a) (b) (c). as well as the different frequencies emanating from the Teslar GNoo3 watch crystal into respectively, an 8.00 Hz E field, an 8.00 Hz B field, and finally an 8.00 Hz impulse wave - true scalar field. The tabulated results are shown in Table I.



FIG. 3 Q CRYSTAL IS PULSED FROM E, 3.0 V. BATTERY THROUGH RC NETWORK TO CREATE A BINARY SERIES OF E FIELD FREQUENCIES, AS SHOWN IN FIG. 4

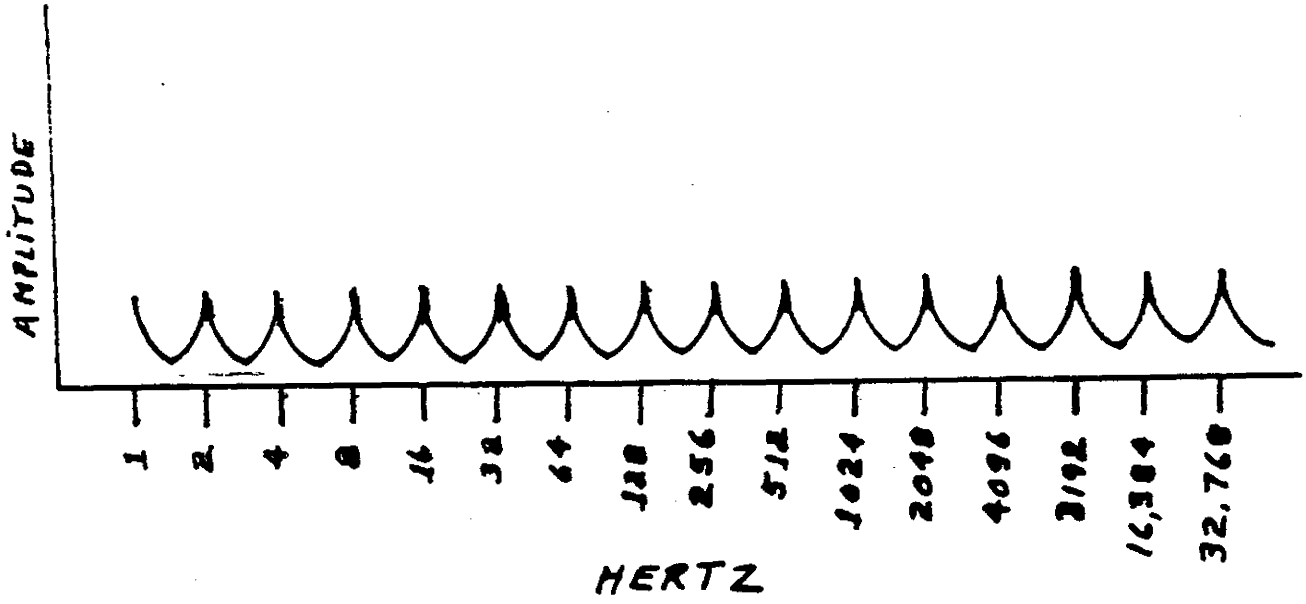

FIG 4 HARMONIC FREQUENCIES (E FIELD) ELICITED BY PULSING CRYSTAL WITH A SINGLE (D.C.) FREQUENCY OF 8.00 Hz.



FIG. 5 SINGLE B FIELD PASSED THROUGH FARADAY CAGE FILTER OF 8.00 Hz AFTER 180° PHASE SHIFT.

[NEXT PAGE]

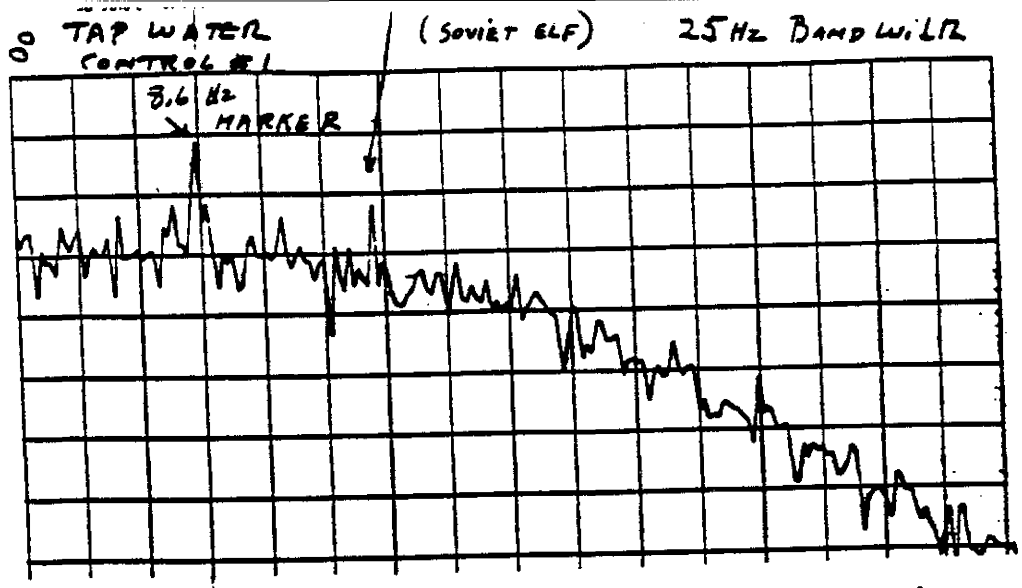

(a)

#4

Paper saturated #1
~6.3Hz 9.3Hz

PUBLICH HANDS ON
CONTROL #1 TAP WATER
25Hz BW.

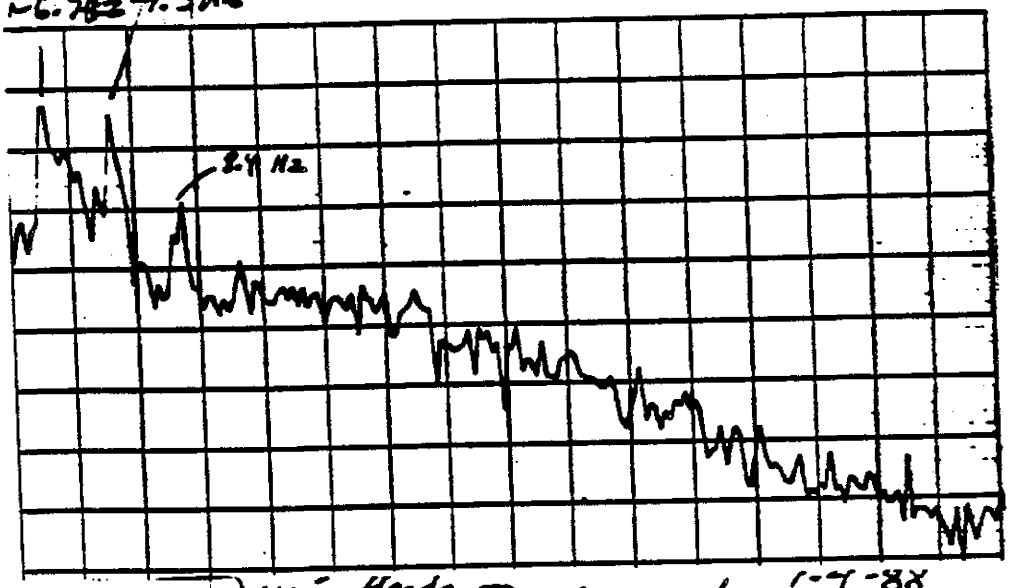

(b)

1-7-88

Marie Hyde saturated tap water

3.1

6.2Hz

25Hz B.W.

#10

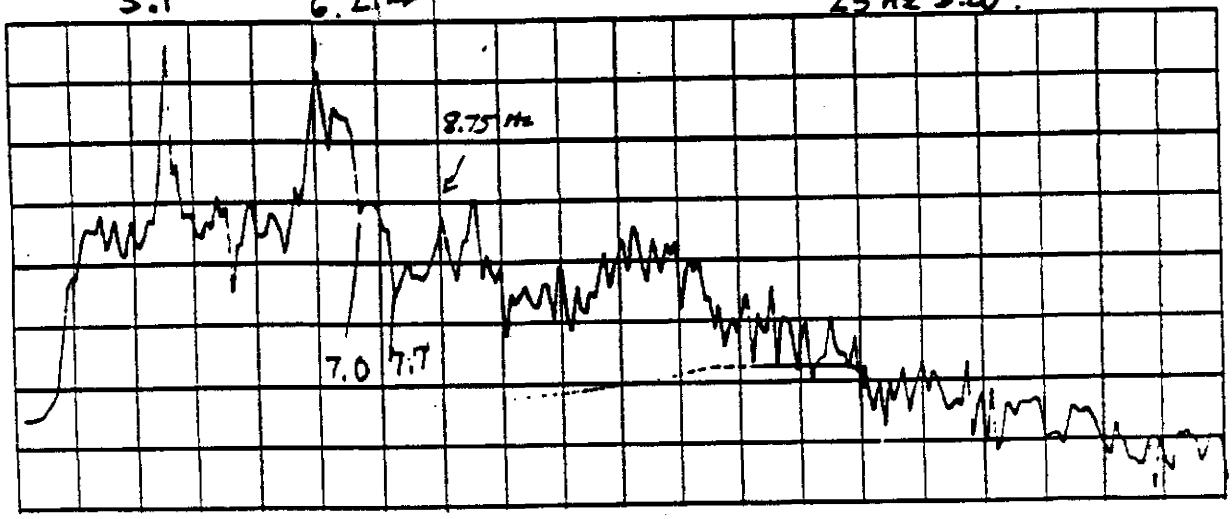

(c)

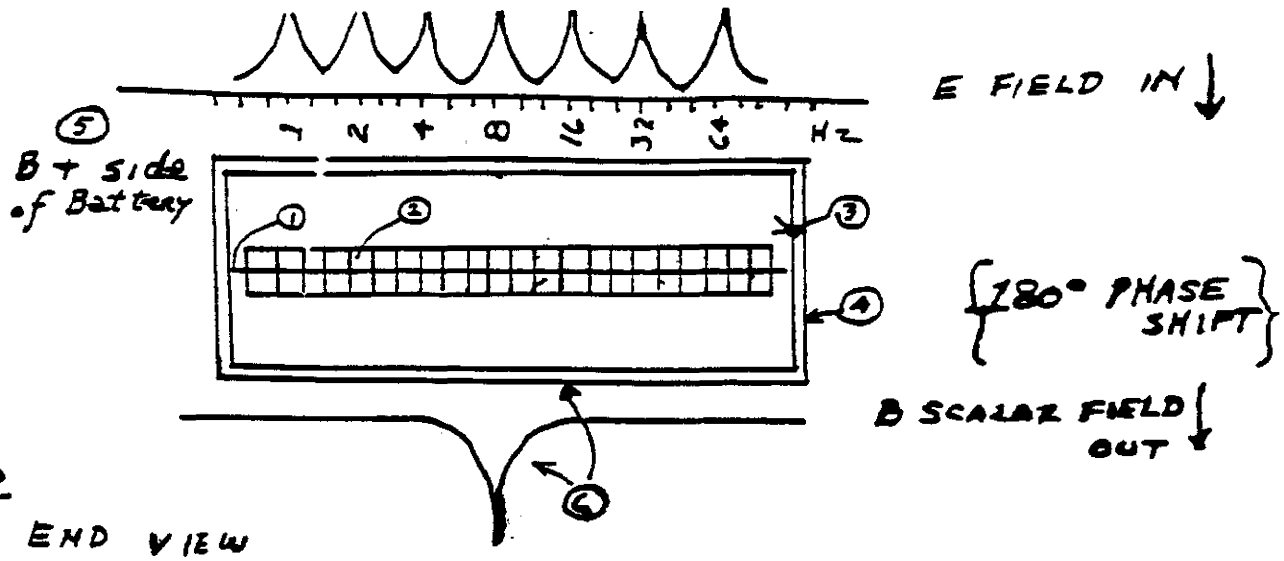

FIG. 6

END VIEW

OF FARADAY CAGE

FILTER. TOP VIEW is 7 m.m. x 7 m.m.

(1) 1 mil thick ALUMINUM FOIL, COATED ON EACH Side with (2) FERRIC OXIDE (Fe_2O_3) GRANULES polarized South - South on ALUMINUM FOIL LAYER THIS IS REAL SEMICONDUCTOR EFFECT.

(3) 1 mil thick Copper Foil configured as a Faraday cage, 4 mils thick overall top dimension, 7 m.m x 7 m.m, and 4 m m. Thick.

(4) Copper Foil coated with 0.5 mil Teflon Coating

(5) TOP SIDE OF FARADAY CAGE FILTER LAID ON B + side BATTERY

(6) BOTTOM SIDE OF FARADAY CAGE FILTER SHOWING FILTERED 8.00 Hz B FIELD SCALAR EMERGING AND DIRECTED INTO HUMAN SKIN

HEWLETT PACKARD

OPERATING MANUAL

MODEL 3582A SPECTRUM ANALYZER

Serial Numbers: 1747A00101 to 1747A00125 and 809A00126 and greater

IMPORTANT NOTICE

This manual applies to instruments with the above serial number prefixes. As changes are made in the instrument to improve performance and reliability, the appropriate pages will be revised to include this information.

WARNING

To help minimize the possibility of electrical fire or shock hazards, do not expose this instrument to rain or excessive moisture.

Manual Part No. 03582-90005

Microfiche Part No. 03582-90855

©Copyright Hewlett-Packard Company 1978
P.O. Box 301, Loveland, Colorado 80537 U.S.A.

Printed: March 1981

FIG. 2

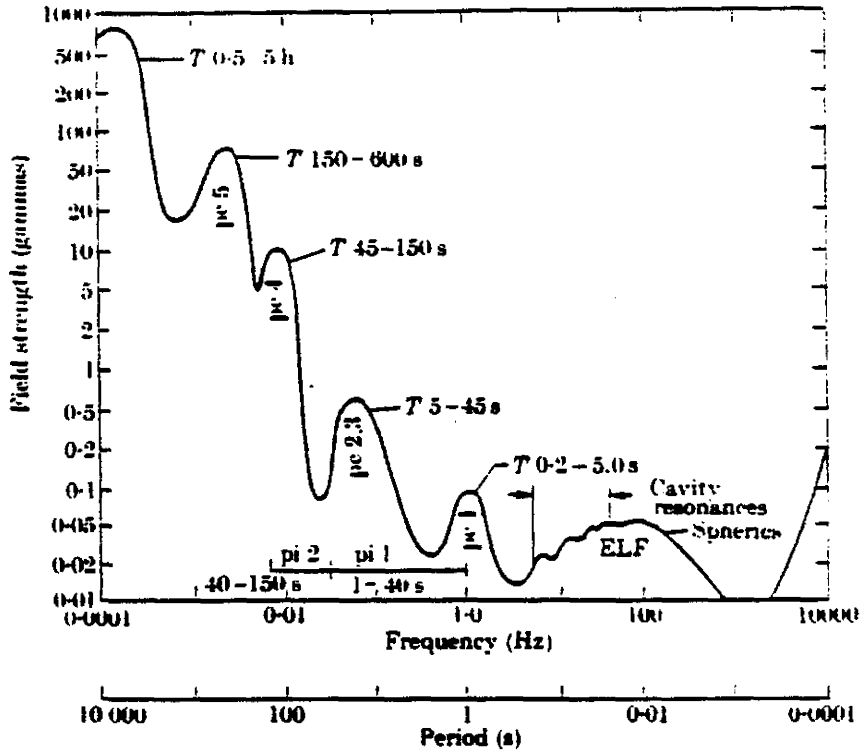

FIG. 6.44. The magnitude of geomagnetic micropulsations of different frequencies (or periods). After Campbell (1967).

The wave that travels with speed $V_A(1-\omega/\omega_i)^{\frac{1}{2}}$ is the pure Alfvén wave or the slow mode; the one that has the speed $V_A(1+\omega/\omega_i)^{\frac{1}{2}}$ is the modified Alfvén wave or the fast mode.

Obayashi (1965) computed the double-hop transit time τ of hydromagnetic waves along a geomagnetic field line: it is defined by

$$\tau = \int ds/v_g,$$

where v_g denotes the group velocity, given by

$$v_g = V_A(1\pm\omega/\omega_i)^{\frac{1}{2}}(1\pm\omega/2\omega_i)^{-1}.$$

Assuming that the plasma density distribution is given by

$$n = n_0(a/r)^3,$$

we have

$$\tau = \frac{4aL^{\frac{1}{2}}}{B_0\sqrt{(4\pi n_0 m)}} \times \times \int_0^{\lambda_m} \cos^4\lambda \left[\left\{1\pm\frac{\omega}{2\omega_c}\frac{\cos^6\lambda}{\sqrt{(1+3\sin^2\lambda)}}\right\}\Big/\left\{1\pm\frac{\omega}{\omega_c}\frac{\cos^6\lambda}{\sqrt{(1+3\sin^2\lambda)}}\right\}^{\frac{3}{2}}\right] d\lambda.$$

ELF COCOON CORP.
RT 1 BOX 545
DOBSON, N.C. 27017

October 13, 1986

CONFIDENTIAL REPORT
LAB REPORT ON (LORUS GN003) TESLAR DIGITAL WATCH

TABLE I

	TEST I SKILLING E- FIELD DETECTOR		TEST II BECK B-FIELD DETECTOR	
FUNCTION	A. WITHOUT CHIP	B WITH CHIP	B. WITH CHIP	A. WITHOUT CHIP
FREQUENCY:	8.00 Hz	8.00Hz	8.00 Hz	8.00 Hz
WAVE FORM:	sine wave	sine wave	impulse wave	sine wave
WRIST LOADING:	gain= 0	gain= 0	gain= x4	gain= 0
MAGNETIC FIELD:	not detectable	N.D.	9-10 nanotesla	N.D.

The above data denotes criteria, as shown in column Test II B , for efficacy of the Teslar, and safety of the Teslar.

We are searching to find a quartz ladies watch that will meet these criteria, as well as a quartz analog watch.

Andrija Puharich, M.D., LLD.
Director of Research
E.C.C.O.

TABLE OF CONTENTS

Section Page

I. GENERAL INFORMATION 1-1
1-1. Introduction 1-1
1-5. Specifications 1-1
1-7. Safety Considerations 1-1
1-9. Instruction Manual Symbol 1-1
1-11. Instruments Covered by Manual 1-1
1-16. Description 1-2
1-27. Options 1-3
1-29. Accessories Supplied 1-3
1-31. Accessories Available 1-4
1-33. Recommended Test Equipment 1-4

Section Page

II. INSTALLATION 2-1
2-1. Introduction 2-1
2-3. Initial Inspection 2-1
2-5. Power Requirements 2-1
2-7. Line Voltage and Fuse Selection 2-1
2-9. Power Cable and Grounding Requirements 2-2
2-11. Operating Environment 2-2
2-12. Temperature 2-2
2-14. Humidity 2-2
2-16. Altitude 2-2
2-18. Cooling Fan 2-2
2-20. Thermal Cutout 2-2
2-22. Installation 2-3
2-23. Mounting 2-3
2-26. HP-IB System Interface Connections 2-3
2-30. Cable Length Restrictions 2-4
2-32. HP-IB Address Selection 2-5
2-34. Storage and Shipment 2-5
2-35. Environment 2-5
2-37. Packaging 2-5

Section Page

III. MANUAL OPERATION 3-1
3-1. Introduction 3-1
3-3. Controls, Connectors, and Indicators 3-1
3-5. Turn-On Procedure 3-1
3-8. About Spectrum Analyzers 3-2
3-10. A Comparison 3-2
3-13. Features 3-2
3-15. The Display 3-2
3-19. Familiarization Exercise 3-3
3-20. Introduction 3-3
3-22. Adjusting the Display 3-4
3-24. The CAL Signal 3-4
3-27. The Input Mode Switch 3-4
3-29. Input Considerations 3-5
3-34. Analyzing an Input Signal 3-5
3-46. The Frequency Span Controls 3-8
3-53. Scales 3-9

Section Page

3-55. Amplitude Reference Level 3-10
3-58. The Passband Shape Controls 3-11
3-61. The Noise Source 3-13
3-65. Impulse Output 3-14
3-68. Dual Channel Measurements 3-15
3-94. Storing Traces 3-24
3-97. Conclusion 3-25
3-99. Operating on Signal Data 3-25
3-100. Introduction 3-25
3-102. Acquiring a Time Record 3-25
3-104. Operating on Stored Time Data 3-25
3-106. Using the Recorder Output 3-26
3-109. Using Probes 3-26
3-111. Probes Are Delicate 3-27
3-113. Probe Compensation Procedure 3-27
3-115. Front Panel Screwdriver Adjustments 3-28
3-117. ASTIG Adjustment 3-29
3-119. BAL Adjustments 3-29
3-122. In Case of Trouble 3-29
3-123. Introduction 3-29
3-125. "Hung UP" 3-30
3-127. Overload 3-30
3-129. Unrelated Spectral Displays 3-31
3-131. Noise Source Output 3-31
3-133. Simplification of Discrete Data Analysis 3-31
3-134. Introduction 3-31
3-136. Time Domain Considerations 3-32
3-139. Frequency Domain Considerations 3-32
3-147. Aliasing 3-34
3-150. Data in Memory 3-35
3-153. Interpreting the Display 3-36
3-156. Leakage 3-37
3-158. Windowing 3-37
3-163. Window Functions 3-38
REMOTE OPERATION 3-39
3-165. Remote Operation 3-39
3-166. Introduction 3-39
3-169. 3582A Remote Functions 3-39
3-170. General Description 3-39
3-172. Remote Front Panel Programming 3-40
3-176. Syntax 3-40
3-180. Delimiters 3-41
3-182. Special Front Panel Commands 3-41
3-184. Using Preset 3-41
3-186. Setting the Marker 3-41
3-189. Instrument Data Output 3-42
3-191. Listing Control Settings 3-42
3-194. Program Examples 3-42
3-199. Program Example 3-45
3-201. Program Example 3-46
3-202. Instrument Data Input 3-47

LIST OF ILLUSTRATIONS

Figure Page

2-1. Line Voltage and Fuse Selection....2-1
2-2. Power Cables....2-2
2-3. Typical HP-IB System Interconnection....2-3
2-4. HP-IB Connector....2-4
3-1. The Channel A CAL Signal....3-4
3-2. Spectrum of a 1 kHz Square Wave....3-6
3-3. Setting the Marker Position....3-7
3-4. Using the SPAN Control to Resolve Sidebands....3-9
3-5. Expanding a Portion of the Display....3-11
3-6. Full Scale Reference in the LINEAR Mode....3-11
3-7. A Sine Wave Spectrum Using the FLAT TOP Passband....3-12
3-8. Sine Wave Spectrum Using the HANNING Passband....3-13
3-9. Sine Wave Spectrum Using the UNIFORM Passband....3-13
3-10. Noise Source Spectrums....3-14
3-11. A Two Port Network....3-15
3-12. Connecting a Single Pole Low Pass Filter....3-15
3-13. Input and Output Spectrum of a Low Pass Filter....3-16
3-14. Transfer Function for a Two Port Network....3-17
3-15. Phase Transfer Function of a Low Pass Filter....3-18
3-16. Phase Spectrum of a Triangle Wave....3-19
3-17. Selecting the Correct Harmonic....3-21
3-18. Modulating a Spectral Line with Noise....3-21
3-19. RMS Averaged Signals....3-21
3-20. TIME Averaged Signals....3-22
3-21. Oscillating Frequency Spectrum....3-22
3-22. Spectrum of an FM Passband....3-23
3-23. The Coherence Relationship Between Two Signals....3-23

Figure Page

3-24. A Two Trace Plot....3-27
3-25. About Scope Probes....3-28
3-26. Probe Compensation....3-28
3-27. Adjusting the BAL Control....3-30
3-28. Sampling an Input Waveform....3-32
3-29. Windowing a Sampled Waveform....3-32
3-30. Frequency Representation of a Cosine Wave....3-33
3-31. Frequency Representation of an Impulse Train....3-33
3-32. Frequency Representation of a Square Pulse....3-33
3-33. Convolving the Cosine Spectrum with the Sampling Pulse Spectrum....3-34
3-34. Convolving a Sampled Cosine Spectrum with a Window Spectrum....3-34
3-35. Increasing the Frequency of a Cosine Wave....3-34
3-36. Aliasing....3-35
3-37. 3582A Antialiasing Filter....3-35
3-38. The Continuous Function....3-35
3-39. Spectrum Points in Memory....3-36
3-40. Memory Data Points Displayed on CRT....3-36
3-41. Leakage of Energy....3-37
3-42. Sidelobes of Transformed Rectangular Window....3-37
3-43. Data Flow....3-38
3-44. Window Functions....3-38
3-45. Words in Memory....3-48
3-46. Storing a Time Record in Memory....3-52
3-47. Reading Binary Data From Memory....3-54
3-48. 3582A Front Panel Controls, Connectors and Indicators....3-69/3-70
3-49. 3582A Rear Panel Connectors, Switches and Filter....3-71/3-72

TABLE OF CONTENTS (Cont'd)

Section Page

3-203. Writing Alphanumeric Messages....3-47
3-205. Program Example.....3-48
3-206. Working With Memory.....3-48
3-208. The Binary Format.....3-48
3-212. Memory Instructions.....3-49
3-215. Memory Locations.....3-49
3-217. Instrument Signal Processing Control and Status.....3-50
3-218. Service Request.....3-50
3-220. Status Word.....3-50
3-223. Program Example.....3-51
3-224. Processor Control Commands.....3-51
3-226. Example Flowcharts and Programs...3-51
3-227. Loading a Time Record Into Memory.....3-51
3-229. Program Example: Writing to Memory.....3-53
3-230. Reading Binary Data From Memory.....3-53
3-232. The Learn Mode.....3-53
3-234. Program Example: The Learn Mode.....3-55
3-235. Program Example: Plotting The Display.....3-56

Section Page

OPERATIONAL VERIFICATION..3-57
3-236. Operational Verification.....3-57
3-238. Required Test Equipment.....3-57
3-240. Preset.....3-57
3-242. Instrument Warmup.....3-57
3-245. DC BAL Verification.....3-59
3-248. ROM Self Test.....3-59
3-252. Display Accuracy.....3-59
3-257. Calibrator Accuracy.....3-60
3-262. Amplitude Accuracy and Flatness...3-60
3-267. Noise Level.....3-61
3-272. Harmonic Distortion.....3-62
3-277. Common Mode Rejection.....3-63
3-282. Frequency Accuracy.....3-64
3-287. Phase Accuracy.....3-65
3-292. Amplitude and Phase Match Between Channels.....3-66
3-297. Controls, Connectors and Indicators.....3-67

APPENDICES
A. HP-IB Command List
B. Condensed Description of the HP-IB
C. Condensed Description of Meta Messages
D. Application Notes

LIST OF TABLES

Table Page

1-1. Options.....1-3
1-2. Accessories Supplied.....1-3
1-3. Accessories Available.....1-4
1-4. Recommended Test Equipment.....1-4
1-5. Specifications.....1-5
2-1. HP-IB Cables.....2-5
2-2. Address Selection.....2-5
3-1. Impulse Output Pulse Period.....3-14
3-2. LDS Points Returned.....3-45
3-3. Output Units.....3-45
3-4. Display-ASCII Equivalents.....3-46
3-5. Recommended Test Equipment for Operational Verification.....3-58
3-6. Recommended Test Accessories.....3-58
3-7. Amplitude Accuracy and Flatness.....3-61

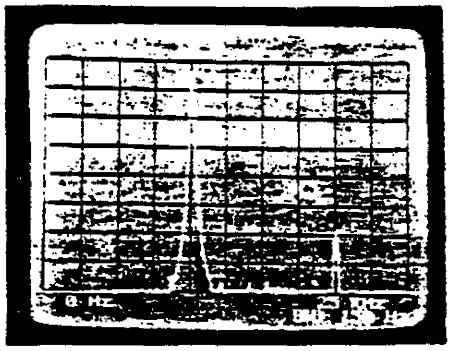

Figure 3-8. Sine Wave Spectrum using the HANNING Passband.

half its previous value. The smaller bandwidth allows for greater selectivity, while the slightly changing shape is due to the discrete sampling and display technique.

g. Set the UNIFORM passband button to ON. The spectrum may appear as in Figure 3-9.

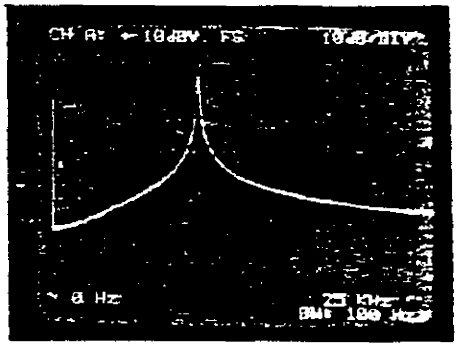

Figure 3-9. Sine Wave Spectrum Using the UNIFORM Passband.

h. Slowly change the frequency of the oscillator. The radically changing shape is due to a bandwidth which is now less than a third that of the FLAT TOP passband. This reveals that the UNIFORM passband should generally not be used except for measuring transfer functions using the PERIODIC NOISE OUTPUT as a source.

3-61. The NOISE SOURCE.

3-62. The NOISE SOURCE is a broadband periodic pseudo random signal. When "PERIODIC" is selected, the period is automatically adjusted so that one period covers one SPAN setting and, therefore, the periodicity does not effect the spectrum analysis. When "RANDOM" is selected, the periodicity of the noise source signal is extended to as much as 14 minutes. In this mode, the 3582A interprets the pseudo random signal as a band limited white noise source. The NOISE SOURCE output may be adjusted through the use of the LEVEL control located adjacent to it. The low impedance output (< 1 ohm) may be used as a source signal for analyzing two port networks.

3-63. To see the spectral output of the NOISE SOURCE, connect the NOISE SOURCE output to the channel A input connector via a shielded cable with suitable adapters. Set the

CHANNEL A COUPLING and the CHANNEL B COUPLING to AC. Adjust the CHANNEL A SENSITIVITY control for an on-scale display. The displayed spectrum is nearly a uniform amplitude across the frequency axis (see Figure 3-10[a]). It is important to note that there is energy at each spectral point, but none in between. If a phase spectrum is observed, the phase will be consistent for corresponding frequencies for each time record taken. Do not use SET START or SET CENTER for making measurements using the Periodic Noise Source within one SPAN width of 0 Hz. Instead, use the 0-START mode as this does not use the Digital Local Oscillator and will avoid L.O. translated noise aliasing around 0 Hz.

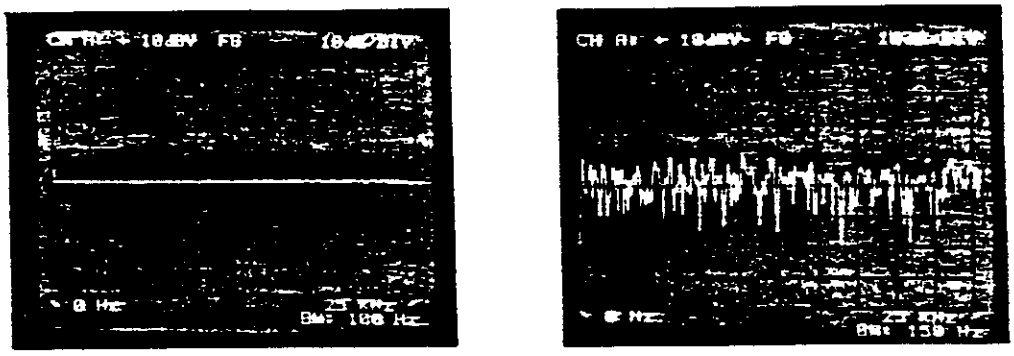

(a) PERIODIC NOISE SOURCE (b) RANDOM NOISE SOURCE

Figure 3-10. Noise Source Spectrums.

3-64. To see the spectral output of the RANDOM noise source, set the PASSBAND SHAPE to HANNING and turn the concentric control of the level switch to RANDOM. The spectrum will appear similar to that in Figure 3-10(b). A smoother display may be obtained by RMS averaging.

3-65. IMPULSE OUTPUT.

3-66. The IMPULSE output signal is a pulse which has an amplitude of +5 V. The period of the pulse is determined by the SPAN control settings (see Table 3-1). The repetition period is the same as the length of the time record. The UNIFORM window should be used

Table 3-1. Impulse Output Pulse Period.

SPAN	0-25 kHz 0-Start	SET START SET CENTER
25 kHz	1.211 μsec	2.441 μsec
10 kHz	2.441 μsec	6.104 μsec
5 kHz	6.104 μsec	12.207 μsec
2.5 kHz	12.207 μsec	24.414 μsec
1 kHz	30.518 μsec	61.035 μsec
500 Hz	61.035 μsec	.12207 msec
250 Hz	.12207 msec	.24414 msec
100 Hz	.24414 msec	.6105 msec
50 Hz	.6105 msec	1.221 msec
25 Hz	1.221 msec	2.441 msec
10 Hz	2.441 msec	6.101 msec
5 Hz	6.101 msec	— — —
1 Hz	30.667 msec	— — —

FIG. 3.

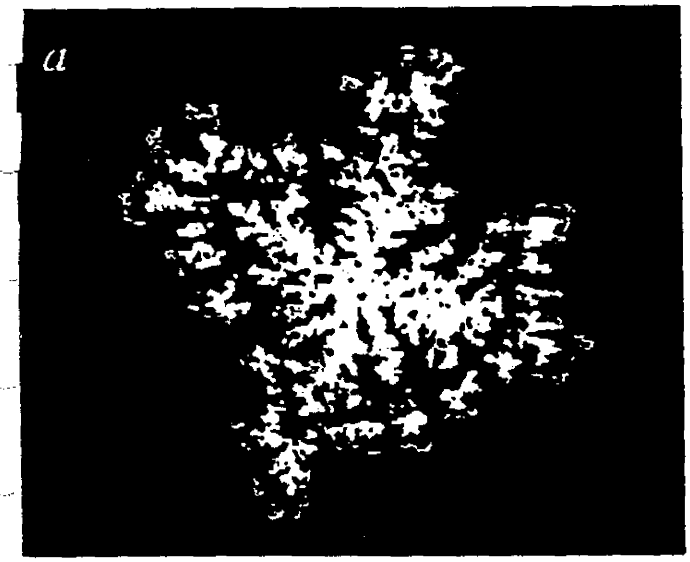

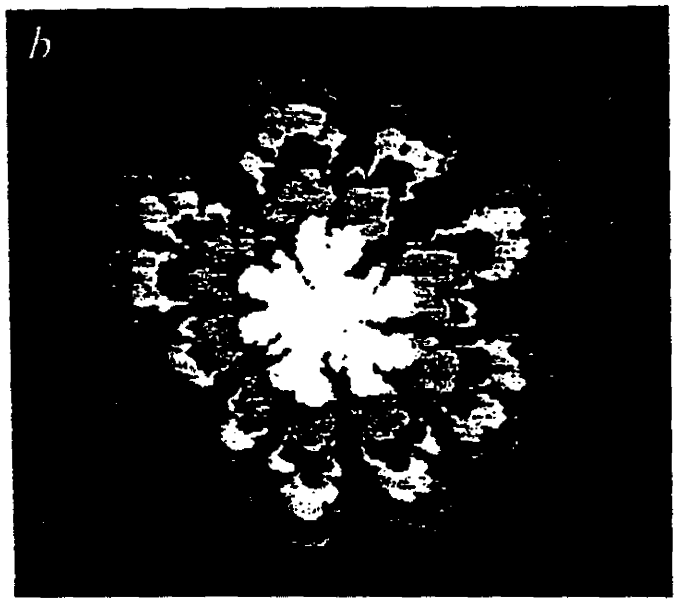

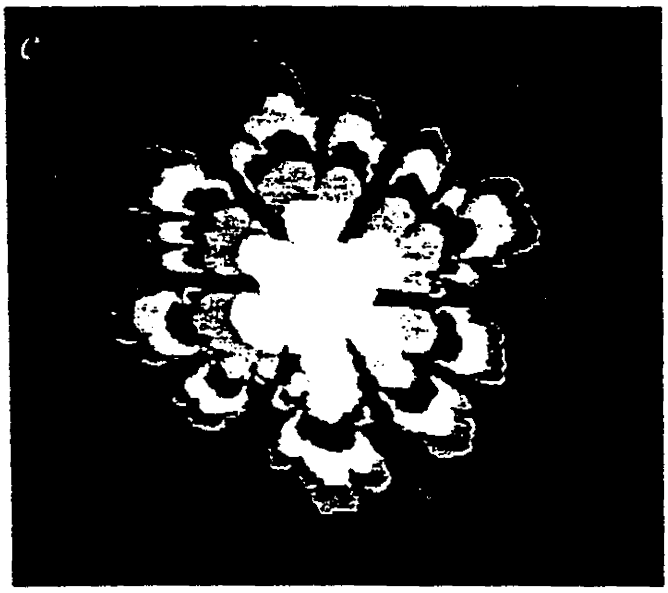

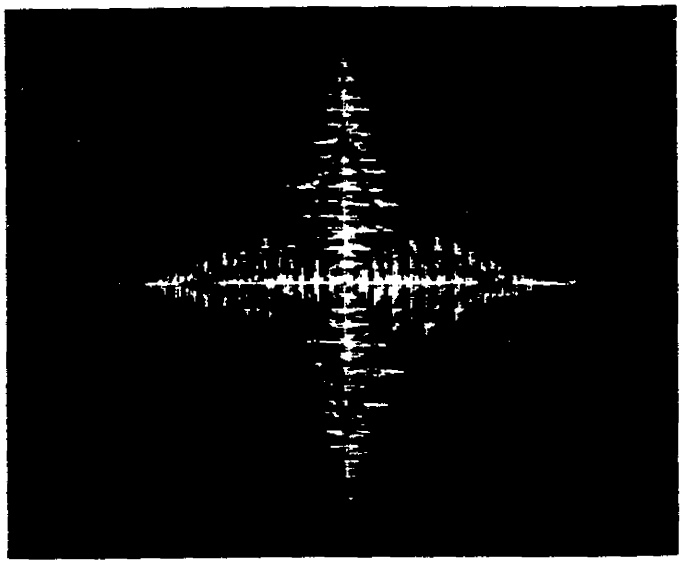

Fig. 2 A typical fractal structure on a square lattice with $s = 50$ and a microscopic anisotropy (defined by equations (6), (7)) of $k - 1 = 10$. The colour coding is the same as in Fig. 1.

($d_f = 1.7$). Here d_f is the fractal dimension obtained, for example, from the slope of a log–log plot of the mass against the caliper diameter. For large s (for example, $s = 20$; Fig. 1*b*), the qualitative appearance appears to differ: the system appears at first sight to cross over to a new 'universality class', with a larger value of d_f. However, when we extrapolate the apparent fractal dimension to large cluster sizes we find that $d_f = 1.7$ for all values of s; that is, the growth forms are quantitatively identical, independent of the degree of noise reduction.

Note that tip splitting always occurs by the same mechanism. First a cluster grows 'smoothly', without tip splitting. However, as the radius of curvature increases, the interface becomes 'rough', with both positive (outward) and negative (inward) fluctuations. The positive fluctuations are not significant, as they are soon damped out; however, the negative fluctuations persis (Fig. 3). This is because, for a charged fractal object, the electri field inside a single notch is very small, and the equation relating the electric field to the gradient of the potential is formally identical to the Darcy law relating growth velocity to the gradien of the pressure. Hence, the tiny notch is not likely to be fille in so quickly as one would expect if interfacial tension were present (Fig. 3*d*). The tiny protrusions on both sides of the notch see a much larger field than does the notch, so they attract mass. The tiny notch thus becomes the terminus of a long fjor (Fig. 3*e*). A fjord is almost perfectly screened, and so is almost never filled in. In Fig. 3, $s = 50$. If $s > 50$ (less noise), then the same tip-splitting mechanism will apply but a negative fluctu ation (notch) will decay more efficiently: the system is les susceptible to negative fluctuations and a fjord is formed only when the cluster has reached a larger radius of curvature.

Although the asymptotic fractal dimension d_f is independen of s, the finger thickness W_f clearly increases with s. Moreover our model explains the existence of a well-defined W_f: the less the noise, the thicker the finger (see Fig. 1). We find the quantitative law:

$$W_f = 4.5 \log s + 2 \qquad (3$$

Fig. 1 Examples of fractal structures generated when the anisotropy parameter k is held fixed at unity, but the noise parameter $1/s$ is decreased. In *a*, *b* and *c*, $s = 2$, 20 and 200, respectively. For all finite values of s, we find that the fractal dimension is equal to the DBM value, $d_f = 1.7$ [illegible]. The colour coding is as follows: the first one-sixth

These biomolecules then build up to proto-life forms which we can photograph under optical microscope, as shown in Part 2 p.57, Fig E. These identical forms can be computer generated and simulate the experimental form by the Fractal geometry of Mandelbrot. See Fig.3, p.5.

This sequence of ELF signalling (8 Hz and higher harmonies to 32,768 Hz); Kervran Transmutation IN VITRO ; and the usefulness of the fractal geometry computer simulation of living forms, gives new insights into the living process.

We can further extend this insight into the living process by briefly reviewing the already cited (PART 2) experiments in simulating sound and voice hearing in totally deaf human beings by means of the TD instrument.

(a) When the two circular flat electrodes carrying the amplitude modulated alternating current are placed on the head skin of a totally deaf person - there is no hearing of the audio information. But - if the electrodes are lightly stroked over the skin - the deaf person will hear linearly to the original audio - tones, voice, or music.

(b) The "stroking" of the skin with the energized electrodes.

It was found that the stroking of the skin chops the carrier signal into 8 Hz (carrier) pulses. This is caused by a half-wave rectification of the carrier leading to sonic transduction in the skin. It is the keratin in the skin (alpha helix protein) which is the (diode) receptor - specifically the protons in the alpha helix keratin. This action on the protons encodes the AM AC half-wave rectified signal into the true auditory pulse code of the central